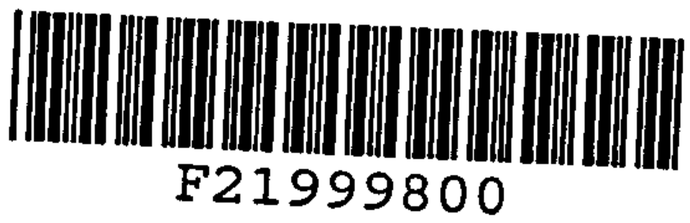

"TROPOMYOSIN HETERODIMERS IN CARDIAC MUSCLE REGULATION"

by Athanasia Kalyva

A thesis submitted to the University of Kent for the degree of Doctor of Philosophy

Department of Biosciences

Faculty of Science, Technology and Medical Studies

2009

Dedication

"The beginning is the most important part of the work"

Plato

To my *teachers*

Anne and Mike

for guiding me through a perfect beginning in research

Declaration

No part of this thesis has been submitted in support of an application for any degree qualification of the University of Kent or any other University or Institute of learning.

21.12.09

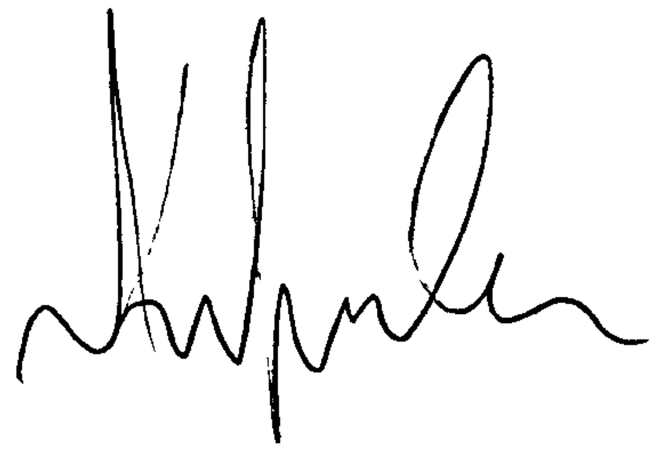

Abstract

The binding of myosin to actin in the skeletal and heart muscles can be regulated by tropomyosin (Tm), troponin (Tn) and Ca^{2+}. Two Tm isoforms are expressed in striated muscles, namely the skeletal α and β isoforms, which are combined *in vivo* to form the αα homodimers and the αβ heterodimers. It is known that, in contrast to the skeletal muscles, the level of the αβ heterodimer in a healthy heart is low. In the hearts of smaller animals, the αα homodimer is predominantly present. Overexpression of the β isoform in transgenic mice, resulted in the formation of the αβ heterodimer in heart and was lethal with the heart exhibiting several pathological abnormalities. It is not known how the skeletal αβ heterodimer regulates heart contraction and why it can be associated with cardiomyopathies. This question has not been addressed to date because purification of the αβ heterodimer was problematic.

The major achievement of the project presented in this thesis was the development of a method to successfully assemble and purify *in vitro* the skeletal Tm heterodimer. The αβ heterodimers were formed by thermally-induced chain dissociation of bacterially expressed αα and ββ homodimers followed by chain exchange and dimer recombination. The ββ homodimers used were tagged at their N-termini (with His or Strep affinity tags). The presence of the small affinity tag prevented the preferential recombination of the tagged-β monomers into the ββ homodimer and allowed the formation of the target αβ heterodimer. This novel method was also applied for the *in vitro* formation of other types of heterodimers that were carries of a cardiomyopathy mutation, namely the α^{D175N} or the α^{E180G} mutations. It is presented here that heterodimers carrying a β subunit are less thermally stable than homodimers or heterodimers composed by α subunits. Also the heterodimers had reduced affinity for actin when compared to the homodimers. However all heterodimers with the skeletal Tn could efficiently regulate the binding of myosin to actin.

The *in vitro* formation and the purification of the αβ heterodimer, now allows the further characterisation of the molecule and will lead in a better understanding of the regulation of heart muscle contraction.

I would like to thank the British Heart Foundation for their generous financial support.

I would also like to thank Dr Stephen Martin for supervising me when I performed the circular dichroism measurements in his laboratory in the Mill Hill institute in London. Also Dr Kevin Howland, the manager of the Biomolecular facility in the Biosciences Department at the University of Kent, for running all the mass spectrometry analysis for me.

I am very thankful to all past and present members of the Geeves group. Especially to Dr Arthur Coulton who has introduced me in the tropomyosin field and supervised me in my first steps. Also to Dr Anja Schmidtman for advising me in molecular biology issues and Dr Nancy Adamek for providing all the technical support and native protein preparations. I would like to thank all the members of the group and the colleagues from other groups in the department for making a friendly work environment especially Marieke, Dave, Sam, Hugh, Maqsood, Heresh, Chris, Eudoxia, Jane, Rebeca, and Sheran. Special thanks to Val, Nancy, Anja and Jane for proofreading the thesis.

I would like to thank my family, Markos, Chrysoula, Anna, Manos and my grandmother Anna for their love and support.

But most importantly, I am truly grateful to my supervisor Professor Michael Geeves for being always available and always most helpful. His guidance was marvellous. In laboratory issues, in thesis writing, in giving me the chance to participate in numerous conferences and even in psychological rescues, he was always most supportive. Quite simply, I could not have possibly asked for anything more.

Abbreviations

Amp	Ampicillin
APS	Ammonium PerSulphate
ATPase	Adenosine 5' Tripohsphatase
DCM	Dilated Cardio Myopathies
DNase	Deoxyribonuclease
DTT	Dithiotreitol
EDTA	Ethylenediaminetetraacetic acid
EGTA	Ethylene glycol bis (b-aminorthyl ether)- N,N,N',N'-tetraacetate)
ELC	Essential Light Chain
FHC	Familial Hypertrophy Cardiomyopathy
FPLC	Fast Performance Liquid Chromatography
HABA	4'-hydroxyazobenzene-2-carboxylic acid
HCM	Hypertrophic Cardio Myopathies
Hepes	N'-(2-Hydroxyethyl) piperazine N'(2-ethane sulphonic acid)
HMM	Heavy MeroMysoin
k_{obs}	Observed rate constant
kDa	Kilo Dalton
LMM	Light Mero Myosin
MHC	Myosin Heavy Chain
MOPS	4-morpholinopropanesufonic acid
Pi	Inorganic Phosphate
Pyrene	N-(1-pyrenyl) iodoacetamide
RLC	Regulatory Light Chain
RNase	Ribonuclease
S1	Myosin Subfragment 1
S2	Myosin Subfragment 2
SDS	Sodium Dodecyl Sulfate
TEMED	N',N',N',N'-tetramethylethylendiamine
Tm	Tropomyosin
Tn	Troponin

Contents

Chapter 3 – Formation of Tropomyosin Heterodimers

Chapter 4 – Characterisation of Tropomyosin Heterodimers

List of Figures

Chapter 3 – Formation of Tropomyosin Heterodimers

Chapter 5 – Cloning, Expression and Purification of TnT1 mutants

Chapter 6 – Closing Discussion

Chapter 1

Introduction

1.1 Introduction

Tropomyosin (Tm) is a coiled-coil dimeric protein that is found associated with actin structures in the cell (Gunning *et al.* 2008). In skeletal and cardiac muscle cells, Tm is associated with the actin filaments of the sarcomere (Bailey 1948). The role of Tm as a regulator of striated muscle contraction has been extensively investigated and is well characterised (Gordon *et al.* 2000). However, there are still questions concerning the regulation of muscle contraction by different types of Tm dimers, more specifically the Tm homodimers that are composed by a single type of subunit vs. the Tm heterodimers that are composed by two different subunits.

In this chapter a literature review on Tm is presented. The chapter starts with the description of Tm genes and isoforms and the description of the coiled-coil Tm structure. The project focuses on the role of Tm in the regulation of skeletal and cardiac muscle contraction, therefore background information is given for the rest of the sarcomeric proteins and then a description of muscle contraction and regulation as it is currently understood follows. The function of Tm is not restricted in regulating the striated muscle contraction; therefore the role of Tm in non-muscle cells is also shortly described. Another aspect of the project is to investigate the effects of

cardiomyopathies on thin filament proteins in cardiac muscle regulation, therefore this chapter ends with general information on cardiomyopathies on Tm and Troponin (Tn).

1.2 Tropomyosin gene structure and isoforms

The most significant property of Tm is its association with actin filaments. In skeletal muscle and heart, Tm is associated with actin filaments in the sarcomere and together with Tn is a regulator of muscle contraction. In the cytoskeleton Tm is also found associated with actin filaments that are involved in a large variety of cellular functions like cell shape, cell motility, vesicle transport, endocytosis and exocytosis. Many different Tm isoforms exist, yet it is not clear why. One of the reasons could possibly be that the different Tm isoforms are expressed in order to satisfy the specific needs of the associated actin filaments.

In eukaryotes a single Tm gene can either give rise to just one Tm isoform or encode for more than one Tm isoform by using alternative promoters and alternative exon splicing. For example in the yeast *Saccharomyces cerevisiae* there are two different Tm genes named TPM1 and TPM2 (Drees *et al.* 1995). Each of them encodes just a single Tm isoform with distinct functions. In *Saccharomyces pombe* there is only one Tm gene known as cdc8 that encodes one Tm isoform (Balasubramanian *et al.* 1992). In more complex organisms like the nematode *Caenorhabditis elegans* a single Tm gene (tmy I) can give rise to four different Tm isoforms using a distal and an internal promoter and alternative splicing as shown in figure 1.1 (Kagawa *et al.* 1995; Anyanful *et al.* 2001). In *Drosophila melanogaster,* there are four different Tm isoforms. Two of the isoforms come from the same mTmI gene by alternative splicing (Basi *et al.* 1984). The other two isoforms mTmII and cTm were originally thought to be products of different genes, but then it was found that they originate from the same gene by alternative splicing (Hanke *et al.* 1987).

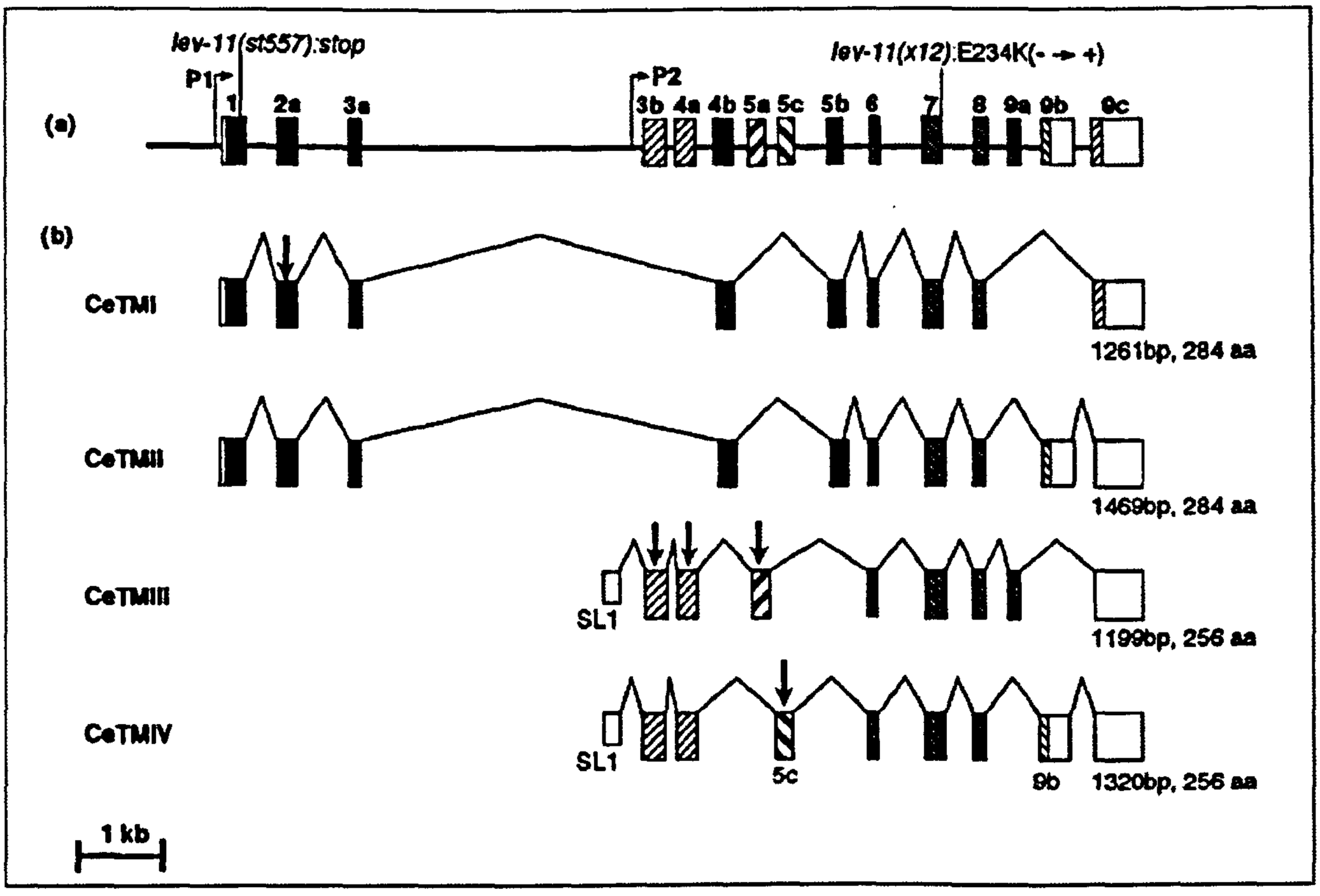

Fig 1.1: Tm isoforms in *Caenorhabditis elegans*. All four isoforms are products of a single gene and formed by using two different promoters and alternative splicing (Anyanful *et al.* 2001).

More than 40 Tm isoforms have been discovered in mammals. The Tm isoforms are encoded by four different genes known either as the α-, β-, γ- and δ-genes or as the TPM1, TPM2, TPM3 and TPM4 genes in humans respectively. These genes are not linked and are found in different location in the genome. For example in humans the four different genes TPM1, TPM2, TPM3 and TPM4 were assigned to bands 15q22 (Eyre *et al.* 1995), 9p13 (Hunt *et al.* 1995), 1q22 (Wilton *et al.* 1995) and 19p13 (Wilton *et al.* 1996) respectively i.e. each is found on a different chromosome. The structural organisation of each mammalian gene is shown in figure 1.2.

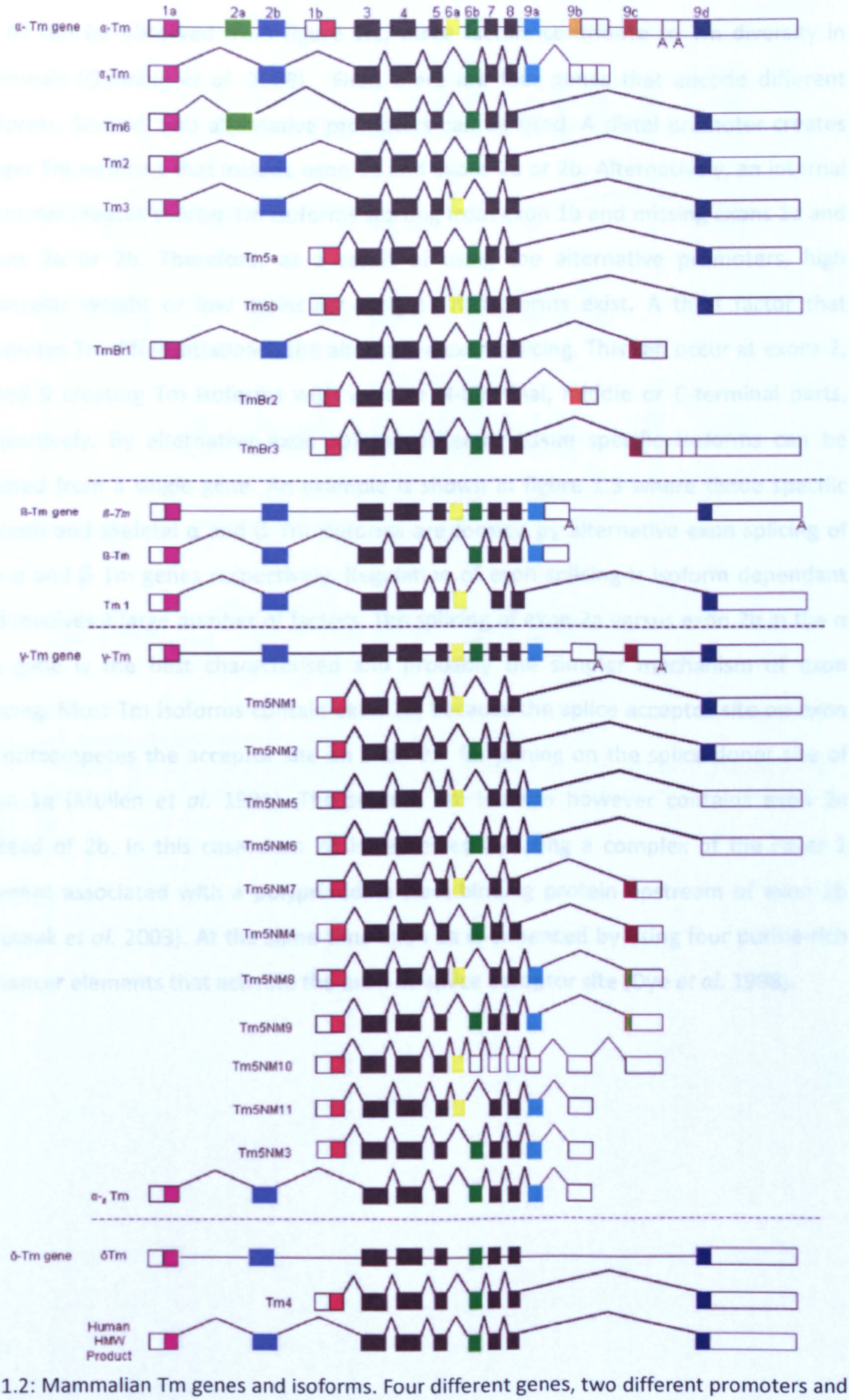

Fig 1.2: Mammalian Tm genes and isoforms. Four different genes, two different promoters and alternative splicing of exons 2, 6 and 9 can produce more than 40 Tm isoforms (not all shown here).In humans the α, β, γ and δ genes are known as TPM-1, 2, 3 and 4 respectively (Gunning *et al.* 2008).

As can be observed from figure 1.2, three factors contribute to Tm diversity in mammals (Gunning *et al.* 2008). First, there are four genes that encode different isoforms. Second, two alternative promoters can be used. A distal promoter creates longer Tm isoforms that include exon 1a and exons 2a or 2b. Alternatively, an internal promoter creates shorter Tm isoforms starting from exon 1b and missing exons 1a and exons 2a or 2b. Therefore, as a result of using the alternative promoters, high molecular weight or low molecular weight Tm isoforms exist. A third factor that promotes Tm differentiation is the alternative exon splicing. This can occur at exons 2, 6 and 9 creating Tm isoforms with variable N-terminal, middle or C-terminal parts, respectively. By alternative exon splicing different tissue specific isoforms can be created from a single gene. An example is shown in figure 1.3 where tissue specific smooth and skeletal α and β Tm isoforms are formed by alternative exon splicing of the α and β Tm genes respectively. Regulation of exon splicing is isoform dependant and involves a large number of factors. The splicing of exon 2a versus exon 2b in the α Tm gene is the best characterised and probably the simpler mechanism of exon splicing. Most Tm isoforms contain exon 2b, because the splice acceptor site on exon 2b outcompetes the acceptor site on exon 2a for joining on the splice donor site of exon 1a (Mullen *et al.* 1991). The smooth Tm isoform however contains exon 2a instead of 2b. In this case exon 2b is repressed by using a complex of the raver 1 element associated with a polyprimidine tract binding protein upstream of exon 2b (Gromak *et al.* 2003). At the same time exon 2a is enhanced by using four purine-rich enhancer elements that activate the exon 2a splice acceptor site (Dye *et al.* 1998).

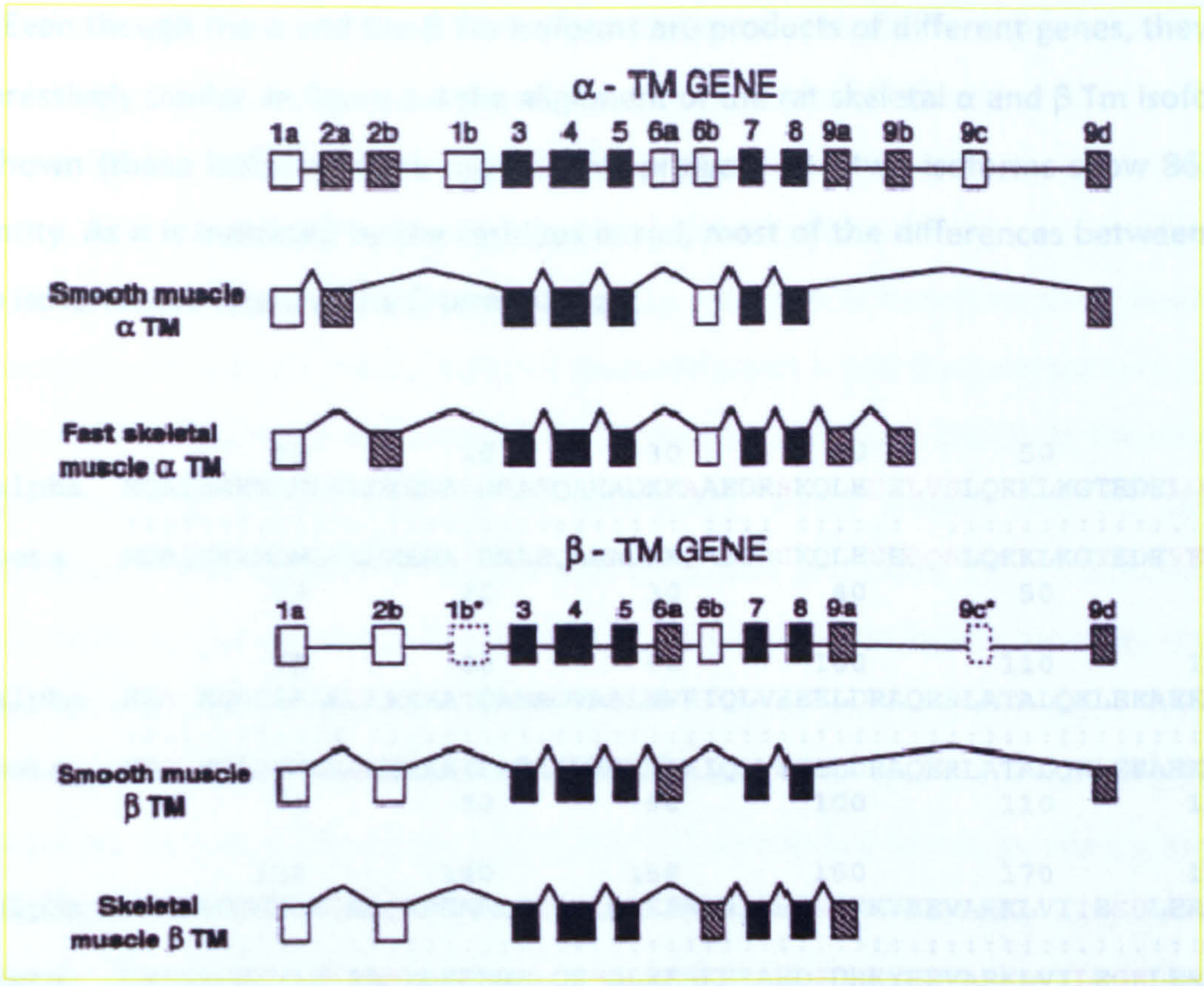

Fig 1.3: Alternative exon splicing in α and β Tm genes results in the production of tissue specific smooth muscle or skeletal muscle α and β Tm isoforms (Perry 2001).
(NB the smooth and skeletal α Tm isoforms are also assigned as Tm6 and α_1Tm respectively in fig 1.2; the smooth and skeletal β Tm isoforms are also assigned as Tm1 and β Tm respectively in fig 1.2).

Even though the α and the β Tm isoforms are products of different genes, they are impressively similar. In figure 1.4 the alignment of the rat skeletal α and β Tm isoforms is shown (these isoforms were used in this project). The two isoforms show 86.4 % identity. As it is indicated by the residues in red, most of the differences between the two isoforms are found in the C-terminal half.

```
                10        20        30        40        50        60
alpha   MDAIKKKMQMLKLDKENALDRAEQAEADKKAAEDRSKQLEDELVSLQKKLKGTEDELDKY
        :::::::::::::::::::.:::::::::::: :::: ::::.:  .:::::::::::..::
beta    MDAIKKKMQMLKLDKENAIDRAEQAEADKKQAEDRCKQLEEEQQALQKKLKGTEDEVEKY
                10        20        30        40        50        60

                70        80        90        100       110       120
alpha   SEALKDAQEKLELAEKKATDAEADVASLNRRIQLVEEELDRAQERLATALQKLEEAEKAA
        ::..:::::::: ::::::::::::::::::::::::::::::::::::::::::::::::
beta    SESVKDAQEKLEQAEKKATDAEADVASLNRRIQLVEEELDRAQERLATALQKLEEAEKAA
                70        80        90        100       110       120

               130       140       150       160       170       180
alpha   DESERGMKVIESRAQKDEEKMEIQEIQLKEAKHIAEDADRKYEEVARKLVIIESDLERAE
        ::::::::::.::.::::::.::.:::::::::::.:::::::::::::::.:..::::.:
beta    DESERGMKVIENRAMKDEEKMELQEMQLKEAKHIAEDSDRKYEEVARKLVILEGELERSE
               130       140       150       160       170       180

               190       200       210       220       230       240
alpha   ERAELSEGKCAELEEELKTVTNNLKSLEAQAEKYSQKEDKYEEEIKVLSDKLKEAETRAE
        :::::.:.::.:::::: :::::::::::::.::: :::::::::.: .::::::::::
beta    ERAEVAESKCGDLEEELKIVTNNLKSLEAQADKYSTKEDKYEEEIKLLEEKLKEAETRAE
               190       200       210       220       230       240

               250       260       270       280
alpha   FAERSVTKLEKSIDDLEDELYAQKLKYKAISEELDHALNDMTSI
        ::::::.::::.:::::::::::.::::::::::::.::::.::.
beta    FAERSVAKLEKTIDDLEDEVYAQKMKYKAISEELDNALNDITSL
               250       260       270       280
```

Fig 1.4: Sequencing alignment of rat skeletal α and β Tm isoforms. The residues shown in red differ between the two isoforms. The two isoforms are 86.4 % identical. (Alignment obdained using the LALIGN tool, http://www.ch.embnet.org/software/LALIGN_form.html)

In any muscle cell both the α Tm and the β Tm isoforms may be expressed. The two isoforms can be combined together to form three possible types of dimers i.e. the αα and ββ Tm homodimers and the αβ Tm heterodimer. The α and β isoforms carry a unique amino acid sequence as shown in fig 1.4, therefore the αα, ββ and αβ dimers will subsequently be different in their amino acid content.

The ratio of Tm homodimers versus heterodimers in muscles is highly variable and largely depends upon the muscle type and the size of organism (reviewed in Perry 2001). Smooth chicken gizzard muscle for example contains roughly equal amounts of smooth α Tm and β Tm isoforms which are found mostly (95%) as heterodimers (Sanders *et al.* 1986; Jancso and Graceffa 1991). Preferential formation of heterodimer in smooth muscle is thermodynamically favoured when α and β monomers are mixed at physiological temperatures of 37- 40 °C (Lehrer and Qian 1990). In the case of skeletal muscles, αα Tm and αβ Tm dimers are mostly present and the ββ Tm homodimer is less stable and rarely found (Cummins and Perry 1973; Cummins and Perry 1974). In general the α Tm isoform is associated with fast contracting muscle fibres and expression of the β Tm isoform occurs in slow contracting muscles (Bronson and Schachat 1982). Heart muscle contains the same α Tm and β Tm isoforms as the skeletal muscle (Lewis and Smillie 1980). In small animals like rabbit, guinea pig and rat which have faster beating hearts the αα Tm homodimer is predominantly present. In contrast, pig, sheep and human hearts that beat more slowly have the αα Tm homodimers but also up to 20 % β Tm isoform present as αβ Tm heterodimer (Leger *et al.* 1976; Pieples and Wieczorek 2000). Interestingly some cardiomyopathies are associated with an increased level in the αβ Tm heterodimer in heart; Overexpression of the β Tm in transgenic mice resulted in higher levels of αβ Tm in the heart and was lethal with death occurring between 10-14 days postnatally (Muthuchamy *et al.* 1995; Muthuchamy *et al.* 1998).

1.3 Tm structure – general features

In every cell Tm is found as a dimer. The dimer can be composed of either identical (homodimer) or highly homologous isoforms (heterodimer). Depending on the length of the isoforms each Tm dimer can span a certain number of actin monomers within an actin filament. For example in mammals the Tm dimers that are composed by the long 284 residues isoforms can span 7 actin monomers, while the dimers composed by the shorter 248 residues isoforms can span 6 actin monomers (Lin *et al.* 1997). In contrast,

the Tpm1 and Tpm2 isoforms of *S. cerevisiae* are only 199 and 161 residues long and span 5 and 4 actin monomers respectively (Drees *et al.* 1995).

In every dimer each of the component subunits has a right-handed α-helix structure. The two α helices are associated in parallel to form a left-handed coiled coil dimer. A crystal structure of α Tm resolved at 7 Å is shown in figure 1.5 (Whitby and Phillips 2000). The Tm coiled-coil dimer is itself further coiled taking approximately three full turns.

Fig 1.5: Crystal structure of α Tm at 7 Å resolution (Whitby and Phillips 2000)

Formation of coiled-coils correlates with the amino acid composition of Tm. Amino acid sequence analysis of Tm reveals that the residues follow a heptad repeat pattern (*a-b-c-d-e-f-g*) (McLachlan *et al.* 1975). In figure 1.6 the heptad repeat pattern in the amino acid sequence of chicken skeletal α Tm is shown together with the position of each residues *a-g* within the coil-coiled dimer. It can be seen that residues at positions *a* and *d* are mainly small and hydrophobic and form the interface of the two helices in the coiled-coil. The coiled-coil is held together mainly by the hydrophobic interactions between residues *a* and *d* in the two chains. The coiled-coil is further stabilised by salt bridges between residues *e* and *g* on the two chains. Residues at positions *b*, *c* and *f* are hydrophilic and face the outside of the coiled-coil, interacting with partner proteins. Observation of the residues arrangement within the Tm coiled coil (fig 1.6) leads to the understanding that Tm heterodimers that possess two different monomers along the coiled-coil may have different residues at positions b, c, f and b',

c', f'. Therefore it is possible that heterodimers could be different in interacting with neighbouring proteins than the homodimers which would be more uniform in the two sides of the coil. Moreover, having different a, d and a', d' residues, the heterodimers could be different from the homodimers in how tight the coiled-coil is held together and therefore in the thermal stability of the molecule.

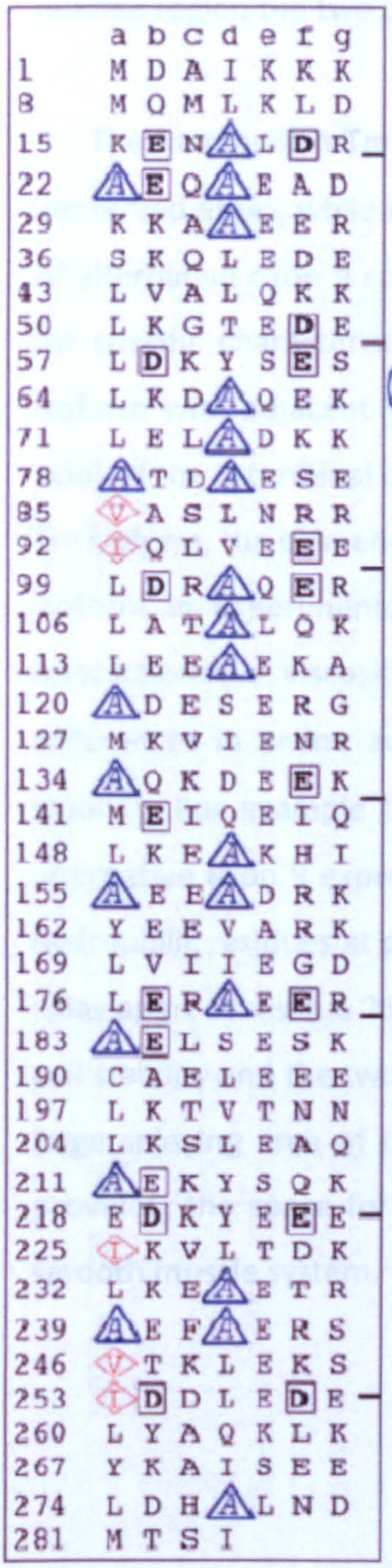

Fig 1.6: Heptad repeat pattern in Tm. Left panel: The amino acid sequence of striated α Tm follows a heptad repeat pattern with residues at positions *a* and *d* being mostly hydrophobic and residues at positions *b, c, e, f, g* hydrophilic. In *a* and *d* positions there are many Ala residues (blue triangles) and in *b* and *f* position many charged residues (black squares) (Brown *et al.* 2001). Right panel: Residues at positions *a-g* occupy specific positions within the coiled-coil. The coiled coil is held together mainly by hydrophobic interactions between residues *a* and *d* and also by ionic interactions between residues *e* and *g*. Hydrophilic residues at positions *b, c* and *f* face the exterior of the coiled-coil and interact with partner proteins. (Wolska and Wieczorek 2003).

In physiological salt concentrations Tm dimers can polymerise forming long Tm filaments. Filament formation is achieved by a head-to-tail overlap between neighbouring Tms. In early X-ray data a head-to-tail overlap in Tm was observed as an area of higher density (Philips et al 1979). Recent data suggest that the two chains at the C-terminal end of one Tm molecule are splayed apart and anchor the two chains of the N-terminal of the next Tm molecule. The first 11 residues from the N-terminal seem to be inserted in the C-terminal cleft (Greenfield *et al.* 2006). At this head-to-tail overlap region the two coiled coils are rotated 90° relative to each other.

The mammalian Tm isoforms are highly homologous. The N-termini are the most conserved areas, while most of differences are found in the C- termini largely because of alternative exon 9 splicing. The C-terminal sequence of a Tm isoform may account for specific characteristics, especially concerning the head-to-tail interaction of this isoform with adjacent Tm molecules. For example, by swapping the last 10 amino acids of the C-terminal of a skeletal β Tm for the corresponding residues of a smooth β Tm isoform, the chimeric construct behaves more like a smooth isoform than a skeletal isoform in experiments that measured parameters dependent on the end-to-end interactions (i.e. viscosity, actin binding, TnT1 binding) (Coulton *et al.* 2008). Moreover, differences in amino acid sequence at the C-terminus can influence the coiled-coil stability. For example the C-termini of skeletal and smooth α Tm isoforms due to alternative exon 9 expression appear very different as shown in figure 1.7. By having hydrophilic residues at positions *a* and *d* the two chains in the skeletal α Tm coiled-coil splay apart at residue 262. In contrast the residues in the smooth α Tm enhance coiled-coil stability and the two chains are splayed apart after residue 270 (Li *et al.* 2002). The large splaying area of the C-terminal in the skeletal isoforms may be important for providing the space for interactions with TnT, something that it is not required in a smooth muscle system.

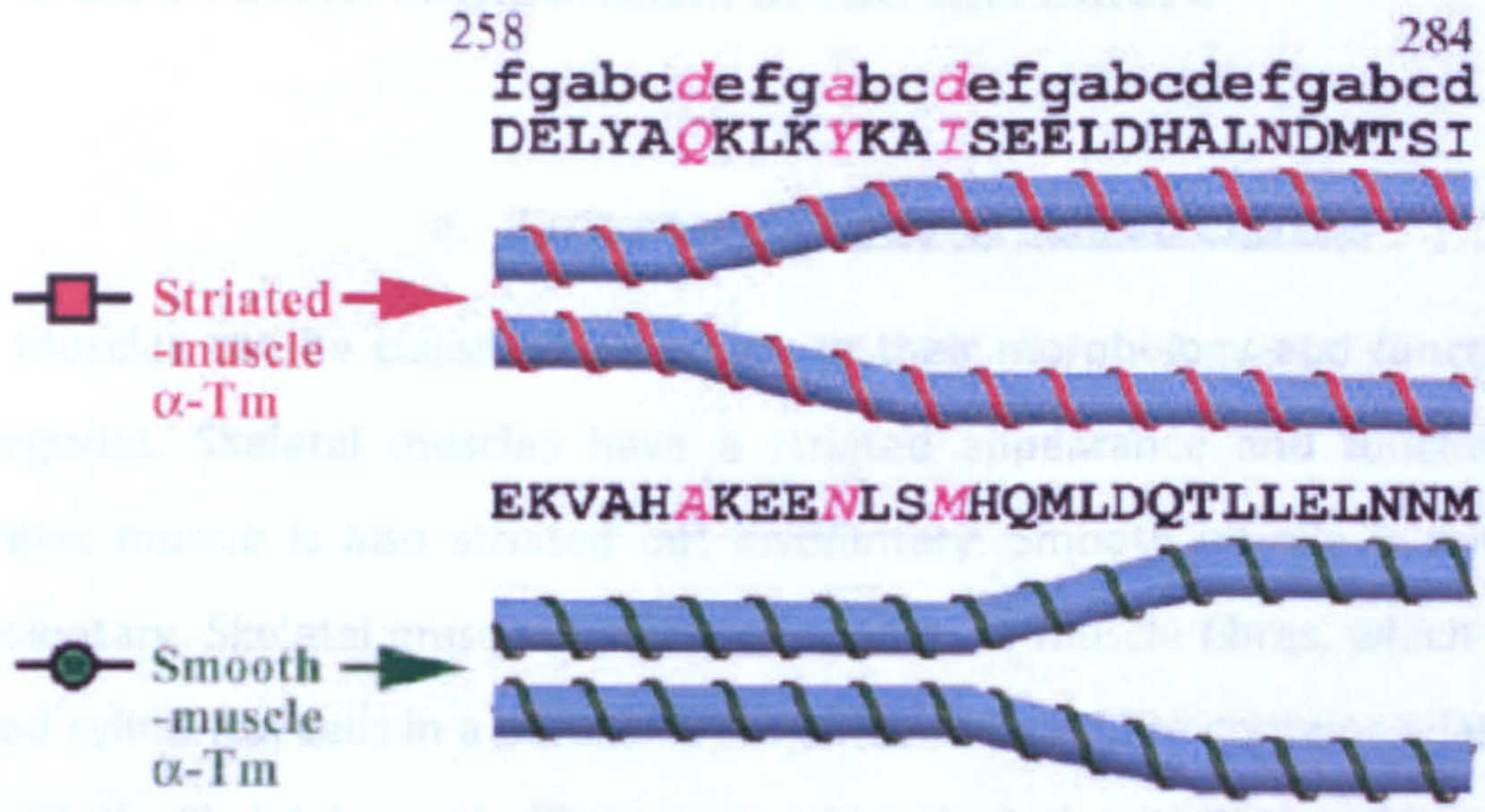

Fig 1.7: C-terminal structural variation in smooth and skeletal Tm isoforms. Coiled-coil structure is extended to residues 262 and 270 for the skeletal and smooth isoforms respectively, thus a larger area at the skeletal Tm C-terminal is spread apart (Li *et al.* 2002).

1.4 Tm function in striated muscle

Tm is mostly known for its role in muscle cells, where it regulates muscle contraction. This thesis focuses on skeletal Tm that is present in striated muscles and investigates if the presence of different Tm isoforms can have an impact on the regulation of muscle contraction. Therefore in the current section background information is given regarding muscle contraction. The muscle sarcomere and its major protein components are described first (1.4.1). Then the mechanism of muscle contraction is explained as it is currently understood (1.4.2). The section ends with the widely accepted three-state model of regulation of muscle contraction (1.4.3).

1.4.1 Protein components of the sarcomere

a. Sarcomere – General characteristics

Muscles can be classified according to their morphology and function into three categories. Skeletal muscles have a striated appearance and function voluntarily. Cardiac muscle is also striated but involuntary. Smooth muscle is not striated and involuntary. Skeletal muscles consist of bundles of muscle fibres, which are elongated fused cylindrical cells in a parallel arrangement. Each fibre contains a large number of myofibrils. Skeletal muscle fibres are multinucleated, with the nuclei arranged at the periphery of the fibres. Cardiac myofibres are shorter than the skeletal ones and can be branched. They only contain one or two nuclei located in the centre of the fibre and not the periphery as in the skeletal case. An additional feature only seen in the cardiac fibres is the presence of intercalated discs, which are membranes linking end to end adjacent cardiac muscle fibres. Smooth muscle fibres are spindle shaped with a wide centre and narrower ends and contain only one centrally located nucleus. Smooth muscles surround the blood vessels and various organs apart from the heart.

Under the microscope, only the skeletal and cardiac muscles appear striated. Each fibre and its component myofibrils have a pattern of alternating dark and light bands. The light bands (I bands) contain thin filaments that extend further into the dark bands as well. In the centre of each I band there is a darker thin line, perpendicular to the filament axis known as the Z line (or Z-disk). The dark bands (A bands) contain both thick filaments and overlapping thick and thin filaments. Therefore within each A band two zones exist; a darker, more dense zone with overlapping thick and thin filaments and a lighter area in the middle of A band with thick filaments only (known also as the H zone). In the overlap area each thick filament is surrounded by six thin filaments. The sarcomere is defined as the area extending between two Z lines and is the basic contractile unit of the muscle (Clark *et al.* 2002, review). The structural organisation of a skeletal muscle from the level of myofibre down to the level of sarcomere is summarised in figure 1.8.

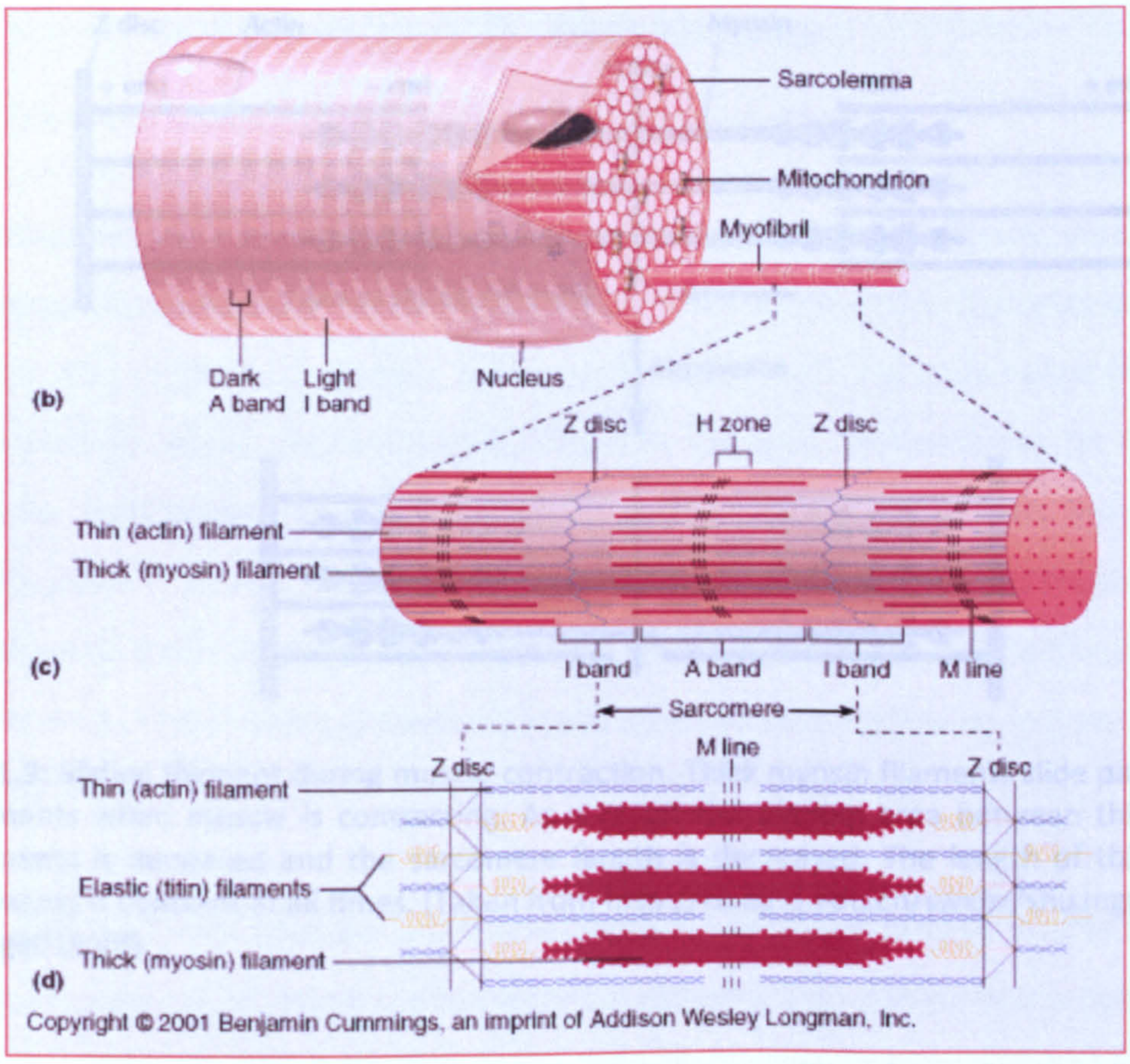

Fig 1.8: Structural organisation of a skeletal muscle fibre. Each fibre consists of a bundle of myofibrils and contains multiple mitochondria and peripheral nuclei. Each of the myofibrils shows a pattern of alternating dark and light bands. The sarcomere is a repeating unit that extends from one Z disc to the next within a myofibril. The location of thin and thick filaments within a sarcomere is indicated. (http://faculty.etsu.edu/forsman/Histologyofmuscleforweb.htm)

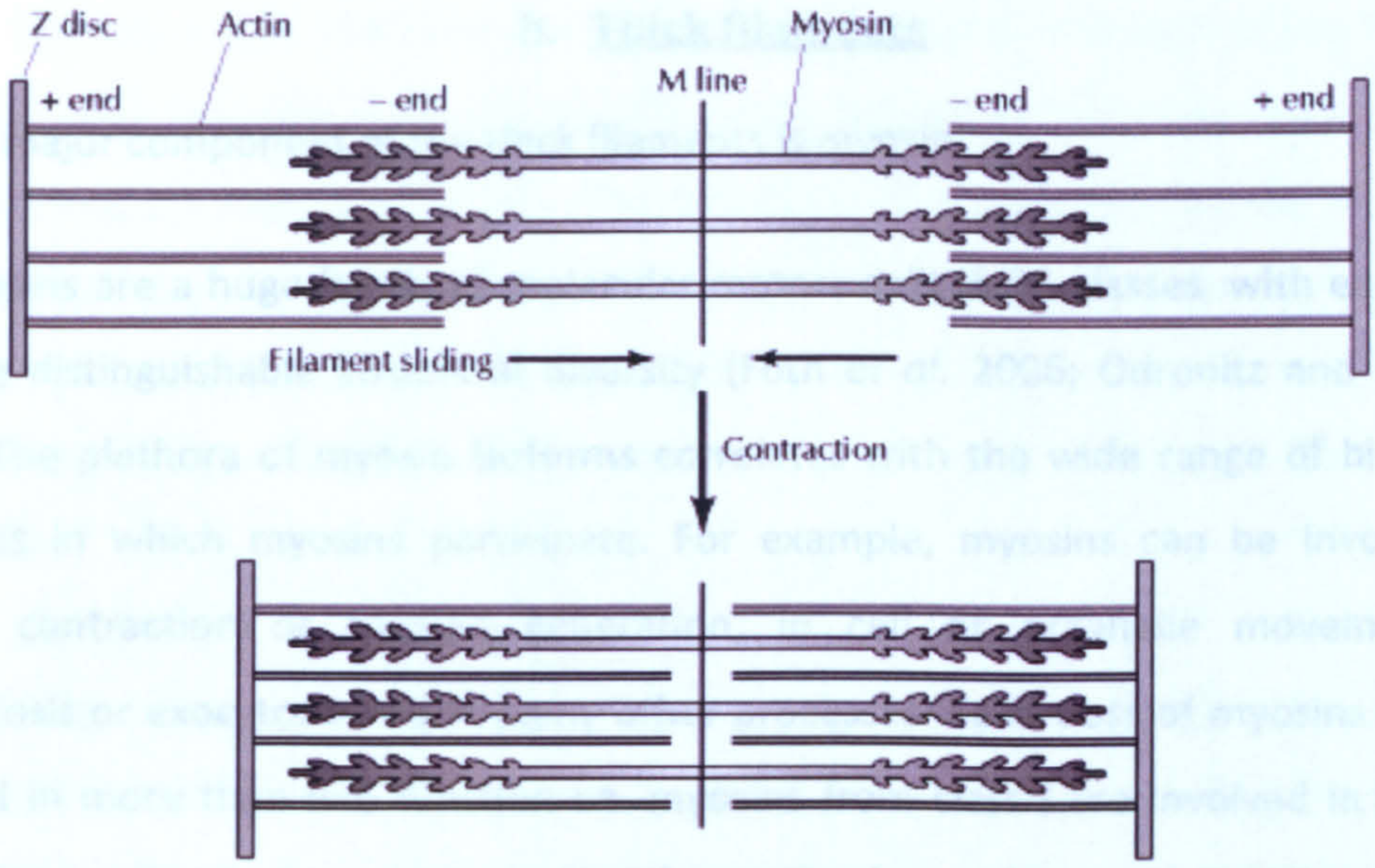

Fig 1.9: Sliding filament during muscle contraction. Thick myosin filaments slide past thin actin filaments when muscle is contracting. As a result the overlap area between thick and thin filaments is increased and the sarcomere length is decreased. The length of thick and thin filaments is constant at all times. (Taken from http://kc.njnu.edu.cn/swxbx/shuangyu/6.files/image016.gif)

As mentioned previously the sarcomere is the basic contractile unit of the muscle. Muscle contraction occurs when the thick and thin filaments slide past each other. The sliding filament theory was described by two independent studies in 1954 (Huxley and Niedergerke 1954; Huxley and Hanson 1954). The major component of the thick filaments is myosin and the major component of the thin filaments is actin. Sliding of filaments is possible because myosin filaments with their protruding heads, also known as cross-bridges, interact with the actin filaments when Ca^{2+} and energy from ATP hydrolysis are available. As the result of filament sliding the two Z discs of a sarcomere approach each other and the overlap area between thin and thick filaments is increased. Therefore the H and I bands appear shorter. The sarcomere length and subsequently the whole myofibril length are decreased. However, the length of the individual thick or thin filaments is constant (fig 1.9).

b. Thick filaments

The major component of the thick filaments is myosin.

Myosins are a huge family of molecular motors split in 35 classes, with each class showing distinguishable structural diversity (Foth *et al.* 2006; Odronitz and Kollmar 2007). The plethora of myosin isoforms correlates with the wide range of biological functions in which myosins participate. For example, myosins can be involved in muscle contraction or tension generation, in cell or organelle movement, in endocytosis or exocytosis and in many other processes. Each class of myosins may be involved in more than one function i.e. myosins from class I are involved in tension generation, endocytosis, exocytosis, signal transduction and transcriptional regulation in the nucleus.

The sarcomeric myosins which take part in skeletal and cardiac muscle contraction belong to class II. Myosin II is a hexamer consisting of two myosin heavy chains (MyHC) and two pairs of calmodulin-like myosin light chains (MyLC) namely the essential MyLC and the regulatory MyLC. In mammals 15 genes encode for MyHC and 8 genes for MyLC. The MyHC products include 6 skeletal, 2 cardiac, 1 smooth muscle, 2 non-muscle and 1 superfast sarcomeric isoforms plus another 3 gene products not well identified. So for example in limb and trunk muscles four MyHCs are expressed: the slow MyHC-1 and the fast MyHC-2A, -2B and -2X. The slow MyHC-1 (also called beta/slow MyHC- β) is also expressed in heart together with the cardiac MyHC-α fast isoform. There are also 4 isoforms for the regulatory MyLCs (a fast, a slow/cardiac, an atrial and a superfast sarcomeric isoforms) and 4 isoforms for the essential MyLCs (a fast, a slow-α, a slow-β and an embryonic/atrial isoforms), (review by Reggiani and Botinelli 2008).

The MyHC has a large globular N –terminal domain of approximately 840 amino acids, also known as the head, followed by an alpha helical neck domain that contains two IQ domains on which one regulatory and one essential MyLC bind. The α-helix is continued for another ~1100 amino acids forming the long myosin tail. The α-helical tail domain follows a heptad repeat sequence that allows formation of a coiled-coil structure between two parallel myosin tails and therefore dimerisation of those two

MyHCs. The tail is also important for aggregating the myosins in such a way that the thick filaments assemble with the myosin heads projecting from the surface of the thick filament at regular intervals. The structure of the coiled-coil tail is slightly disturbed by four skip residues that are inserted within the heptad repeat sequence. The skip residues promote thick filament packing by causing bends at the myosin tail and increase charge complementarity between myosin rods (Offer 1990; Straussman *et al.* 2005).

In practice, it is easier to work with the soluble myosin head domain only, also known as S1, than with the whole myosin. S1 contains the actin binding site and the nucleotide binding site. S1 alone can therefore bind to actin filaments and perform the ATPase activity as successful as the whole native myosin. S1 with the essential light chain bound can be easily obtained by chymotrypsin digestion of myosin as explained in section 2.2.4. Alternatively, to obtain S1 with both the essential and the regulatory light chains bound, myosin can be digested with papain.

Further limited proteolysis of S1 breaks the molecule into three fragments; the N terminal 25K, the middle 50K and the C terminal 20K domains (Mornet *et al.* 1979). The surface loop 1 connects the 25K to the 50K domain and the surface loop 2 connects the 50K to the 20K domain. X-ray crystallography revealed structural details within S1. The first X-ray crystal structure was of S1 from chicken muscle in the post-rigor state (Rayment *et al.* 1993). Since then many more crystal structures of S1 have been published with all showing the same basic structure (Bauer *et al.* 2000; Gulick *et al.* 2000; Holmes *et al.* 2004). Overall the head consists of 7-stranded β sheets surrounded by numerous α helices. In the crystal structure of S1 shown in figure 1.10 below, the N-terminal 25K domain is shown in green. The 50K domain is split into two parts the upper 50K (in red) and the lower 50K (in grey) domains. The C-terminal domain, also known as the lever arm, is shown in blue.

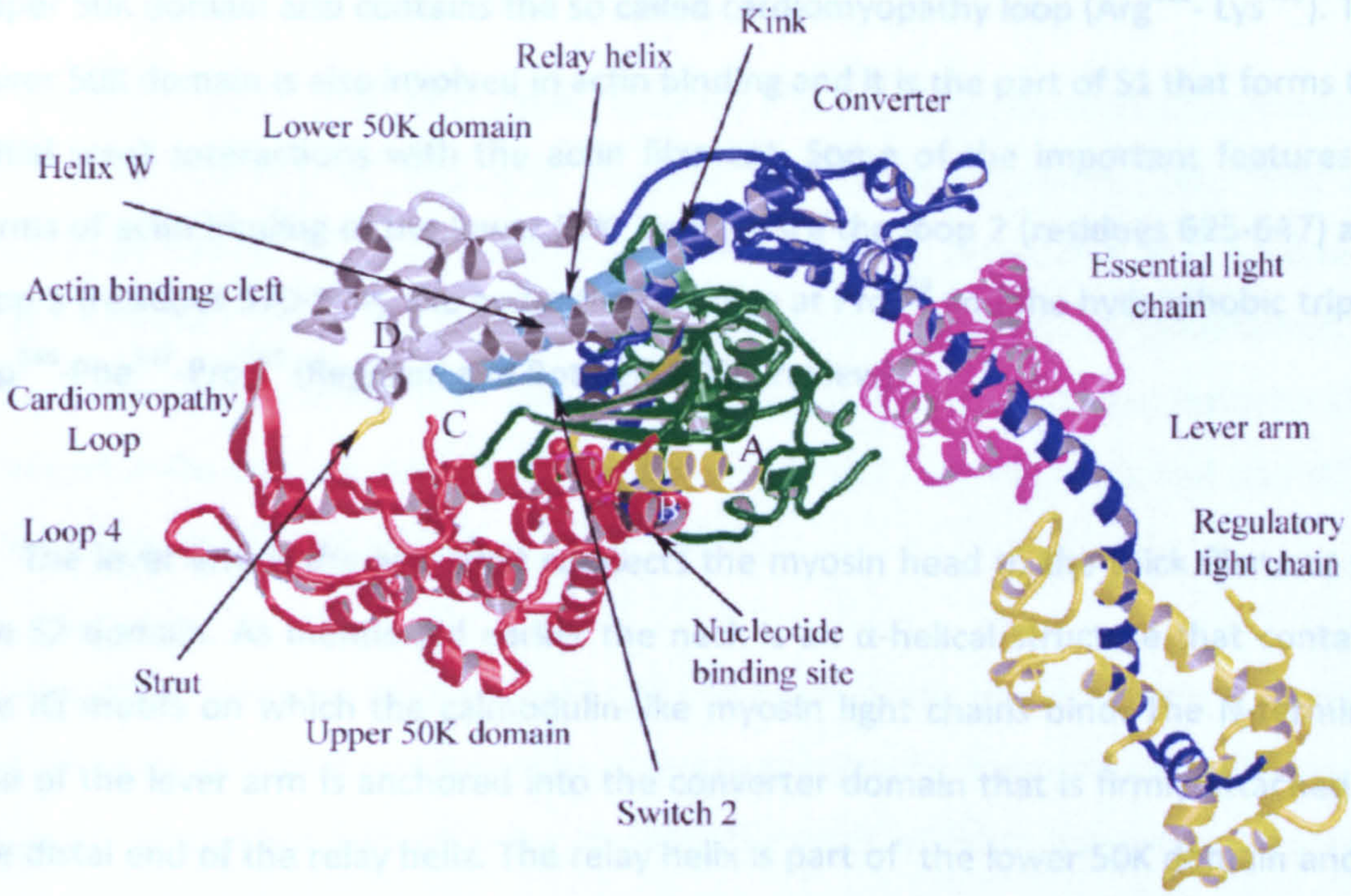

Fig 1.10: Crystal structure of chicken S1 at the post-rigor state. The various domains within S1 are colour-coded. N-terminal is in green. The upper 50K domain is in red, the lower 50K domain is in grey. The actin binding cleft is found between the upper and the lower 50K domains. Close to the actin binding cleft is the nucleotide binding site, located between the upper 50K and the N-terminal domains. The C-terminal domain or lever arm is in blue and is associated with an essential (magenta) and a regulatory (yellow) light chain. The converter domain at the start of the lever arm communicates with the lower 50K domain via the relay helix (Geeves and Holmes 2005).

Figure 1.10 shows that the N-terminal domain lies near the start of the lever arm. The nucleotide pocket is found between the N-terminal and the upper 50K domain and contains a characteristic P-loop (Gly^{179}- Thr^{186}) similar to other ATPases and G proteins. The P-loop lies between two segments namely the switch 1 and switch 2 (Geeves and Holmes 2005). The N-terminal domain ends with the surface loop 1 located at the opening of the nucleotide binding pocket.

The 50K fragment spans two domains which are the upper 50K domain (in red) and the lower 50K or actin binding domain (in grey). The upper and the lower domains are separated by the large actin binding cleft. Part of the upper 50K domain is involved in the nucleotide binding pocket and part in the actin binding site. The ATP-binding site is approximately 4 nm away from the actin binding site (Geeves and Holmes 1999). The

upper 50K domain also contains the so called cardiomyopathy loop (Arg^{403}- Lys^{415}). The lower 50K domain is also involved in actin binding and it is the part of S1 that forms the initial weak interactions with the actin filament. Some of the important features in terms of actin binding of the lower 50K domain are the loop 2 (residues 625-647) and loop 3 (residues 570-574), the hydrophobic bulge at Pro^{529} and the hydrophobic triplet Trp^{546}-Phe^{547}-Pro^{548} (Reggiani and Botinelli 2008, review).

The lever arm is the neck that connects the myosin head to the thick filament via the S2 domain. As mentioned earlier the neck is an α-helical structure that contains the IQ motifs on which the calmodulin-like myosin light chains bind. The N-terminal end of the lever arm is anchored into the converter domain that is firmly attached to the distal end of the relay helix. The relay helix is part of the lower 50K domain and is connected via switch 2 (Geeves and Holmes 2005).

c. Thin filaments

The proteins of the thin filaments that play an important role in muscle contraction are actin, the Tn complex and Tm. Fig 1.11 below shows schematically the organisation of these proteins within the thin filament.

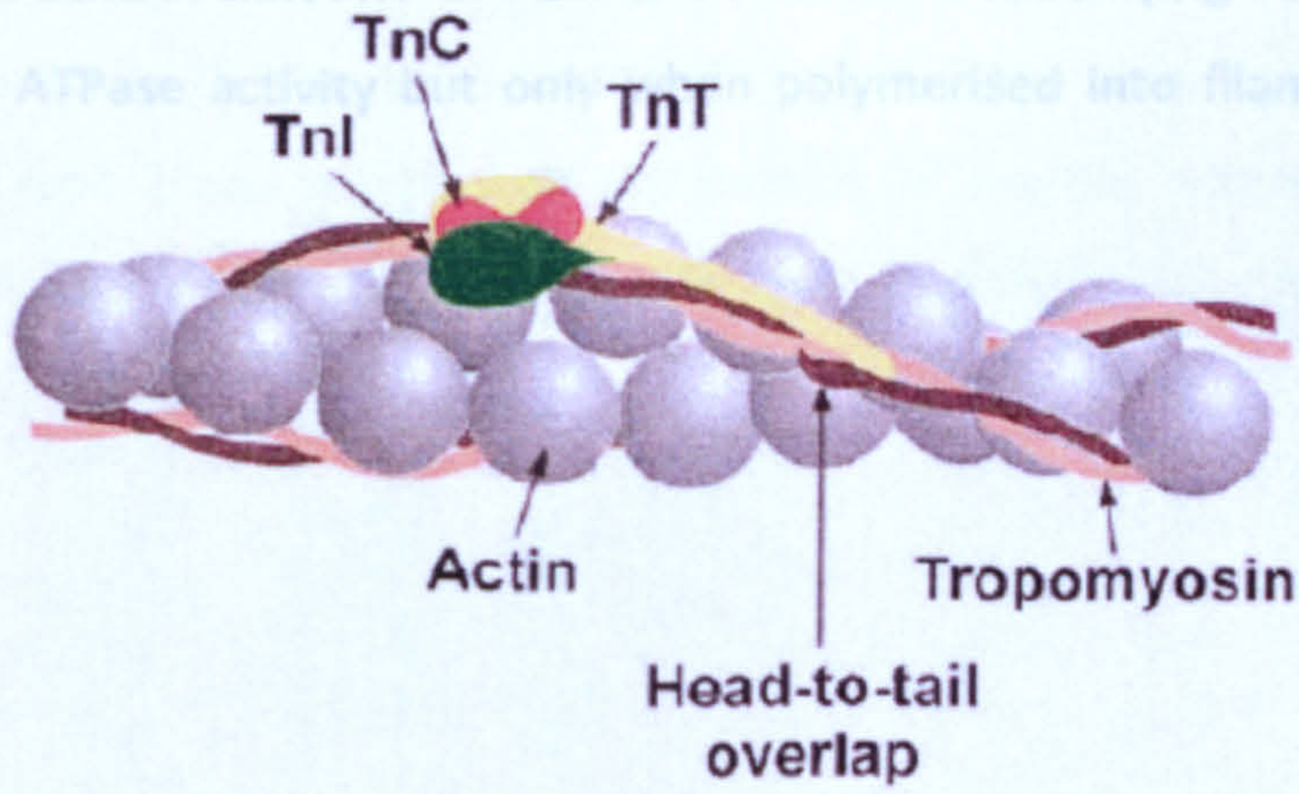

Fig 1.11: Proteins of the thin filament. The Tm coiled-coil and the Tn complex lie along the actin filament. Part of the TnT lies on the top of the head-to-tail overlap region (Gordon *et al.* 2000).

- Actin

The major component of the thin filaments is actin. Although actin is involved in a very wide spectrum of biological functions, only a few isoforms exist that are remarkably similar. In mammals there are only six actin genes and each encodes a single isoform. These are the α-skeletal, α-smooth, α-cardiac, β-cytoplasmic, γ-cytoplasmic and γ-enteric actin isoforms. The α-skeletal and α-cardiac isoforms that take part in the striated muscle contraction are both 377 residues long and only differ in 4 residues (Herman 1993; Nowak *et al.* 2009).

The actin monomer is 42 kDa and has a globular shape, thus is known as G-actin. The structure of G-actin was solved by X-ray crystallography in complex with DNase I in 1990 but since then various other crystal structures of actin have been reported (Kabsch *et al.* 1990; McLaughlin *et al.* 1993; Graceffa and Dominguez 2003; Klenchin *et al.* 2006; Rould *et al.* 2006). G-actin is composed of four subdomains, from which subdomains 1 and 3 are larger than subdomains 2 and 4 (fig 1.12). Subdomains 1 and 3 contain a central five-stranded β-sheet surrounded by short α-helices. The smaller subdomains 2 and 4 are primarily β-sheet with small amount of α-helix. Both the N- and C- termini of G-actin are in subdomain 1. At the centre of G-actin a cleft is formed that separates the molecule into two halves. One half contains subdomains 1 and 2 and is known as the outer domain of actin because it occupies the outside of actin filaments. The other half contains subdomains 3 and 4 and is known as the inner domain. In the central cleft ATP or ADP and a bivalent cation (Mg^{2+} or Ca^{2+}) can bind. Actin exhibits ATPase activity but only when polymerised into filamentous actin (F-actin).

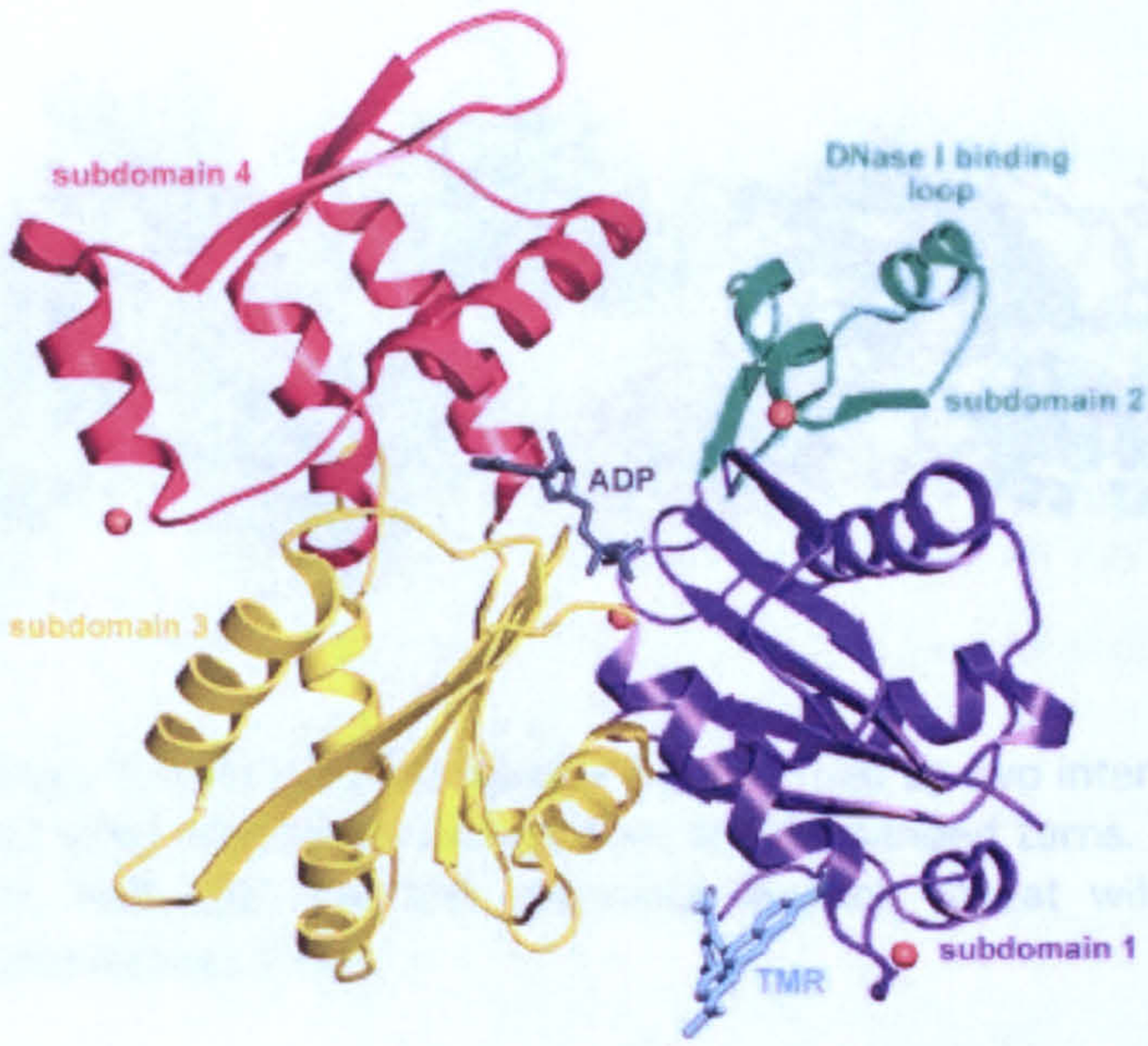

Fig 1.12: G-actin structure. G-actin has a globular shape and shows four subdomains. Subdomains 1 and 2 form the outer domain of actin and are separated by a central cleft from subdomains 3 and 4 that form the inner domain of actin. In the cleft one ATP or ADP molecule and one bivalent cation bind (Otterbein *et al.* 2001).

G-actin monomers polymerise to form F-actin. The F-actin structure is shown in figure 1.13. F-actin is composed of two chains of actin polymers that turn around each other forming a right-handed α-helix. The F-actin helix is a repeat of 13 actin monomers that are arranged in six left-handed turns and occupy 36 nm (2.75 nm per molecule). The first monomers in each repeat share identical orientations. Each monomer is positioned with the subdomains 3 and 4 facing the inside of F-actin, where they can interact with the subdomains 3 and 4 from neighbouring monomers. Subdomains 1 and 2 are oriented on the outside of F-actin, with the subdomain 1 being the primary binding site for a myosin head (Holmes *et al.* 1990; Lorenz *et al.* 1995; Oda *et al.* 2009).

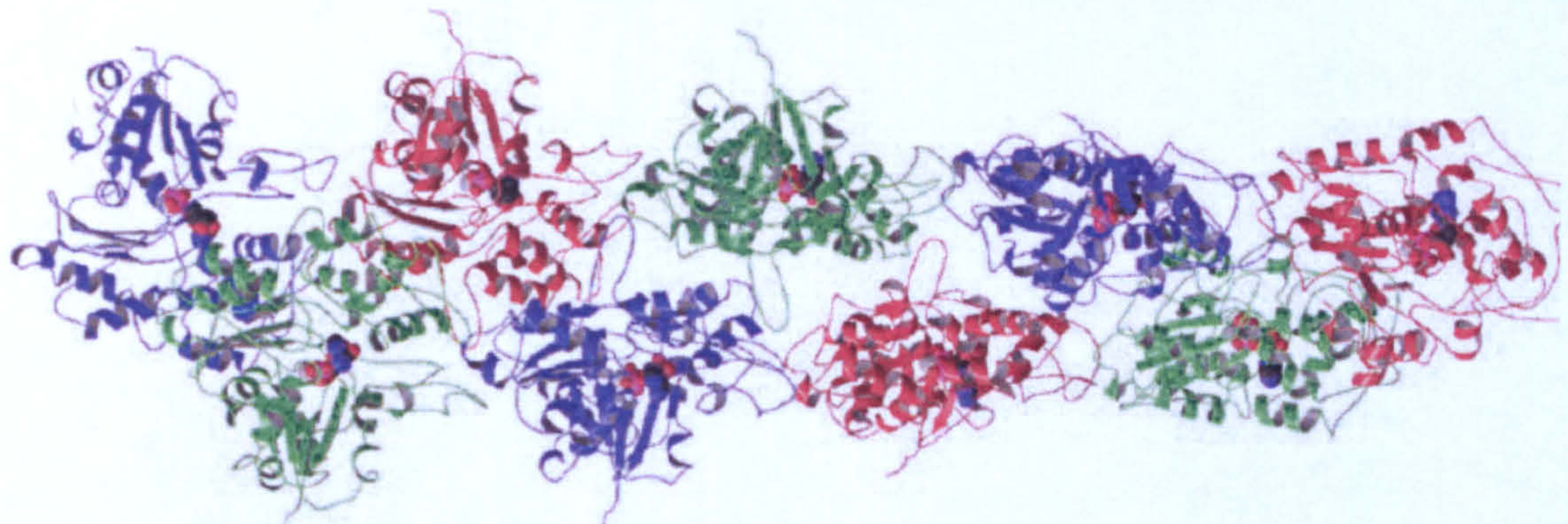

Fig 1.13: F-actin structure. F-actin is a right-handed helix formed by two intertwined chains. F-actin helix contains 13 actin monomers arranged on six left-handed turns. The F-actin helix repeats every 36 nm, such that the first monomer in each repeat will share identical orientations (Geeves and Holmes 1999).

High resolution X-ray diffraction data revealed that the outer domain of an actin monomer rotates 20° relative to the inner domain, when the monomer undergoes a G- to F-actin transition. The rotational axis is about at 90° to the filament axis. This rotation results in a flattened conformation of the F-actin monomers. Also the flexible DNase I loop found on subdomain 2 adopts an open-loop conformation in F-actin monomers (Oda *et al.* 2009). The new F-actin model proposed by Oda *et al.* explains from a structural point of view why the ATPase of actin is active only in F-actin and not in G-actin molecules. As shown in figure 1.14, the 20° rotation of the domains in F-actin changes the position of the residue Gln137 (which is known to be involved in ATP hydrolysis) and brings it in closer proximity with the γ-P of an ATP molecule sitting in the cleft.

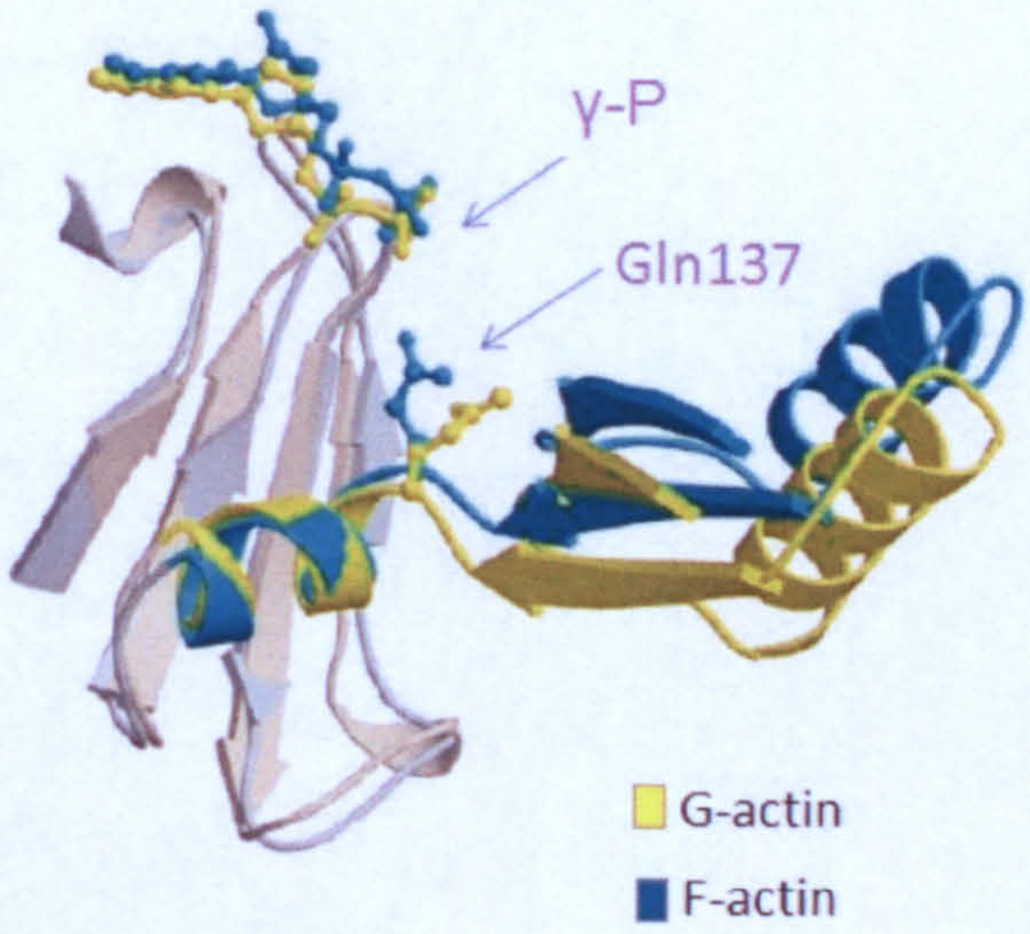

Fig 1.14
Rotation between inner and outer domains of monomeric actin during its transition into F-actin. The rotation causes a structural change in the ATPase site. G-actin in yellow is superimposed to F-actin in cyan. The residue Gln137 that takes part in ATP hydrolysis is moved in the vicinity of the γ-P only in the F-actin monomers (modified from figure 6 of supplementary data from Oda *et al.* 2009).

- Troponin complex

The Tn complex is composed of three proteins; TnC- the Ca^{2+} binding subunit, TnT- the Tm binding subunit and TnI- the inhibitory subunit. The three subunits function with high co-ordination to accomplish regulation of muscle contraction together with Tm. The Tn regulation is only found in striated muscle contraction and does not occur in smooth muscle systems. A crystal structure of the cardiac Tn complex solved by Takeda *et al* is shown in figure 1.15 below. The crystal structure of skeletal Tn complex has also been solved (Vinogradova *et al.* 2005)

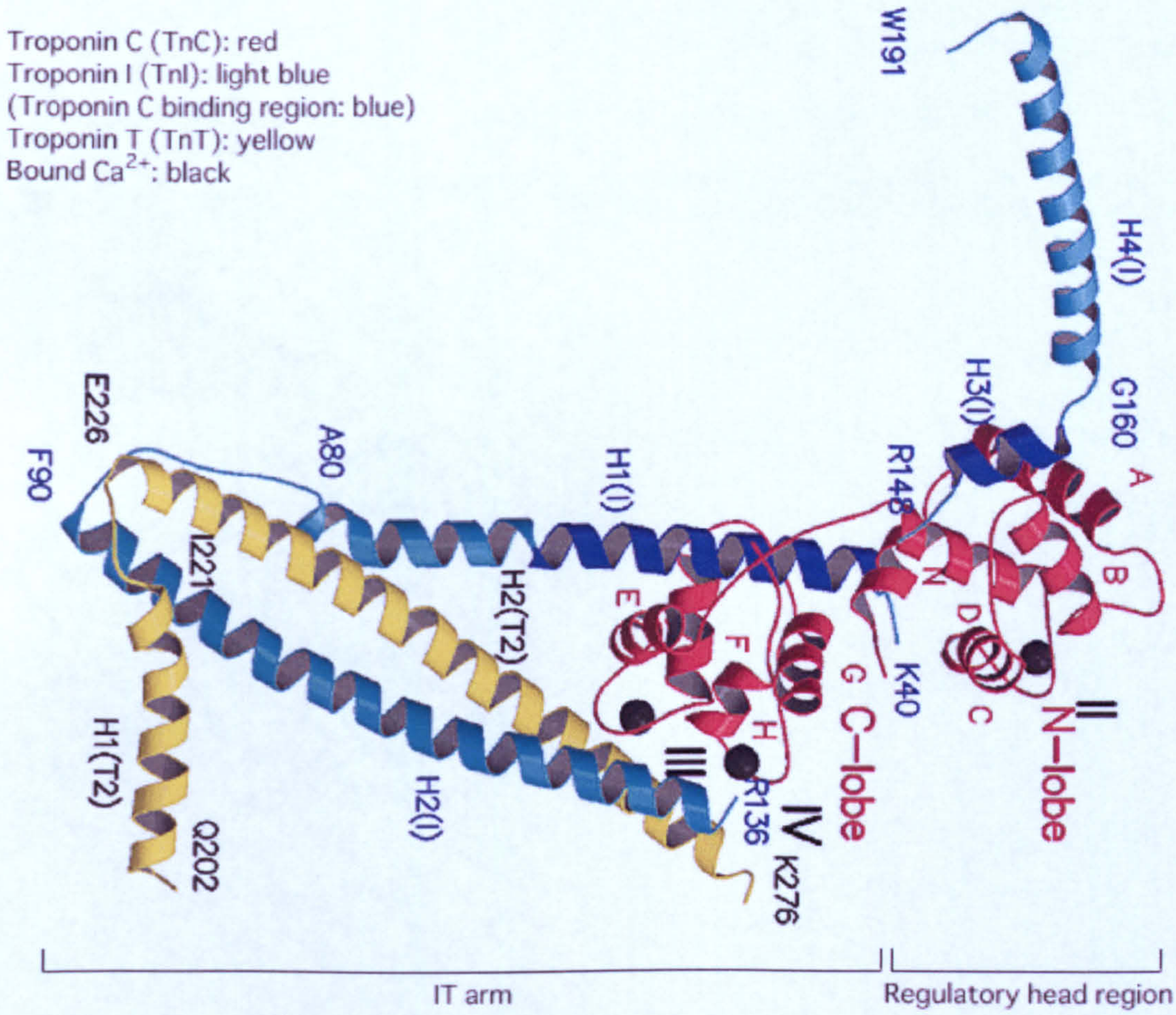

Fig 1.15: Crystal structure of the human cardiac Tn complex with Ca^{2+} bound in the TnC subunit. TnC is in red. TnT is in yellow. TnI is in cyan apart from the residues that interact with TnC that are shown in blue. Ca^{2+} is in black spheres (taken from http://www.riken.go.jp/engn/r-world/info/release/news/2003/sep/index.html); (Takeda *et al.* 2003).

TnC is an 18 kDa protein that acts as the Ca^{2+} receptor of the thin filaments. X-ray crystallography revealed that TnC (shown in red in fig 1.15) has a very similar structure to other members of the calmodulin superfamily. TnC has a dumbbell-like shape, with the N- and C-termini forming two globular domains that are connected by a long central α-helix (Herzberg and James 1985). Both N- and C- terminal domains contain EF hand motifs, where the cation binding loop connects two α-helices, forming a binding pocket for the cation. The skeletal TnC isoform has two EF hand motifs at the C-terminal lobe and another two at the N-terminal lobe. In contrast the cardiac TnC isoform has two EF hand motifs at the C- and only one EF hand motif at the N-terminal. At the C-terminal EF cation binding sites Ca^{2+} or Mg^{2+} can bind. These sites are known as structural sites because binding of either Ca^{2+} or Mg^{2+} enhances interactions of TnC with TnI, thus promoting structural stability of the Tn complex. The affinity is higher for Ca^{2+} than for Mg^{2+} (10^7 M^{-1} vs. 10^3 M^{-1} respectively), therefore after Ca^{2+} influx from the sarcoplasmic reticulum (10 μM Ca^{2+}) these sites are occupied by Ca^{2+} (Potter and Gergely 1975). Under relaxed conditions when the Ca^{2+} concentration is low, Mg^{2+} can outcompete Ca^{2+} for the C-terminal binding sites. The C-terminal sites are therefore occupied at all times by either Ca^{2+} or Mg^{2+} (Zot and Potter 1982). Moreover, when Mg^{2+} replaces Ca^{2+} at the C-terminal sites, it opposes Ca^{2+} binding to the N-terminal sites (Pearson *et al.* 2008). The N-terminal binding sites have higher specificity but lower affinity for Ca^{2+}. Therefore in these sites only Ca^{2+} can bind (and not Mg^{2+}) but with lower affinity than it does for the C-terminal sites (10^5 M^{-1}). Ca^{2+} binding at the two N-terminal sites of skeletal TnC occurs sequentially (Li *et al.* 1995) and is the trigger for muscle contraction.

In mammals there are three genes encoding TnT, known as the slow skeletal T1, the cardiac T2 and the fast skeletal T3 genes. All of TnT genes can be alternatively spliced and produce a very large number of isoforms. TnT isoform expression is tissue specific and developmentally regulated (Perry 1998). TnT has an asymmetric structure, with a globular C-terminal region and an extended α-helical N-terminal domain. The two domains can be separated by chymotryptic digestion into the N-terminal TnT1 (residues 1-158) and the C-terminal TnT2 (residues 159-258) fragments. TnT2 is more conserved whereas TnT1 is highly variable amongst different TnT isoforms. TnT is known as the Tm binding subunit and it has the important role of linking the Tn

complex to the rest of the thin filament via its connection to Tm. TnT also holds together the Tn complex itself by interacting with both TnC and TnI. The major interaction of TnT with Tm happens on the TnT1 domain. The N-terminal of TnT1 lies antiparallel along the C-terminal of Tm in the thin filaments and covers the end-to-end overlap region of adjacent Tms. The TnT2 domain also binds to Tm; TnT2 also binds TnC and TnI. Apart from its important structural role, TnT has modulatory roles in thin filament regulation. Because of its position at the Tm overlap region, TnT influences the communication between Tm molecules and enhances their binding affinity to actin filaments (Palm *et al.* 2001). Moreover, when TnT1 or TnT are added in actin/Tm filaments the cooperativity unit size is increased from 6 to 9 in the case of TnT1 and to 12 in the case of TnT (Schaertl *et al.* 1995). Also the actin/Tm/TnT1 filaments have a 10-fold reduction in K_T (the equilibrium constant from the closed to the open state, explained in section 1.3c) thus the closed state occupancy is preferred. For this reason the rate of S1 binding onto actin and of the actin activated S1 ATPase are reduced in comparison to Actin/Tm filament without TnT or TnT1 (Maytum *et al.* 2002).

TnI is expressed by three different genes, as in the case of TnT. However TnI genes are not alternatively spliced, thus encoding only three isoforms namely the slow skeletal, the fast skeletal and the cardiac (Wilkinson and Grand 1978; Koppe *et al.* 1989). The cardiac isoform is larger than the skeletal isoforms because it carries a ~30 residues N-terminal extension. TnI can be phosphorylated at multiple sites by PKA after adrenergic stimulation in heart. This phosphorylation event reduces the affinity of TnI for TnC and the affinity of TnC for Ca^{2+} and decreases the Ca^{2+} sensitivity of the system (Kranias and Solaro 1982). TnI is known as the inhibitory subunit of the Tn complex because it inhibits the S1 ATPase activity in the presence of Tm and Tn and absence of Ca^{2+}. The inhibitory activity of TnI is abolished when Ca^{2+} is bound on TnC. In the absence of Ca^{2+} TnI binds with its inhibitory peptide region (residues 137-148) on actin. In the presence of Ca^{2+} another peptide of TnI (residues 150-159) preferentially binds on TnC translocating the inhibitory peptide away from actin. The conditionally inhibition of TnI is supported by its structure, which allows particular domains within TnI to change conformation depending on Ca^{2+} availability. As was shown on figure 1.15 the TnI has a helical structure. Four helices can be observed in the crystal structure named H1-H4. The H1 helix (residues 43-79) binds with its N-terminal to the

C-lobe of TnC and with its C-terminal to the TnT. The H2 helix (residues 90-135) forms a parallel α-helical coiled-coil with TnT (known as the IT arm of the Tn complex). H3 helix (residues 150-159) can interact with the N-lobe of TnC. H4 helix (residues 164-188) is projecting out of the complex and does not show interactions with other Tn fragments. The crucial inhibitory peptide of TnI that can bind actin includes residues 137-148 and is located between helices 2 and 3.

The C-terminal of TnT and the N-terminal of helix H1 of TnI bind at the TnC C-lobe, holding together the Tn complex. In the absence of Ca^{2+}, the structural sites of TnC are occupied by Mg^{2+}. The inhibitory peptide of TnI binds with high affinity on actin. The helix H3 of TnI is not bound on TnC. Upon Ca^{2+} binding to the N-terminal sites of TnC, the EF hand motifs of the regulatory sites open, exposing hydrophobic domains within the N-lobe of TnC. The helix H3 of TnI binds to the exposed hydrophobic sites on TnC with high affinity. Because the TnI inhibitory peptide is proximal to helix H3 it moves along with H3 transition uncovering the actin surface. Amongst the various domains of the Tn complex, those exhibiting the highest conformational changes upon Ca^{2+} binding to TnC are the inhibitory peptide and the helices H3 and H4 of TnI (schematic representation in figure 1.16 below) (Takeda *et al.* 2003; Vinogradova *et al.* 2005; Sun *et al.* 2009).

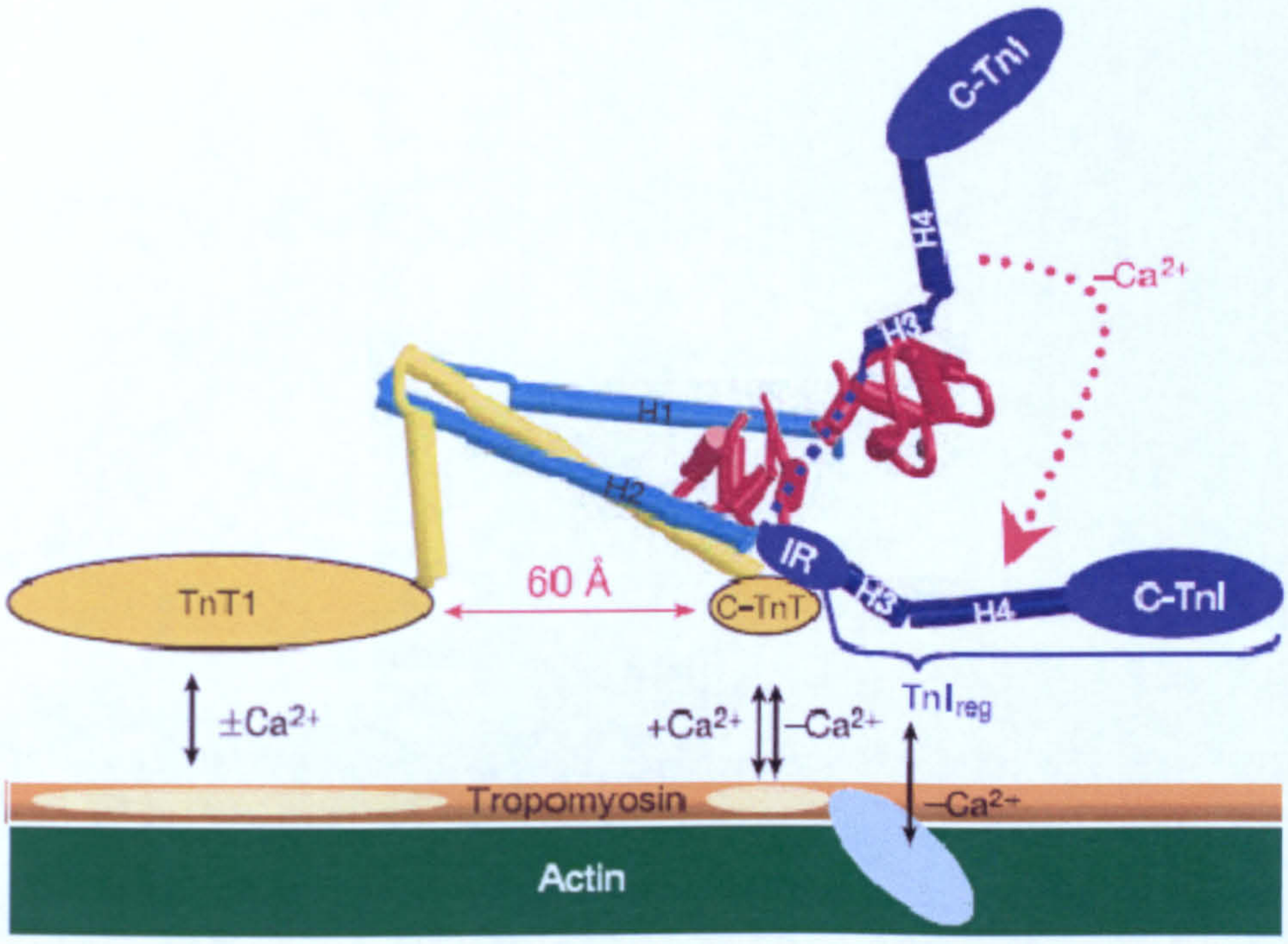

Fig 1.16: Schematic representation of Tn complex and interactions with actin and Tm in the presence and absence of Ca^{2+}. TnC is shown in red, TnT in yellow and TnI in blue. The part of TnI that undergoes major conformational changes upon binding of Ca^{2+} in the N-lobe of TnC is shown in dark blue. Actin and Tm is in green and brown respectively (Takeda *et al.* 2003).

- Tm

Tm appears as a very simplistic and uniform coiled-coil rod. However, within the Tm molecule key structural features exist which perturb the ordered structure of the coiled-coil. Subsequently a Tm dimer gains the correct structural conformation and shape complementarity to bind on actin filaments (Hitchcock-DeGregori 2008; Holmes and Lehman 2008; Lehman and Craig 2008). The features within the Tm molecule that destabilise the coiled-coil can be grouped into two categories; the alanine clusters and the broken core regions. Figure 1.17 below shows schematically the Ala clusters and the broken core regions along a Tm molecule.

Fig 1.17: Location of Ala clusters (pink) and broken core regions (green) along the Tm molecule. The residues in the core of the coiled-coil at positions *a* and *d* of the heptad repeat that participate in the above structural features are indicated in the boxes (Minakata *et al.* 2008).

The Ala clusters are regions where Ala or other unbranched residues are clustered at the core of the coiled-coil at positions *a* and *d* of the heptad repeat. The segment of the coiled-coil that is rich in core Ala appears axially out of register by ≈1Å and narrowed by ≈2 Å. The side chain of a core Ala is found to interact with three residues at most from the neighbouring chain. In contrast, when the coiled-coil has other hydrophobic residues with longer side chains at the core, for example Leu, it appears more canonical with the two chains in register (fig 1.18). The core Leu can contact four residues of the neighbouring chain. The sequencing of striated muscle Tm shows that there are seven Ala cluster regions along the Tm core, which are separated by intermediating Leu and other hydrophobic residues. At the position where an axially staggered segment of the coiled coil (due to Ala cluster effect) is continued by a canonical in-register segment, the coiled-coil bends noticeably by ≈6°. The bending occurs away from the locally longer helix (Brown *et al.* 2001; Brown *et al.* 2005). Bends along the coiled-coil promote a shape for Tm that is complementary to the surface of the actin intertwined helix, therefore the bends promote actin binding (Brown *et al.* 2001; Holmes and Lehman 2008). When core Ala residues were mutated into residues that would remove the bend from the coiled-coil (A74L-A78V-A81L), the actin binding affinity was reduced 10-fold, although the mutant appeared more stable in circular dichroism studies (Singh and Hitchcock-DeGregori 2003). It is also considered that bending areas within the Tm coiled-coil have some degree of flexibility (Minakata *et al.* 2008). Tm flexibility could possibly further assist Tm binding onto actin and is thought

to be important for the Tm movement over the actin surface (Singh and Hitchcock-DeGregori 2006; Minakata *et al.* 2008).

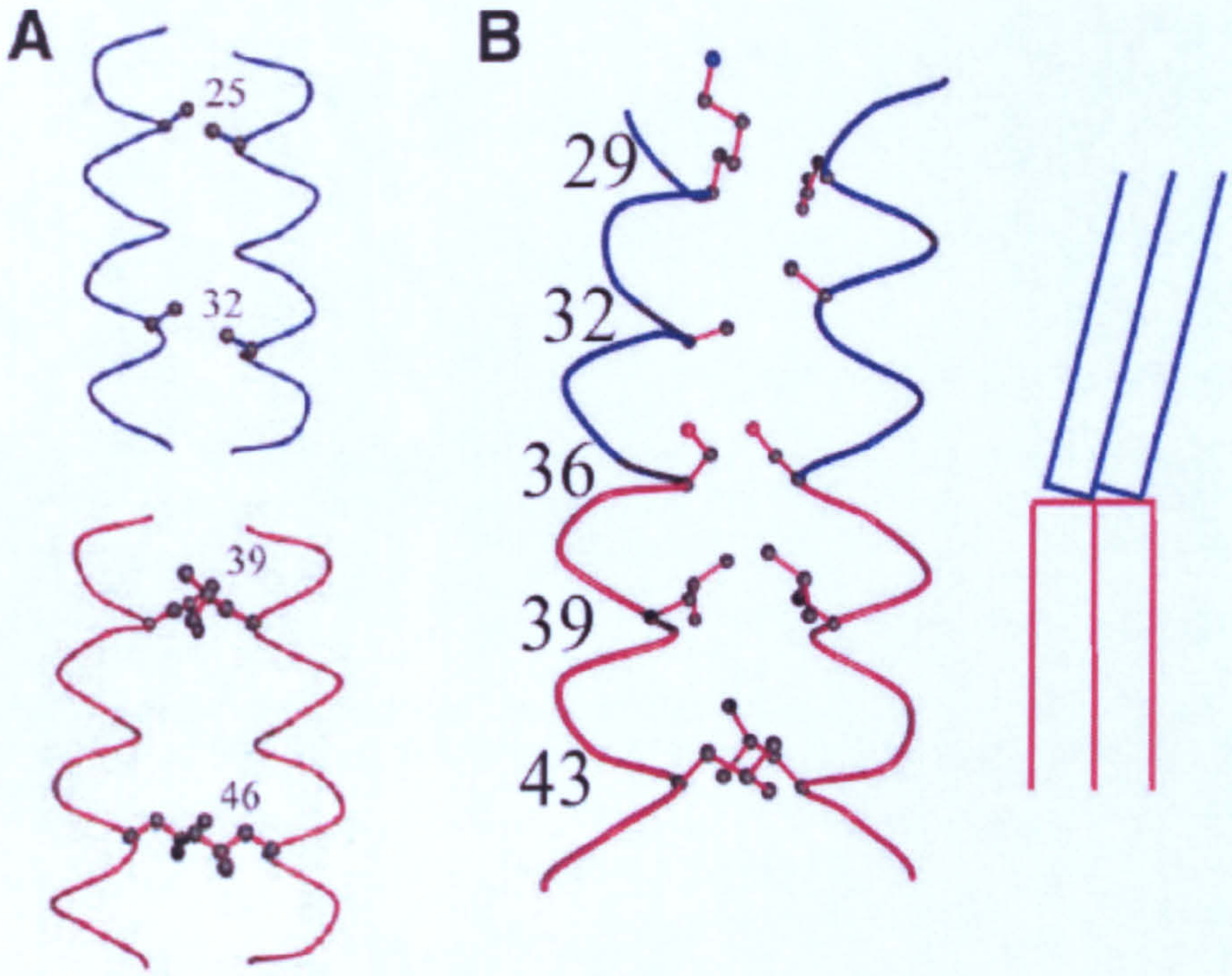

Fig 1.18: Bend formation on a Tm peptide due to Ala staggering. **A:** a Tm peptide rich in Ala core residues in blue and a Tm peptide rich in Leu residues in red are compared. The two chains in the Ala rich peptide appear axially out of register (staggered) and narrower than in the Leu rich peptide. **B:** At the point where an axially staggered region is followed by an in-register region, a bend in the coiled-coil axis is formed (taken from figures 2 and 3, Brown *et al.* 2001)

As shown in figure 1.17 three broken core regions exist along Tm. The broken core regions are formed when instead of the typical hydrophobic residues other residues are positioned in the core of the coiled coil. Thus two of the broken core regions are formed around the acidic core residues Asp137 and Glu218 and the third broken core is formed around the hydrophilic core residue Gln263. At the broken core regions the radius of the coiled-coil is increased, leaving a hole in the middle of the core. Crystals of a Tm peptide that included the residues Glu218 and Gln263 revealed the presence of water molecules in the holes of the broken core, suggesting that the residues around these broken core regions are exposed to the solvent. Also both broken core regions were bent and flexible (Minakata *et al.* 2008). On the other hand the broken core around Asp137, which is a highly conserved residue, is associated with increased instability in the middle of Tm; Asp137 appears to be the preferable site due to local

unfolding for tryptic digestion to occur. In the mutant Asp137Leu, digestion by trypsin is inhibited and the thermal stability of the molecule is increased by 5 °C. The mutant does not differ in the actin binding from the wild type. However it shows greater acto-S1 ATPase activity compared to the wild-type. This might suggest that the Leu mutant shows an increase in the cooperative unit size (n) of the thin filaments consistent with reduction in flexibility (Sumida *et al.* 2008).

From the Ala clusters and the broken core regions described above it is likely that those causing bends (which are probably associated with some degree of flexibility) along the Tm molecule are important in actin binding, simply because they provide shape complementarity and help Tm to wind around actin. However apart from the shape complementarity there is also sequence complementarity between Tm and actin (McLachlan and Stewart 1976; Phillips 1986). The 284 residues long Tm isoforms show seven periodic repeats, each being ≈40 residues long and provides a potential binding site for an actin subunit (Brown *et al.* 2001). The importance of each periodic repeat was evaluated in experiments where specific repeats were deleted or replaced by Leu zippers (Landis *et al.* 1999; Hitchcock-DeGregori *et al.* 2002; Siththanandan *et al.* 2009). With relation to actin binding, mutants with single periods deleted had variable effect; the worst actin binding affinity was observed for the Tm peptide lacking period 5 (Hitchcock-DeGregori 2008). However in other experiments where the actin binding site on period 5 was replaced by equivalent actin binding sites from period 1 or period 2, the mutant peptide could retain its actin binding thus suggesting that the actin binding sites amongst the seven periods of Tm are quasi-equivalent (Singh and Hitchcock-DeGregori 2007; Hitchcock-DeGregori 2008). The potential actin binding sites on the surface of the Tm coiled-coil are rich in charged residues (positions *b, c, f* of the heptad repeat) that can interact with charged residues on the actin surface (Lorenz *et al.* 1995). Different Tm isoforms can occupy slightly different positions on the surface of actin, with the cardiac and smooth isoforms shifted towards the inner part of the outer domain as opposed to the skeletal isoforms that were found on the outer edge of the inner domain under the same conditions (Lehman *et al.* 2000). Tm binding on actin however is not a strong interaction and should not be considered of a lock-and-key type, despite the complementarity between the two proteins. Instead Tm form only weak electrostatic interactions with the actin filament, and for this reason

Tm is found at a large radius of ≈40 Å away from the actin filament axis in the atomic model of the actin/Tm complex or the actin/Tm/Tn complex (Lorenz *et al.* 1995; Poole *et al.* 2006). The weak electrostatic interaction between actin and Tm meets Tm's requirements of moving freely and rapidly over the actin surface to regulate precisely the muscle contraction at low energy cost.

A model describing Tm binding onto actin filaments was recently suggested by Lehman and Holmes (fig 1.19), (Holmes and Lehman 2008). This Gestalt-binding model emphasises the importance of Tm to attain a 3-D form that is designed to be complementary to the actin filament surface. Both shape and sequence complementarity, as described previously, contribute in the correct conformation of Tm. Because of their complementary form, individual Tm dimers are able to associate with actin filaments although their binding affinity for actin is extremely low. The weak electrostatic interactions between actin and Tm hold individual Tm dimers on actin surface very weakly and this is the initial step of Tm filament formation on actin. When Tm dimers on actin surface reach a critical concentration, the subsequent Tm dimer to bind on actin will have to interact end-to-end with another Tm dimer pre-existing on actin surface. Thus polymerisation of Tm is initiated on actin surface. As a result Tm polymers of varying lengths are formed and populate actin filament, assuming that there are more than one initiation points for Tm polymerisation along the actin filament. It is expected that there will be places along the actin filament where a short Tm polymer will be separated by a long Tm polymer by gaps of less than 7 free actins that are not big enough to accommodate one more Tm and fill the space between the two Tm polymers. At these places a sorting process is likely to exist that will favour longer Tm polymers over the shorter ones and eventually Tm will be zipped along the length of actin filament, leading to a fully decorated actin.

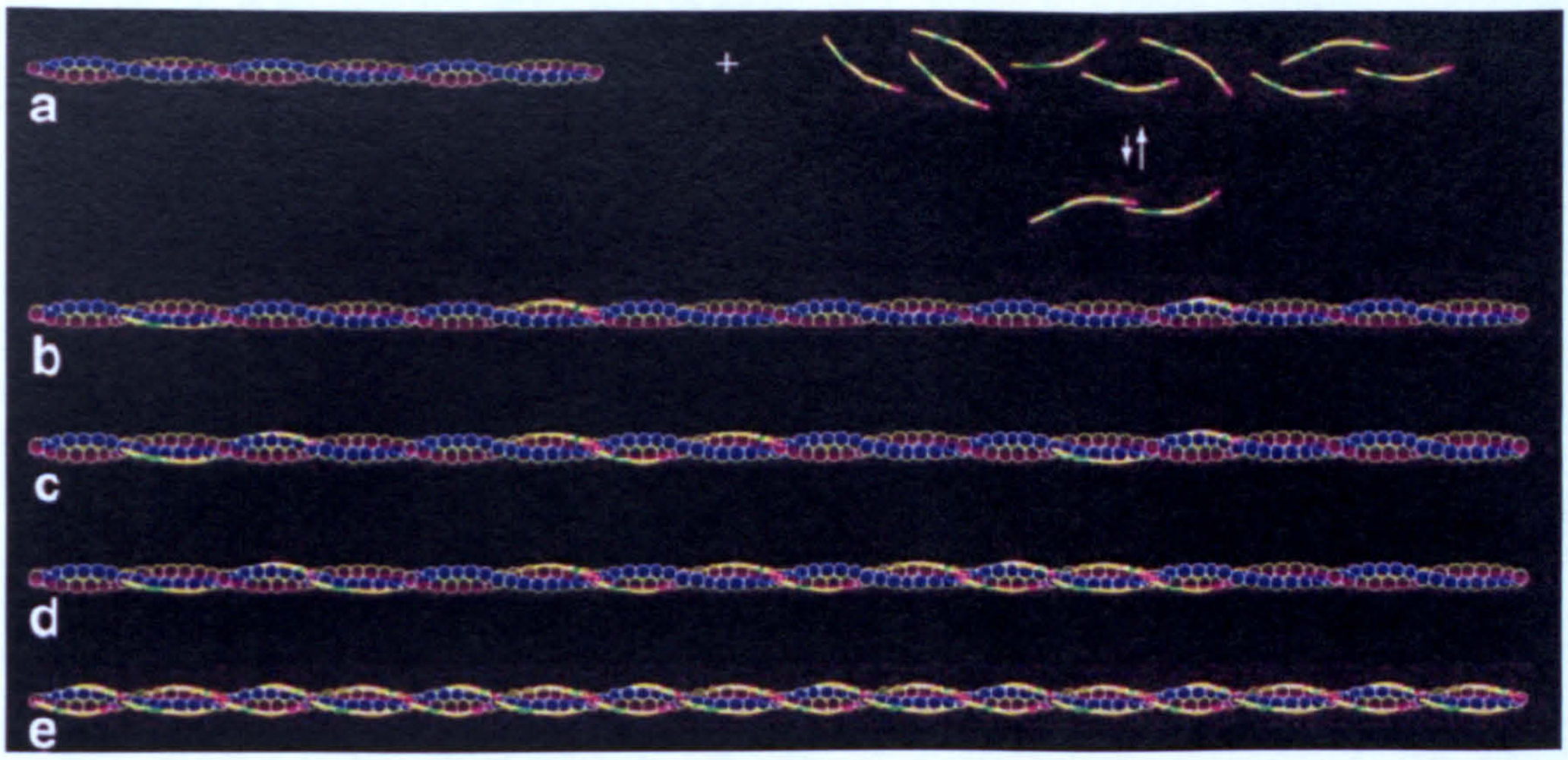

Fig 1.19: Gestalt binding and polymerisation of Tm on actin filaments. a) Initial mixture of actin filaments and Tm molecules. b) Weak binding of complementary Tm molecules on the actin surface. c) Initiation of Tm polymerisation on actin filaments. d) Sorting process between long and short Tm polymers. e) Fully decorated actin filament with Tm (Holmes and Lehman 2008).

In fully decorated filaments, individual Tm molecules behave as part of the larger Tm filament system, where adjacent Tm molecules communicate and act co-operatively as one unit. The Tm's affinity for actin in this case is very strong in comparison to the affinity of the individual Tm molecules. However the Tm filament is only held on actin's surface with the same very weak electrostatic interactions as do the single Tm molecules. It is still a controversy whether or not the regions of Tm that show some degree of flexibility may promote binding to actin. In the Gestalt binding model for example, Tm flexibility is considered to be irrelevant for actin binding. Other groups believe that Tm is flexible around the bend areas and that this flexibility may well contribute in binding to actin (Singh and Hitchcock-DeGregori 2006; Minakata *et al.* 2008). Despite this argument, the Tm filament as an entity should be fairly rigid in order to provide stability for actin filaments. Actin filaments upon binding Tm become more stable and stronger and are less likely to break (Wegner 1982; Hitchcock-DeGregori *et al.* 1988; Cooper 2002). It is likely that if Tm was a very flexible coiled-coil, then perhaps it would have failed to provide the required stability for actin. In contrast, some degree of flexibility would be very valuable for the movement of the Tm filament over the surface of actin. A very rigid Tm rod perhaps would not be able to cope with the strain produced during Tm filament movement, especially at the joints between adjacent Tms.

In order for Tm to be a continuous and cooperative filament, polymerisation of adjacent Tm molecules (described in section 1.3) must be successful. If the end-to-end interaction between neighbouring Tms is somehow disturbed, a decreased binding affinity or even a total loss of binding to actin can be observed. Two factors enhance the end-to-end interactions in Tms; the N-terminal acetylation of Tm and the interaction of the Tm overlap region with TnT1 (Hitchcock-DeGregori and Heald 1987; Monteiro *et al.* 1994; Schaertl *et al.* 1995). Native Tm is acetylated and can bind actin. Bacterially expressed Tm does not undergo post-translational modifications and therefore cannot be acetylated; hence bacterially expressed Tm cannot bind actin. As shown in fig 1.20 below the structural difference at the N-terminal between acetylated and unacetylated Tm peptides is remarkable. The splayed ends of the unacetylated Tm are likely prohibited from insertion into the C-terminal cleft of the preceding Tm molecule and with lack of Tm polymerisation strong actin binding is abolished. It has been reported that having an Ala-Ser extension at the N-terminal of recombinantly expressed Tm can mimic the N-terminal structure of acetylated native Tm and restore actin binding (Monteiro *et al.* 1994; Boussouf *et al.* 2007). On the other hand as already mentioned on the TnT section (pg 25), TnT1 strengthens the end-to-end interactions between Tm and creates a more cooperative filament.

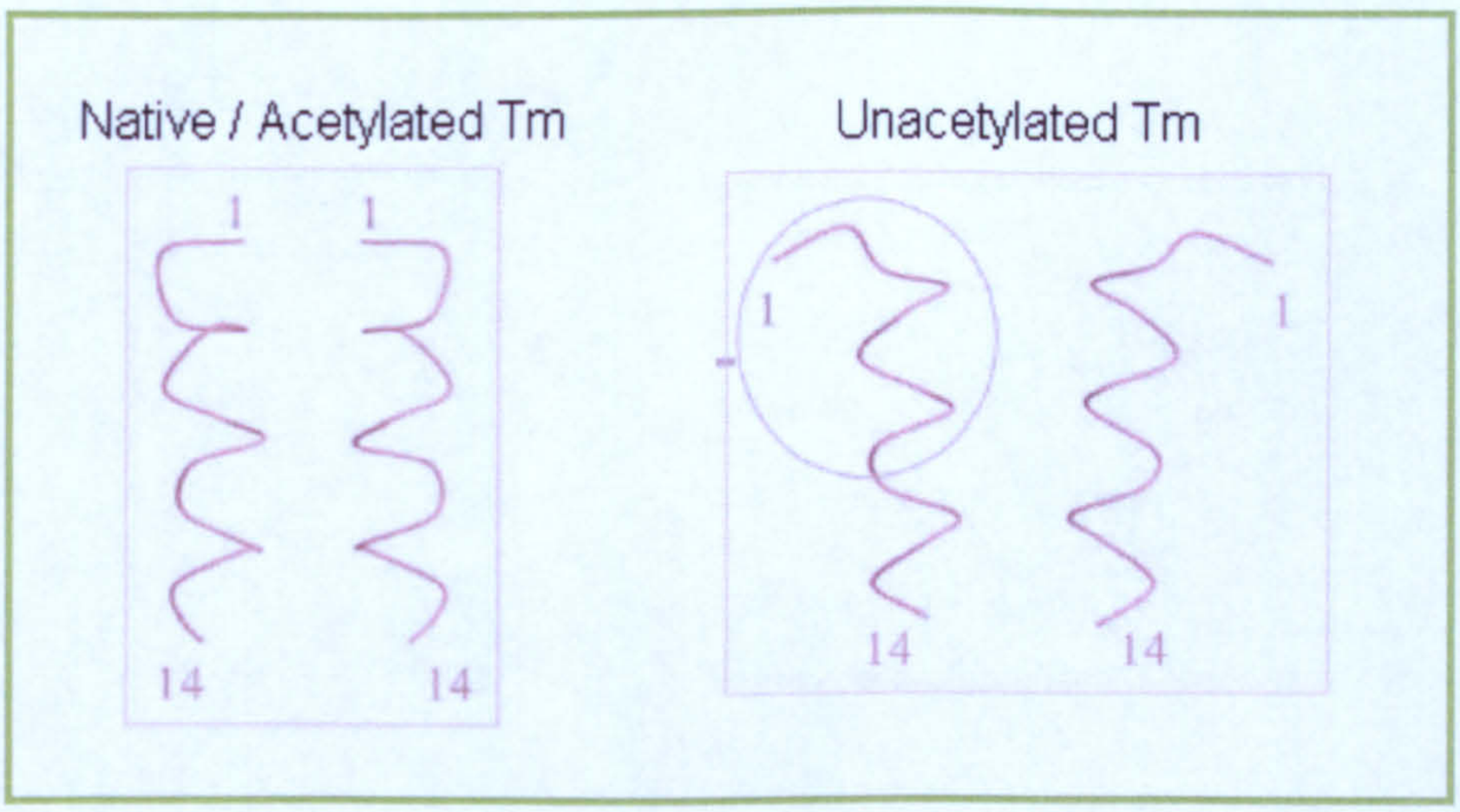

Fig 1.20: N-terminal structural differences between acetylated and unacetylated Tm peptides. Loss of actin binding of unacetylated Tm must be due to the splayed N-terminal ends that fail to overlap with the C-terminal ends of adjacent Tm molecules (Brown *et al.* 2001).

Apart from the interactions of Tm with actin and TnT in the thin filaments, it is also found to interact with Tropomodulin (Tmod). Tmod is used to cap actin filaments at their pointed ends, thus regulating the actin filament dynamics and assisting them to retain a constant length (Weber *et al.* 1994; Gregorio *et al.* 1995). For optimal function, Tmod requires binding to Tm. Two Tm molecules can bind at the N-terminal of Tmod and their binding is necessary for Tmod capping activity. In contrast, the C-terminal of Tmod does not have Tm binding sites and can cap actin by itself (Kostyukova 2008). It can be concluded that Tm stabilises actin filaments both directly by its binding onto actin and indirectly by enhancing Tmod capping activity.

d. Other proteins of the sarcomere

Apart from myosin other proteins are also found in the thick filaments of the sarcomere. These are the myosin binding proteins C and H (MyBP-C, MyBP-H) and the enzyme adenosine monophosphate deaminase. MyBP-C consists of 10-11 domains with fibronectin (Fn3) and immunoglobulin (Igl) homology. MyBP-C binds to the thick filament and promotes their structural organisation. In the case of cardiac and fast skeletal MyBP-C isoforms, three molecules of MyBP-C bind via their C-terminal around thick filaments forming a trimeric collar structure (Flashman *et al.* 2008). MyBP-C binds also the titin elastic filament via its C-terminal and actin on thin filaments via its N-terminal. Binding on actin is reduced upon phosphorylation of MyBP-C by PKA (Shaffer *et al.* 2009). Also upon phosphorylation, MyBP-C is dissociated from the S2 region of myosin, leaving myosin in a more favourable conformation for actin binding (Weisberg and Winegrad 1996). Adenosine monophosphate deaminase (AMPD) is involved in the regulation of adenosine metabolism. In muscles it is particularly important when ATP hydrolysis outpaces ATP supply during vigorous muscle contraction. Under these conditions ADP accumulation must be prevented in order to maintain the energy for further ATP hydrolysis. ADP removal is achieved by the coupled action of adenylate kinase (AK) and AMPD. First ADP is converted into AMP via AK and AMP is then irreversibly broken down by AMPD (Hancock *et al.* 2006). AMPD interacts with both myosin heavy chain and titin. There are also numerous proteins located at the M-line of the thick filament, which is a line found vertically in the middle of the sarcomere

(shown in fig 1.9). Proteins of the M-line include myomesin, M-protein, MURF-1, the cystein protease p94 (a muscle specific Calpain 3) and a muscle isoenzyme of creatine kinase (MM-CK) (Clark *et al.* 2002, review).

Numerous other proteins also exist in a sarcomere. Titin is a giant protein that can be up to 4.2 MDa depending on the isoform and expands from the Z-disk to the M-line in a sarcomere. At the Z-disks two titins from adjacent sarcomeres overlap with their N-termini. At the M-line the two titins of a sarcomere interact with their C-terminal ends. Thus titin forms a continuous filament system in myofibrils. The N-terminal part of titin found at the Z-disks is critical for maintaining sarcomeric structure. The part that spans the I-band shows elasticity and is considered as a spring that regulates myofibril stiffness. The part that spans the A-band is thought to have a structural role and contributes to the assembly of the thick filaments. Finally the C-terminal end of titin found at the M-line has a kinase domain which when activated can phosphorylate myosin (Trinick 1996; Fukuda *et al.* 2008; Tskhovrebova and Trinick 2008). Another large protein of the sarcomere is nebulin that can be up to 900 kDa. Nebulin extends from the Z-disks to the pointed end of the actin filaments, where it interacts with the capping Tmod. Nebulin is considered to be the ruler that specifies the thin filament length and appears early in myofibrillogenesis before actin filaments gain their complete length and organisation (Clark *et al.* 2002; McElhinny *et al.* 2003). Numerous other proteins are found in the sarcomere like α-actinin that is found in the Z-disks together with many α-actinin associated proteins (for example Muscle Lim Protein, the ALP-enigma family, the FATZ family). Other proteins of the Z-disks include obscurin, filamin, telethonin and MURF-3. There are also numerous intermediate filament proteins that organise the nuclei and the mitochondria in the muscle cytoskeleton; these include desmin, vimentin, nestin, synemin, paranemin, desmulin, syncoilin and lamins A B1 and B2. Microtubules are also found between myofibrils and it is thought that they play a role in myofibrillogenesis. Other proteins are used to link the sarcomere to the sarcolemma - the cell membrane of the muscle fibre. These include integrins, spectrin and the dystroglycan complex (composed by dystrophin, sarcoglycans, dystrobrevin, syntrophins). All of the above proteins are reviewed in Clark *et al* (2002).

Even non-muscle Tm isoforms (Tm5NM1 and Tm5NM-34kd) are found in the sarcomere. These are located along the Z-disc and provide the link between the sarcomere with the integrins and the dystroglycan complexes (fig 1.21). Tm5NM1 is associated with γ-actin and is highly populated in the inter-myofibril space and also around the mitochondria. Tm5NM-34kd is also thought to be associated with an actin isoform (not known which one) and is found also around the myofibrils. Tm5NM1 knock-out mice showed impaired T-tubule function, indicating that it may be required for normal excitation-contraction coupling in muscles. Another cytoskeletal Tm, the Tm4, was found associated with the sarcoplasmic reticulum. Tm4 was shown to be upregulated during muscle regeneration (Kee *et al.* 2004; Vlahovich *et al.* 2008; Vlahovich *et al.* 2009).

The large number of proteins associated with the sarcomere indicates that the sarcomere is an extremely complex structure. The recent view of the sarcomere is far more complex than the original view of a simple thick and thin filament structural arrangement.

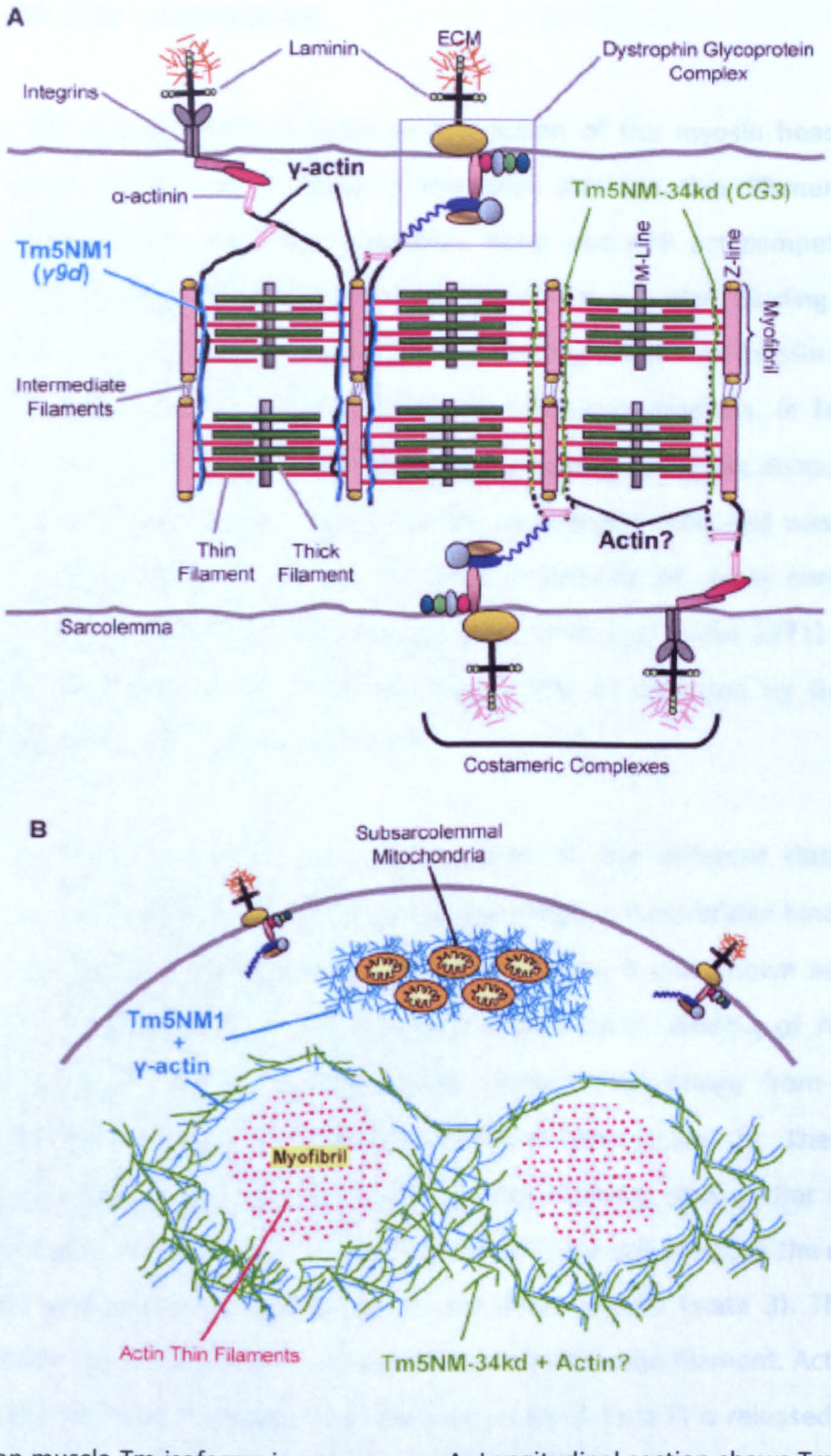

Fig 1.21: Non muscle Tm isoforms in sarcomeres. A: Longitudinal section shows Tm5NM1 and Tm5NM-34kd perpendicular to the filament axis along-side the Z-disks. B: Transverse section shows both isoforms to populate the space between myofibrils. The Tm5NM1 isoform associated with γ-actin is also found around the mitochondria of the sarcoplasm (Kee *et al.* 2004).

1.4.2 Muscle contraction

Muscle contraction occurs through an interaction of the myosin head with the actin filaments resulting in a sliding of the thick and the thin filaments of the sarcomere using energy from ATP hydrolysis. Actin and ATP act competitively for binding onto their specific binding sites in the myosin cross bridge. Binding of ATP on myosin rapidly dissociates myosin from actin and binding of actin on myosin stimulates the myosin ATPase cycle by displacing the ATP hydrolysis products. In fact muscle contraction can be described by a cycle of events occurring during the dissociation and association of actomyosin. This is known as the cross-bridge cycle and was proposed by Lymn and Taylor back in 1971 and still stands at present, of course enriched with newly discovered structural and biochemical data (Lymn and Taylor 1971) . In figure 1.22 the recent perspective of the cross-bridge cycle as proposed by Geeves and Holmes is shown (Geeves and Holmes 2005).

In the cross-bridge cycle myosin can be found in four different states. In the absence of bound nucleotide in the myosin pocket, myosin cross-bridge binds strongly on actin filaments. This tightly actin-bound conformation is also known as the rigor state and is depicted as state 1 in the cross-bridge cycle. Binding of ATP in the nucleotide pocket of myosin dissociates the myosin cross-bridge from the actin filaments. Myosin enters the post-rigor conformation (state 2). Then myosin undergoes a conformational change, known as the recovery stroke, that is coupled with ATP cleavage. The hydrolysis products ADP and Pi are still bound in the nucleotide pocket. This conformation is known as the pre-power stroke (state 3). The myosin enters then the top-of-power-stroke (state 4) and rebinds actin filament. Actin binding stimulates the ADP and Pi release from the myosin head. First Pi is released, then the power-stroke follows that will move the actin filament by ≈10 nm and lastly ADP is released. After these events, the myosin cross-bridge is back in the rigor conformation and ready to repeat the cycle.

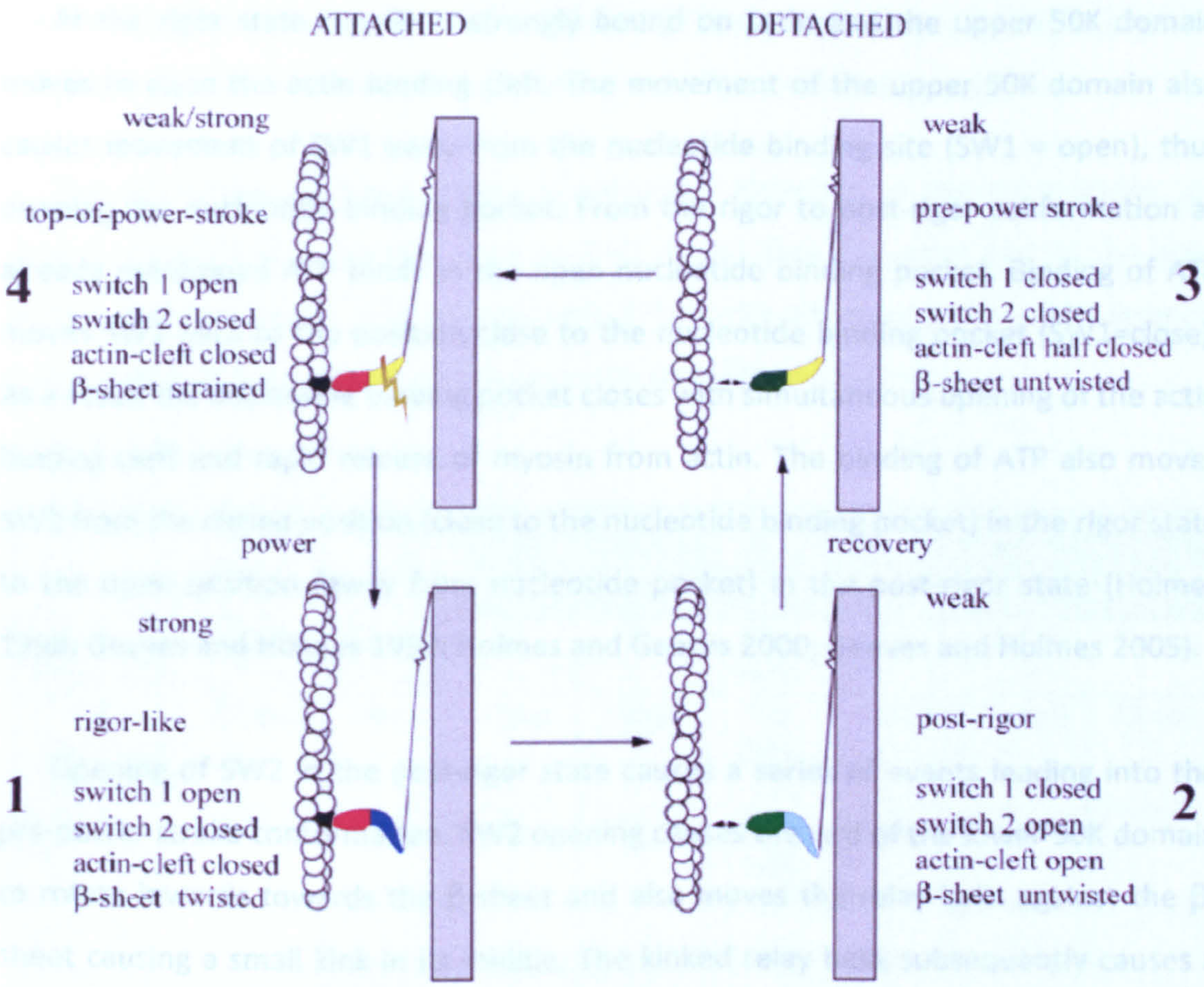

Fig 1.22: The cross-bridge cycle. At the rigor state (state 1) myosin binds strongly to actin filaments. ATP binding to myosin dissociates myosin from actin and myosin gains the post-rigor conformation (state2). Then the cross-bridge undergoes further conformational changes and enters the pre-power stroke (state 3) where the myosin ATPase is active and hydrolyses ATP. Then the cross-bridge re-binds to actin (top-of-power-stroke conformation, state 4) and subsequently the hydrolysis products are released and the power stroke executed (Geeves and Holmes 2005).

In order for a myosin cross-bridge to adopt the different conformations seen in the cross-bridge cycle, it is required that its structural attributes will have to undergo strictly orchestrated movements. The individual structural attributes of a myosin head are strongly linked; hence a conformational change in one of them will have an impact on the next like a domino-type effect. The elements that contribute in adopting the required myosin conformation are the actin binding cleft, switch 1 (SW1), switch 2 (SW2), P-loop, β-sheet, relay helix, converter domain and lever arm (these were described in the myosin section pg 18-19).

At the rigor state myosin is strongly bound on actin and the upper 50K domain moves to close the actin binding cleft. The movement of the upper 50K domain also causes movement of SW1 away from the nucleotide binding site (SW1 = open), thus opening the nucleotide binding pocket. From the rigor to post-rigor conformation as already mentioned ATP binds in the open nucleotide binding pocket. Binding of ATP moves SW1 back to the position close to the nucleotide binding pocket (SW1=close). As a result the nucleotide binding pocket closes with simultaneous opening of the actin binding cleft and rapid release of myosin from actin. The binding of ATP also moves SW2 from the closed position (close to the nucleotide binding pocket) in the rigor state to the open position (away from nucleotide pocket) in the post-rigor state (Holmes 1998; Geeves and Holmes 1999; Holmes and Geeves 2000; Geeves and Holmes 2005).

Opening of SW2 in the post-rigor state causes a series of events leading into the pre-power stroke conformation. SW2 opening causes the rest of the lower 50K domain to rotate inwards towards the β-sheet and also moves the relay helix against the β-sheet causing a small kink in its middle. The kinked relay helix subsequently causes a 60° rotation of the converter domain and the lever arm. The SW2 moves back in the closed position. Since both SW1 and SW2 are in the closed position the nucleotide is completely enclosed in the nucleotide binding pocket and ATP cleavage is initiated. The bound nucleotide holds the P-loop in the "down" position and restrains the β-sheet in the un-twisted conformation. The movement of SW2 into the closed position also causes a conformational change that closes the inner part of the actin binding cleft (Holmes 1998; Geeves and Holmes 1999; Holmes and Geeves 2000; Geeves and Holmes 2005).

At this pre-power stroke state myosin can bind actin entering the top-of-power-stroke conformation. Actin binding causes the β-sheet to twist. The twisted β-sheet rotates the converter domain. Rotation of the converter domain releases the pressure and removes the kink from the relay helix. P-loop moves in the "up" position and SW1 opens. Following this, the Pi is released, myosin binds strongly to actin and drives the power stroke and by reaching the rigor-state the ADP is also released (Geeves and Holmes 2005). There are still questions concerning the sequencing of the events during

the conversion from the pre-power stroke state to the rigor state and this is because there is no crystal structure of myosin in the top-of-power-stroke conformation.

The movement of some individual structural elements of the cross-bridge are strongly coupled. For example an open SW1 means that the outer part of the actin binding cleft is closed or P-loop facing up is linked with a twisted β-sheet. The strongly linked elements are shown with the same colour in figure 1.23 below.

State	SW1	Outer cleft	Inner cleft	SW2	β-sheet	P-loop	Relay helix	Conv-erter-lever
1 Rigor A.M	Open	Closed	C_1	C_1	Max twist	Up	straight	Down
2 Post-rigor M#ATP	Closed	Open	Open	Open	No-twist	Down	straight	Down
3 Pre power-Stroke M*ATP/ M*ADP.P_i	Closed	Open	C_2	C_2	No-twist	Down	kinked	Up
4 Strongly attached top M*ADP.P_i	*open*	*closed*	C_2	C_2	*No-twist*	*Down*	*kinked*	*Up*

Fig 1.23: Moveable structural elements of the cross-bridge. The moveable structural elements cause the cross-bridge to adopt specific conformations during the cross-bridge cycle. The elements include SW1 and SW2 the inner and outer parts of the actin binding cleft, the β-sheet, P-loop, relay helix and the converter domain. The suggested position of each structural element during the four states of the cycle is indicated. Elements depicted in the same colour have strongly linked movements (Geeves and Holmes 2005).

The structural changes occurring across the cross-bridge cycle can also be decrypted with kinetic data. Transient kinetic techniques like stopped-flow, flash photolysis, pressure jump and temperature jump can all give information on individual steps during actomyosin dissociation by ATP or during the association of actin with myosin. The tools used for kinetic studies are the light scattering (relates to the size of the actomyosin complex), the fluorescence on actin by covalent addition of extrinsic pyrene fluorophore and the intrinsic fluorescence of myosin at W501 of the relay helix.

The ATP induced dissociation of the actomyosin complex is a three-step process (scheme 1). Binding of ATP into the actomyosin complex is the first fast step. The second step is an isomerisation event during which there is a perturbation in the pyrene signal. The final step is the rapid dissociation of Myosin-ATP from actin. During dissociation of myosin from actin there is no perturbation on the W501 signal indicating that changes in the relay helix occurring at a later stage after the post-rigor state.

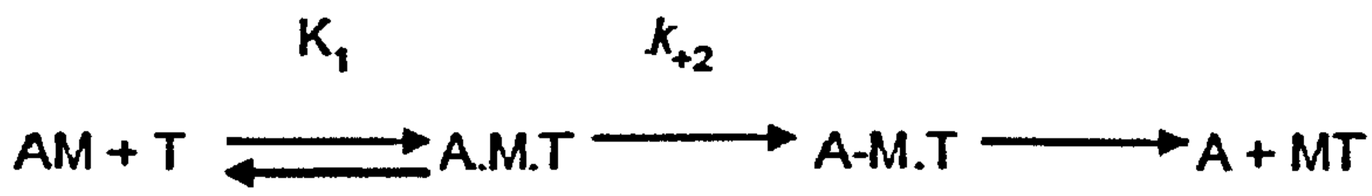

Scheme 1: Actomyosin dissociation by ATP (Nyitrai *et al.* 2006)

Three distinct steps are identified by kinetics that describe the binding of myosin to actin and the transition from the pre-power stroke conformation to the power stroke (scheme 2). In the first step myosin with the hydrolysis products ADP and Pi bound, interacts very weakly with actin via the lower 50K domain (state 1). In the second step myosin binds strongly to actin and the actin binding cleft closes (step 2). This is accompanied by major isomerisation changes since perturbations in pyrene-actin, the nucleotide (mant-ADP) and W501 occur at the same time. The strong actin binding after cleft closure is coupled with weaker nucleotide binding in the myosin pocket (state 3) and finally leads to Pi release (step 4).

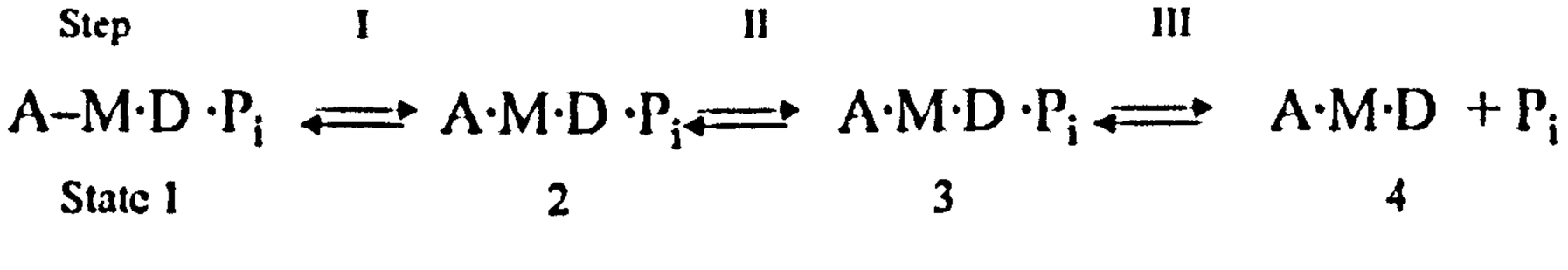

Scheme 2: Formation of the actomyosin complex (Geeves and Holmes 2005)

1.4.3 Ca^{2+}–dependent thin filament regulation of muscle contraction

The interaction of actin and myosin is finely regulated. Depending on the system there are different means of regulation. The actomyosin interaction in a striated muscle for example is regulated by Tm, Tn and Ca^{2+} and is known as the thin filament regulation (Ebashi 1963; Ebashi and Kodama 1965; Szent-Gyorgyi 1975). In other systems like the smooth muscle that lacks Tn, regulation is achieved by Ca^{2+} dependent phosphorylation of the myosin light chains as well as Ca^{2+} dependent release of caldesmon inhibition of actomyosin interaction (details in section 1.5) (Webb 2003, review).

The availability of Ca^{2+} in the thin filaments is a crucial element in thin filament regulation of muscle contraction. In the absence of Ca^{2+} from TnC the regulatory proteins inhibit myosin binding on actin, while in the presence of Ca^{2+} interaction of myosin with actin is permitted. A muscle cell spends a very large amount of energy to ensure that Ca^{2+} will be present in the thin filaments only when it is required. It is important to have Ca^{2+} available for muscle contraction but it is of equal importance to remove Ca^{2+} from the system to allow muscle relaxation. It was estimated that 70 % of energy in muscle cells is consumed during the cross-bridge cycle and the rest 30 % is spent to regulate the Ca^{2+} circulation in and out of the cell (Rall 1985). Figure 1.24 shows the pathways involved in Ca^{2+} circulation in a muscle cell. Ca^{2+} ions constantly flow in the T-tubules of the sarcoplasmic membrane. When an action potential arrives, the numerous Ca^{2+}-channels on the T-tubules open and allow Ca^{2+} to enter the cell. In cardiac fibres the influx of Ca^{2+} stimulates further Ca^{2+} release from the sarcoplasmic reticulum (SR) and muscle contraction is initiated. In contrast, in skeletal fibres the release of Ca^{2+} from the SR is not stimulated by the influx of Ca^{2+} from the T-tubules. Instead the Ca^{2+} channels on SR are coupled to plasma membrane voltage sensors and stimulate Ca^{2+} release from the SR after membrane depolarisation upon arrival of the action potential (Rios and Pizarro 1991; Lamb 2000). At the end of muscle contraction Ca^{2+} is removed from the sarcoplasm by Ca^{2+}-ATPases found on the SR thus returning the Ca^{2+} ions back into the SR. It is also removed by Ca^{2+}-ATPases and Na/Ca^{2+} antiporters found on the sarcoplasmic membrane thus returning the Ca^{2+} ions against

their concentration gradient back in the T-tubules. Finally Ca^{2+} can be removed from the sarcoplasm by entering the mitochondria through Ca^{2+} uniporters on the mitochondrial membrane (Bers 2002).

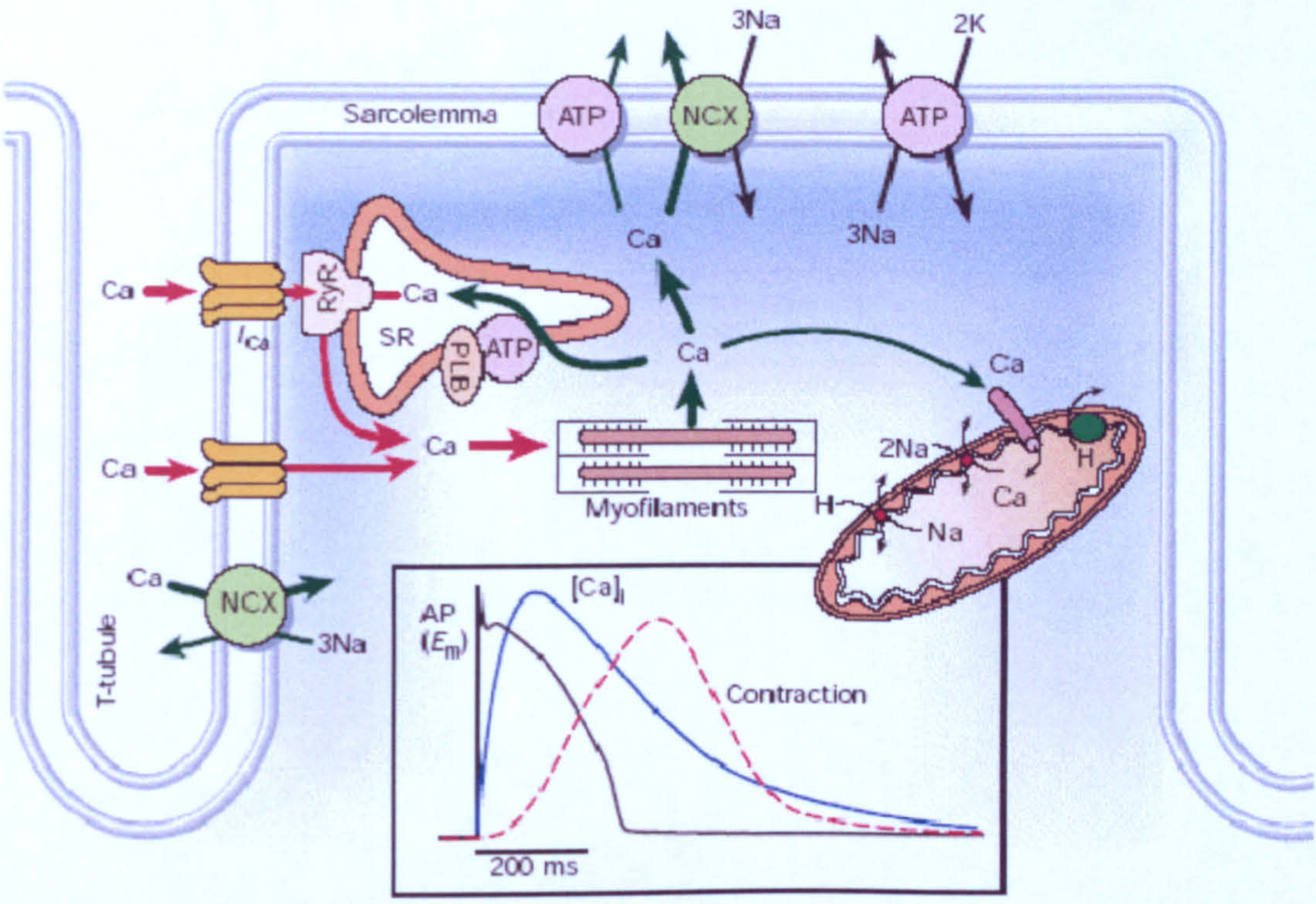

Fig 1.24: Ca^{2+} circulation in and out of the cardiac sarcoplasm. Upon action potential stimulation, Ca^{2+} enters the cell through opening of the Ca^{2+}-channels on T-tubules and stimulates further release of Ca^{2+} from the sarcoplasmic reticulum (red arrows). To remove Ca^{2+} away from the thin filaments Ca^{2+}-ATPases, Ca^{2+}/Na antiporters and Ca^{2+} uniporters are used (green arrows). The panel shows the time course of the action potential, of the intracellular Ca^{2+} concentration and of the muscle contraction (Bers 2002).

In the earlier years muscle contraction was thought to be regulated by a steric blocking mechanism of the thin filaments. This model proposed that thin filaments were blocked by the regulatory proteins Tm and Tn in the absence of Ca^{2+}, thus myosin could not bind. Addition of Ca^{2+} alone was sufficient to remove the block and allow actomyosin association. In this model the thin filament was considered as a series of repeating structural units, with each unit composed by seven actins one Tm and one Tn (A_7·Tm·Tn). Later Hill et al proposed a model, according to which the thin filaments could be found in either the Off or the On states (i.e. weakly and strongly bound myosin respectively). Based on this two state model of regulation, thin filaments were predominantly found in the Off state independently on the presence of Ca^{2+} ; binding

of myosin was required to turn the filament in the On state (Hill *et al.* 1980). However based on the two state model by Hill, experimental results from kinetic measurements using the stopped-flow and results from equilibrium binding of myosin on actin measured by myosin titrations were not in agreement. The kinetic results showed that 30 % of the thin filaments were in the On state in the absence of Ca^{2+} and increased up to 95 % upon addition of Ca^{2+}. On the other hand, the equilibrium titration results showed that 5 % of the filaments were in the On state and increased only up to 20 % upon Ca^{2+} addition. The enigma was solved by introducing a third state in the model.

The three state model of thin filament regulation was introduced by McKillop and Geeves (McKillop and Geeves 1993). According to the three-state model the filament exists in a dynamic equilibrium between three different states; the Blocked (B state), the Closed (C state/ Ca^{2+} induced) and the Open (M state / Myosin induced) states (fig 1.25). In the blocked state myosin cannot bind actin since Tm is sterically blocking the actin binding sites. In the closed state myosin can only weakly bind to the actin filaments because Tm moves away from the blocking position, partially exposing the actin binding sites. In the open state myosin can bind to actin and isomerise into the strongly bound rigor form (R state). Transition from the blocked to the closed state is characterised by the K_B equilibrium and is dependent on the Ca^{2+} presence and on the thin filament proteins. Transition from the closed to the open state is characterised by equilibrium K_T and is less dependent on Ca^{2+}; transition to the open state is promoted by the weak binding of S1 into the closed state of actin that traps Tm at the inner domain of actin filaments, thus fully exposing the actin binding sites. The K_1 and K_2 equilibrium define the transition to the weakly myosin bound state and to the strongly myosin bound state respectively. The ATPase activity is On, (or to be more precise the Pi from ATP hydrolysis is released) only in the open state during isomerisation of myosin into the rigor conformation.

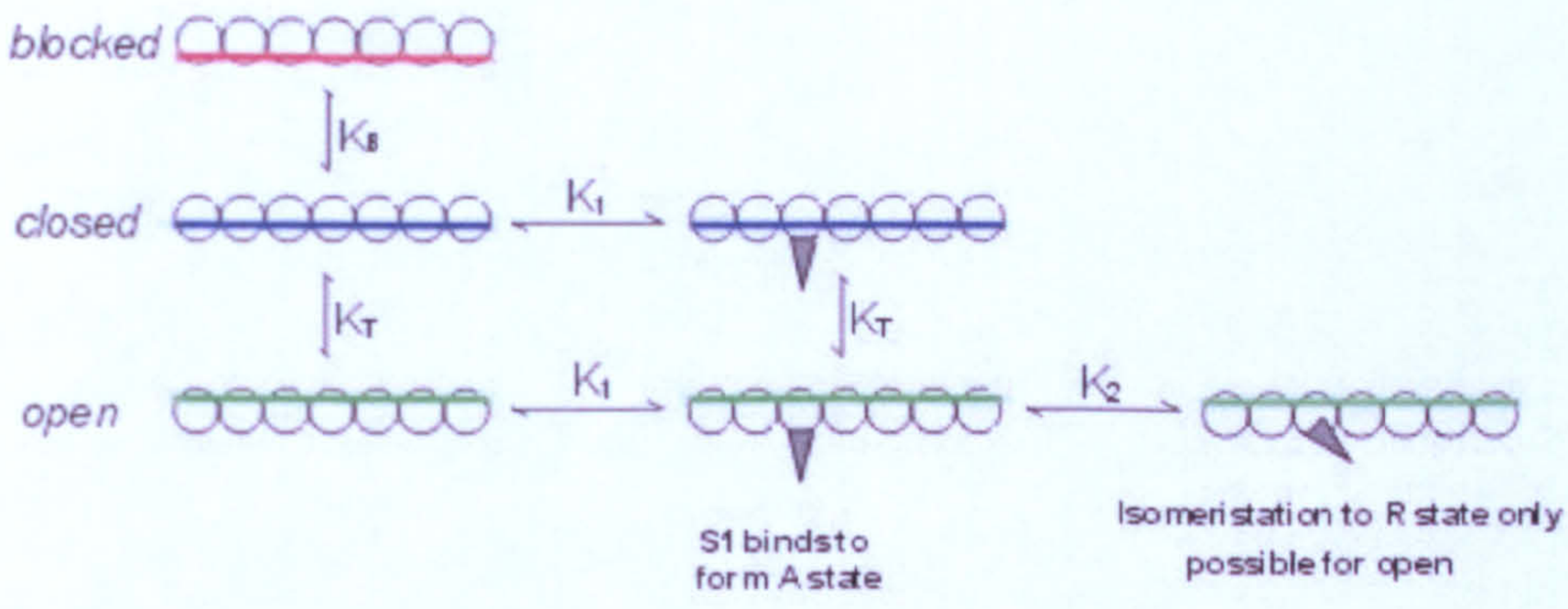

Fig 1.25: Three-state model of thin filament regulation. The thin filaments exist in a dynamic equilibrium between the blocked, the closed and the open states. Myosin can only bind weakly in the closed state, promoting transition of the filament into the open state. Strong actin binding occurs only in the open state (from http://www.kent.ac.uk/bio/geeves/research.html).

Based on the three-state model of regulation, thin filaments containing Actin/Tm or thin filaments of Actin/Tm/Tn in the presence of Ca^{2+} was found to be distributed between the closed state by 80 % and the open state by 20 %. The filaments of Actin/Tm/Tn in the absence of Ca^{2+} were found to be 75 % in the blocked , 25 % in the closed and less than 5 % in the open states. Therefore the results of the above kinetic measurements are in agreement with the titration equilibrium data (i.e. 5 % and 20 % of filaments in the On state in the absence and presence of Ca^{2+} respectively), (McKillop and Geeves 1993).

The three-state model of thin filament regulation was supported by structural data. Electron microscopy reconstructions of filaments in relaxed ($-Ca^{2+}$), activated ($+Ca^{2+}$) and rigor conditions showed that in each case Tm occupied different positions on the actin filament (Craig and Lehman 2001). More recent models were produced by the Holmes group where they have fitted a model of Tm and a model of actin (or the model of actin with myosin for the open state) in the electron microscopy 3D reconstruction of thin filaments (Holmes *et al.* 2003; Pirani *et al.* 2005). Their work is shown in figures 1.26 and 1.27. It is clear that Tm can occupy the blocking position and inhibit sterically the binding of myosin on actin (blocked state). Tm moves 25° away from its blocking position on addition of Ca^{2+} and permits weak binding of myosin (closed state). In the open state, Tm is found 35° away from the initial blocking position and myosin heads can interact freely and strongly with the exposed actin binding sites (Poole *et al.* 2006).

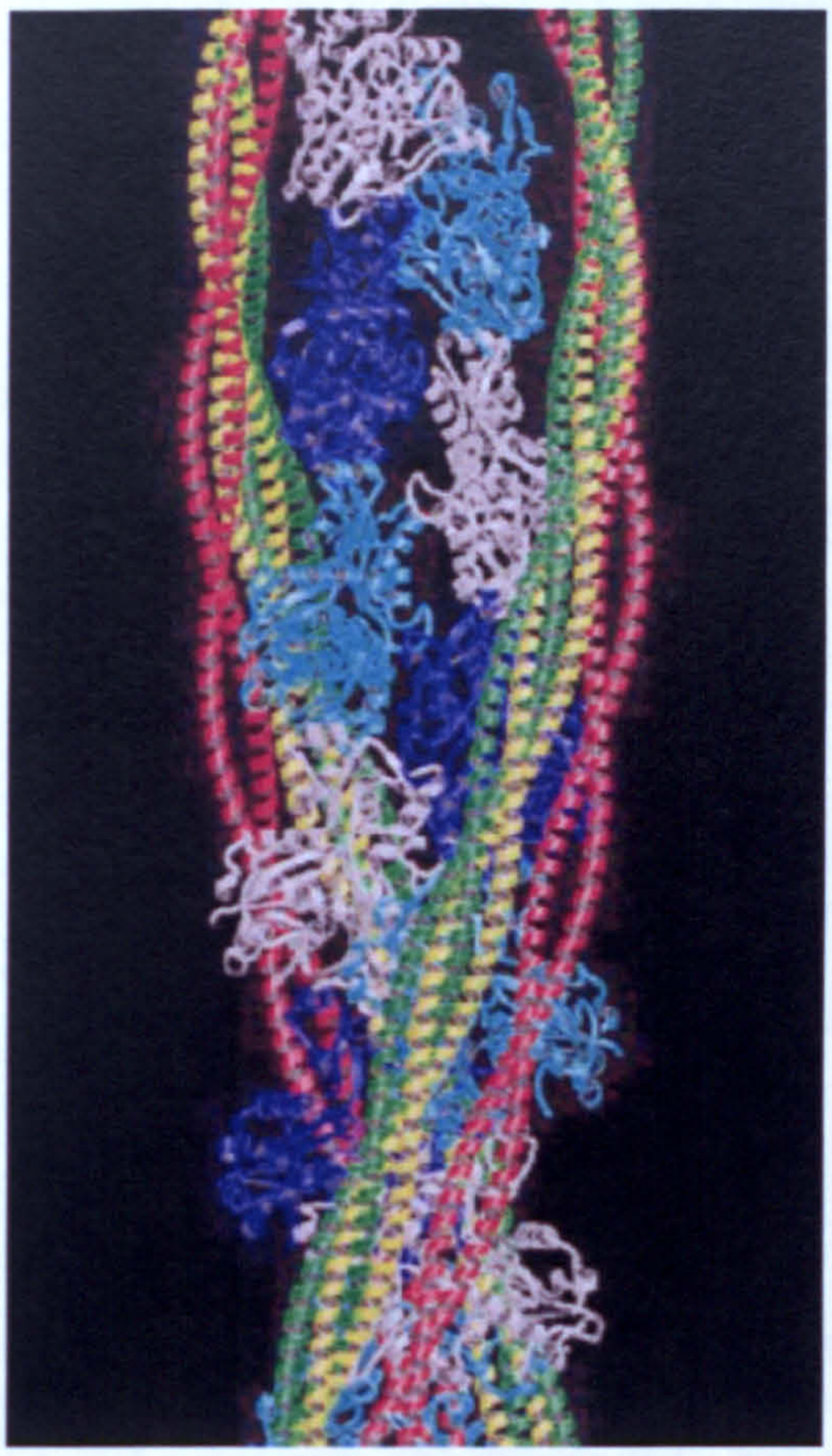

Fig 1.26:
Tm can occupy three different positions on actin filament. In the blocked state (red) Tm fully inhibits myosin binding on actin. In the closed state (yellow) Tm moves 25° away from its blocking position and permits weakly binding of myosin on actin. In the open state (green) Tm moves 10° further, fully exposing the actin binding sites and allowing strong myosin binding on actin (Poole *et al.* 2006).

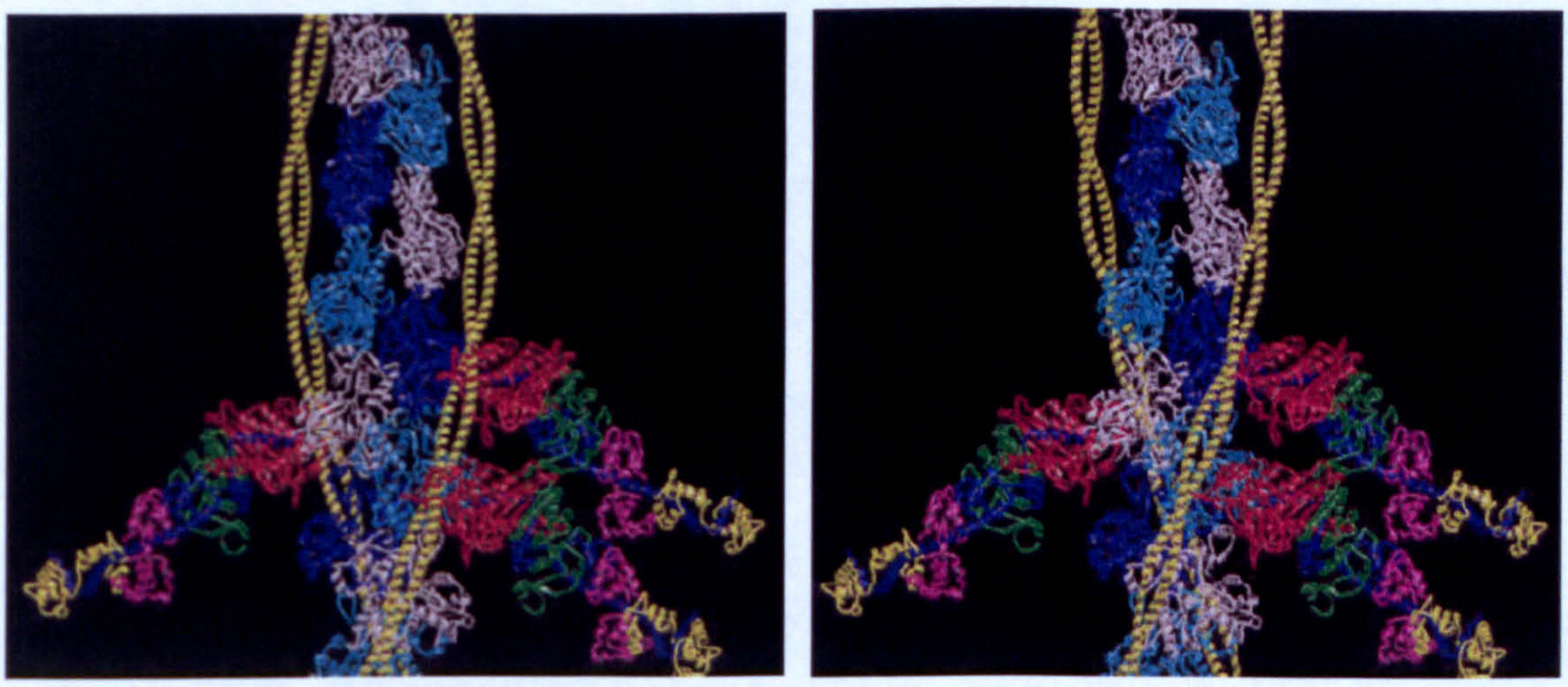

Fig 1.27: The thin filament model of actin/Tm together with myosin in the rigor conformation. In left panel Tm is in the blocked state thus directly preventing myosin cross bridges to interact with actin. In right panel Tm is in the closed state and myosin cross-bridges can interact weakly with the partially exposed binding sites on actin (Poole *et al.* 2006).

According to the McKillop and Geeves model myosin can only bind to actin filaments found in two states i.e. the closed and the open states. The thin filament transition from the closed to the open state occurs cooperatively after myosin binding. This can be observed by association or dissociation experiments of myosin from filaments of Actin/Tm or Actin/Tm/Tn that show typical sigmoidal curves consistent with cooperativity (Geeves and Lehrer 1994). When one S1 initially binds to a single actin in the thin filament, the filament turns itself on such that more S1 will bind cooperatively. Cooperative binding of myosin on the thin filaments occurs only when Tm is present. Thus the cooperativity phenomenon is considered as a Tm filament property. Initial weak S1 binding on actin will occur only if at this time Tm is found away from the blocking position. The occupancy of the outer domain of actin by S1 will subsequently restrict the dynamic movement of Tm over the closed and open state positions at the inner domain of actin. The myosin binding on an actin subunit only locally prevents Tm to move back towards its blocking position. But this local restriction of movement in a segment of Tm is transmitted to adjacent periods within the Tm molecule itself and subsequently further to the adjoining Tm molecules. As a result the restricted movement of Tm away from the blocking position will leave the myosin binding sites on actin monomers within the vicinity of this particular cooperative unit partially uncovered permitting more myosin molecules to bind (Geeves and Lehrer 2002).

The cooperative unit size in the thin filament is defined by the number of actin monomers in this unit that will be turned on after binding of a single myosin to permit cooperative binding of subsequent myosins. For example, a cooperative unit of 11 would mean that a single myosin binding on an actin monomer within this unit would turn on another 5 actin monomers to the left and 5 monomers to the right of the myosin-bound actin monomer. The cooperative unit must not be confused with the structural unit. As already mentioned a structural unit is composed by 7 actins, 1 Tm and 1 Tn. The cooperative unit size of filaments containing Actin and Tm is found to be 5-6 i.e. is smaller than the structural unit. On the other hand the cooperative unit size of filaments containing Actin, Tm and Tn in the presence of Ca^{2+} is found to be 10-12 i.e. larger than the structural unit but it is decreased in the absence of Ca^{2+} (6-8). Therefore the cooperative unit size depends on both Tn and Ca^{2+} (Geeves and Lehrer

1994; Maytum *et al.* 1999; Maytum *et al.* 2001; Maytum *et al.* 2002). Furthermore the cooperative unit size is likely to be influenced by the Tm coiled-coil flexibility and by the degree of communication between adjacent Tm molecules along the continuous Tm filament. A stiffer Tm filament and stronger end-to-end interaction between Tms will result in a greater cooperative unit (Geeves and Lehrer 2002).

Interestingly when Tm decorates actin filaments without the Tn present it is found mostly in the closed state (80 %) and does not occupy the blocked state. Tm is found on the blocked state only in the presence of Tn and in absence of Ca^{2+}. Structural evidence for this observation arose recently by fitting actin and Tm models on electron microscopy reconstructions of filaments containing actin, Tm and the C-terminal of TnI (Galinska-Rakoczy *et al.* 2008). The C-terminal TnI was found to span two actin monomers across the F-actin double helix, more specifically it extended from subdomain 1 of one actin to subdomain 4 of the second actin, crossing the cleft between them (fig 1.28). At subdomain 4, the C-terminal TnI had a fist-like structure located against the Tm coil. The last bit of C-terminal TnI was found to drape over Tm. Parts of the actin surface that were covered by the TnI peptide contained several amino acids which are thought to interact electrostatically with Tm in the closed state. It can be concluded that the TnI peptide in the absence of Ca^{2+} competes with Tm for this common binding site on the actin surface and constrains Tm away into the blocking position. After Ca^{2+} binding on TnC, the TnI peptide will be subsequently removed from the actin site and Tm will be able to return to its preferable closed state position.

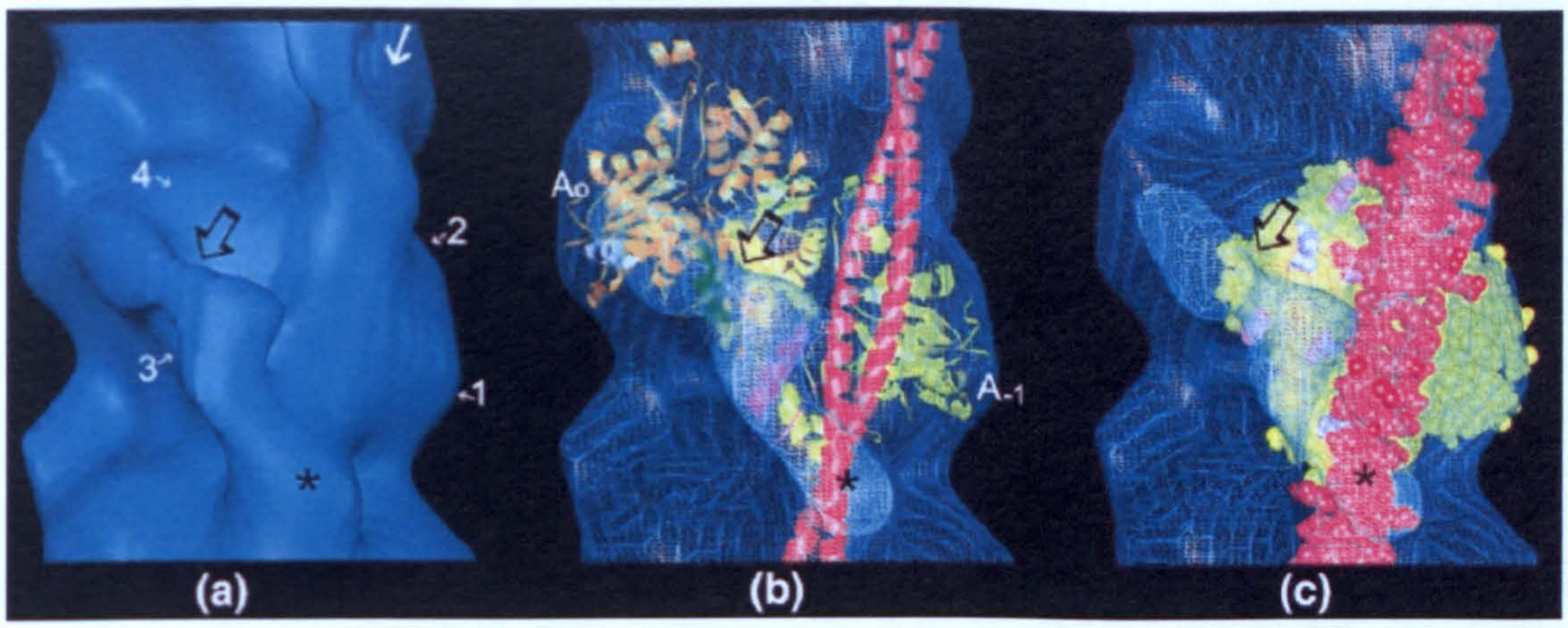

Fig 1.28: The C-terminal peptide of TnI constrains Tm coiled-coil in the blocked state in the absence of Ca^{2+}.(a) EM of thin filaments containing actin, Tm and TnI peptide. (b) and (c) Fitting models of actin and Tm on the EM shown in a. The TnI peptide crosses the cleft between two actin monomers in the F-actin helix. The distal end of TnI forms a fist like structure against the Tm coil (over magenta residues in b). Also the TnI peptide covers residues on actin know to interact with Tm in the closed state position (pink and white residues shown in c over the actin monomer shown in yellow) (Galinska-Rakoczy *et al.* 2008).

1.5 Tm function in smooth muscle and non-muscle cells

Apart from the striated muscle system, tropomyosin is also involved in smooth muscle contraction. In this case the tissue specific smooth muscle Tm isoforms are involved. The regulation of smooth muscle contraction differs from the regulation of skeletal muscle since Tn is absent from smooth muscle cells. Regulation can instead be achieved by two independent ways (Somlyo and Somlyo 1994; Marston *et al.* 1998; Gusev 2001). One way of regulation involves the activation of myosin by phosphorylation of its light chain by myosin light chain kinase. The stimulus for the myosin light chain kinase is the Ca^{2+} binding on calmodulin. Myosin becomes deactivated upon dephosphorylation by a myosin phosphatase (Webb 2003). The second route for the regulation of smooth muscle contraction involves the inhibition of actomyosin complex formation by caldesmon and Tm. A model of cooperative allosteric inhibition was proposed where caldesmon is the allosteric inhibitor and switches the thin filament from the On state to the Off state and Tm propagates the signal (Marston and Redwood 1993; Alahyan *et al.* 2006; Ansari *et al.* 2008). The

cooperativity unit is larger in smooth muscles compared to the skeletal muscles, presumably due to the stronger end-to-end interactions between smooth Tm isoforms. Ca^{2+} binding on the Ca^{2+}-binding protein releases the caldesmon inhibition and initiates muscle contraction.

In non-muscle cells, Tm obeys the same fundamental theorem as in the muscle cells; that is to stabilise actin filaments and to control the interactions of actin with other actin binding proteins. The actin binding candidates in non muscle cells could be for example non-muscle myosins or proteins involved in the regulation of actin dynamics. It has been shown that binding of Tm on actin protects actin from the actin depolymerising factor cofilin (Bernstein and Bamburg 1982) or from fragmentation by gelsolin (Ishikawa *et al.* 1989). Also Tm inhibits the Arp2/3 complex from creating branch points along actin filaments (Blanchoin *et al.* 2001). Some of the Tm functions are isoform specific. The fibroblast TM3 isoform for example was shown to stimulate the retrograde movement of organelles such as mitochondria and lysosomes towards the periphery of cell nucleus. Together with the transported organelles both myosin I and dynein were found to redistribute at the perinuclear area, indicating that the organelle transport occurred via actin filaments and microtubule tracks. On the other hand the Tm5NM1 isoform had no effect in organelle redistribution (Pelham *et al.* 1996).

Another interesting observation is the distribution of different Tm isoforms within a single cell. For example in brain tissue, more than one Tm isoforms are found in a neuron. In early stages of development the Tm5NM-1 or -2 isoforms are mostly found in the neuronal axon together with β and γ actin. However in mature neurons the Tm5NM-1 or -2 isoforms in axon are replaced by the brain specific isoforms TmBr1 and TmBr3. β-actin is also lost from the axon, while γ-actin is distributed all over the neuron. The Tm5NM-1 and -2 isoforms are limited in the cell body of the neuron (Weinberger *et al.* 1996). A comparative study between the Tm5Nm1 and TmBr3 isoforms showed that they differentially regulated the actin filament organisation with impact in the cell shape and migration. So actin filaments with Tm5NM1 isoform could be associated with myosin II and induced stress-fibre formation. On the other hand the actin/TmBr3 filaments could bind to coffilin and the stress-fibre formation appeared

reduced. Other morphological characteristics were the increased cell surface and the inhibition of lamellipodia formation in the Tm5NM1 transfected cells. The transfected cells with TmBr3 had the opposite effects (decreased cell surface, induced lamellipodia formation) (Bryce *et al.* 2003). However it is unclear what controls Tm localisation in a cell.

The yeast *S. cerevisiae* has two Tm isoforms as mentioned in section 1.2. Tpm1 is associated with the actin cables running along the yeast's cytoplasm and is involved in the polarised transport of vesicles, in mating projection formation and in cell fusion of mating cells (Liu and Bretscher 1989; Liu and Bretscher 1992). The second shorter isoform Tpm2 does not seem to have significant physiological defects upon deletion. Overexpression of Tpm2 does not seem to affect the actin cytoskeleton however the cell's polarity can be altered. The commonly seen axial budding pattern (cells polarize and divide adjacent to the previous site of cell separation) was shifted upon Tpm2 overexpression to a bipolar budding pattern (cells may divide adjacent or opposite to the previous site of cell separation) in 40 % of the haploid cells (Drees *et al.* 1995). Another yeast the *S. pombe* expresses only a single Tm isoform, the cdc8. 80 % of cdc8 is found to be acetylated at all times while the rest of the protein remains unacetylated. From kinetic and structural experiments the acetylated cdc8 is found predominantly at the closed state on actin filaments with only 2 % found at the open state (the blocked state is not occupied because the thin filaments were not decorated with Tn since yeast cells lack Tn). On the other hand the percentage of the unacetylated cdc8 that is found at the open state is very much increased up to 32 %, suggesting that the two molecules can differentially regulate myosin binding on actin (Skoumpla *et al.* 2007). As an exception to the general rule, the cdc8 can be associated with different actin structures according to its post-translational modification state, without the need of *S. pombe* to express a second isoform. Acetylated cdc8 is associated with the actin ring during cytokinesis while unacetylated cdc8 is associated with the actin cables in *S. pombe* (Mulvihill lab, unpublished observation).

Other recent investigations in Drosophila assigned a novel role for the Tm/Tn complex in maintaining nuclear integrity. Embryonic lethal mutant alleles for two Tm isoforms Tm1 and Tm2 or a mutant for TnI had all similar defects. In the mutant

embryos the tubulin structure was abnormal and nuclear divisions occurred asynchronously. In some cases chromosomes were fragmented and nuclei appeared clumped. Moreover the Tm2 mutant embryos at the metaphase stage failed to achieve proper spindle orientation and chromosome alignment. Each of the mutants also caused defects in actin cytoskeleton, cell shape and cell polarity (Sahota *et al.* 2009).

1.6 Hypertrophic Cardiomyopathies

Cardiomyopathy literally means heart (=cardio) muscle (=myo) disease (=pathy) and it can be classified according to the morphology of the diseased heart into three main types; the hypertrophic, the dilated or the restrictive cardiomyopathy. In figure 1.29 each of the above cardiomyopathy types are schematically represented and compared to a normal heart. The hypertrophic cardiomyopathy (HCM) shows extensive thickening of the myocardium particular in the ventricles area. The ventricles are also stiff and show myocardial disarray. The major characteristic of dilated cardiomyopathy (DCM) is the enlarged heart; the myocardium is weakened and thinner and pumps blood less strongly. In the restrictive cardiomyopathy (RCM) the ventricular walls become stiff mainly because of the presence of scar tissue. Thus the ventricles resist filling with blood and this may cause fluid accumulation in tissues and cardiac arrhythmias. Any of the above cardiomyopathies can be caused by mutations in proteins of the sarcomere or even by other diseases (like diabetes or thyroid disease) (Fatkin and Graham 2002; Chang and Potter 2005; Morimoto 2008; Mudd and Kass 2008).

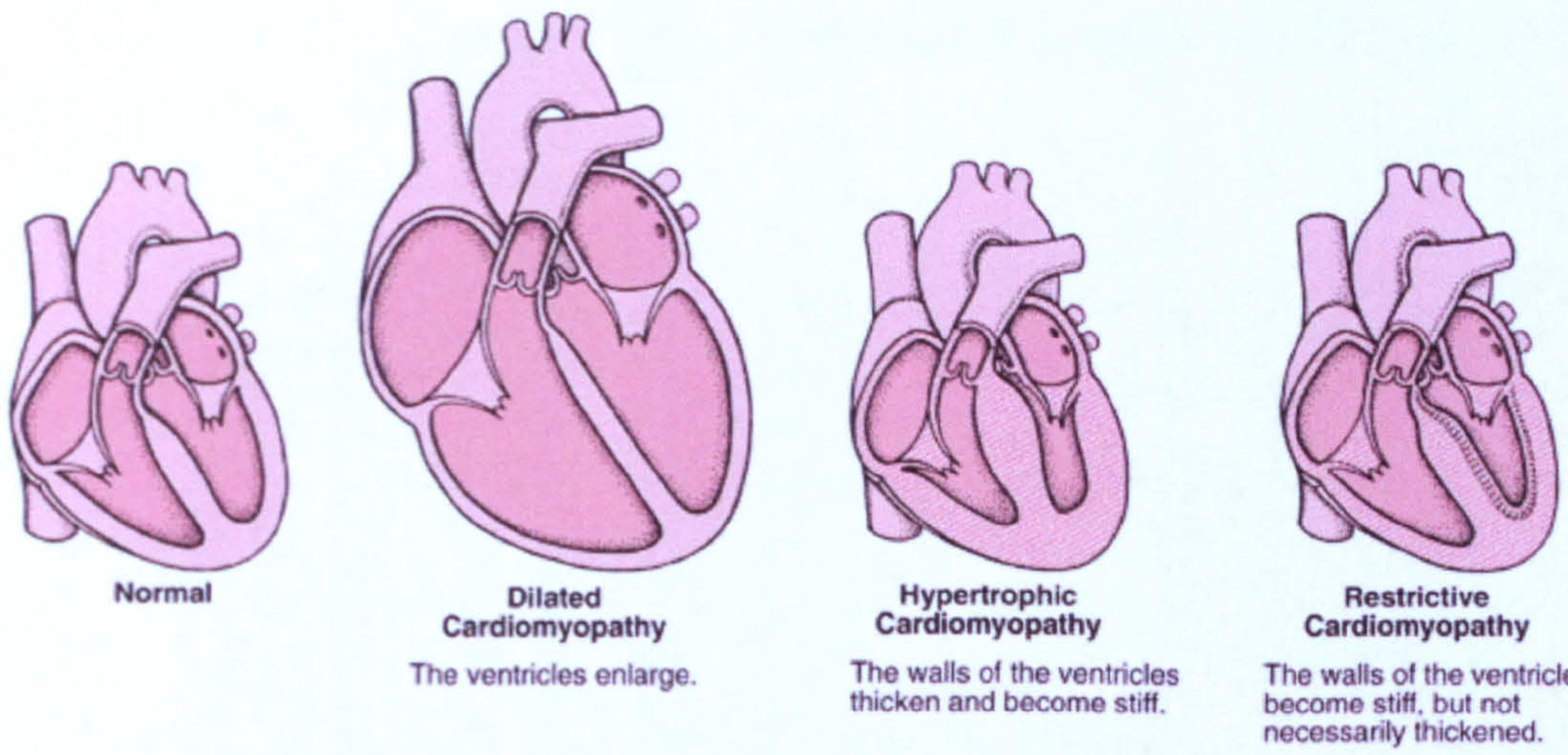

Fig 1.29: The morphology of a cardiomyopathy disease heart. Compared to the normal healthy heart, the DCM heart appears enlarged, the HCM heart has thickened and stiff ventricular walls and the RCM heart has stiff ventricular walls (from http://www.merck.com/mmhe/print/sec03/ch026/ch026a.html).

Hypertrophic Cardiomyopathy (HCM) is a very common cause of heart disease affecting one in every 500 individuals (Maron *et al.* 1995). The most common cause of HCM is mutations in almost any of the sarcomeric proteins either of the thick or the thin filaments (fig 1.30), (Redwood *et al.* 1999; Taylor *et al.* 2004). Other more rare forms of HCM are due to metabolic defects that result in glycogen accumulation in cardiac myocytes (Arad *et al.* 2005). Mutations in β-myosin heavy chain, myosin-binding protein C and TnT are the most frequent cause of the sarcomeric-related cardiomyopathies (~35, ~15 and ~15 % frequency respectively) (Geisterfer-Lowrance *et al.* 1990; Watkins *et al.* 1995).

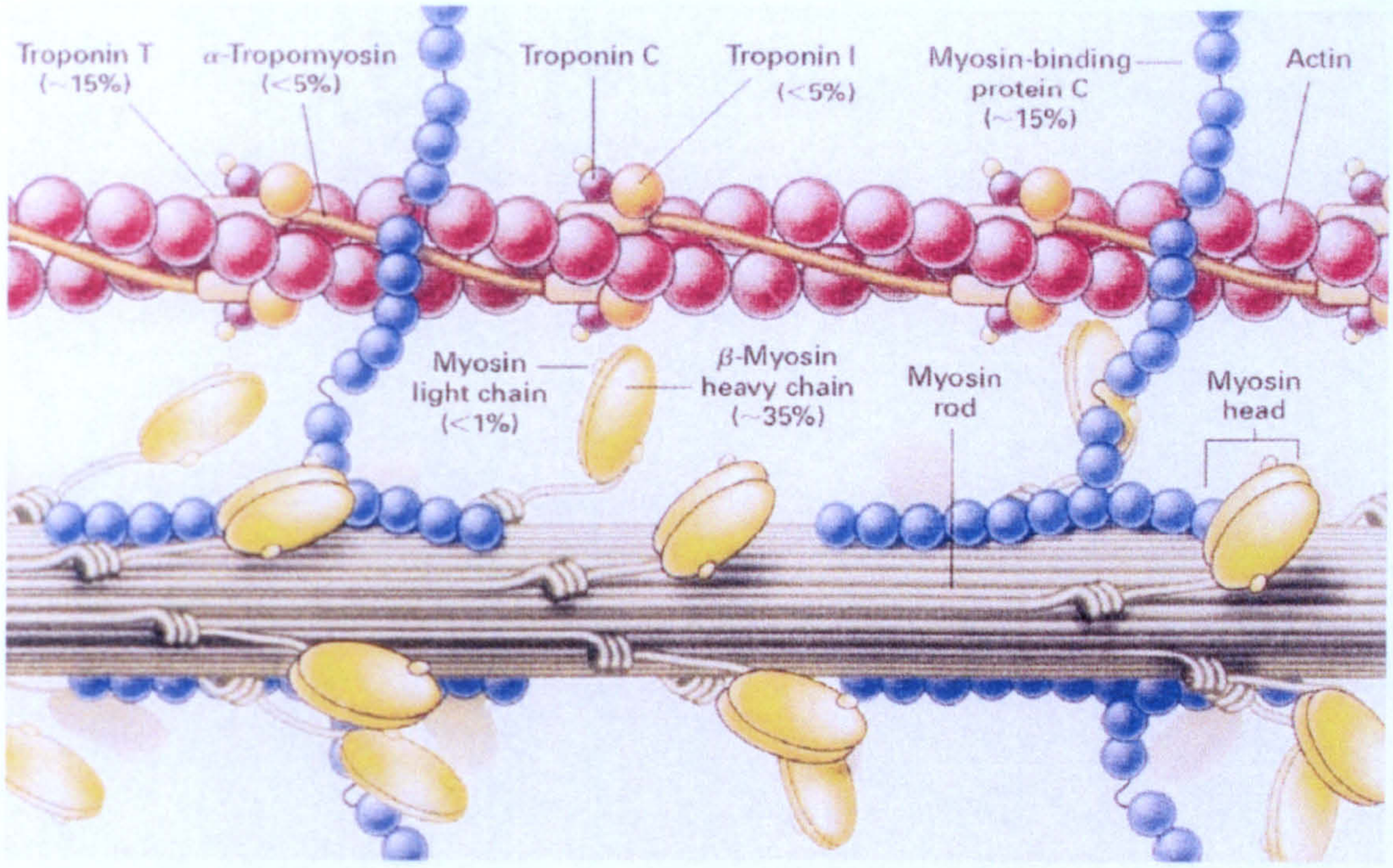

Fig 1.30: Schematic representation of the distribution of mutations causing HCM amongst the various proteins of the sarcomere. Mutation in β-myosin heavy chain, TnT and myosin-binding protein C is the most popular cause of HCM (Watkins *et al.* 1995; Redwood *et al.* 1999).

The effects of HCM mutations on Tm and TnT is of particular interest to this thesis as will be explained in section 1.7. In the case of tropomyosin, there are four autosomal dominant mutations in the gene encoding α Tm that cause hypertrophic cardiomyopathy (HCM) but none yet has been reported on the gene encoding for β Tm (apart from the Arg91Gly mutation that only affects skeletal muscle (Sung *et al.* 2003)). The α Tm HCM mutations include the Ala63Val, Asp175Asn (Nakajima-Taniguchi *et al.* 1995), Lys70Thr(Yamauchi-Takihara *et al.* 1996) and the Glu180Gly (Thierfelder *et al.* 1994), making the α Tm mutations responsible for the 5 % of the total HCM cases. Amongst the proteins of the thin filaments, mutations in Troponin T gene are the most frequent (~15 %) cause of HCM. To date 30 mutations on TnT that are linked to HCM have been reported (reviewed in Gomes *et al.* 2004). Most of the HCM mutations are associated with hypertrophic-thickened walls of the left ventricle, which result in reduced size of the left ventricular cavity. However, most of HCM TnT mutations show myocardial disarray and no or mild hypertrophy, prognosis of the disease is really poor and patients have a high incidence of sudden cardiac death (Varnava *et al.* 2001. a;

Varnava *et al.* 2001. b). From figure 1.31 below it can be observed that the TnT1 fragment (as well as the helix 4 of TnI) is a hotspot for cardiomyopathy mutations.

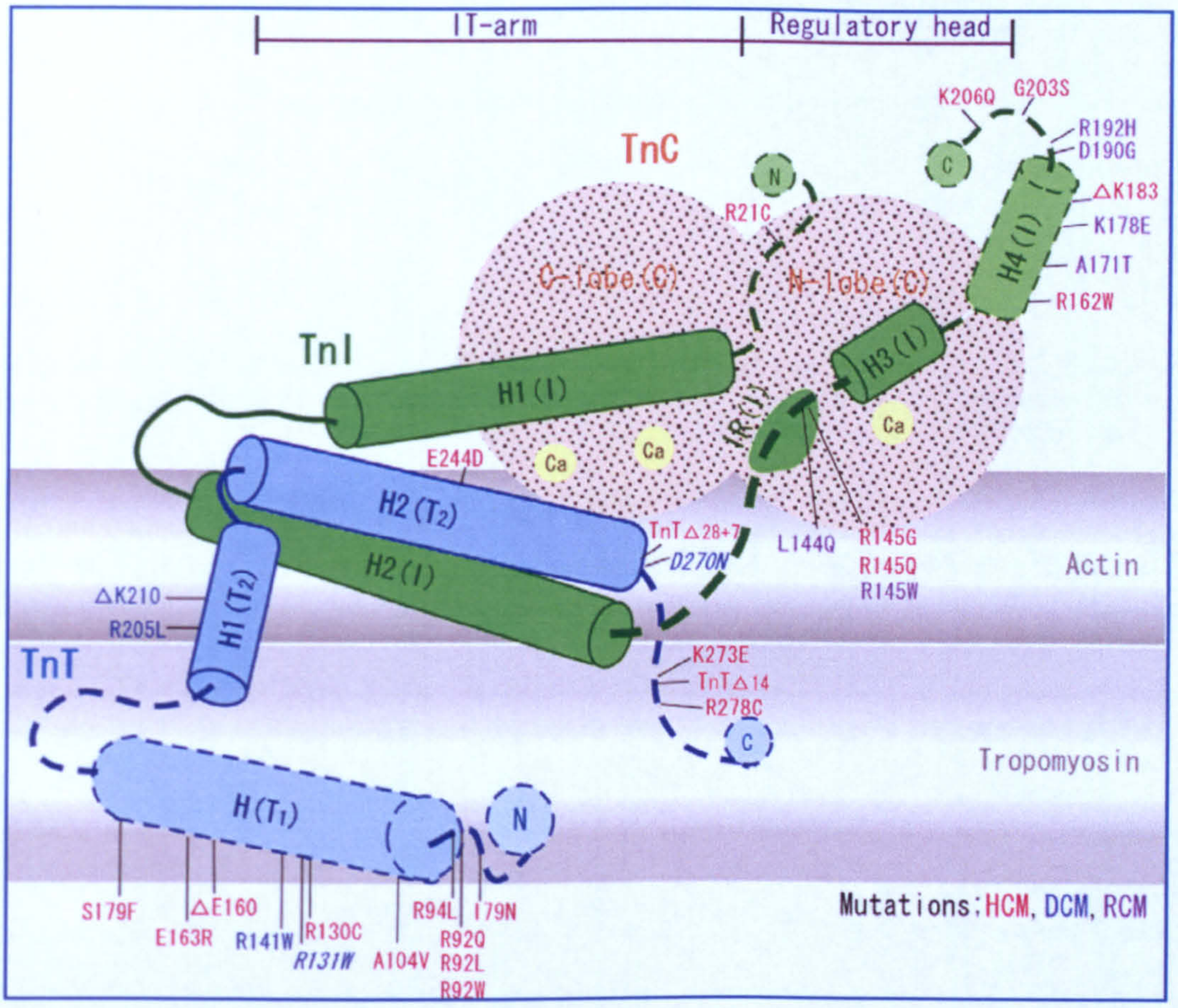

Fig 1.31: Location of cardiomyopathy-causing mutations within the Tn complex. HCM mutations are shown in red, DCM mutations in blue and RCM in purple. Hotspots for mutations include the TnT1 fragment and helix 4 of TnI (Ohtsuki and Morimoto 2008).

The heart muscle functions very similarly to skeletal muscles, i.e. during systole Ca^{2+} levels rise and bind to cardiac TnC stimulating heart contraction. It is not clear how mutations in the sarcomeric proteins can cause cardiomyopathies. But in general it is widely accepted that mutations that cause HCM increase the Ca^{2+} sensitivity of the system. On the other hand mutations that cause DCM are associated with decreased Ca^{2+} sensitivity (Robinson *et al.* 2007).

In general, HCM mutations on sarcomeric proteins may affect the protein's structure and function. The hypertrophic response is not considered as the primary manifestation of the HCM mutations, but progressively develops as a mechanism to compensate sarcomere dysfunction. There are two models for the primary signal that arises from the mutant sarcomeric proteins. In the dominant negative model both mutant and wild-type proteins are expressed in equal proportions with the mutant protein acting as the "poison polypeptide" that can be successfully incorporated into the sarcomere and disrupt normal function. The second model is the haploinsufficiency model according to which the mutation can cause null alleles or a reduction in the amount of the wild-type protein expressed (Bonne *et al.* 1998; Fatkin and Graham 2002; Maass and Leinwand 2003). In any case this primary signal may trigger further cascade pathways that will eventually result in a hypertrophic response. Many factors can be involved in the progression of hypertrophy and these can be either extrinsic or intrinsic to the cardiac myocyte. Intrinsic stimuli may include elevated intracellular Ca^{2+} concentration, activation of kinases, phosphatases and transcription factors. Extrinsic stimuli may include activators of protein kinase C and growth factors, α-adrenergic agonists or vasoactive peptides like angiotensin (Sugden 2001).

For example it is widely accepted that most of the HCM mutants show altered Ca^{2+} sensitivity. It was reported that the intracellular Ca^{2+} can play a role in the calcineurin signalling pathway which can cause left ventricular hypertrophy. Intracellular Ca^{2+} can activate calcineurin, which in turn dephosphorylates the NFAT3 transcription factor. NFAT3 in turn translocates in the nucleus, combines with the cardiac restricted GATA4 trasncription factors and together they stimulate expression of embryonic cardiac genes leading to a hypertrophic response (Molkentin *et al.* 1998). Ca^{2+} can also activate the calmodulin dependent protein kinase (CaMK) pathway that can stimulate hypertrophy. Activated CaMK can stimulate the transcription factor MEF2, which is a putative marker of hypertrophy. The MEF2 transcription factor is associated with transcriptional repressor proteins thus failing to initiate transcription. However upon stimulation by CaMK the inhibition on MEF2 is released, the transcriptional activity is carried out leading eventually to hypertrophy (Passier *et al.* 2000). The Ca^{2+} signalling pathways that are involved in the hypertrophy response are summarised in figure 1.32.

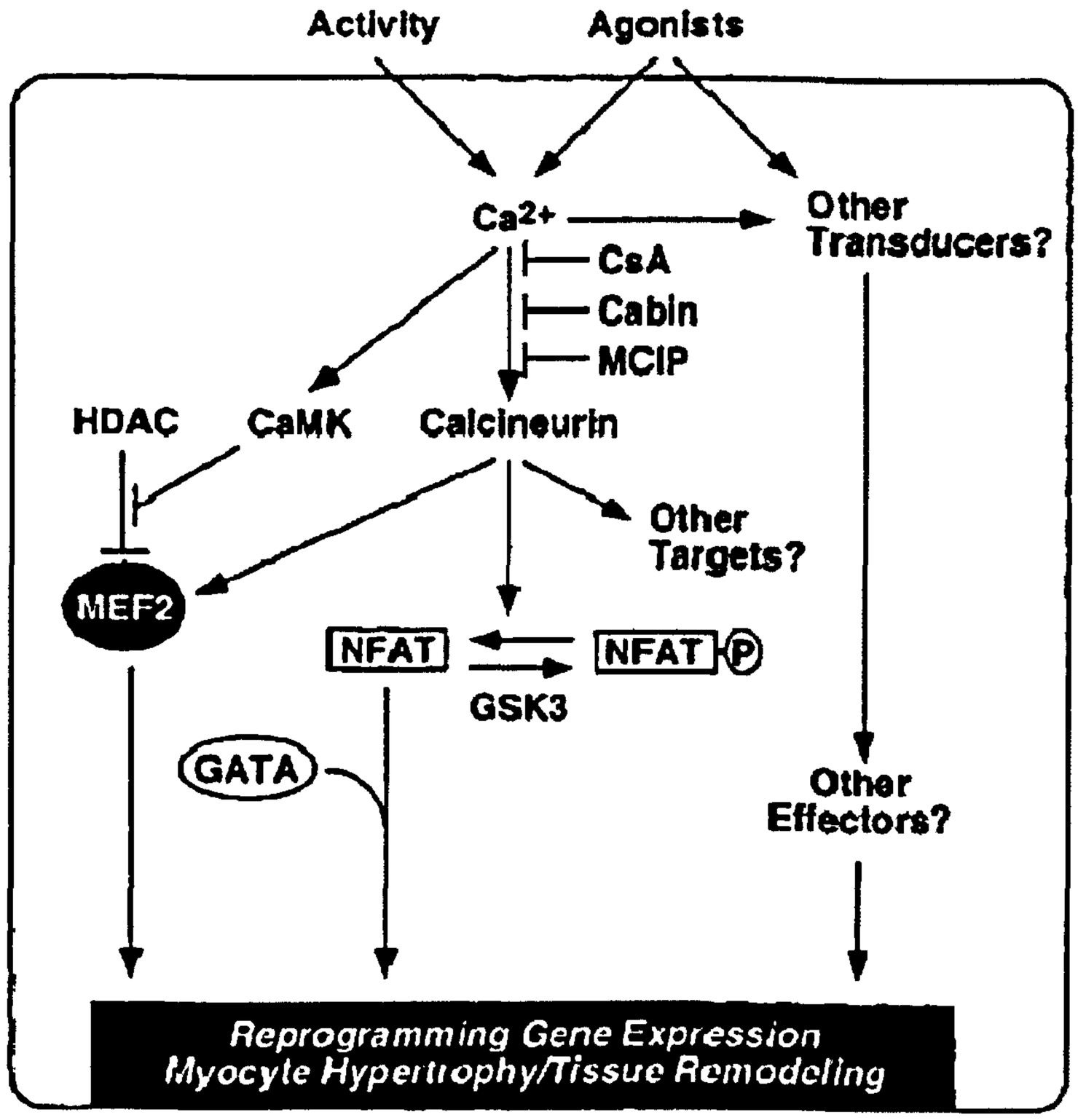

Fig 1.32: Ca^{2+} signalling pathways that result in cardiac hypertrophy (Olson and Williams 2000)

1.7 Aim of project

Some interesting aspects of the αβ Tm heterodimer were already mentioned in the current chapter in section 1.2. To summarise, the αβ Tm heterodimer is preferentially assembled in smooth muscles. The skeletal αβ Tm heterodimer levels can vary in skeletal fast or slow muscle fibres. Also the presence of αβ heterodimer in heart is dependent on the size of organism but if increased it is associated with cardiomyopathies. These observations make the αβ Tm heterodimer a very interesting subject to study. It is of interest to investigate if the Tm heterodimer is capable of differentially regulated muscle contraction in comparison to the Tm homodimer. Many studies were reported on Tm dimers, with the majority of them on Tm homodimers or the smooth Tm heterodimer, but very little is known about skeletal Tm heterodimers, mainly because their *in vitro* formation was not successful. Therefore, the formation and characterisation of the αβ Tm heterodimer is the major aim of this project.

A second aim of this study is to form and characterise Tm heterodimers that will be composed of one wild-type Tm copy and one mutant Tm copy that can cause cardiomyopathy. Many of the Tm cardiomyopathy mutants have been successfully cloned and expressed in bacteria cells and characterised. However, most characterisation experiments to date were performed using homodimers of these Tm mutants (section 4.1). It is likely that a particular mutation will not have the same effects if it is present as a double copy i.e. in homodimers or as a single copy i.e. in heterodimers. Therefore, to learn more about a particular mutation, it is of great interest to form and characterise the heterodimers carrying that mutation and compare them with the corresponding wild type and mutant homodimers. The aim is to use the hypertrophic cardiomyopathy mutations α^{D175N} and α^{E180G}, both of which are well characterised as homodimers, and combine them with either an α or a β wild-type subunit to make heterodimers.

Finally it is of interest to check the effect of TnT1 fragment on the Tm filaments. TnT1 is expected to stabilise the end-to-end interactions between adjacent Tm molecules and therefore influence the binding affinity of Tm for actin. Using PCR site-directed mutagenesis and the wild-type TnT1 template, the aim is to produce three TnT1 mutants that are known to cause cardiac hypertrophy. The TnT1 mutants that were chosen for this study include the R92Q, A104V and F110I, thus all of them lie in the TnT1 area directly involved in the Tm overlap region. The aim is to investigate the effects of each of the TnT1 fragments on the binding affinity of αα and αβ dimers to actin (because these two Tm dimers exist naturally in the heart and thus are potential binding partners). It is also of interest to measure the binding affinities of each TnT1 fragments to αα and αβ Tm dimers.

The protocol developed for the formation and purification of the different types of Tm heterodimers is explained in chapter 3. Characterisation experiments of the Tm heterodimers produced are shown in chapter 4. Finally in chapter 5 the interactions of the various TnT1 fragments with Tm are investigated.

Chapter 2

Materials and Methods

2.1 Molecular biology materials and methods

All enzymes used for molecular biology were purchased from Promega unless otherwise stated and all DNA purification kits were from Qiagen.

2.1.1 PCR for Site directed mutagenesis of DNA encoding TnT1

Point mutations were introduced in the TnT1 DNA template (encoding for amino acid residues 1-160 of human cardiac Troponin T, type-2, isoform 3) using the specific mutagenic forward and reverse primers listed below. The original TnT clone was a gift from I. P. Trayer, University of Birmingham. Three TnT1 mutants were created i.e. the R92Q, A104V and F110I using the DpnI-mediated site directed mutagenesis technique (Fisher and Pei 1997). The PCR recipe and conditions used were the same for each TnT1 mutant.

PCR Recipe	PCR Conditions
0.5 µl DNA template (10-50 ng/ µl)	Initial heating of the PCR mix →1 min @ 95 °C
0.5 µl Forward Primer (25 pmol/ µl)	Then thermocycles of:
0.5 µl Reverse Primer (25 pmol/ µl)	Denaturation step → 30 sec @ 95 °C
1 µl Pfu DNA polymerase (2-3 unit/ µl)	Annealing step → 1 min @ 55 °C
5 µl Pfu 10 x buffer	Elongation step → $7_{1/2}$ min @ 68°C
1 µl DNTPs (10 mM)	
41.5 µl sterile H_2O	Repeated for 18 amplification cycles

Mutagenic Primers used (the changed codons are shown in red)

R92Q Forward Primer
5' GAT GAC ATC CAC CAG AAG CGC ATG GAG AAG G 3'

R92Q Reverse Primer
5' C CTT CTC CAT GCG CTT CTG GTG GTG TCA TC 3'

A104V Forward Primer
5' C CTG AAT GAG TTG CAG GTG CTG ATC GAG GC 3'

A104V Reverse Primer
5' GC CTC GAT CAG CAC CTG CAA CTC ATT CAG G 3'

F110I Forward Primer
5' G CTG ATC GAG GCT CAC ATT GAG AAC AGG 3'

F110I Reverse Primer
5' CCT GTT CTC AAT GTG AGC CTC GAT CAG C 3'

- Summary of the TnT1 mutants cloning procedure

For the PCR step, the pGEM-T Easy vector in which the wild type TnT1 sequence was inserted was used as the parental DNA. With the mutagenic primers used, the whole plasmid was amplified i.e. both the TnT1 sequence and the pGEM-T Easy vector sequence. The difference between the two plasmids is that the parental one obtained from a bacterial miniprep is methylated while the PCR amplified plasmid is unmethylated.

At the end of the PCR, the reaction mixture was left to cool and then treated with DpnI endonuclease for 1 h at 37 °C. DpnI digests the methylated parental plasmid but not the unmethylated PCR-amplified product. The DpnI-digested mixture was then used to transform DH5α cells (bacteria cell transformation is described in section 2.1.8). The transformed cells were then streaked onto LB/Amp agar plates because the pGEM-Teasy vector has an ampicillin resistance gene (details of vectors in section 2.1.3). (NB any plate on which cells were streaked or any liquid media that were inoculated with cells were incubated overnight at 37 °C unless stated otherwise).

Single colonies were then used to inoculate 5 ml of LB/Amp media. From each culture, 1.5 ml of cells were centrifuged and DNA was purified using the QIAprep spin miniprep kit following the product manual. For each mutant 5 minipreps were prepared and were sent for sequencing to MWG . The sequencing was carried out using the universal M13(-21) forward and M13(-29) reverse primers. The inserts of the correct sequence were subcloned from the pGEM-T Easy vector into the pJC20 vector. First the insert was digested from pGEM-T Easy using the NdeI and BamHI restriction sites. Then the insert was ligated into the pJC20 vector that was previously cut by the same NdeI and BamHI enzymes to produce compatible ends (restriction enzyme digest is described in section 2.1.6 and plasmid ligation in section 2.1.7). This pJC20/TnT1 of interest ligation mixture was then used to transform DH5α cells. The transformed cells were streaked onto LB/Amp agar plates because the pJC20 vector has ampicilin resistance and single colonies were then picked up to inoculate 5ml LB/Amp liquid cultures. From these cultures 1 ml was used to produce minipreps that were double digested by NdeI and BamHI to check if they were positive for the insert. The digestion mixtures were separated on 1 % agarose gels and samples that showed a ~500 bp band corresponding to the size of the insert accounted as positive. 1 ml of the minicultures that were found positive for the insert was then added into cryotubes containing 500 µl of 60 % glycerol to create clonning stocks of DH5α/pJC20/TnT1 of interest and stored at -80 °C.

The minipreps from the positive 5 ml minicultures of DH5α/pJC20/TnT1 of interest were also used to transform BL21 cells. The transformed cells were spread on LB/Amp plates and single colonies were then used to inoculate 5 ml of LB/Amp media. 1 ml of these starter cultures were then used to inoculate 25 ml of NZY/Amp media. Cells were grown until they reached an OD_{600}= 0.4. Then 1 ml of each culture was aliquoted out to act as a control and the rest of the culture was induced by addition of 100 mg/l IPTG. Cells were incubated for a further 3 h. 1 ml of the induced cultures and 1 ml of the non-induced controls were then centrifuged at 6.4 rpm for 7 min. The pellets of cells were resuspended in 100 µl H_2O plus 20 µl sample loading buffer, heated at 90 °C for 5 min and loaded onto 10 % Polyacrylamide Gel (for PAGE details please see section 2.2.1). The initial 5 ml LB/Amp culture that gave the best protein expression level (as was observed after polyacrylamide gel electrophoresis) was then used to make

expression glycerol stocks. 1 ml of BL21/pJC20/TnT1 insert cells were added into cryotubes containing 500 µl of 60 % glycerol and stored at -80˚C.

2.1.2 PCR for the amplification of DNA encoding for Tm and for tag insertion at the 5' end of Tm sequence

Amplification of the DNA sequences of interest was performed by PCR using the high fidelity Pfu DNA polymerase. Genes encoding the rat skeletal α Tm or β Tm were modified at their 5' end using specially designed forward primers. The primers were designed to include an Ala-Ser extension at the 5' end of α Tm or β Tm as previously reported (Kremneva *et al.* 2004; Boussouf *et al.* 2007). Other primers were designed to insert a His- or a Strep-tag followed by factor Xa protease sequence prior to the Ala-Ser extension at the 5' of α Tm or β Tm. These forward primers could be used for the amplification of both αTm and βTm since they contained the starting 5' nucleotide sequence which is identical in the two genes.

The forward primers used for the Tm amplification also contained the NdeI restriction site sequence and the reverse primers contained the BamHI restriction site sequence, for subsequent cloning of the amplified Tm fragments into the appropriate vectors. The PCR recipe and conditions were unchanged for all of the Tm sequences that were amplified.

PCR Recipe

1 µl DNA template (100-500 ng/ µl)
1 µl Forward Primer (25 pmol/ µl)
1 µl Reverse Primer (25 pmol/ µl)
1 µl Pfu DNA polymerase
5 µl Pfu 10 x buffer
1 µl DNTPs (10 mM)
40 µl sterile H_2O

PCR Conditions

Denaturation step → 1 min 94˚C
Annealing step → 1 min 50˚C
Elongation step → 2 min 68˚C

Repeated for 35 amplification cycles

Details of the forward and the reverse primers used are shown below.

Forward AS-αTm Primer

5' GG CAT ATG GCG AGC ATG GAC GCC ATC AAG AAG AAG ATG CAG ATG 3'

NdeI AS αTm

Forward AS-βTm Primer

5' G GAA TTC CAT ATG GCG AGC ATG GAC GCC ATC AAG AAG AAG ATG C 3'

NdeI AS βTm

Forward StrepFXaAS Tm primer

5' GG CAT ATG TGG AGC CAC CCG CAG TTC GAA AAA ATC GAA GGG CGC GCG AGC ATG GAC GCC ATC AAG AAG 3'

NdeI Strep tag FactorXa AS Tm

Forward HisFXaAS Tm primer

5' GG CAT A TG AGA GGA TCG CAT CAC CAT CAC CAT CAC ATC GAA GGG CGC GCG AGC ATG GAC GCC ATC AAG AAG 3'

NdeI 6 His tag FactorXa AS Tm

Reverse α Tm Primer

5' CC GGA TCC TTA TAT GGA AGT CAT ATC GTT GAG AGC GTG GTC 3'

BamHI

Reverse β Tm Primer

5' CGC GGA TCC TCA GAG GGA AGT GAT GTC ATT GAG CG 3'

BamHI

➢ summary of the Tm cloning procedure

The amplified PCR products were then tagged at their 5' ends by adding adenine nucleotides using Taq DNA polymerase (method described in section2.1.4). The DNA fragments were then loaded onto agarose gels to check if the amplified DNA was of the correct size by comparing to a standard 1 kb DNA ladder. The fragments corresponding to ~ 900 bp were then gel extracted and DNA was purified using the QIAquick gel extraction kit according to the manufacturer's instructions. The purified DNA fragments with the 5' adenine overhangs were then ligated into the pGEM-T easy linear vector which is designed with 3' thymine overhangs. The ligation mixture was then used to transform DH5α cells. The transfromed cells were then spread onto LB/Amp/Xgal plates. From the plates single colonies were picked and used to inoculate 5 ml LB/Amp liquid cultures. 1.5 ml of each culture was then used to purify DNA using the QIAprep spin miniprep kit according to the manufacturer's instructions. For a quick check to verify if the plasmids contained the insert DNA, small amount of each miniprep was digested by EcoRI since the pGEM Teasy vector has EcoRI sites at either end of the insert area. The EcoRI digestion mixture was loaded on agarose gel to check for the presence of the 900 bp Tm DNA insert. Minipreps positive for the insert were then send for sequencing (i.e. the original undigested miniprep solution). The DNA fragments of the correct sequence were then digested from the pGEM-T easy vector and ligated into the pJC20 vector as explained previously. The pJC20/Tm insert plasmid was used to transform DH5α and BL21 cells and thus make the cloning and expression glycerol stocks using the same methodology as described in section 2.1.1.

The following Tm glycerol stocks were made:

- α Tm
- His α Tm
- Strep α Tm
- β Tm
- His β Tm
- Strep β Tm

Also glycerol stocks of mutants α^{D175N} Tm and α^{E180G} Tm previously made in our lab by Dr Maytum were used.

2.1.3 Information on the vectors used for cloning

The pGEM-T Easy vector is about 3 k bp long (fig 2.1). It is designed with 3' thymine overhangs that will provide compatible ends for the ligation of DNA inserts designed to have 5' adenine overhangs. The multiple cloning region is between the lacZ reporter gene. Therefore when the sequence of interest is successfully ligated, the lacZ gene sequence is disrupted and cannot produce beta-galactosidase. This means that transformed bacteria with the plasmid that contains the insert cannot break down XGalactose and thus produce white colour colonies. On the other hand transformed bacteria with vector in which the insert is not successfully ligated can produce beta-galactosidase and break down XGalactose and this reaction can be observed by a blue by-product, thus the colonies appear blue. Moreover the pGEM-T Easy vector has an Ampicillin resistance gene. Also from either side of the insert there are restriction sites sequences for EcoRI and NotI enzymes, thus by digesting the plasmid with either of these enzymes one can check quickly if the insert of interest is ligated.

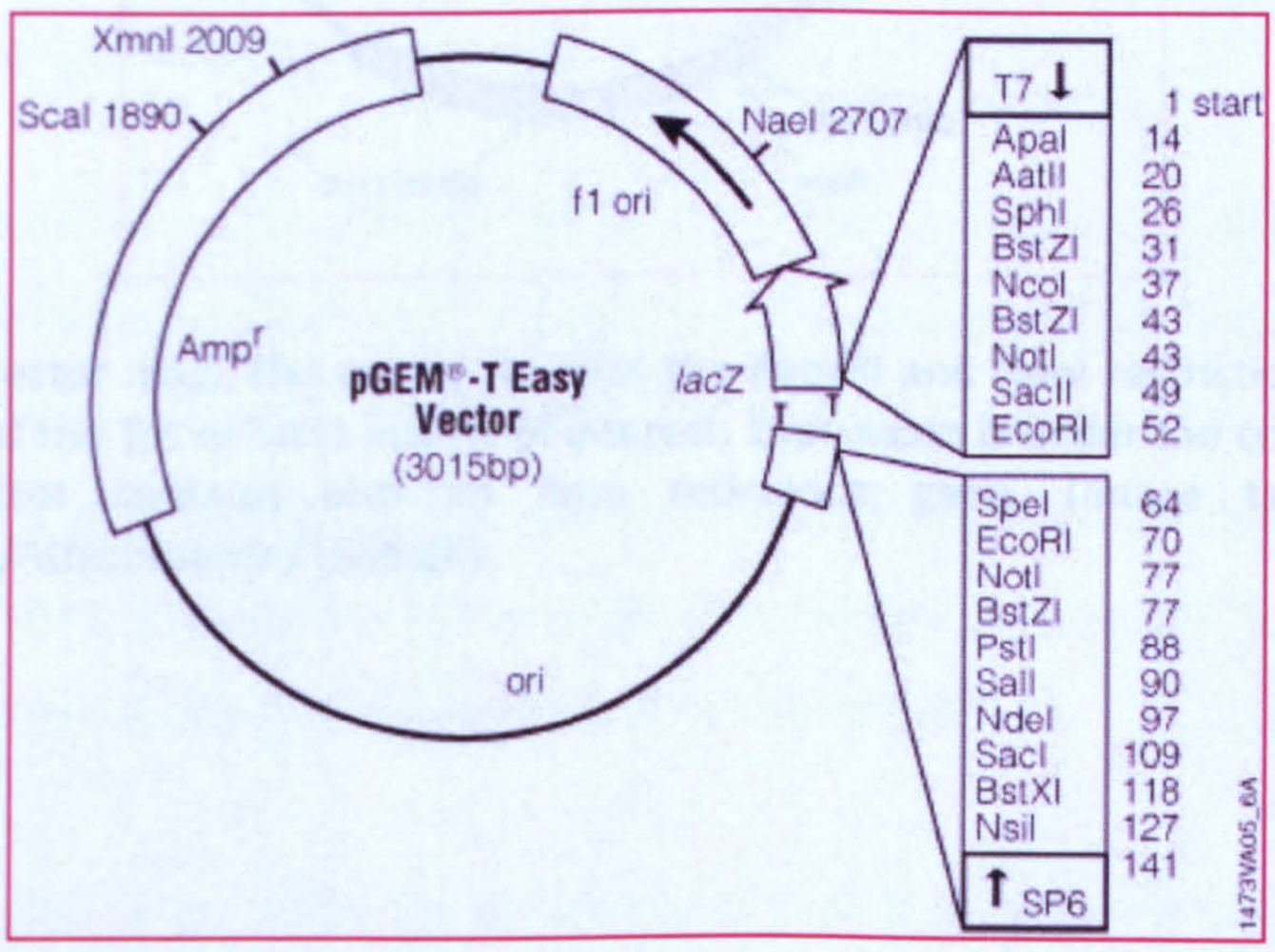

Fig 2.1: pGEM-T Easy vector map and sequence reference points. The vector contains the lacZ reporter gene and an Amp resistance gene. The thymine overhangs on the vector make ligation of adenine-tagged inserts very easy. There are two sites for EcoRI digestion at either side of the insert, allowing quick scanning for positive clones (taken from http://www.promega.com/paguide/chap13.htm).

The pJC20 vector is 2.3 k bp long and is a very simple and easy to handle vector (fig 2.2), (Clos and Brandau 1994). It has an Ampicillin resistance gene and a small multiple cloning region, which contains the restriction sites for the most commonly used enzymes. For cloning of either Tm or TnT1, the NdeI and BamHI sites were used. This vector can give very good expression of protein when transformed in BL21 cells. Expression is under the control of the T7 promoter and can be induced by IPTG.

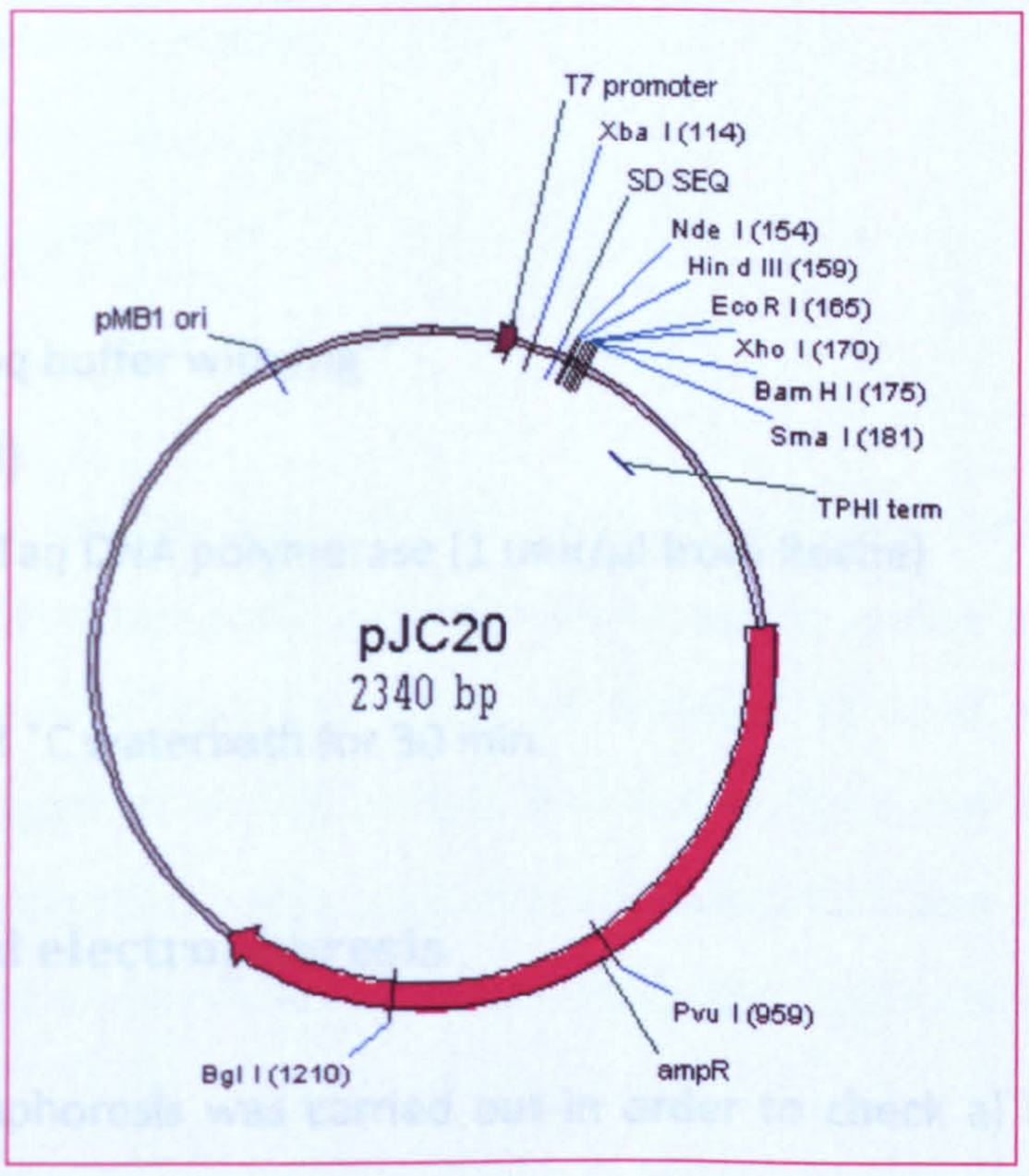

Fig 2.2: The pCJ20 Vector map. The vector contains the BamHI and NdeI restriction sites for convenient ligation of the Tm or TnT1 inserts of interest. Expression is under the control of T7 promoter. The vector contains also an Amp resistance gene. (Image taken from http://www.atcc.org/Attachments /1588.gif).

2.1.4 Deoxyadenosinetriphosphate addition onto the PCR product

In the case where the PCR amplified product was to be ligated into the pGEM-T Easy vector it needed to be tagged by deoxyadenosinetriphosphate at its 5' end. Thus the deoxyadenosine overhangs onto the insert DNA would complement the deoxythymidine overhangs of the vector. The PCR product was treated with deoxyadenosinetriphosphate and High Fidelity Taq polymerase enzyme from Roche in order to create the desired overhang onto the 5' end of the DNA strands.

Typical reaction

15 µl PCR product

2 µl High Fidelity Taq buffer with Mg^{2+}

0.5 µl dATP (10 mM)

0.5 µl High Fidelity Taq DNA polymerase (1 unit/µl from Roche)

2 µl H_2O

Incubation at 72 °C waterbath for 30 min.

2.1.5 Agarose gel electrophoresis

Agarose gel electrophoresis was carried out in order to check a) if the amplified DNA after PCR was of the correct size, b) if the vectors were successfully cut such that they would be able to accept the insert DNA, c) if the DNA fragment of interest was successfully ligated into the plasmids (this was achieved by double digestions at either side of the insert and loading the whole digestion mixture on the gel to check for bands with sizes corresponding to the insert and to the cut vector).

1 % agarose gels were made by dissolving 1 g of high melting point agarose (BioRad) in 100 ml of TAE buffer (40 mM TRIS pH 8.0, 20 mM glacial acetic acid, 1 mM EDTA). 10 µl of the DNA of interest together with 2 µl of 6x DNA sample buffer were loaded. The electrophoresis was performed in TAE buffer under constant 60 V. The 1 kb DNA ladder from Promega was used as a marker for estimation of the size of the DNA samples. Ethidium bromide (6 µl per gel) was used for detection of DNA bands on the agarose gel by UV light.

2.1.6 Restriction enzyme digests

For a quick check to test if the pGEM-T Easy vector was ligated with the adenine-tagged DNA insert a digestion with the EcoRI enzyme was carried out, since EcoRI sites exist on either side of the insert area and the digestion products were visualised on agarose gels.

Typical restriction enzyme digestion

10 µl DNA from miniprep

1.5 µl EcoRI (12unit /µl)

2 µl 10x EcoRI buffer

6.5 µl H_2O

In order to remove the insert of interest from the pGEM-T Easy vector, it was double digested by NdeI and BamHI enzymes. Moreover to create compatible ends between the pJC20 vector and the insert of interest so that they would be subsequently ligated together, the vector was also cut by the same BamHI and NdeI enzymes. Also double digestions were carried out in order to check if pJC20 plasmid was successfully ligated with the insert by checking the digestion products on an agarose gel.

Double digestions of DNA

5 µl plasmid

1.5 µl BamHI (10 unit /µl)

1.5 µl NdeI (10 unit /µl)

4 µl 10x buffer D

28 µl H_2O

For the double digestions both enzymes and enzyme buffer were ordered from the same company (Promega). Each of the digestion reactions was incubated at 37 °C for 1 h.

2.1.7 Ligation of DNA fragments into vectors

a. Ligation of Adenine overhang DNA insert into pGEM-T Easy vector

In order to ligate the adenine-tagged DNA insert into the pGEM-T Easy vector the following reaction mixture was set up.

Ligation Mixture

10 µl adenine-tagged DNA insert

1 µl pGEM-T Easy vector

1 µl T4 DNA ligase (1-3 unit /µl)

1.5 µl 10x DNA ligase buffer

1.5 µl H_2O

Mixture was incubated overnight at 4°C.

b. Ligation of the Tm or TnT1 insert into pJC20 vector

Ligation of the insert of interest which was double digested by NdeI and BamHI into the pJC20 vector that was cut by the same restriction enzymes was performed using the same method as described above. 10 µl of insert and 1 µl of pJC20 vector were ligated in the presence of 1 µl T4 DNA ligase enzyme and 1.5 µl 10x ligase buffer. The total reaction volume adjusted to 15 µl with H_2O and the ligation mixture was incubated overnight at 4 °C.

Before procceding in the ligation reaction, any of the DNA fragments to be ligated were first run on agarose gel, and they were puirifed using the QIAquick gel extraction kit.

2.1.8 Transformation of *E. coli* competent cells

The insert and vector mixture that was ligated overnight as described in section 2.1.7 above was then used to transform competent bacteria cells (*E.coli* DH5α or BL21 cells). 50 µl aliquots of the cells that were stored at - 80 °C were defrosted on ice. Then 7.5 µl of the ligation mixture was added into the cells and the mixture left on ice for further 20 min. The cells were then transformed by heat-shock at 42 °C for 75 sec and then transferred immediately onto ice for 2 min. 250 µl of SOC media was then added and cells left to recover for 1 h at 37 °C. After this short recovery, cells were streaked onto agar plates (LB/Amp/XGal or LB/amp plates for the plasmids containing the pGEM-T Easy vector or pJC20 vector respectively) and incubated overnight at 37 °C.

2.1.9 Production of Ca^{2+} competent *E. coli* cells

Single colonies of DH5α or BL21 cells were inoculated into 5 ml broth (2 % tryptone, 0.5 % yeast extract, 0.4 % $MgSO_4$, 10 mM KCl, pH 7.6) and left to grow overnight at 37 °C. This culture was then used to inoculate a fresh 500 ml broth. Cells were grown at 37 °C until $OD_{600} = 0.4$ and chilled on ice afterwards for 15 min. The cells were then centrifuged down at 2,500 rpm for 5 min at 4 °C. Pellets were then resuspended gently in 130 ml ice-cold TFB I buffer (100 mM RbCl, 50 mM $MnCl_2$, 30 mM KOAc, 10 mM $CaCl_2$, 15 % v/v glycerol, pH 5.8) and left on ice for 15 min. Then cells were centrifuged for a second time at 2,500 rpm for 5 min at 4 °C and pellets resuspended gently in 20 ml ice-cold TFB II buffer (10 mM MOPS, 10 mM RbCl, 75 mM $CaCl_2$, 15 % v/v glycerol, pH 7). 100 µl aliquots of the cells were then frozen in liquid nitrogen and stored at -80 °C.

2.1.10 Media recipes

LB/Amp : 5 g NaCl, 5 g bactopeptone, 2.5 g yeast extract dissolved in 500 ml H_2O. Media were autoclaved and 500 µl of 50 mg/ml Amp added after the solution was cooled down. In order to make plates, 7 g of agar was added into the above mixture.

NZY/Amp: 10 g NZ amine, 5 g NaCl, 5 g yeast extract dissolved in 1 l H_2O. Media was autoclaved and then 12.5 ml of 1 M $MgCl_2$, 12.5 ml of 1 M $MgSO_4$, 20 ml 20 % w/v glucose and 1 ml 50 mg/ml Amp was added.

LB/Amp/XGal plates: As in LB/Amp plates above but with extra 500 µl (per 500 ml LB medium) of 40 mg XGal dissolved in 1 ml N'N' dimethylformamide.

SOC: 20 g bactotryptone, 5 g yeast extract, 2 ml of 5 M NaCl, 2.5 ml of 1 M KCl, 10 ml of 1 M $MgCl_2$, 10 ml of 1 M $MgSO_4$, 20 ml of 1 M glucose dissolved in 1 l H_2O.

2.2 Protein Biochemistry Materials and Methods

2.2.1 SDS PAGE

Protein samples were analysed by SDS Polyacrylamide gel electrophoresis. Depending on the resolution required, 7.5 % and 10 % acrylamide gels were used. In all samples before loading, x6 sample buffer was added. In the case where samples were needed under reducing conditions, the sample buffer contained 2-mercaptoethanol and was heated at 90 °C for 5 min before loading. In the case where samples were needed under non-reducing conditions 2-mercaptoethanol was excluded from the sample buffer and samples were not heated. Identification of proteins of interest was possible by comparison with kaleidoscope prestained standards (ranging from 200 to 6.5 kDa from BioRad). Recipes for resolving gel, stacking gel, electrode buffer and sample buffer are adopted from the standard Laemmli recipe (Laemmli 1970).

2.2.2 Recombinant protein expression

BL21 *E. coli* cells transformed with the pJC20 vector containing the Tm or the TnT1 gene of interest were streaked onto an LB/Amp agar plate and left to grow overnight at 37 °C. From this plate single colonies were picked and used to inoculate 3 ml of LB/Amp media to create mini cultures. Each of these minicultures was used to streak fresh LB/Amp agar plates. Typically 4 mini cultures were prepared for each protein of interest. The minicultures were grown at 37 °C until an OD_{600} of 0.6 was obtained. Then the minicultures were induced by IPTG (100 mg/l) and incubated for a further 3h. 0.5 ml of each miniculture before and after induction with IPTG were aliquoted out and the cells were centrifuged down at 6400 rpm for 7 min. Cells were resuspended in 50 µl H_2O and 10 µl sample buffer and loaded onto 10% SDS gels. From the gel the miniculture that gave the best protein expression level was detected and used for a large scale protein expression. This was achieved by transferring a single colony from the LB/Amp agar plate of the selected miniculture into 1l of NZY/Amp media. The cells were grown at 37 °C until OD_{600} reached 0.4-0.6 and then induced with 100 mg/l IPTG for 3 h. The cells were then centrifuged at 6,000 rpm for 20 min and the cell pellet stored at -20 °C.

2.2.3 Recombinant protein purification

2.2.3.a Recombinant Tm purification with an Ala-Ser N-terminal extension

Pellets of Tm expressing cells were resuspended in 30 ml of ice-cold lysis buffer (0.3 M NaCl, 20 mM TRIS pH 7.5, 5 mM EGTA) and homogenised. Cells were then lysed on ice by sonication (2 min sonication followed by 1 min rest and another 2 min sonication). The lysate was transferred to an 80 °C waterbath and incubated for 10 min. During this step most of the lysate contaminant proteins were denatured but Tm is heat stable and after cooling on ice Tm could be refolded. After cooling on ice the lysate was centrifuged at 10,000 rpm for 20 min and most of cell debris was pelleted down. The supernatant containing Tm was collected and the pH dropped to 4.6 to precipitate Tm. After centrifugation at 10,000 rpm for 20 min Tm was pelleted down.

The Tm pellet was then resuspended in buffer A (0.1 M NaCl, 5 mM $MgCl_2$, 5 mM KPi pH 7) and treated with 100 µl DNase (10 mg/ml) and 100 µl RNase (10 mg/ml) and incubated for a minimum of 1 h at 4 °C. Tm was then purified by FPLC using the 5 ml anion exchanger HiTrap Q HP sepharose column (from Amersham Pharmacia). Elution of Tm from the column occurred at 40-60 % buffer B (1 M NaCl, 5 mM $MgCl_2$, 5 mM KPi pH 7) using a linear gradient 0-90 % buffer B. The purification onto the HiTrap Q HP column was repeated twice to obtain a Tm sample free of protein and nucleotide contaminants (as shown in fig 2.3). This was achieved by pooling together the Tm-containing fractions at the end of each run, precipitating Tm by dropping the pH to 4.6, and pelleting the sample by centrifugation as described previously. Finally the Tm pellet was resuspended in buffer A in order to prepare it for the next purification run.

In the final purification run fractions containing Tm were collected and Tm was precipitated by pH cut to 4.6. Tm was then centrifuged at 10,000 for 20 min and the pellet was resuspended in 3 ml of 5 mM TRIS buffer pH 7. Tm was then ultracentrifuged at 100,000 rpm for 20 min to precipitate any impurities. Using the Beer-Lambert law ($A = \varepsilon c l$), the concentration of the purified Tm was then calculated by measuring the absorbance A using a UV spectrophotometer at 280 nm. The value of ε is 17,880 l mol^{-1} cm^{-1} and 18,130 l mol^{-1} cm^{-1} for α Tm and β Tm respectively. A typical yield of Tm purification was 50 mg/l of culture.

Using the above method wild type AS- α Tm and AS- β Tm as well as mutant AS-α^{E180G} Tm and AS-α^{D175N} Tm were purified. All purified products had the expected molecular mass as measured by mass spectrometry (section 3.6).

In any of the experiments that involved recombinant Tm, all of the Tm used had the Ala-Ser N-terminal extension.

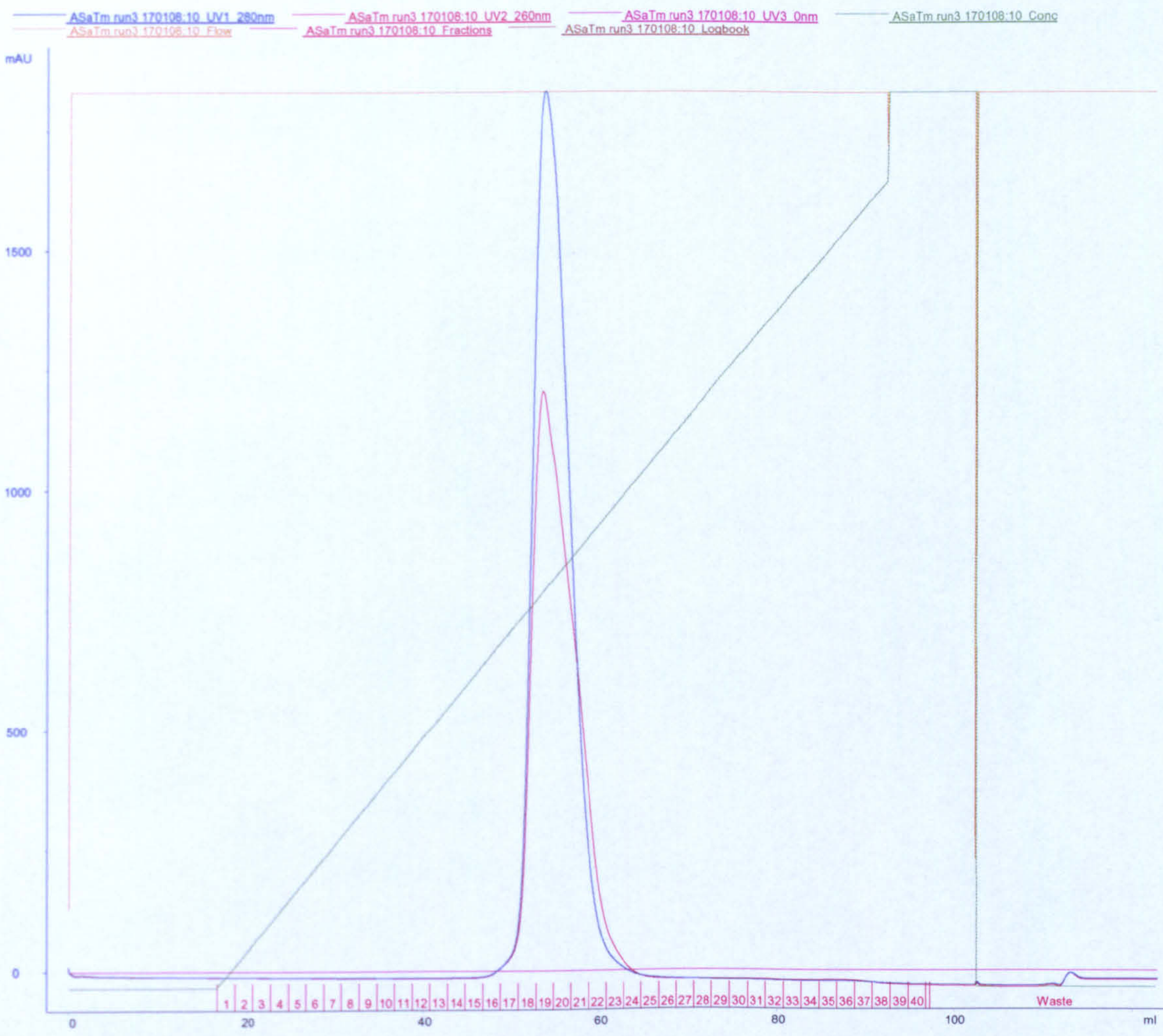

Fig 2.3: α Tm purification on HiTrap Q HP sepharose column. In blue the protein peak measured in absorbance units at 280 nm. The red peak corresponds to the absorbance measurement at 260 nm. Protein is eluted by a linear gradient of 0.1 – 1 M NaCl shown in green. Protein elution occurs at ~40-60 % buffer B (fractions 17-23). y axis shows absorbance at 280 nm and x axis is the volume of buffer in ml passed through the column. The red numbers on x axis indicate the fraction tubes number. This was the third/final purification run of α Tm, thus sample is free from nucleotide or protein contaminants.

2.2.3.b Strep-tagged Tm purification

The Strep-tagged proteins were purified using a Strep-Tactin column following the steps of the purification cycle as shown in figure 2.4.

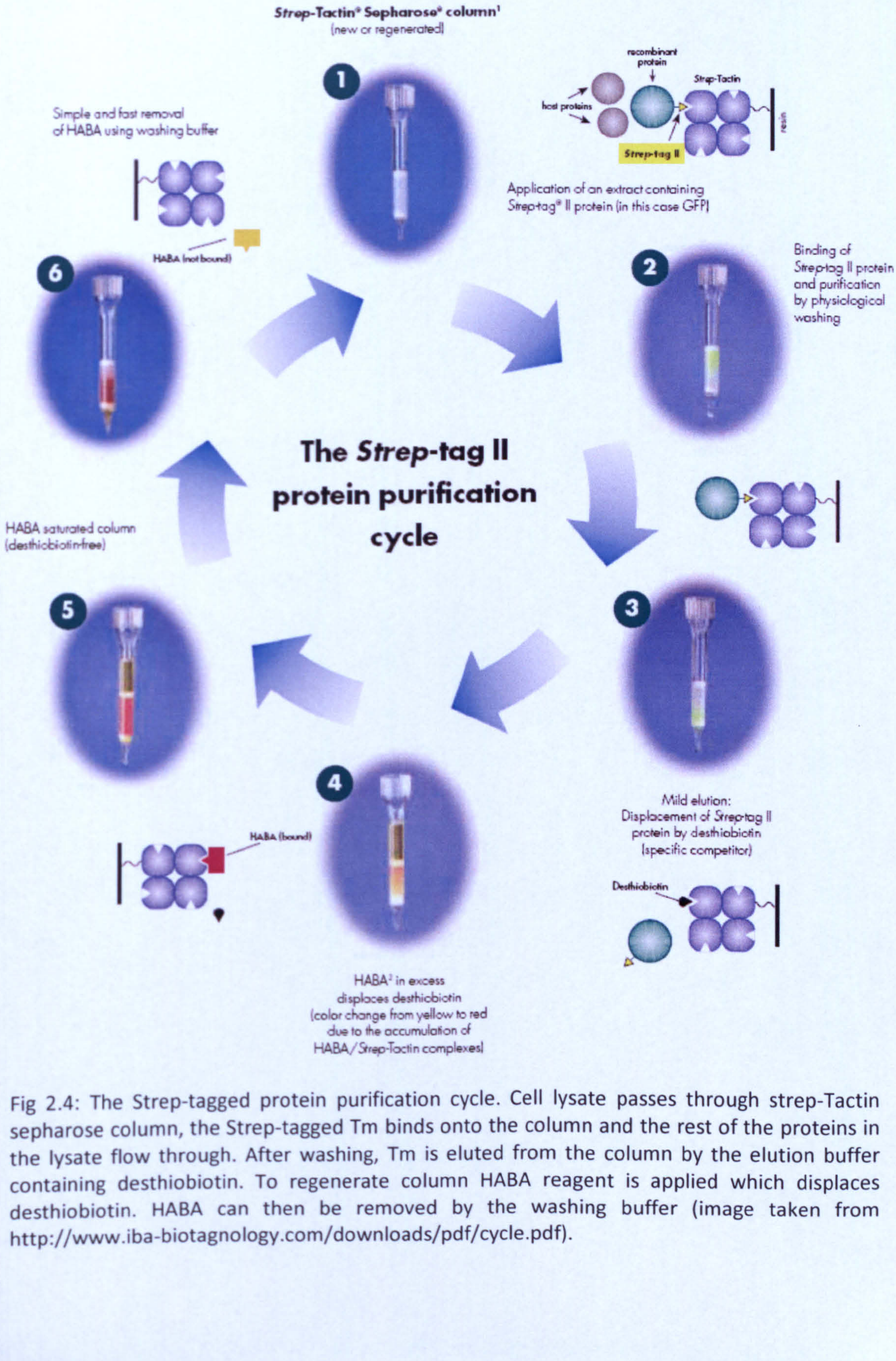

Fig 2.4: The Strep-tagged protein purification cycle. Cell lysate passes through strep-Tactin sepharose column, the Strep-tagged Tm binds onto the column and the rest of the proteins in the lysate flow through. After washing, Tm is eluted from the column by the elution buffer containing desthiobiotin. To regenerate column HABA reagent is applied which displaces desthiobiotin. HABA can then be removed by the washing buffer (image taken from http://www.iba-biotagnology.com/downloads/pdf/cycle.pdf).

Pellets of BL21 cells expressing the Strep-tagged Tm, were resuspended and homogenised in 30 ml lysis buffer (0.3 M NaCl, 20 mM TRIS pH 7.5, 5 mM EGTA). Cells were then lysed on ice by sonication (2 min sonication followed by 1 min rest and another 2 min sonication). The lysate was centrifuged twice at 12,000 rpm for 30 min to spin down cell debris. The Strep-tagged Tm was then precipitated by dropping the pH to 4.7 and pelleted down by centrifugation at 10,000 rpm for 20 min. The Tm pellet was then resuspended in 12 ml of Strep-Tactin column wash buffer (Buffer W = 150 mM NaCl, 1 mM EDTA, 100 mM Tris-Cl pH 8) and ultracentrifuged at 100,000 rpm for 20 min. The cleared lysate in the supernatant was collected and applied onto the Strep-Tactin column previously equilibrated with Buffer W. The Strep-Tactin column was a gravity flow column packed with 3 ml Strep-Tactin sepharose. Thus purification of the Strep-tagged proteins occurred manually and not via an FPLC machine.

After applying the Strep-tagged protein, the column was then washed 5 times with 1 CV (i.e. column volume) of Buffer W. The bound Strep-tagged Tm was eluted by applying 6 times 0.5 CV elution buffer (Buffer E = 150 mM NaCl, 1 mM EDTA, 100 mM Tris-Cl pH 8, 2.5 mM desthiobiotin). In the elution buffer desthiobiotin acts as a specific competitor of Strep-tagged Tm for the Strep-Tactin matrix. After elution of the protein, the column was regenerated by washing with regeneration buffer R (Buffer R = 150 mM NaCl, 1 mM EDTA, 100 mM Tris-Cl pH 8, 1 mM hydroxy azophenyl benzoic acid (HABA)). The HABA reagent in buffer R in excess displaces desthiobiotin from Strep-Tactin column. As a final step, the column was washed with buffer W to remove HABA and stored at 4 °C. To monitor the purification of Strep-tagged Tm, small aliquots from the washing and the elution samples were run on 10 % SDS gels. Because of the small capacity of the gravity Strep-Tactin column that was used, a quite large amount of the Strep-tagged protein was found in the flow through. This protein was collected and subjected to a second purification cycle. The purification yield of the Strep-tagged Tm using the 3 ml Strep-Tactin gravity column was ~20 mg per litre of bacterial culture.

The result of Strep-tagged protein purification is shown in section 3.3.1.

2.2.3.c His-tagged Tm purification

Pellets of BL21 cells expressing the His-tagged Tm were resuspended and homogenised in 30 ml lysis buffer (0.3 M NaCl, 50 mM NaH_2PO_4, pH 8). Cells were then lysed on ice by sonication (2 min sonication followed by 1 min rest and another 2 min sonication). The lysate was centrifuged twice at 12,000 rpm for 30 min to spin down cell debris. The His-tagged Tm was then precipitated by dropping the pH to 4.8 and pelleted down by centrifugation at 10,000 rpm for 20 min. The Tm pellet was resuspended in 12 ml of lysis buffer and ultracentrifuged at 100,000 rpm for 20 min. The cleared lysate was then applied onto a 5 ml gravity NiNTA column and the His-tagged protein was purified manually and not via an FPLC machine. In figure 2.5 below the interaction of the NiNTA matrix with a 6x His tag protein is shown schematically.

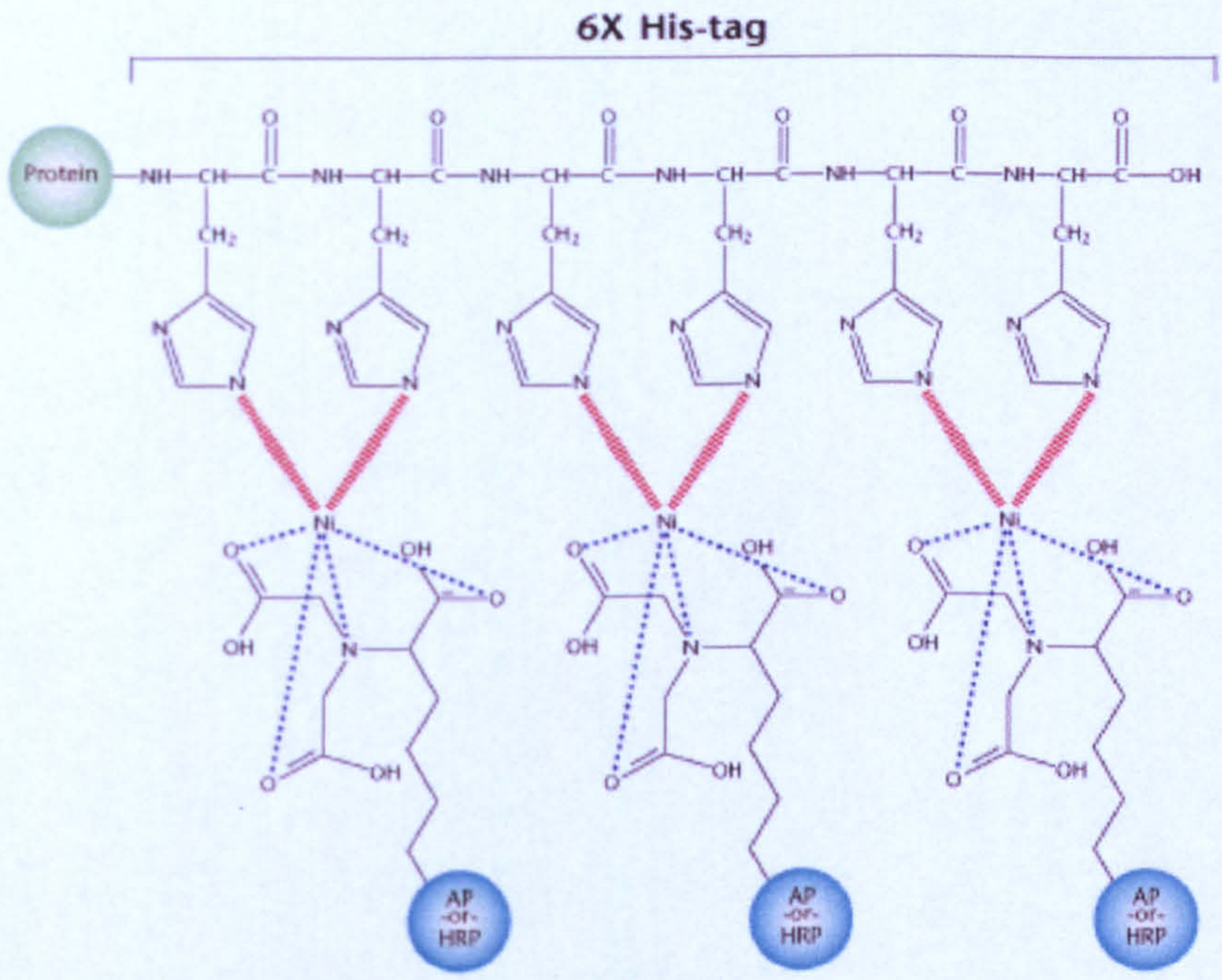

Fig 2.5: Interaction of a 6x His tagged protein with immobilised Ni ions (in our procedure on a highly cross-linked NTA- agarose matrix) (taken from http://www.kpl.com/images/His-tagged2.jpg).

The NiNTA column was then washed to remove any unbound or non-specific bound proteins of the cleared lysate 4 times with 4 CV Wash Buffer (0.3 M NaCl, 50 mM NaH_2PO_4 pH 8, 20 mM imidazole). The His-tagged Tm was then eluted by washing 6 times with 1 CV Elution Buffer (0.3 M NaCl, 50 mM NaH_2PO_4 pH 8, 250 mM imidazole). Imidazole competes with the His-tagged proteins for the immobilised Ni ions therefore

the His-tagged protein was eluted by the high concentration of imidazole in the elution buffer. The column can be regenerated by washing with 5 CV 0.5 M NaOH followed by 5 CV H_2O and 3 CV 20 % ethanol. To monitor the purification of His-tagged Tm, small aliquots from the washing and the elution samples were run on 10 % SDS gels. As in the case of Strep-tagged Tm purification, a significant amount of the His-tagged protein was found in the flow through because of the small capacity of the gravity NiNTA column. The unbound protein was collected from the flow through and subjected to a second purification cycle on the NiNTA column. The purification yield of His-tagged Tm using 5 ml NiNTA gravity column was ~20 mg of protein per litre of bacterial culture. The result of a His-tagged protein purification is shown in section 3.3.1.

The purified His-tagged protein was then dialysed overnight to remove imidazole. Because the protein was to be used in the heterodimer formation experiment, it was dialysed in the experimental buffer (0.5 M KCl, 20 mM KPi pH 7, 5 mM $MgCl_2$). Due to the high salt concentration in this buffer and also because the sample was kept diluted in a large volume (~1 mg/ml), there were no problems with the His-tagged Tm precipitation upon removal of imidazole.

2.2.3.d TnT1 Purification

Pellets of BL21 cells that expressed TnT1 were resuspended and homogenised in 30 ml lysis buffer (0.3 M NaCl, 20 mM TRIS pH 7.5, 5 mM EGTA) in which a protease cocktail inhibitor tablet (from Roche) was dissolved. Cells were then lysed on ice by sonication (2 min sonication followed by 1 min rest and another 2 min sonication). The lysate was then ultra-centrifuged at 100,000 rpm for 20 min at 4 °C. The supernatant was kept and treated with 200 µl DNase (10mg/ml) and 200 µl RNase (10mg/ml) and incubated at 4 °C for 2 h. After this incubation, TnT1 was precipitated by dropping the pH to 4.4. The sample was then centrifuged and the pellet of TnT1 was resuspended and homogenised in 30 ml of DEAE buffer A (6 M urea, 50 mM Tris-HCl, 1 mM EGTA, 1.4 mM β-mercaptoethanol, pH 8). The sample was then applied onto the DEAE sepharose column and proteins were eluted using a salt gradient from 0 to 0.6 M KCl (i.e. DEAE buffer B: 0.6 M KCl, 6 M urea, 50 mM Tris-HCl, 1 mM EGTA, 1.4 mM β-

mercaptoethanol, pH 8) over 24 column volumes (120 ml). At the end of this first purification cycle aliquots from the various fractions were loaded onto 10 % SDS gels. Those fractions containing TnT1 were pooled together, dialysed in equilibration buffer A and a second purification cycle was performed under exactly the same conditions as in the first cycle. Again, aliquots from the various fractions were loaded onto 10 % SDS gels to check for the presence of TnT1. The fractions containing TnT1 appeared free from most protein contaminants and were pooled together. However, there were still nucleotide contaminants present (as shown in chromatograms by the peak showing absorbance at 260 nm) but these should not interfere with the future experiments where the TnT1 would be involved. The concentration of each TnT1 protein was measured by the Bradford method instead of the routinely used UV spectroscopy to avoid inaccuracies due to the nucleotide contamination. The purification yield was ~25 mg of TnT1 per litre of bacterial culture. Because the TnT1 protein is quite sensitive to degradation, it was aliquoted into small volumes (50 µl) prior storing at - 20 °C; after defrosting an aliquot for use, the remaining sample was disposed.

The results of TnT1 purification are shown in section 5.3.

2.2.4 Purification of Native proteins from rabbit muscle tissue

Muscle tissue dissected from the backs and legs of rabbits was used as the source of all of the native proteins used in the experiments. Purification of the native proteins is a routine procedure in the group and was carried out by the lab technicians. To start the purification, the muscle was minced and dialysed in 3 l of Guba-Straub buffer (100 mM KH_2PO_4, 50 mM K_2HPO_4, 0.3 M KCl). Then the mixture was stirred for 15 min and centrifuged at 4,500 g for 30 min. After centrifugation, the thin filaments were pelleted down while myosin remained in the supernatant (Spudich and Watt 1971).

Myosin was purified as described by Margossian and Lowey (Margossian and Lowey 1982). Myosin from supernatants was dialysed in high salt buffer and glycerol stocks of myosin were prepared before storage at -20 °C. When S1 only needed for experiments myosin was precipitated from glycerol stock by mixing with large volume

of H_2O and the pellet was then dissolved in digestion buffer (125 mM KCl, 10 mM KPi, 2 mM EDTA, 2 mM DTT pH 6.5). Chymotrypsin was added (0.1 mg per ml of solution) and the mixture was stirred for 10 min exactly at 23 °C. Chymotrypsin digestion was quenched by adding 0.5 mM PMSF. The digested S1 was then further purified by ion exchange chromatography using the DEAE-sephacel column. Elution of protein was achieved by a 0-250 mM KCl gradient in presence of 50 mM imidazole at pH 7. The eluted S1 was freeze-dried in presence of sucrose and stored at -20 °C. Before experimental use, S1 powder was dialysed against 30 mM KCl, 20 mM MOPS, 5 mM $MgCl_2$ at pH 7.

The thin filament pellets (obtained after centrifugation for the separation of myosin as explained before) were dialysed in actin buffer 1 (4 % $NaHCO_3$, 0.1 mM $CaCl_2$) and filtered through a cheesecloth. The solid residue was then dialysed in actin buffer 2 (10 mM $NaHCO_3$, 10 mM Na_2CO_3, 0.1 mM $CaCl_2$) and filtered through a cheesecloth again. The solid residue was washed in excess of acetone and then sandwiched between blotting papers and left to air-dry for a couple of days. The dried acetone powder preparation containing the G-actin with the Tm/Tn complex was then stored at -20 °C.

The dried acetone powder was then dissolved in a pre-chilled at 0 °C buffer containing 10 mM TRIS, 0.5 mM ATP, 0.2 mM $CaCl_2$, 1 mM DTT pH 8.0 and filtered through cheesecloth. This resulted in separation of (1) G-actin passed through in the filtrate from (2) the Tm/Tn mixture that remained in the solid residue.

1) The filtrated G-actin was then centrifuged at 30,000 rpm and collected from the supernatants and then polymerised by stirring for 1 h in 100 mM KCl and 2 mM $MgCl_2$ buffer. By centrifugation at 30,000 rpm the polymerised F-actin was pelleted down. F-actin was resuspended and dialysed overnight in de-polymerising buffer (5 mM TRIS, 0.2 mM $CaCl_2$, 1 mM NaN_3 pH 7.5), and then centrifuged. G-actin collected from supernatants was then re-polymerised and centrifuged. The pelleted F-actin was then resuspended in experimental buffer (50 mM KCl, 20 mM MOPS, 5 mM $MgCl_2$, 1 mM NaN_3 pH 7). In cases where F-actin needed labelling for fluorescence experiments, actin was treated with

pyrene iodoacetamide solution (Criddle *et al.* 1985). Pyrene was added into the F-actin solution (0.6 -1 % w/w pyrene/actin) and the mixture was wrapped in foil and left stirring for 18 h. The mixture was then centrifuged at low speed (8,000 rpm) to precipitate any unbound pyrene and then at higher speed (30,000 rpm) that precipitated the pyrene-labelled F-actin. Pellets were then resuspended in experimental buffer (100 mM KCl, 20 mM MOPS, 5 mM $MgCl_2$, 1 mM NaN_3 pH 7). To obtain pure F-actin, clean from Tn and Tm contaminants, the unlabelled or the pyrene labelled F-actin was treated with high salt buffer. KCl was added in the actin solution to a final concentration of 0.6 M and the solution incubated for 1 h at room temperature. Then the sample was ultra-centrifuged at 100,000 rpm for 20 min to pellet down the clean F-actin. The actin pellet was resuspended and dialysed in experimental buffer (100 mM KCl, 20 mM MOPS, 5 mM $MgCl_2$, 1 mM NaN_3 pH 7). In cases where actin was needed in very low concentrations, it was stabilised by the fungal toxin phalloidin. Phalloidin was added into pyrene actin solution in a 1:1 ratio and the mixture was incubated at 4 °C for at least 4 h prior to use.

2) The solid residue containing the Tm/Tn mixture was dissolved in 10 mM TRIS, 20 mM DTT, 1 mM NaN_3 at pH 8, stirred for 5 h at room temperature and then filtered through cheesecloth again. This time the Tm/Tn mixture passed through in the filtrate. The filtrate was then subjected into 40 % ammonium sulphate cut (by adding slowly ammonium sulphate into the solution continuously stirred on ice) and then the sample was centrifuged (9,000 rpm for 30 min). The pellet was discarded and the supernatant brought to 60 % saturation in ammonium sulphate. The mixture was again centrifuged at 9,000 rpm for 30 min and the Tm/Tn containing pellet was resuspended and dialysed in 5 mM TRIS, 0.5 mM DTT, pH 8 buffer.

2.2.5 Purification of Tm and Tn complex from the native Tm/Tn mixture

The native Tm was further purified from the Tm/Tn mixture that was obtained as explained in section 2.2.4 above. The Tm/Tn mixture was dialysed overnight in buffer 1 (50 mM KCl, 0.5 mM DTT, 10 mM TRIS, pH 8). The dialysed mixture was then adjusted to a final concentration of 1 mg/ml using buffer 1. Then the mixture was pH cut by dropping 0.1 M HCl very slowly into the solution to bring its pH to 4.6 to precipitate down Tm and then stirred for 20-30 min on ice. This was followed by centrifugation at 12,000 rpm for 20 min and Tm was pelleted down. Pellets containing Tm were resuspended in buffer 1 using 85 % of the starting volume. Supernatants were also collected and used for the preparation of troponin. The pH cut was repeated twice more and Tm pellets were resuspended using 75 % and 65 % of the starting volume. The final Tm pellet was then resuspended in buffer 2 (250 mM KCl, 5 mM TRIS, 0.2 mM EDTA, 0.2 mM DTT, pH 7.5) using 45 % of the starting volume. This was followed by a 53 % ammonium sulphate cut to precipitate any contaminant Tn and the sample was then stirred on ice for 30 min and then centrifuged at 12,000 rpm for 20 min. Supernatant containing Tm was collected and placed in a 30 °C waterbath for 30 min. This step precipitated Tm which was then centrifuged at 12,000 rpm for 30 min. The pellet Tm was then dialysed in storage buffer (10 mM KCl, 10 mM MOPS, 0.2 mM EDTA, 0.2 mM DTT, 1 % w/v sucrose, pH 7.5) , aliquoted and stored at -20 °C.

The supernatants containing Tn were adjusted to pH 8. Then 70 % ammonium sulphate cut was used to precipitate Tn and the sample was stirred on ice for 30 min. The sample was then centrifuged at 12,000 rpm for 30 min and Tn was pelleted down. The pellet Tn was resuspended and dialysed in storage buffer (10 mM KCl, 10 mM MOPS, 0.2 mM EDTA, 0.2 mM DTT, 1 % w/v sucrose, pH 7.5) aliquoted and stored at -20 °C.

Protein concentrations were estimated by UV spectroscopy using extinction coefficient ε for Tm = 0.24 mg^{-1} ml cm^{-1} (MW = 66 kDa) and ε for Tn = 0.45 mg^{-1} ml cm^{-1} (MW = 70 kDa). Each preparation yielded roughly 9 mg of native Tm and 5 mg of native Tn.

2.2.6 Mass spectrometry

Electrospray Mass spectrometry was performed in order to verify that the various purified recombinantly expressed proteins were of the correct molecular mass. Proteins were dialysed in 5 mM Tris buffer at pH 7. The spectrometry was performed by Kevin Howland in Biomolecular Science facility of the department. The Tm proteins tested were found to be of the expected molecular mass and the results are shown in section 3.6. The TnT1 wild-type and mutant proteins had an extra mass, and this is explained in section 5.3.

2.2.7 Extinction coefficients of various Tm dimers

To estimate the concentration of the various Tm dimers after measuring their absorbance at 280 nm the following extinction coefficients (in l mol^{-1} cm^{-1} units) were used.

Tagged Dimers		Untagged dimers	
Strepα-Strepα	28880	αα	17880
Strepβ-Strepβ	29130	ββ	18130
Hisα-Hisα	17880	αβ	18005
Hisβ-Hisβ	18130	α^{D175N}-β	18005
Strepα-α^{D175N}	23380	α^{E180G}-β	18005
Strepα-α^{E180G}	23380	α-α^{D175N}	17880
α- Hisβ	18005	α-α^{E180G}	17880
α^{D175N}-Strepβ	23505	α^{D175N}- α^{D175N}	17880
α^{E180G}-Strepβ	23505	α^{E180G}- α^{E180G}	17880

2.3 Biochemical techniques for Protein Characterisation

2.3.1 Thermal unfolding of Tm using Circular Dichroism

The thermal stability of various Tm homodimer and heterodimer samples was measured by circular dichroism (CD). The measurements were carried out in Mill Hill institute using a Jasco J-715 spectropolarimeter under the supervision of Dr Stephen Martin. The scan was performed automatically over a temperature range from 5 to 65 °C using a Peltier instrument. The heating rate was 1.5 °C per min. The data were collected at a constant 222 nm wavelength that can report for changes in the α-helical content of the proteins. The protein concentration was 5 μM and the sample was dissolved in 200 μl of the CD buffer (0.5 M NaCl, 20 mM KPO_4 at pH 7.0, 5 mM $MgCl_2$, 1 mM DTT) (Coulton *et al.* 2008). Stoppered 1 mm cuvettes were used for the measurements. Because the heterodimer Tm samples had been previously cross-linked during their formation, each sample's thermal denaturation scan was repeated twice. Therefore, each protein sample was heated up to 65 °C, then cooled back to 5 °C and then the same sample was unfolded for a second time under exactly the same conditions. By this method structural changes due to cross-link breakage in the heterodimer molecule after heating during the first scan or structural changes due to the recombination of the denatured heterodimer subunits into a population of homodimers and heterodimers would show up if the first thermal scan was different from the second scan.

The Tm thermal unfolding results are shown in section 4.2

2.3.2 Actin cosedimentation assays

In order to calculate the affinity of a Tm sample for actin, actin co-sedimentation assays were performed. The basis of this experiment is that filamentous actin can be pelleted down when ultra-centrifuged at 100,000 rpm. So if any protein is bound on the actin filaments, it will be co-sedimented together with actin in the pellet. Any protein that is not bound onto actin is expected to be in the supernatant after ultra-centrifugation.

In the cosedimentation assays the concentration of actin was constant (9 μM) and the concentration of Tm was varied (0.2 - 5 μM). The specific concentrations of actin and Tm were chosen for the cosedimentation assays because first they were within range for actin affinity and second they were quantifiable when loaded on the SDS gels. Tm was mixed with actin and the volume in each centrifuge tube was adjusted to 100 μl with the experimental buffer (100 mM KCl, 20 mM MOPS, 5 mM $MgCl_2$, pH 7). The mixture was incubated for 1 h at room temperature for binding to occur.

Control samples were prepared as well that contained Tm alone or actin alone. It was important to check that the Tm would be found in the pellets only because it was cosedimented with actin. Therefore in the control Tm sample that lacked actin, after ultra-centifugation Tm should stay in the supernatants. On the other hand, in the control actin sample, F-actin should be pelleted down after ultra-centrifugation. The actin used in the cosedimentation assays was previously treated with high salt buffer to remove any Tm and Tn contaminants (as explained in pg 81) and dialysed afterwards in the cosedimentation experimental buffer.

Then all tubes were ultra-centrifuged at 100,000 rpm for 20 min at 20 °C. After this step, the pellets were separated from the supernatants. Pellets were resuspended in 100 μl H_2O and 20 μl of sample buffer was added. In 50 μl of supernatants 10 μl of sample buffer was added. Then 10 μl from pellets and 10 μl of supernatants were loaded onto 10 % SDS gels. After electrophoresis, the gels were stained using a standard Coomassie blue stain solution and then destained.

An example of the pellets and supernatant gels of a cosedimentation assay is shown in fig 2.6.

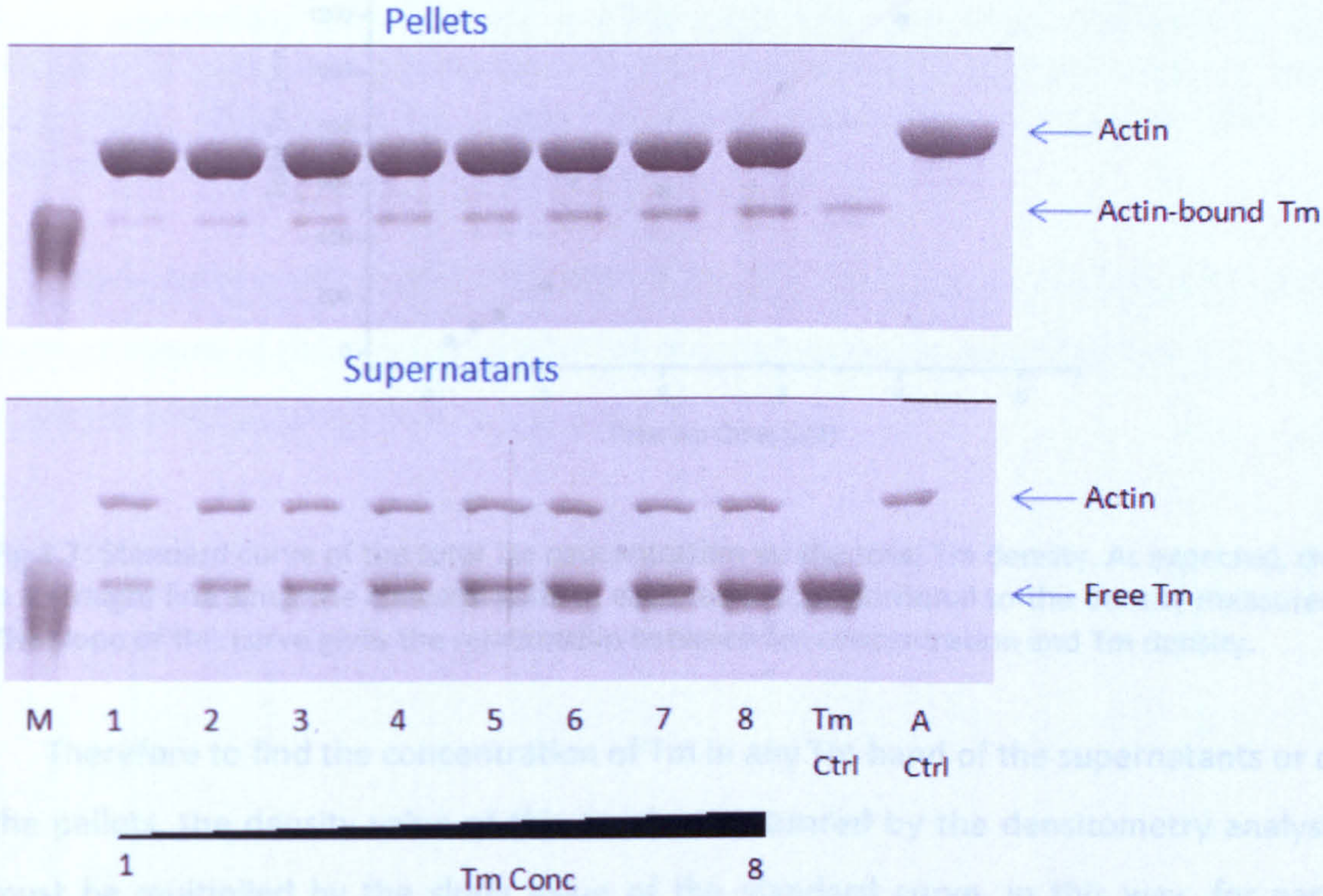

Fig 2.6: Actin and Tm cosedimentation assay. The two proteins were mixed in a tube and ultracentrifuged. Pellets were separated from supernatants and loaded onto SDS gels. Actin was constant (9 μM) and Tm was increased (0.2- 5 μM in tubes 1-8 respectively). Control samples containing Tm alone or actin alone were also loaded. The Tm control sample showed that after ultracentrifugation most of Tm remained in supernatants. Therefore in samples 1-8, the presence of Tm in pellets is the result of the association and co-sedimentation of Tm with actin.

The density of each protein band on the pellets and supernatants SDS gels was then measured using the ScionImage software. For each sample 1-8 of the assay, the total density of Tm was estimated by adding the densities of the Tm bands from both the pellet and the supernatant gels. By plotting for each sample the total amount of Tm density as calculated after the densitometry analysis versus the known Tm concentration as used in the beginning of the experiment, a standard graph was created. The slope of this graph shows the relationship between Tm concentration and Tm density (fig 2.7).

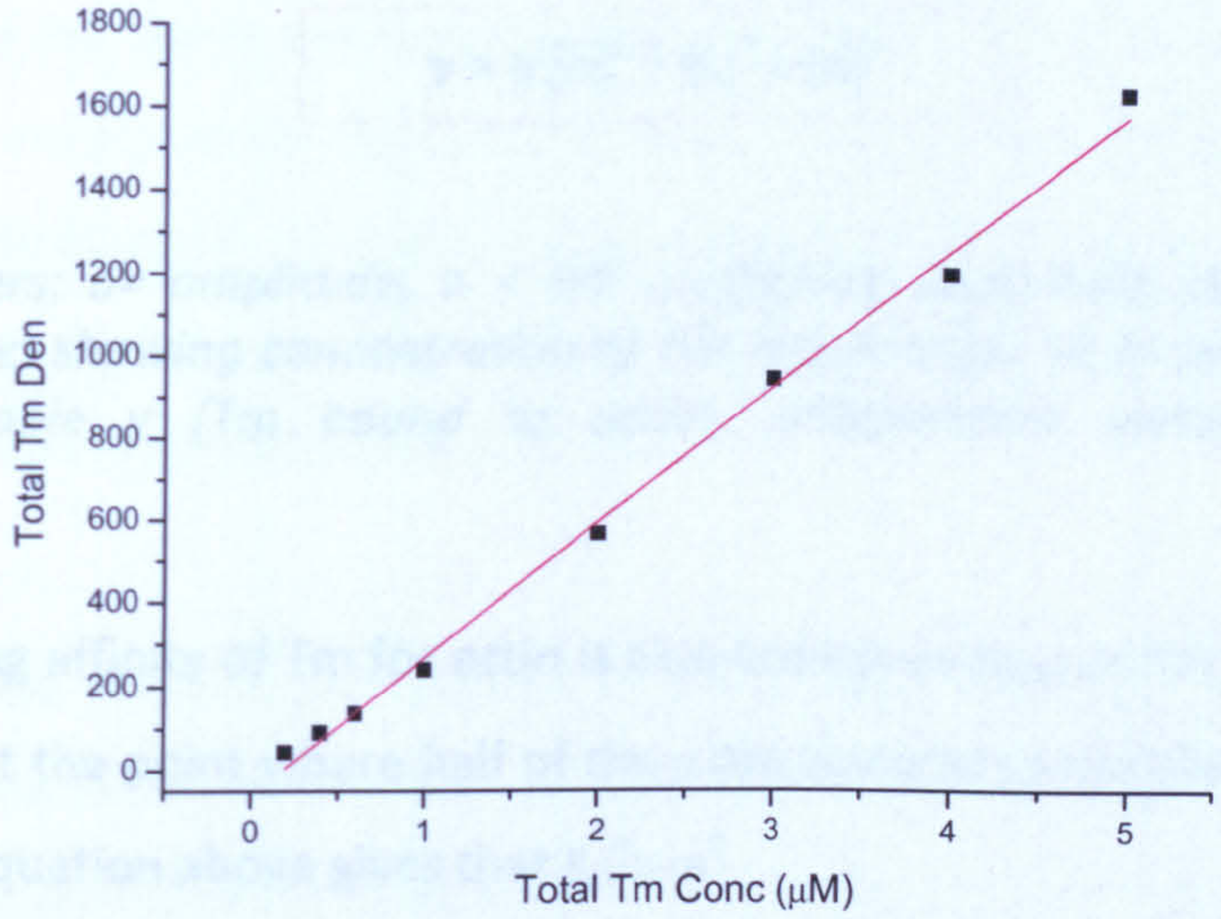

Fig 2.7: Standard curve of the total Tm concentration vs. the total Tm density. As expected, this is a straight line since the concentration in each tube is proportional to the density measured. The slope of this curve gives the relationship between Tm concentration and Tm density.

Therefore to find the concentration of Tm in any Tm band of the supernatants or of the pellets, the density value of this band as measured by the densitometry analysis must be multiplied by the slope value of the standard curve. In this way, for each sample of the assay, the concentration of Tm found free in the supernatants can be estimated.

To obtain information for the binding affinity of Tm to actin, as described by the following reaction:

$$Tm_{free} + Actin \rightarrow Tm_{bound} \cdot Actin$$

one must know the relationship between the reactant (free Tm) and the product (bound Tm).

When the free Tm concentration is plotted against the bound Tm, a typical sigmoid curve can be obtained. The sigmoidal shape of the graph, suggests that Tm binding to actin is cooperative. The graph can be fitted using Origin software with the Hill equation shown below, which describes cooperative binding. From the fit the binding affinity of Tm for actin (K_d) and the Hill coefficient (n) of binding were estimated (fig 2.8).

$$y = a\,[x]^n / K_d{}^n + [x]^n$$

Fitting *parameters: a= amplitude,* n *= Hill coefficient, describing cooperativity,* K_d *= midpoint of curve, showing concentration of Tm required for 50 % saturation of actin. Dependent variable y (Tm bound to actin), Independent variable x (free Tm concentration)*

The K_d binding affinity of Tm for actin is also known as $K_{50\%}$ or the mid-point of the curve, because at the point where half of the actin becomes saturated then y = ½ and solving the Hill equation above gives that $K_d{}^n = x^n$.

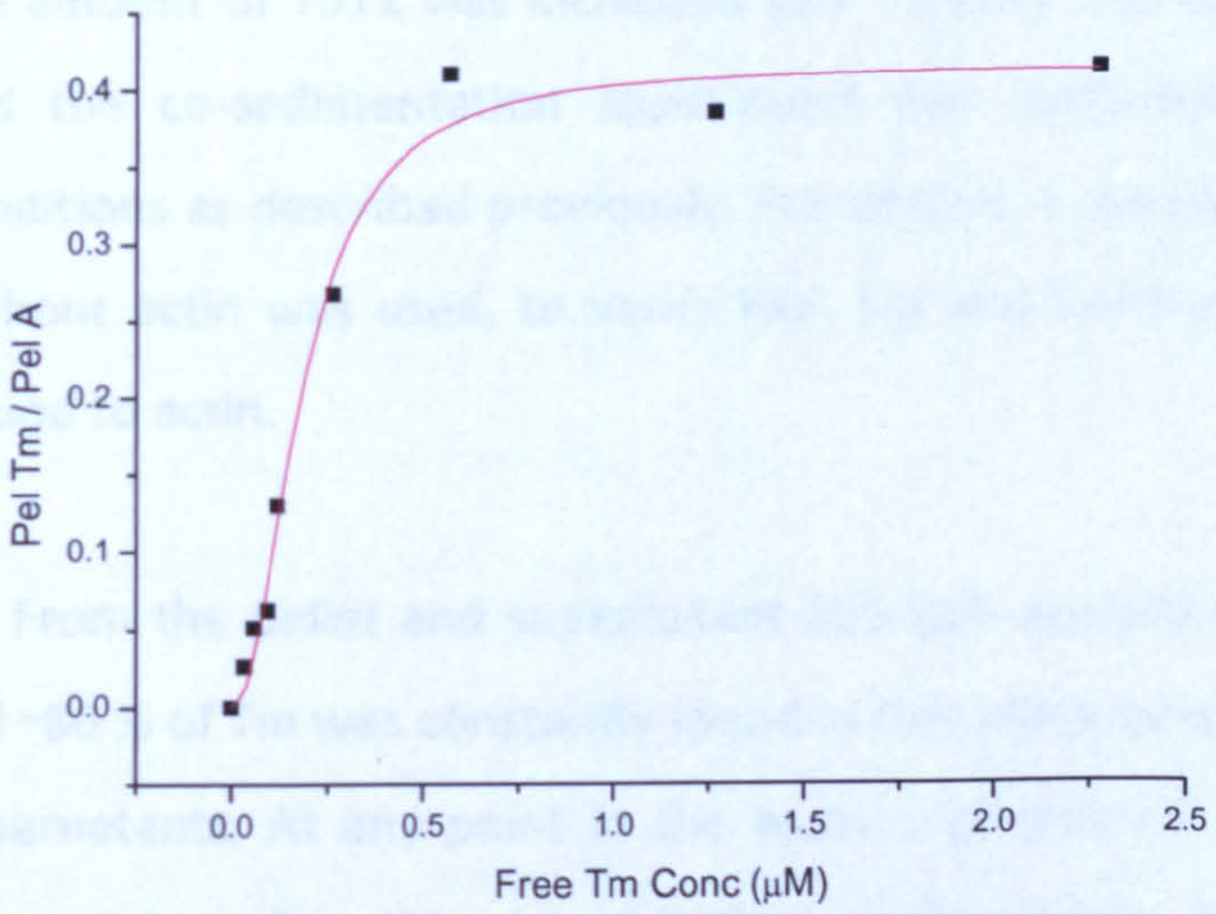

Fig 2.8: Calculation of the Tm binding affinity for actin. The free Tm densities from the supernatant gels were converted into free Tm concentrations (by multiplying with the slope value of the standard curve shown in fig 2.7) and plotted against the bound to actin Tm (for correction bound Tm / pellet actin); a sigmoidal curve was obtained as a result of Tm's cooperative binding. The actin binding affinity was estimated by fitting to the Hill equation.

In order to correct for sample loading and pipetting errors the pellet Tm was divided by the pellet of actin. Therefore, if for example in a sample of the assay more actin was pipetted in the tube (actin is quite viscous and such errors are possible), then more Tm would be found in the pellets. By dividing the pellet of Tm with the pellet of actin, the bound Tm per unit of actin for each sample is estimated, thus enhancing the accuracy of the measurement.

Results of the cosedimentation assays of Tm with actin are shown in section 4.3.

A variation of the above experiment of the cosedimentation of Tm with actin, is to include the TnT1 protein in the mixture. By adding a constant amount of excess TnT1 in each vial, the affinity of Tm for actin in the presence of TnT1 can be estimated (using exactly the same analysis as before). The results of this type of cosedimentation experiments are shown in sections 4.3 and 5.4.

Using the basic principle of the actin cosedimentation assay, the affinity of the various TnT1 constructs for Tm can also be estimated. In these experiments the amounts of actin and Tm were constant in each vial (9 μM actin and 2 μM Tm), while the amount of TnT1 was increased (0.4 - 6 μM). The samples were incubated for 1 h and the co-sedimentation experiment was performed under the same standard conditions as described previously. For control, a sample containing Tm and TnT1 only without actin was used, to verify that Tm and TnT1 were pelleted down only when bound to actin.

From the pellet and supernatant SDS gels analysis, it was estimated that in each vial ~80 % of Tm was constantly found in the pellets and the rest 20 % was found in the supernatants. At any point in the assay a portion of TnT1 was bound onto the Tm filament in pellet; the rest of TnT1 was found free in supernatants. The TnT1 was binding to the Tm/Actin filaments found in the pellets until Tm became saturated. From this point on the amount of TnT1 was constant in pellets and increased in supernatants. The stoichiometry of TnT1 : Tm at saturation is expected to be 1:1, since one TnT1 molecule binds to every Tm overlap region along the Tm filament.

As in the Tm and actin cosedimentation experiment, the density of each protein band on the pellets and supernatants gels can be estimated using the ScionImage software. A standard graph of the total TnT1 concentration as used in the beginning of the experiment versus the total TnT1 density as measured by densitometry can be plotted for each sample of the assay. The slope of this linear graph can give the concentration of TnT1 per unit of density, thus the free TnT1 densities can be converted into free TnT1 concentrations by multiplying with this slope value. Plotting

the free TnT1 concentration versus the bound TnT1 and fitting the resulting curve into a hyperbola ($y = a [x] / K_d + [x]$), estimates the affinity K_d of TnT1 for Tm.

The cosedimentation experiments that were carried out for the measurement of the affinities of the various TnT1 proteins for Tm are shown in section 5.5.

2.3.3 Kinetic analysis of S1 binding on thin filaments by Stopped Flow

Binding of S1 onto actin filaments is a fast reaction and it can be monitored using the stopped-flow technique. The S1 binding on actin filaments labelled by pyrene fluorophore at Cys374 can be measured by monitoring the change in pyrene fluorescence. The stopped-flow machine that was used in the experiments is the SF-61DX2 spectrophotometer (from HiTech Scientific). Pyrene was excited at 365 nm and the fluorescence emitted was detected using a 389 nm cut off filter. The data was analysed using the Kinetasist software.

Because there are two reactants (i.e. actin filaments and myosin heads) that interact to give the acto-myosin product, the reaction followed is a second order. However, because second order reactions are very complex and difficult to analyse, the experiment is carried out under pseudo-first order conditions. To obtain a pseudo-first order reaction, one of the reactants must be in great excess over the second reactant. Thus in practice the reactant in excess should be constant throughout the course of the reaction.

There are two ways by which pseudo-first order conditions can be met; either when actin is in excess or when S1 is in excess. Therefore in the reaction of S1 binding on actin for the formation of the acto-myosin complex:

$$A + S1 \xrightarrow{k} A\text{-}S1$$

a) In the excess actin case, the actin concentration will remain unchanged throughout the reaction and the observed rate constant (k_{obs}) will have a linear relationship with the actin concentration. At the same time, the S1 concentration will be decreased exponentially:

$$[S1]_{(t)} = [S1]_0 e^{(-k_{obs}t)}$$

b) In the excess S1 case, the S1 concentration will be constant throughout the reaction and the observed rate constant will be a linear function of the S1 concentration. Actin will be decreased exponentially:

$$[A]_{(t)} = [A]_0 e^{(-k_{obs}t)}$$

In practice, in the excess S1 case, the initial binding of S1 on the thin filaments will be dependent on the actin sites available for binding. If a portion of the thin filaments is in the blocked state, then a lag phase is expected to be observed. That would correspond to an initial slow binding of S1 followed by an accelerated faster S1 binding phase. After the initial cooperative binding of S1 on actin, the actin filaments will be turned On to allow faster binding of the subsequent S1 molecules.

We chose S1 to be in excess over the thin filaments (5 μM S1 pushed against 0.5 μM actin, 0.2 μM Tm and 0.2 μM Tn syringe concentrations before mixing) in order to be economical with the quantity of Tm heterodimer used. Because actin was at low concentration it needed to be stabilised by phalloidin (as explained in pg 81). For the reconstitution of actin by the regulatory proteins a larger amount of Tm and Tn was used (instead of 7 actins: 1 Tm: 1 Tn) to ensure full thin filament reconstruction.

For each of Tm dimer of interest four experiments were performed. The first one served as control and only contained pyrene-actin pushed against S1. The second set was the binding of S1 to pyrene-actin reconstituted with the Tm dimer of interest. The third set monitored binding of S1 onto actin reconstituted with both Tm and Tn in the absence of Ca^{2+} (i.e. 2 mM EGTA in the buffer). The last set monitored binding of S1 to pyrene-actin decorated with Tm and Tn in the presence of Ca^{2+} (i.e. 1 mM $CaCl_2$ in the buffer). In every set of experiments binding of S1 to actin filaments caused a quenching of the pyrene fluorescence, as expected. The experiment was carried out in the

presence of 100 mM KCl, 20 mM MOPS, 5 mM $MgCl_2$, pH 7 buffer. The Tn used was the rabbit skeletal tissue purified Tn complex.

The results showing excess S1 binding on the actin filaments as monitored by the Stopped flow experiments are presented in section 4.4.

Chapter 3

Formation of Tropomyosin Heterodimers

3.1 Introduction

Although regulation of muscle contraction has been widely studied over a few decades now (Ebashi *et al.* 1971; Squire 1975), there are still areas that have not been fully investigated. One area that lacks important information is the regulation of skeletal or cardiac muscle contraction by different Tm dimers i.e. the homodimers vs. the heterodimers. In contrast to the skeletal Tm homodimers, which are well characterised (review by Perry 2001), there is very little known on skeletal Tm heterodimers mainly because their *in vitro* formation has not been successful. Apart from experiments where native skeletal Tm was used (mixture of homodimers and heterodimers), there is no information on pure skeletal Tm heterodimer characterisation.

The two skeletal isoforms α and β when expressed *in vivo* can be combined into both αα homodimers and αβ heterodimers, while the ββ homodimer is unstable and not found (Bronson and Schachat 1982). It is not at all clear what regulates the level of αα and αβ dimers in the different tissues and what are the functional consequences. In order to investigate the functional properties of the different Tm dimers, homodimers and heterodimers should be isolated and characterised separately. This could be

possible by two methods: A) using as starting material muscle tissue to be able to separate the native homodimers from heterodimers and B) by developing a method that will enable the formation of heterodimers *in vitro* using as starting materials bacterially expressed proteins and then compare the heterodimers to the well characterised homodimers.

To date there is no method available in literature for the *in vitro* formation of skeletal Tm heterodimers. However, there are methods that have been developed for the formation of smooth Tm heterodimers. In smooth muscle cells the αβ heterodimer is the predominant form and it can also be preferentially formed *in vitro*. Two independent studies (Lehrer and Qian 1990; Jancso and Graceffa 1991) showed that native smooth muscle homodimers via chain dissociation and chain exchange would preferentially form heterodimers. Coulton *et al* more recently made use of the method of Jancso and Graceffa to successfully assemble smooth heterodimers using bacterially expressed and purified smooth Tm homodimers (Coulton *et al.* 2006).

In this chapter I describe the different approaches taken in order to obtain skeletal Tm heterodimers.

A) It is shown here that from a mixture of native αα and αβ Tm dimers that were extracted from rabbit skeletal muscle, the native αβ heterodimer was successfully purified by hydroxyapatite chromatography. The hydroxyapatite chromatography has been widely used by other research groups in order to separate the Tn complex from Tm in the native Tn/Tm mixture extracted from skeletal muscles. In the past, during the separation of Tm from Tn by hydroxyapatite chromatography, it was observed that Tm was separated into two fractions, which were likely the αα and αβ dimers (Eisenberg and Kielley 1974).

B) Also it is shown here that by modifying the method described by Jancso and Graceffa for the *in vitro* formation of smooth Tm heterodimers, it was possible to form and purify skeletal αβ Tm heterodimers *in vitro* (procedure described in detail in section 3.3.2). To achieve this, recombinantly expressed αα and ββ skeletal Tm homodimers were used as starting materials. The ββ homodimer was molecularly

modified to carry an affinity tag (His-tag) at its N-terminal. After thermal denaturation of the homodimers, the reduced chains were mixed together and cooled in order to be recombined into dimers. The resulting mixture of dimers was then chemically cross-linked to allow the observation of the assembled dimers on SDS gels using non-denaturing PAGE. It was revealed that the monomers were recombined back into the original homodimers and into the newly formed α-Hisβ heterodimer. The newly formed heterodimer was successfully purified from the homodimers by affinity chromatography. After purification was completed, the affinity tag was removed from the heterodimer. The purified heterodimer when loaded on SDS gels under non-reducing conditions appeared as a single band, while when run under reducing conditions two bands were observed that run at the same level as the control stock of α and β monomers.

The novel method developed for the *in vitro* formation and purification of the skeletal αβ heterodimer, was also applied for the formation of additional skeletal Tm heterodimers which were carriers of hypertrophic cardiomyopathy mutations. Two recombinantly expressed skeletal Tm mutants were used i.e. the α^{D175N} and the α^{E180G} (described in section 1.6). Each of the mutants was combined either with a wild-type α or with a wild-type β subunits. The wild-type subunits were tagged at their N-terminal either with a His- or a Strep- tag and accordingly the resulting heterodimers were purified on NiNTA or Strep-Tactin columns.

Therefore in total five skeletal Tm heterodimers were successfully formed and purified namely the αβ, $\alpha^{WT}\alpha^{D175N}$, $\alpha^{WT}\alpha^{E180G}$, $\alpha^{D175N}\beta$ and $\alpha^{E180G}\beta$ heterodimers.

3.2 Purification of native skeletal αβ Tm heterodimers

Back and leg muscles from rabbit were used for the purification of native skeletal Tm. This was done according to a multiple-step protocol. Firstly the thin filaments were purified. The thin filaments were then further separated into actin and control proteins (i.e. Tn and Tm mixture), (described in section 2.2.4). Lastly Tm was separated from Tn complex by a series of ammonium sulphate cuts (section 2.2.5).

According to the literature, Tm extracted from skeletal muscle is expected to exist as a mixture of αα and αβ dimers, while the ββ homodimer is unlikely to be found. Indeed, when the mixture was chemically cross-linked (as described below), the different dimers could be visualised when loaded onto an SDS gel and run under non-reducing conditions. From the gel, two different bands of ~66 kDa indicative of Tm dimer species could be seen and these were most likely the αα and the αβ dimers (this sample is labelled as "ctrl" in gel 2 of figure 3.3). It was observed that the lower band was roughly twice the density of the upper band. According to the literature the lower band is expected to be the αα homodimer and the upper band the αβ heterodimer (Lehrer and Joseph 1987).

The next step was to separate and purify the two different dimer species from the muscle-extracted Tm mixture. This was achieved by ion exchange and hydroxyapatite FPLC. However, because the chromatography method applied was very long (i.e. the hydroxyapatite chromatography purification step lasted more than 6 h), the dimers were previously chemically cross-linked in order to improve their stability. Therefore, the initial dimers that were cross-linked prior to chromatography would have less chance to dissociate during their purification procedure. For the chemical cross-linking, the Tm dimers (2 mg/ml) were mixed with the oxidation buffer (10 mM $K_3Fe(CN)_6$, 2 μM $CuSO_4$, 2 M NaCl, 10 mM MOPS pH 7) in a 2:1 volume ratio (Coulton *et al.* 2006). Samples were left to oxidise for 90 min at room temperature and dialysed afterwards in buffer A (0.1 M NaCl, 5 mM KPi pH 7) to remove the oxidation buffer and prepare the sample for the first purification step. Disulphide cross-linking of the Tm dimers, catalysed by Cu^{+2}, $K_3Fe(CN)_6$, is schematically shown in figure 3.1.

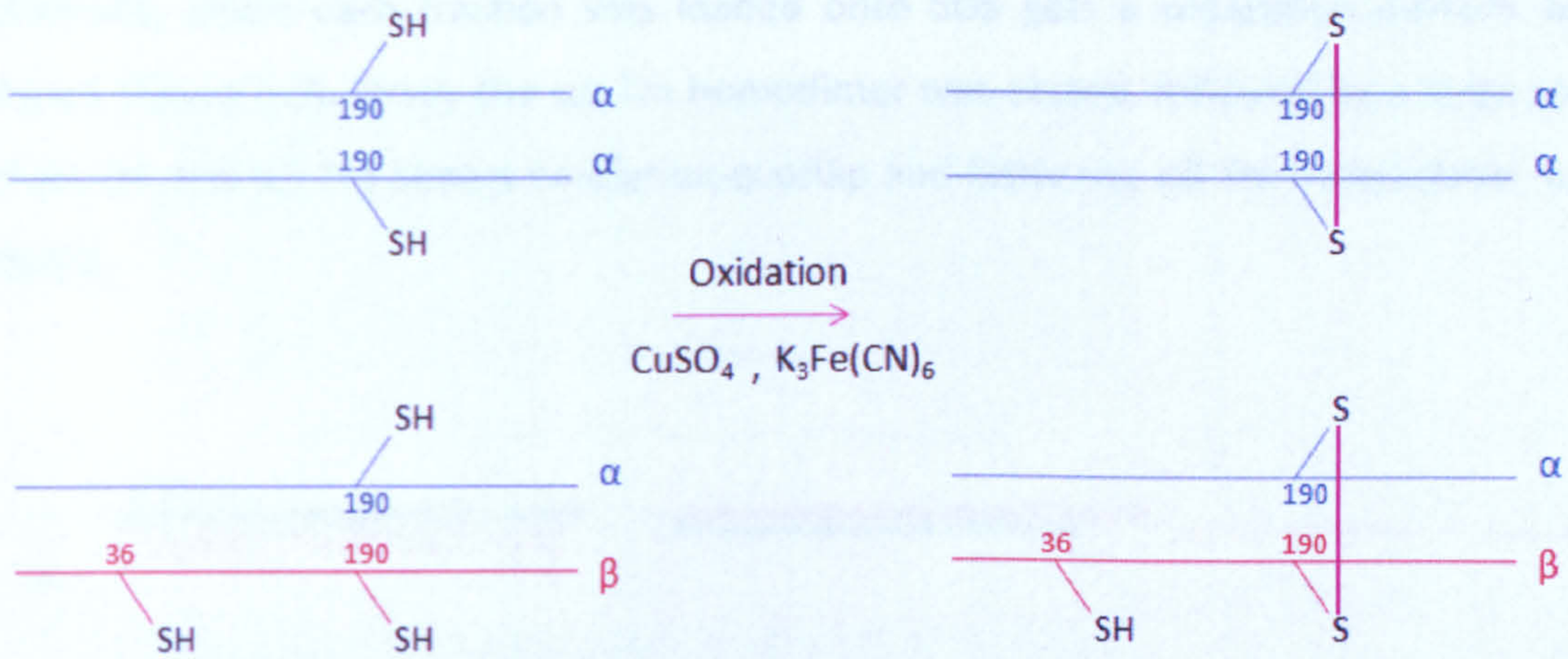

Fig 3.1: Schematic representation of disulphide cross-linking in Tm dimers. The native αα and αβ dimers are not found cross-linked. However both α and β subunits have a Cys at position 190. Therefore after chemical cross-linking both αα and αβ dimers can form a single cross-link. In the case of the ββ homodimer there are two Cys at positions 36 and 190, thus up to two cross-links can be formed. Cross-linking allows the detection of dimers on non-reducing SDS gels and also enhances the dimers' stability.

The first purification step was performed on a HiTrap Q HP anion exchanger. Both αα and αβ dimers were co-eluted using a 0.1 – 1 M NaCl gradient. This purification step was not performed to separate the two dimers, but was only performed in order to remove any other contaminants from the rabbit preparation and obtain a cleaner Tm sample. This would prolong the life-time of the very delicate hydroxyapatite column used in the next purification step.

For the second purification step the Tm dimers mixture was dialysed against equilibration buffer (0.5 M KCl, 100 mM KPi, pH 7) and applied onto the ceramic hydroxyapatite column CHT10 (from BioRad). The hydroxyapatite column results in essentially a mixed-mode ion exchange separation since the hydroxyapatite matrix provides both negatively charged (PO_4^{-3}) and positively charged (Ca^{2+}) centres. Thus it is a more sensitive chromatography method than the classic ion exchange chromatography. The Tm dimers were eluted using a 100 – 150 mM linear KPi gradient and in order to separate the two dimers a large 50 column volumes were used. The flow rate was also kept very low at 2 ml/min to improve the purification. The chromatogram obtained is shown in figure 3.2. Although from the chromatogram two different peaks that would correspond to the two different αα and αβ dimers were not

observed, when each fraction was loaded onto SDS gels a separation pattern was shown (figure 3.3). Firstly the αα Tm homodimer was eluted, followed by a large area of αα Tm and αβ Tm dimers co-elution overlap and lastly the αβ Tm heterodimer was eluted.

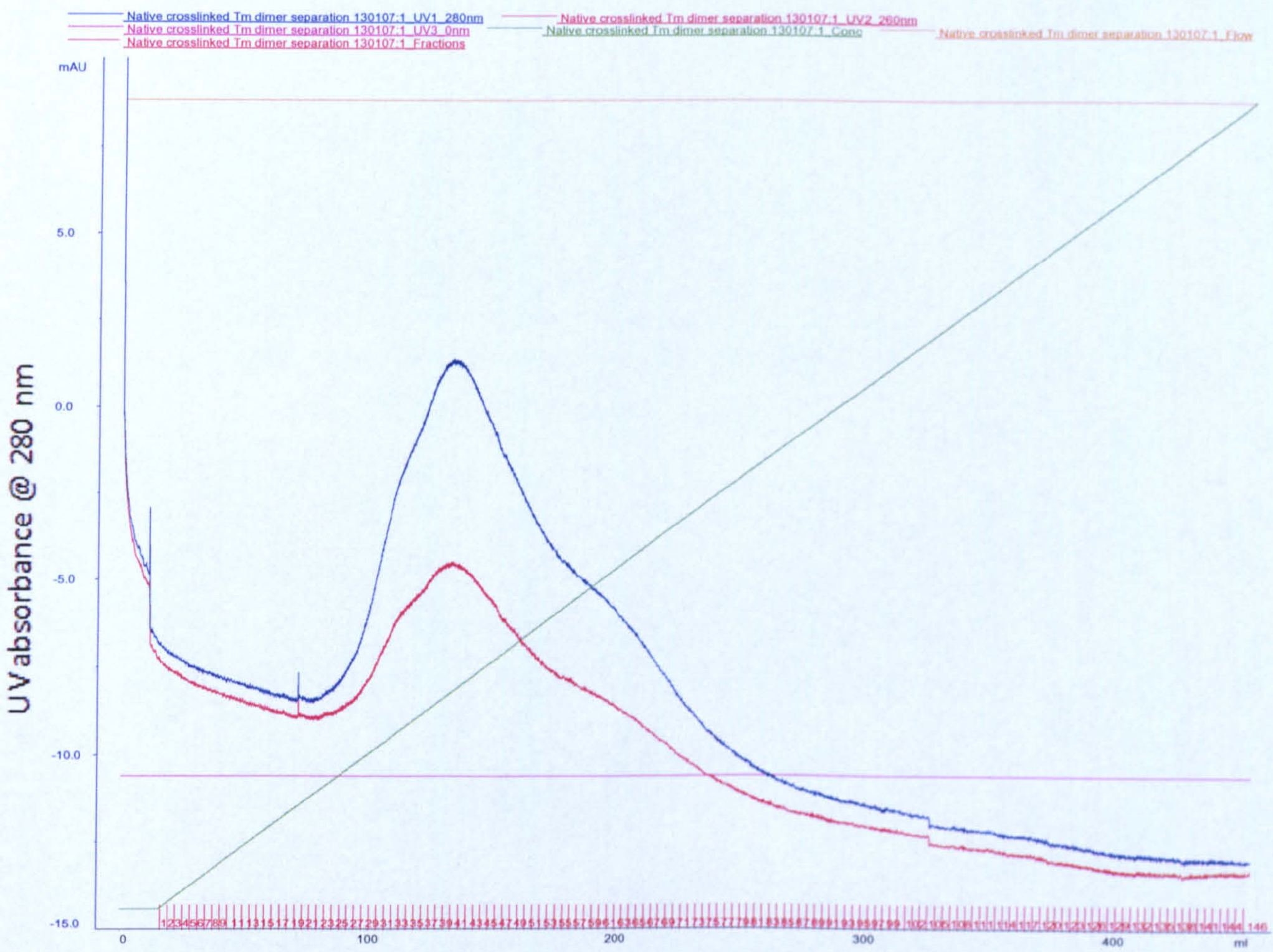

Fig 3.2: Hydroxyapatite chromatography of cross-linked αα Tm and αβ Tm dimers mixture using ceramic hydroxyapatite column CHT10. A linear phosphate gradient (100 mM – 150 mM in green) was used for protein elution. The line in blue is the UV absorption at 280 nm and the line in red is the UV absorption at 260 nm. For successful separation of the two dimers a very large 50 column volumes gradient was used and sample was fractionated in 146 tubes (marked in red in x-axis).

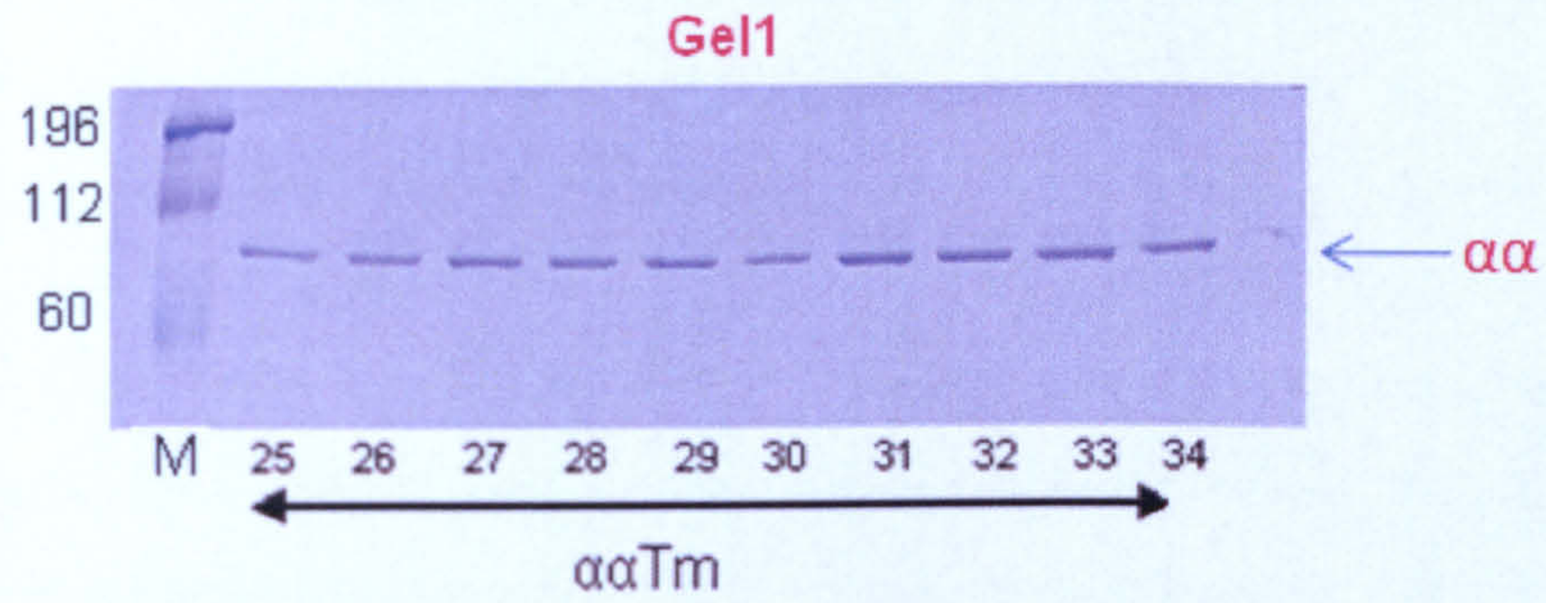

Fig. 3.3: Elution profile of αα Tm and αβ Tm cross-linked dimers. According to the literature (Lehrer and Joseph 1987) αβ is the top band and αα Tm is the lower band. Fractions 25-66 corresponding to the peak of the chromatogram in fig 3.2 were loaded onto 9 % SDS gel in order of elution. αα Tm was eluted first and αβTm was eluted last, but there was a big overlap of co-elution of the two dimers in between. The two last gels were silver stained for better visualization of the αβ Tm heterodimer to make sure that only those fractions with pure heterodimer would be collected.

Using hydroxyapatite chromatography it was possible to purify the native αβ heterodimer from a mixture of αα and αβ Tm dimers. The purified native αβ heterodimer when run under reducing PAGE, was split into two bands i.e. the α and the β subunits. The purified αα homodimer under reducing PAGE showed one major band i.e. the α subunit (fig 3.4). There was small protein contamination in both samples (i.e. in the heterodimer samples there was small αα contamination, since the α subunit band appeared slightly denser than the β subunit band; in pure heterodimer samples the two bands should be of equal densities. In the αα homodimer sample there was small αβ heterodimer contamination since traces of the β subunit could be seen on the gel).

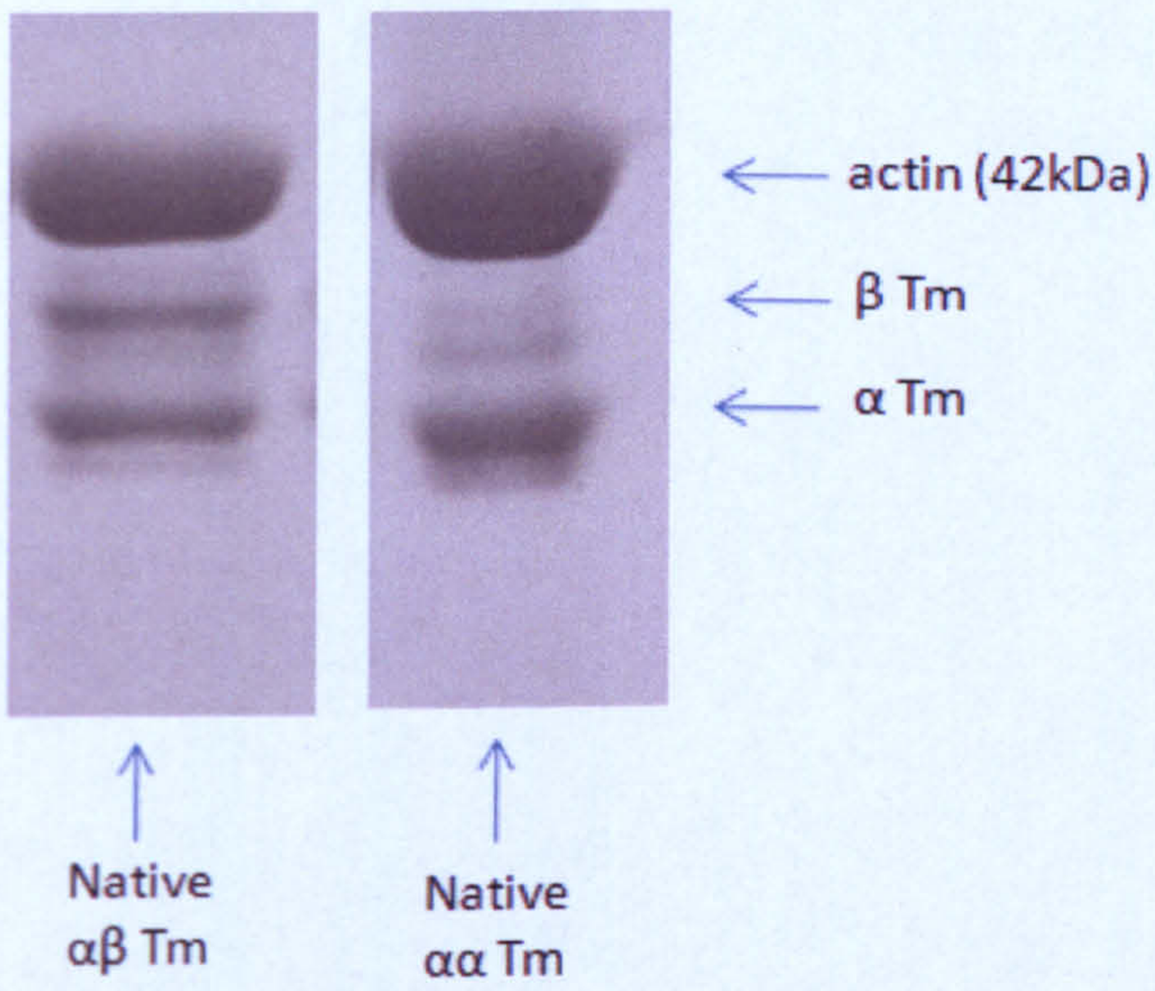

Fig 3.4: Native αα and αβ dimers on reducing SDS gel. The purified top band as shown in figure 3.3 was indeed the αβ heterodimer which under reducing conditions was split into the two α and β monomers. The purified lower band of αα homodimer as shown in fig 3.3 gave only one major band under reducing conditions as expected.

The αβ purification yield was very low (maximum of 0.6 mg of heterodimer purified from a total of 10 mg mixture). The amount of pure native αβ heterodimer obtained was insufficient for a complete set of characterisation experiments.

3.3 *In vitro* formation of Tm heterodimers

In theory, the *in vitro* formation of Tm heterodimers could be very valuable since it could overcome the disadvantages of wasting animal tissue for a very low yield of native heterodimer. Also by using a variety of recombinantly expressed Tm monomers as starting materials, many different types of heterodimers can be formed. For example, apart from the wild-type αβ heterodimer, other heterodimers carrying mutations or labels in one of their chains could be formed. In this section a reproducible method for the *in vitro* formation of Tm heterodimers is presented.

3.3.1 Tools for the *in vitro* heterodimer formation and purification method

The novel method for the *in vitro* formation of skeletal Tm heterodimers has similarities to the method described by Coulton et al. for the formation of smooth Tm heterodimers (Coulton *et al.* 2006). In both methods bacterially expressed and purified Tm homodimers were used as starting materials.

However, in order to increase the efficiency of the formation and subsequent purification of the skeletal Tm heterodimers, two different types of Tm homodimers were used as starting materials. One of the homodimers carried an N-terminal affinity tag while the second homodimer was untagged.

The expression and purification of the untagged Tm homodimers was performed as previously reported (Boussouf *et al.* 2007) and can be seen in section 2.2.3.a. About 60 mg of protein was purified per litre of bacterial culture using ion exchange chromatography on HiTrap columns. All of the untagged proteins were expressed with an Ala-Ser dipeptide extension, to mimic the native acetylated protein (as described in pg 33).

On the other hand, novel N-terminally tagged Tm homodimers were molecularly designed, expressed in bacterial cells and purified by affinity chromatography. The N-terminal affinity tags that were used for the formation and purification of the heterodimers were either a Strep-tag or a His-tag. Both affinity tags are small; the Strep tag has the sequence WSHPQFEK and the His tag has the sequence RGSHHHHHH. (http://www.iba-go.com/prottools/prot_fr01_01.html and http://www.iba-go.com /downloads/pdf/2-1437-000pASK-IBA37plus.pdf). Each tag sequence was followed by the four residue sequence IEGR which can be recognised and digested by Factor Xa (FXa) protease. FXa recognises this restriction site and cuts after the last Arg, thus removing the leading Strep or His tag and the FXa restriction site completely (Assouline *et al.* 1995). The primers used for the insertion of the tag sequence at the 5' end of the original Tm sequence template are shown in detail in section 2.1.2. After FXa treatment the digested proteins would be left with the AlaSer dipeptide N-terminal extension, which was positioned after the FXa sequence and before the original Tm sequence. Therefore after FXa digestion, these bacterially expressed proteins would possess the AlaSer extension and would mimic the native N-terminal acetylated protein.

The novel N-terminal tagged Tms that were designed for the heterodimer formation experiment were expressed in BL21 cells and purified using the appropriate affinity columns. Thus the Strep-tagged Tm was bound onto a gravity flow Strep-Tactin column and eluted with desthiobiotin. The His-tagged Tm was bound onto a gravity flow NiNTA column and eluted with imidazole. Details of the Strep- and His-tagged protein purification are shown in sections 2.2.3 b and c. Purification of the tagged proteins on the affinity columns was straight forward and yielded about 20 mg of protein per litre of IPTG induced bacterial culture. In figure 3.5 and 3.6 below the purification profile of Strep-α Tm and His-α Tm is shown as an example. It can be seen that a quite large amount of protein was eluted in the flow through and first washes due to the small gravity flow column having reached its capacity limit. The unbound protein was collected and subjected to a second purification cycle.

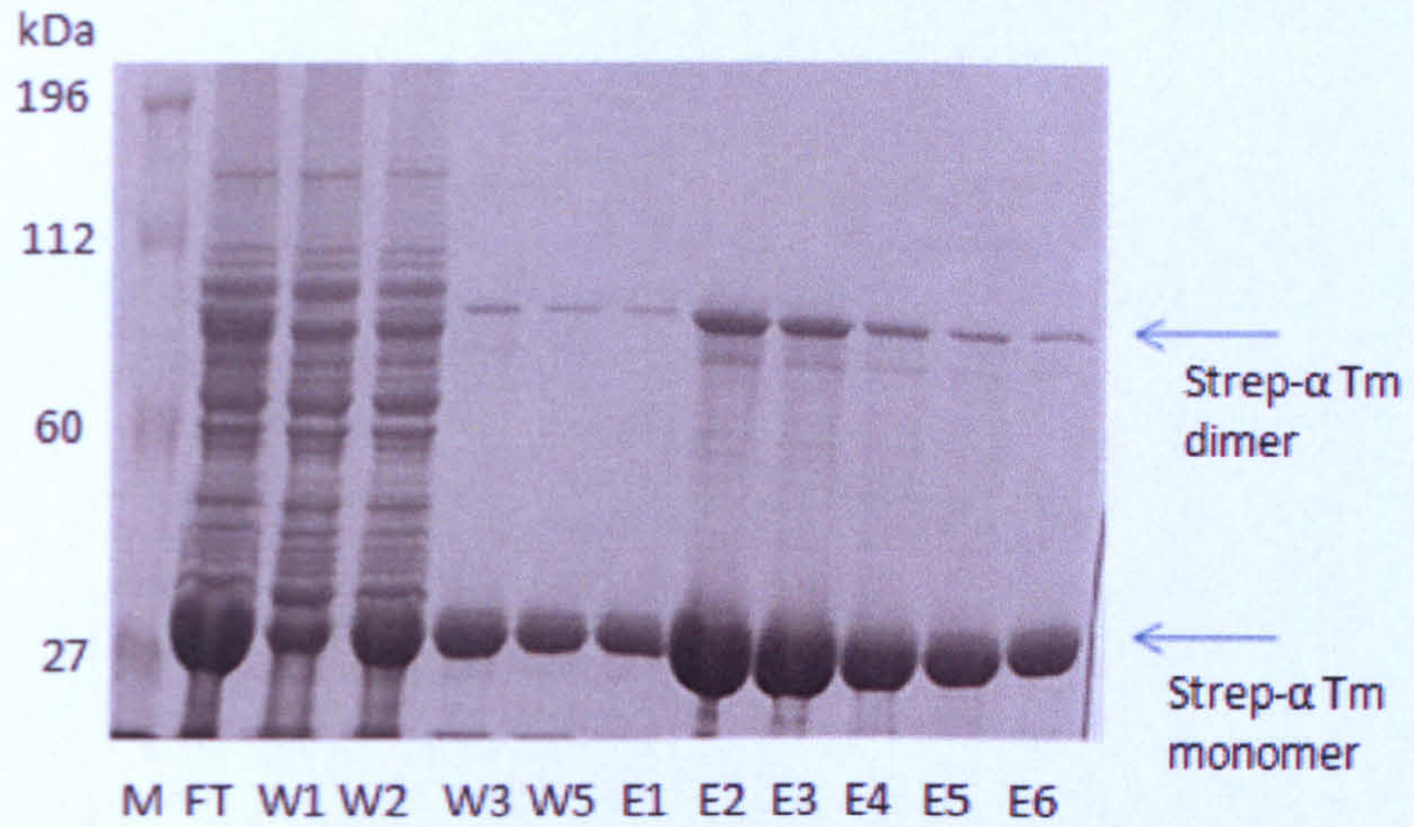

Fig 3.5: Strep-α Tm elution profile. Aliquots from each step were loaded on 10 % SDS gel and ran under non-reducing conditions. The gels were stained using Coomassie blue. In detail M is the marker; FT is the flow through; W1-W5 the washing products with Buffer W; E1-E6 the elution products with Buffer E containing 2.5 mM desthiobiotin. Strep-α Tm can be isolated in fractions W3-E6 (details of the buffers used are given in section 2.2.3b).

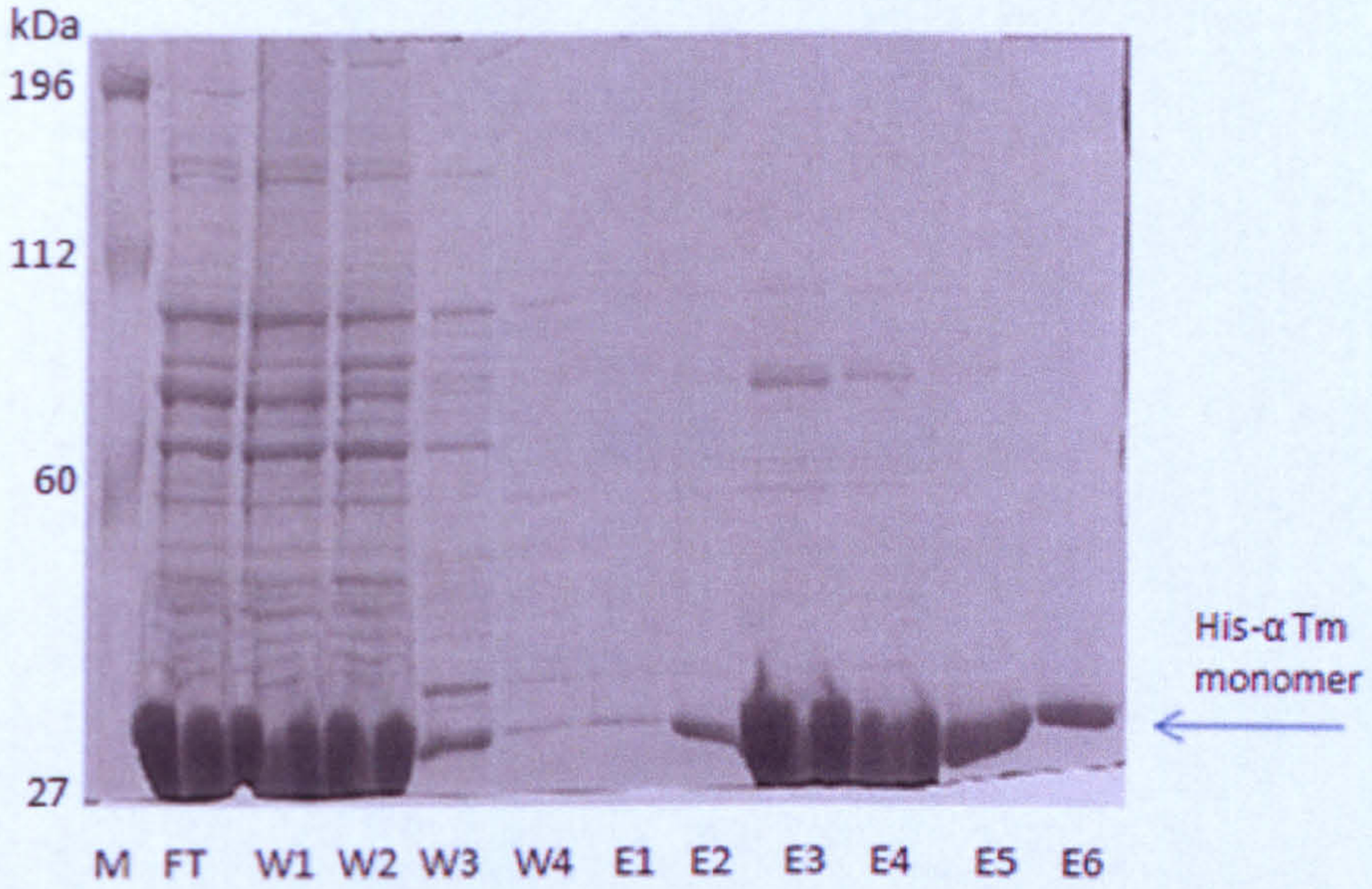

Fig 3.6: His-α Tm elution profile. Aliquots from each step were loaded on 10 % SDS gel and ran under reducing conditions. The gels were stained using Coomassie blue. M is the marker FT is the flow through W1-W4 the washing products and E1-E6 the products after elution with 250 mM imidazole. His-α Tm can be isolated in fractions E1-E6 (details of the buffers used are given in section 2.2.3c).

3.3.2 *In vitro* formation of α - His β heterodimer

The α-Hisβ heterodimer was formed according to the basic method described schematically in figure 3.7 below using as starting materials α Tm and His-β Tm homodimers.

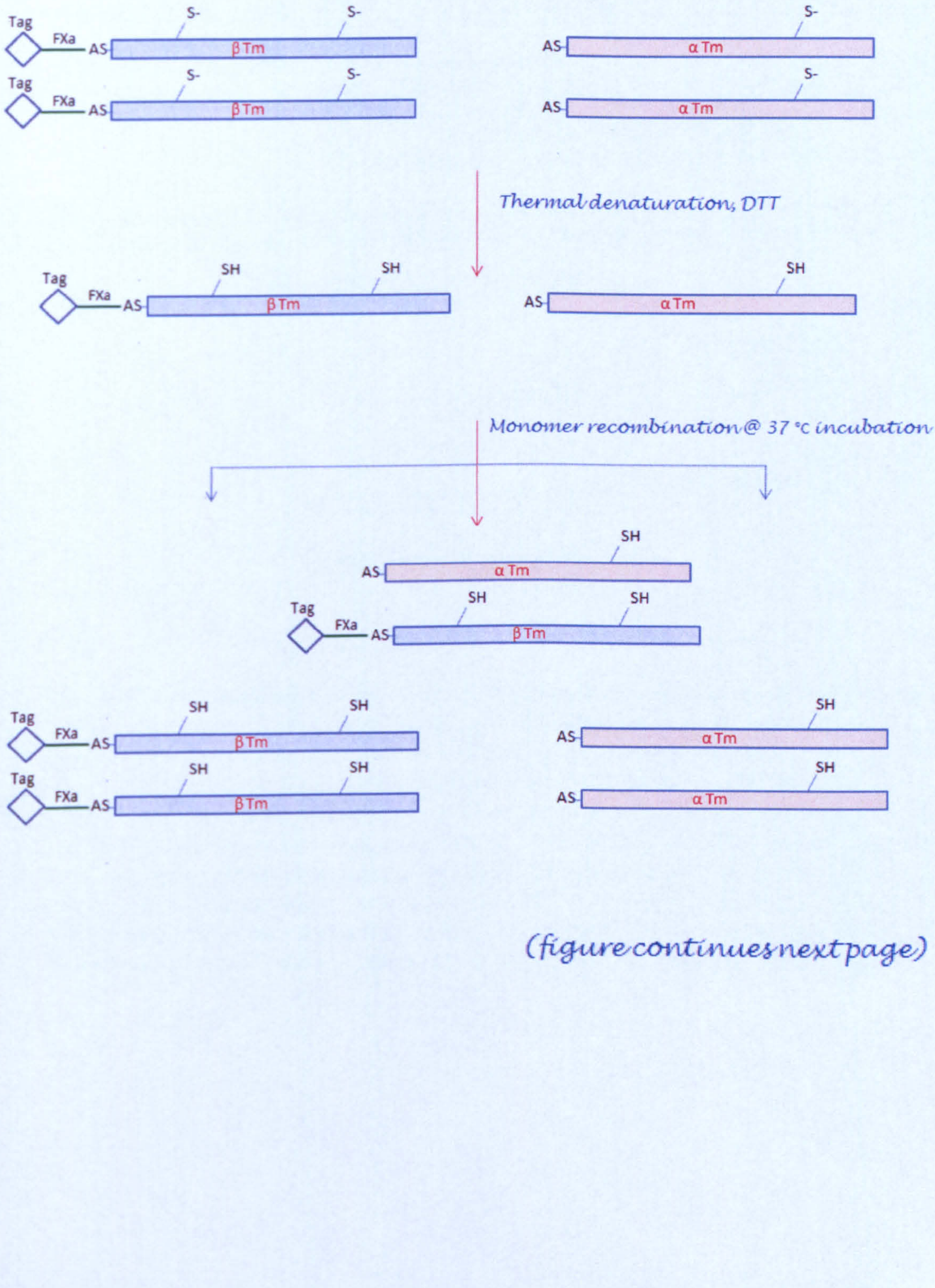

(figure continues next page)

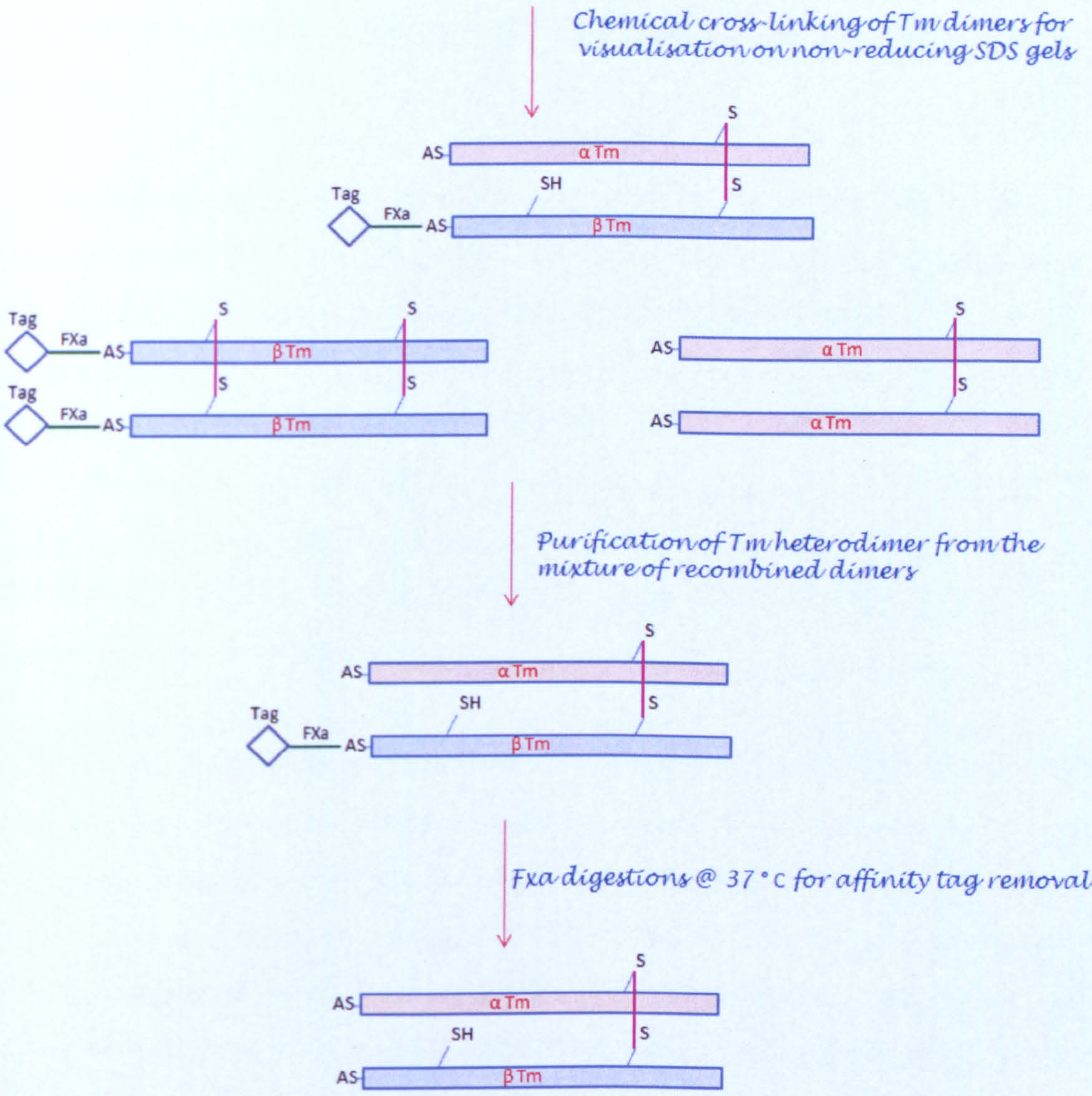

Fig 3.7: Cartoon representation of the *in vitro* αβ heterodimer formation process. There are two major steps during heterodimer formation; the first step includes the homodimers' dissociation into monomers and the second step is the recombination of the reduced monomers into dimers. It is expected that after monomer recombination the two original homodimers and the target heterodimer will be formed. After cross-linking the different dimers can be visualised on non-reducing SDS gels. The heterodimer can be purified from the mixture of dimers by affinity chromatography; the three dimers carry 0, 1 or 2 affinity tags thus each dimer binds differentially on the appropriate affinity column. After purification of the heterodimer the affinity tag can be cleaved by FXa digestions. For successful formation of the αβ heterodimer it was necessary to use an affinity tag at the N-terminal of the β subunit.

For the *in vitro* formation of the skeletal Tm heterodimer, the experimental conditions were similar as for the formation of smooth Tm heterodimers (Coulton *et al.* 2006).

The first step was the reduction of homodimers into monomers. 750 µg of α Tm were suspended into 1500 µl high salt experimental buffer (0.5 M KCl, 20 mM KPi, 5 mM $MgCl_2$ pH 7). 20 mM DTT was added to ensure reduction of the Cys side chain and sample was placed at 58 °C. At the same time 250 µg of Hisβ Tm was diluted into 500 µl experimental buffer and as before 20 mM DTT was added and sample was heated at 58 °C. The homodimers were thermally denatured, after incubating the samples at 58 °C for 10 min. Then the reduced α and Hisβ Tm were mixed together into a single tube (i.e. 750 µg : 250 µg or 3:1 ratio to improve heterodimer purification yield as will be explained further on in section 3.4).

α Tm and Hisβ Tm samples that were not mixed together after the heating step were also kept to serve as homodimer controls. The control homodimer samples and the mixed sample were then transferred at a lower temperature of 37 °C for 45 min to allow the recombination of the reduced monomers into dimers (i.e. at physiological temperature). After this incubation period, DTT was removed from all samples by gel filtration using gravity columns at room temperature. DTT was removed from the samples in order to allow the chemical cross-linking of the recombined dimers at a later stage. After DTT removal, the samples were loaded onto reducing SDS gels as shown in figure 3.8. In order to verify that samples were not damaged during the process, stock controls of α and Hisβ were loaded as well to check that identical monomers were running at the same level on the gel. It can be seen in fig 3.8 that the α Tm sample shows traces of a second band which corresponds to an N-terminal truncated product as obtained after mass spectrometry analysis. This truncation is also noticed in other bacterially expressed proteins (like α^{D17SN} and β Tm).

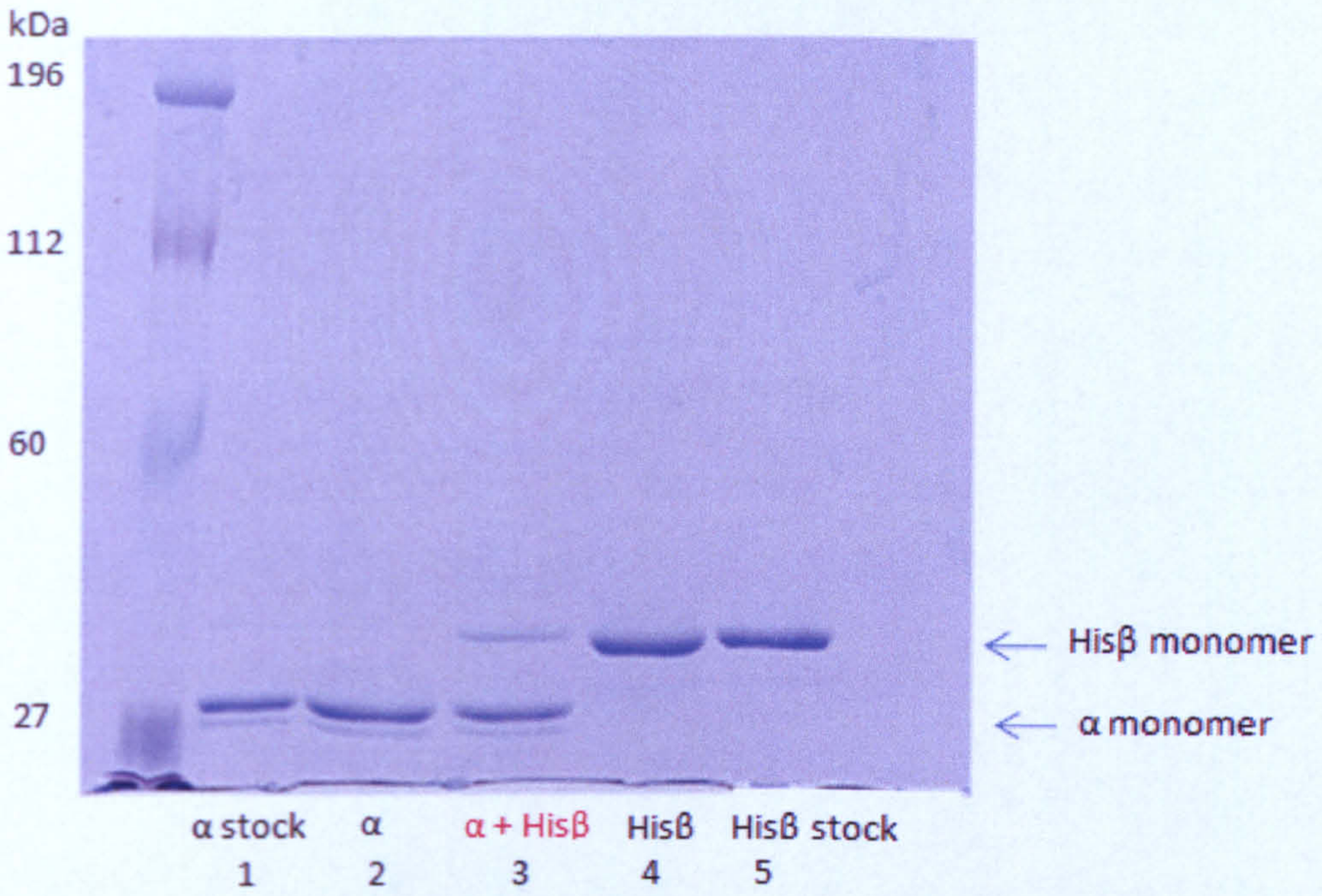

Fig 3.8: Presence of α and Hisβ monomers in unmixed homodimer samples (lane 2 & 4 respectively) and in mixed samples (lane 3) prior to cross-linking. Stock α and Hisβ controls were also loaded (lanes 1 and 5 respectively) to ensure that the samples were running on the same level as the corresponding controls, thus were not damaged during the thermal denaturation process. Samples were ran on 7.5 % SDS gels under reducing conditions. In the sample shown in lane 3, the α band is denser than the Hisβ band because they were mixed in a 3:1 ratio respectively.

After DTT removal the samples were chemically cross-linked, in order to be able to visualise the different dimers on non-reducing SDS gels. Instead of cross-linking just a small sample that would be enough to detect on the gel, the whole sample was cross-linked to have it ready for the subsequent FXa digestion step (explained in section 3.5). The control samples containing a single type of monomer (either α or Hisβ), were expected to be re-assembled into the original type of homodimer. The mixture of α with Hisβ monomers was expected to form three different types of dimers i.e. the α-α and Hisβ-Hisβ homodimers and the α-Hisβ heterodimer. For cross-linking each sample was mixed with the oxidation buffer (10 mM $K_3Fe(CN)_6$, 2 μM CuSO4, 2 M NaCl, 10 mM MOPS at pH 7) and incubated for 90 min at room temperature. The oxidation buffer was then removed from all samples by dialysis. The α-α and the α-Hisβ dimers can be cross-linked at Cys190 while the Hisβ-Hisβ can be double cross-linked at Cys36 and Cys190 (as was shown schematically in figure 3.1) . After cross-linking the samples were loaded onto SDS gels and ran under non-reducing conditions (fig 3.9). From the gel it was clear that three different dimers were assembled after recombining the

reduced α and Hisβ monomers. Two of the bands were exactly the same as the re-assembled homodimer controls of α-α and Hisβ-Hisβ. The third band ran between the two homodimer bands and was most likely the α-Hisβ heterodimer. This band could not be seen in the homodimer control samples. If this band was not the heterodimer (if it was for example a cleaved homodimer product) it would appear in the homodimer control samples as well, since all samples were treated under the same conditions. The formation of the α-Hisβ heterodimer was verified again at a later stage after its purification; when the purified α-Hisβ heterodimer was loaded on a gel under reducing conditions it was split into the two components, the α and Hisβ subunits (this is shown later on, in figure 3.17).

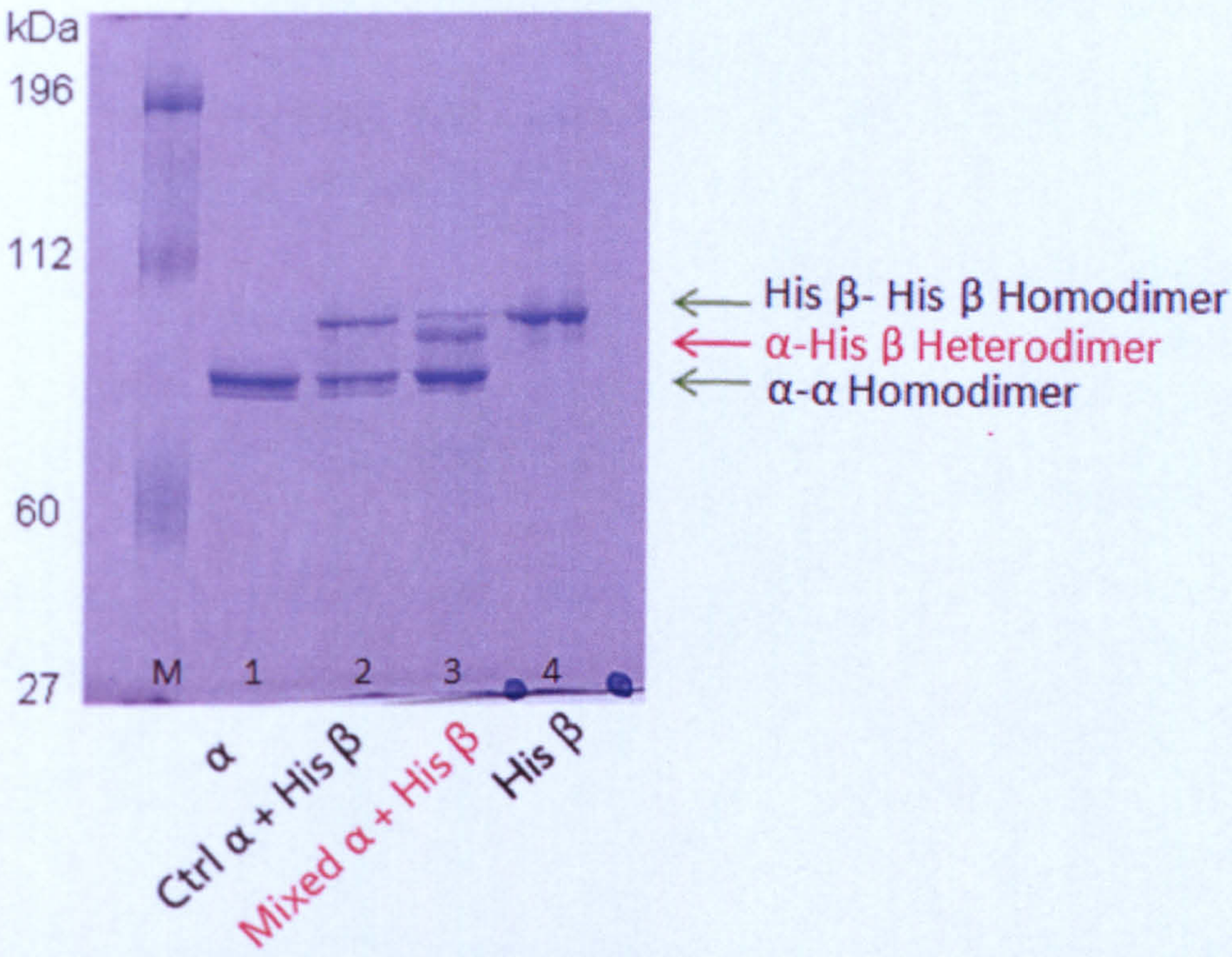

Fig 3.9: *In vitro* formation of α-Hisβ heterodimer. Lane 1 and 4 contain the α-α and Hisβ-Hisβ homodimer controls that were formed after cooling and cross-linking of the dissociated α and Hisβ monomers respectively. Lane 2 is a control with the homodimers (as in lane 1 & 4) loaded together. Lane 3 shows the dimers formed after mixing and recombining α with Hisβ monomers in a 3:1 ratio; the two homodimer bands (same as in lane 2) are shown plus the new band of α-Hisβ heterodimer running between the homodimer bands. 7.5 % SDS gel was used with samples ran under non-reducing conditions.

3.3.3 *In vitro* formation of Strep α^{WT} - α^{mutant} heterodimer

Using exactly the same procedure as was described in the previous section 3.3.2, it was possible to form heterodimers containing one wild-type copy of α Tm and one hypertrophic cardiomyopathy mutant copy of α Tm. Two HCM mutations were used namely the α^{D175N} and the α^{E180G}. In the current case, as starting homodimer materials, the N-terminal Strep-tagged α^{WT} Tm and the untagged α^{D175N} or α^{E180G} Tm were used.

Formation of the Strep$\alpha^{WT}\alpha^{D175N}$ heterodimer is shown in figure 3.10 and formation of the Strepα^{WT} α^{E180G} heterodimer is shown in figure 3.11.

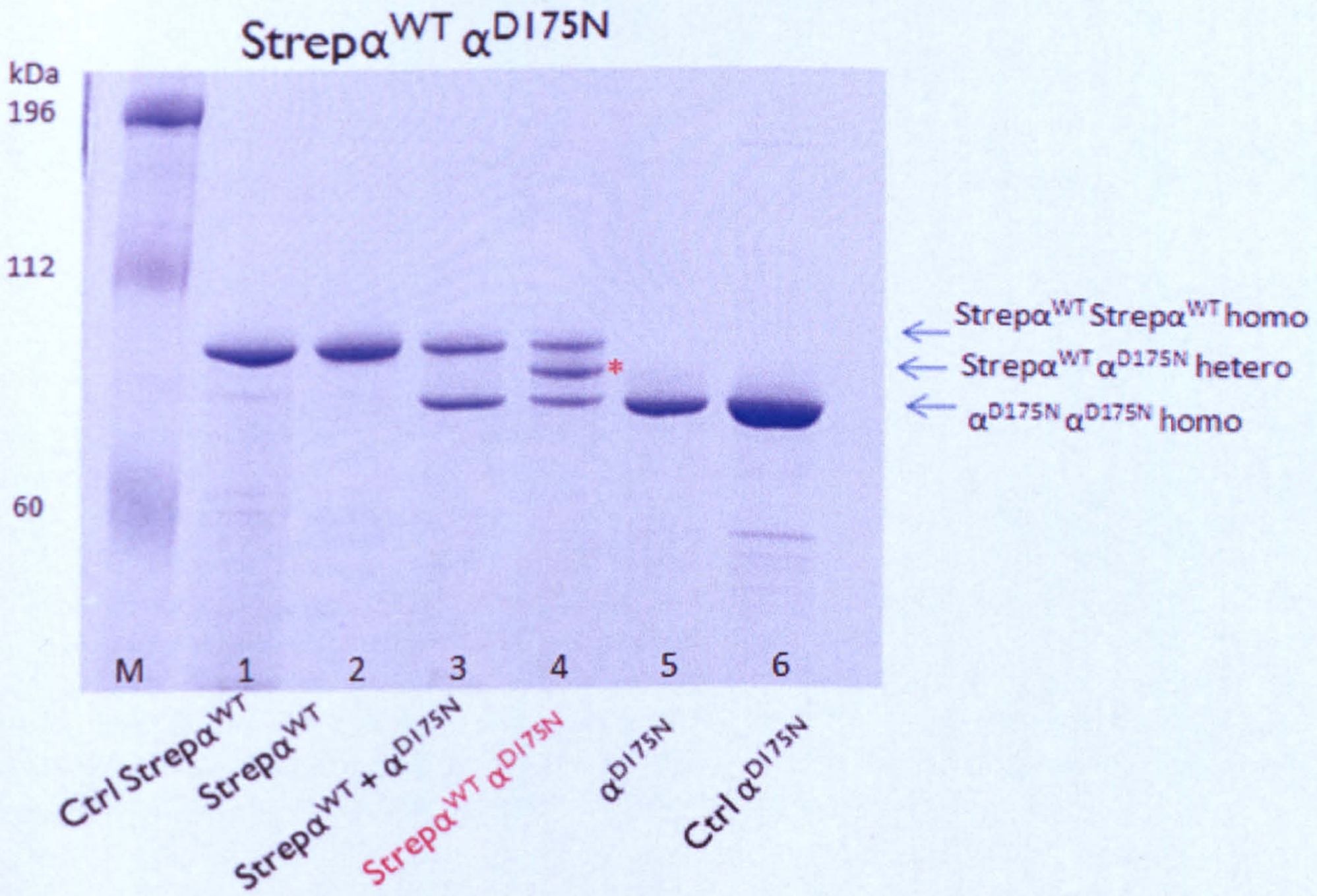

Fig 3.10: *In vitro* Strep$\alpha^{WT}\alpha^{D175N}$ heterodimer formation. Lane 1 and 6 contain stock controls of the Strepα^{WT} and the α^{D175N} homodimers, respectively. Lanes 2 and 5 are Strepα^{WT} and α^{D175N} homodimer controls formed after homodimer dissociation and re-assembly. It is clear that samples in lanes 2 and 5 are the same as the stock controls in lanes 1 and 6 as expected. Lane 3 is a loading control with both samples of 2 & 5. Lane 4 shows the resulting dimers after mixing Strepα^{WT} and α^{D175N} monomers (1:1 ratio) and allowing dimer re-assembly; the homodimers Strepα^{WT} and α^{D175N} can be seen again and are the same as in the loading control of lane 3, but also the newly formed Strep$\alpha^{WT}\alpha^{D175N}$ heterodimer can be seen (indicated by red asterisk) running between the two homodimer bands. 7.5 % SDS gel was used with samples ran under non-reducing conditions and stained using Coomassie blue. NB the homodimers were routinely mixed in a 3:1 ratio in large scale experiments, to improve the heterodimer purification yield.

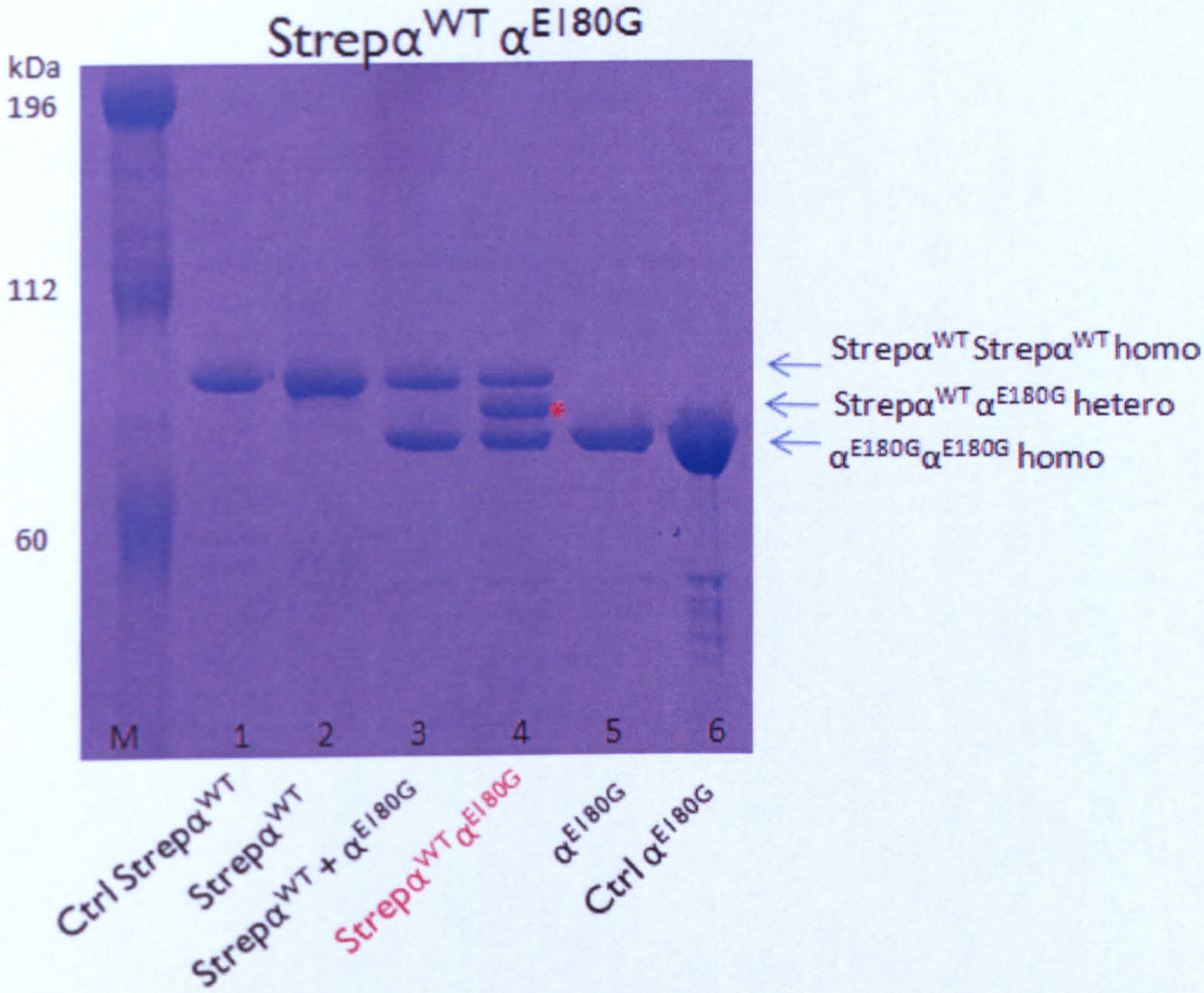

Fig 3.11: *In vitro* Strepα^{WT}α^{E180G} heterodimer formation. Lane 1 and 6 contain stock controls of the Strepα^{WT} and the α^{E180G} homodimers and lanes 2 and 5 are Strepα^{WT} and α^{E180G} homodimer controls formed after homodimer dissociation and re-assembly. Lane 3 is a loading control with both samples of 2 & 5. Lane 4 shows the resulting dimers after mixing Strepα^{WT} and α^{E180G} monomers (1:1 ratio) and allowing dimer re-assembly; the homodimers Strepα^{WT} and α^{E180G} can be seen again and are the same as in the loading control of lane 3, but also the newly formed Strepα^{WT}α^{E180G} heterodimer can be seen (indicated by red asterisk) running between the two homodimer bands. 7.5 % SDS gel was used with samples ran under non-reducing conditions and stained using Coomassie blue. NB the homodimers were routinely mixed in a 3:1 ratio in large scale experiments, to improve the heterodimer purification yield.

In the case of α^{WT}α^{mutant} heterodimers it was not necessary to use a Strep tag (or a His tag) on one of the subunits in order to form the heterodimers. Using the same heterodimer formation method, the α^{WT}α^{D175N} heterodimer (and possibly the α^{WT} α^{E180G} heterodimer) could be formed using non-tagged homodimers as starting materials as shown in figure 3.12. However, the heterodimer formed was impossible to be purified from the re-assembled dimer mixture although various conditions on ion exchange or hydroxyapatite chromatography were attempted. The presence of the N-terminal tag proved to be necessary for the subsequent purification of the

heterodimer. Also the tagged α^{WT} homodimer runs further apart on SDS gels from the mutant homodimers in comparison to the untagged α^{WT} homodimer. Therefore, it was also useful to use the tagged α^{WT} homodimer as starting material in order to distinguish the three different homodimers and the heterodimer when their mixture was loaded on SDS gels.

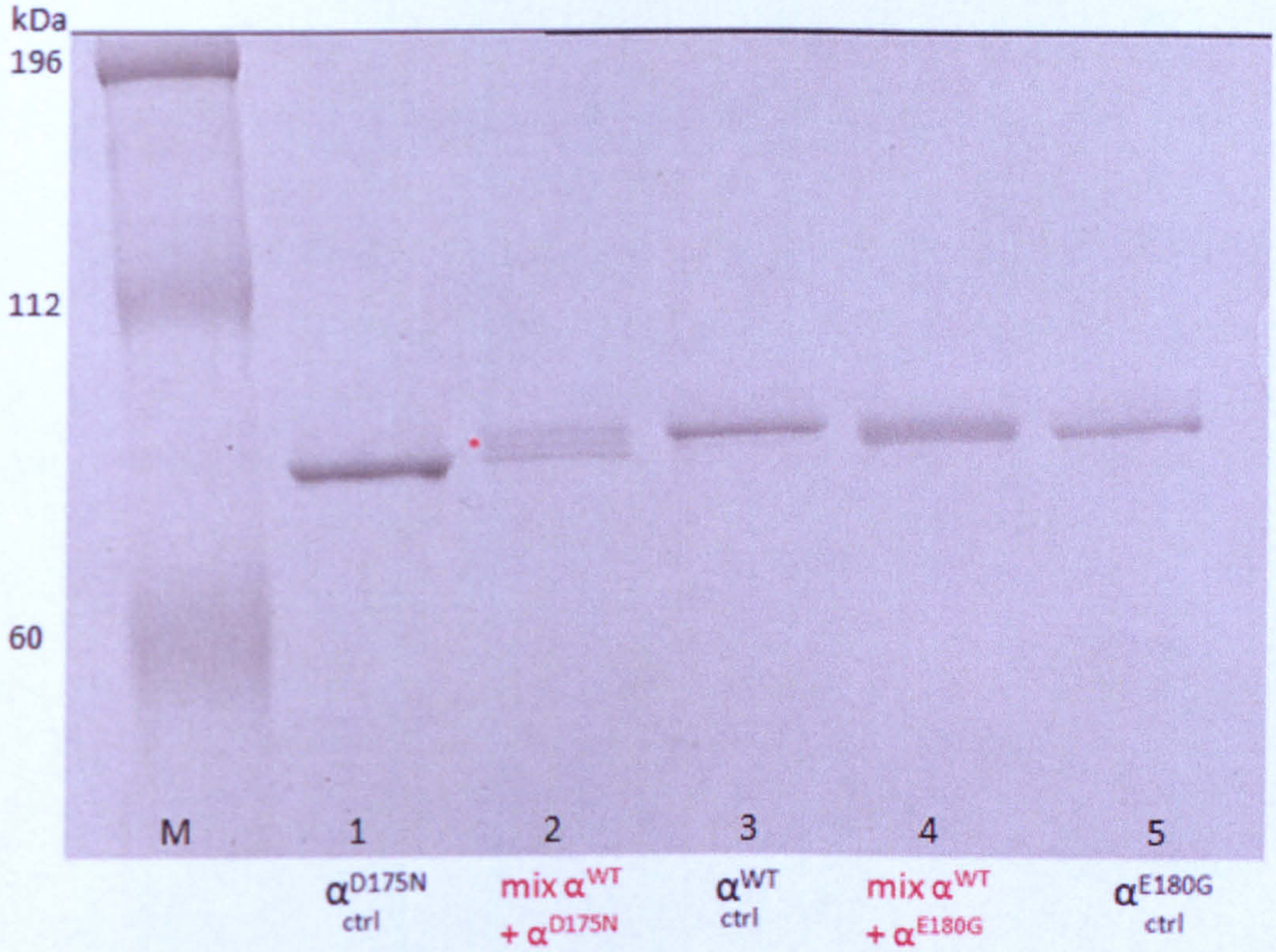

Fig 3.12: *In vitro* formation of untagged $\alpha^{WT}\alpha^{D175N}$ and $\alpha^{WT}\alpha^{E180G}$ Tm heterodimers. Lane 1 is the cross-linked $\alpha^{D175N}\alpha^{D175N}$ homodimer (obtained after re-assembly of the reduced α^{D175N} monomers). Similarly, lane 3 and 5 are the cross-linked $\alpha^{WT}\alpha^{WT}$ and $\alpha^{E180G}\alpha^{E180G}$ homodimers respectively. Lane 2 shows the mixture of dimers formed after recombination of α^{WT} & α^{D175N} subunits with the new band (*) of the $\alpha^{WT}\alpha^{D175N}$ heterodimer running between the control homodimers. Lane 4 shows the dimers formed after recombination of α^{WT} & α^{E180G} subunits but since $\alpha^{WT}\alpha^{WT}$ & $\alpha^{E180G}\alpha^{E180G}$ homodimers run very close together it is hard to visualise three distinct bands. 7.5 % SDS gel was used with samples ran under non-reducing conditions and stained using Coomassie blue.

3.3.4 *In vitro* formation of α^{mutant} – Strepβ heterodimer

Using exactly the same procedure as was described in section 3.3.2 for the α-Hisβ heterodimer formation, it was possible to form heterodimers containing one wild-type copy of β Tm and one hypertrophic cardiomyopathy mutant copy of α Tm (α^{D175N} or α^{E180G}). As starting homodimer materials, the N-terminal Strep-tagged or His-tagged β Tm and the untagged α^{D175N} or α^{E180G} Tm were used. Strepβ was used preferentially because it was easier to handle than the Hisβ.

Formation of the α^{D175N}Strepβ heterodimer is shown in figure 3.13 and formation of the α^{E180G}Strepβ heterodimer is shown in figure 3.14. As it can be observed from both figures, the stock solution of Strepβ homodimer appeared as a double band on the gel. The two bands correspond to single and double cross-linked Strepβ homodimers (at Cys36 or Cys190). However, the Strepβ homodimer samples that were chemically cross-linked showed only one band corresponding to the double cross-linked state.

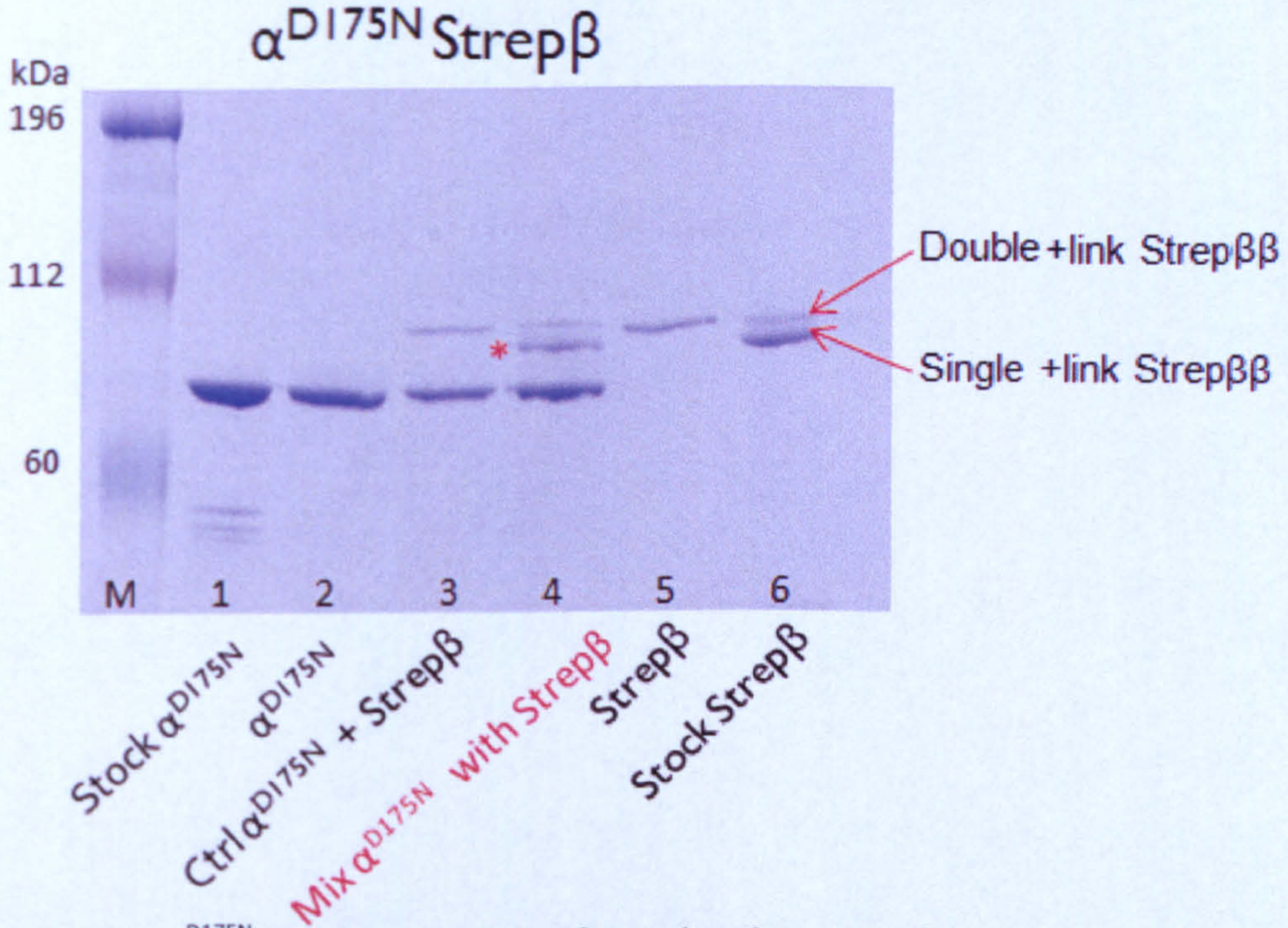

Fig 3.13: *In vitro* α^{D175N}Strepβ heterodimer formation. Lane 1 and 6 contain stock controls of α^{D175N} and Strepβ homodimers and lanes 2 and 5 are α^{D175N} and Strepβ homodimer controls formed after homodimer dissociation and re-assembly. The stock control of Strepβ which is not chemically cross-linked can be both single and double crosss-linked thus two bands appear, while the Strepβ homodimers in lane 3,4,5 are chemically cross-linked at both Cys36 and Cys190 sites. Lane 3 is a loading control with both samples of lanes 2 & 5. Lane 4 shows the resulting mixture of dimers after mixing monomers (1:3 ratio of Strepβ: α^{D175N}) and allowing dimer re-assembly; the newly formed α^{D175N}Strepβ heterodimer can be seen (indicated by red asterisk) running between the two homodimer bands. 7.5 % SDS gel was used with samples ran under non-reducing conditions and stained using Coomassie blue.

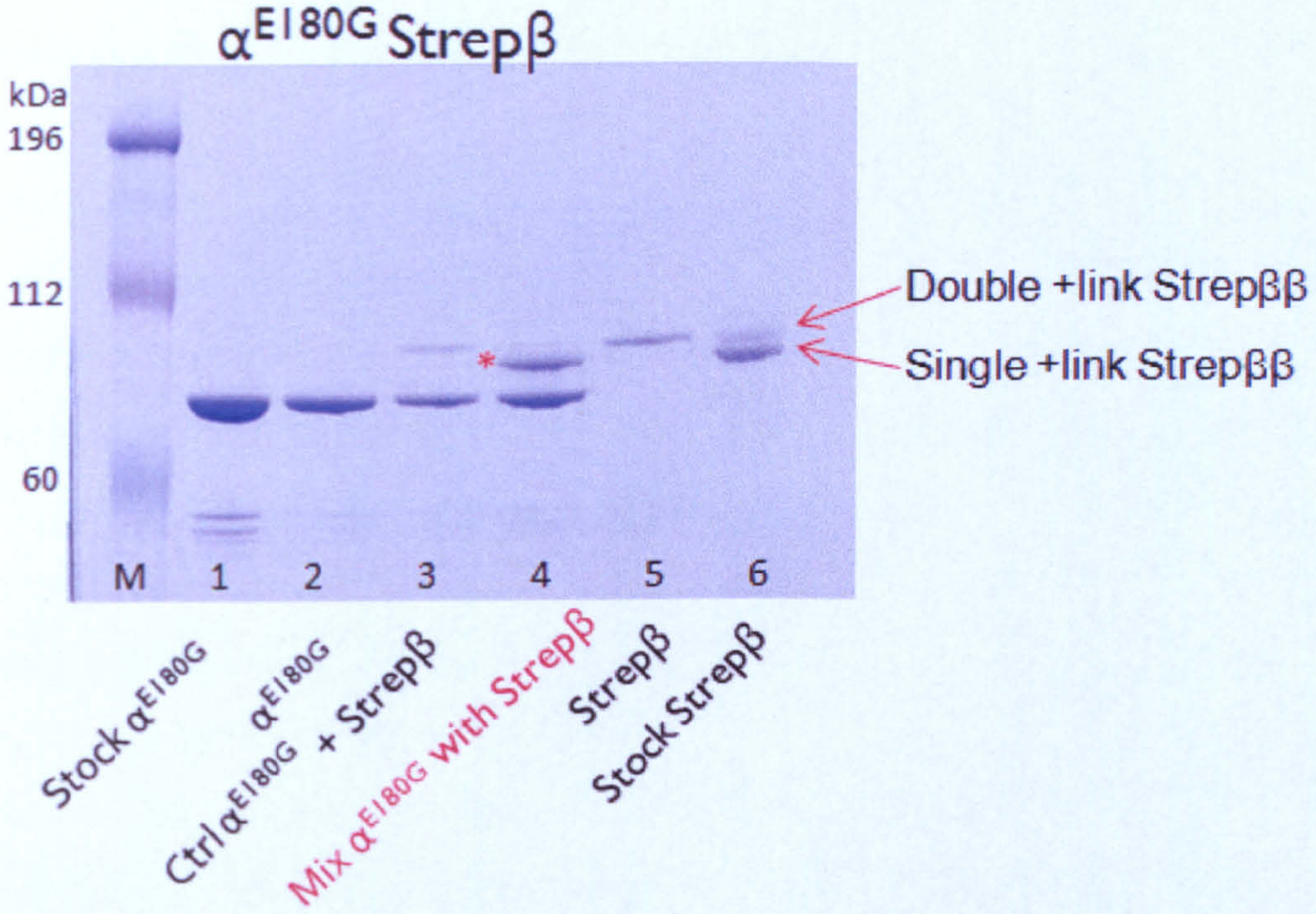

Fig 3.14: *In vitro* α^{E180G}Strepβ heterodimer formation. Lane 1 and 6 contain stock controls of α^{E180G} and Strepβ homodimers and lanes 2 and 5 are α^{E180G} and Strepβ homodimer controls formed after homodimer dissociation and re-assembly. As in figure 3.13, the stock control of Strepβ was not chemically oxidised and was both single and double cross-linked thus two bands appeared. Lane 3 is a loading control with both α^{E180G} and Strepβ chemically cross-linked homodimers (same as in lanes 2 and 5). Lane 4 shows the resulting mixture of dimers after mixing monomers (1:3 ratio of Strepβ : α^{E180G}) and allowing dimer re-assembly; the newly formed α^{E180G}Strepβ heterodimer is indicated by a red asterisk and appeared between the two homodimer bands. 7.5 % SDS gel was used with samples ran under non-reducing conditions and stained using Coomassie blue.

3.4 Affinity purification of Tm heterodimers

Each heterodimer of interest was purified by affinity chromatography from the mixture of homodimers and heterodimers formed after dimer re-assembly. In each recombined dimer mixture there were three types of dimers; one homodimer that did not carry any tag, the heterodimer of interest which was single tagged and a homodimer that was double tagged. It was expected that when the mixture of these dimers would be applied onto the appropriate column, the non-tagged homodimer would be eluted first since it could not bind the matrix. Then the single-tagged

heterodimer elution would follow and last the double-tagged homodimer, which had the strongest affinity for the column matrix, would be eluted.

The challenging part in the above purification procedure was to separate the single tagged heterodimer from the double tagged homodimer. To improve the yield of heterodimer purification a 3:1 molar ratio of untagged : tagged homodimer was used at the beginning of the *in vitro* heterodimer formation experiment, as explained in section 3.3.2. This resulted in less double-tagged homodimer formation when the monomers were allowed to re-assemble. Figure 3.15 below shows the resulting dimers that were formed after mixing the starting reduced monomers in different molar ratios. It can be seen that when using a 1:2 or 1:4 ratio of tagged : non-tagged monomers, the amount of the recombined double tagged homodimer was reduced. Therefore during the formation experiment of any of the heterodimers of interest the initial reduced monomers were mixed together with a higher ratio of the non-tagged over the tagged monomer (i.e. 3:1 ratio). This was done only in order to maximise the purification yield of the heterodimer from the recombined dimer mixture.

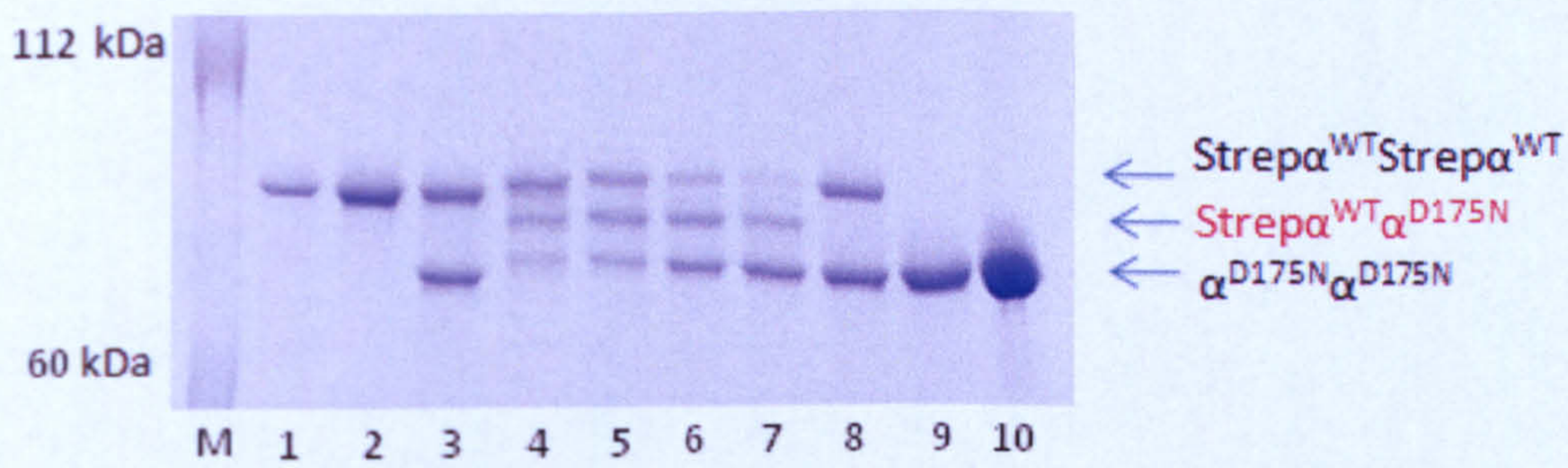

Fig 3.15: Formation of Strepα^{WT}α$^{D\ 175N}$ heterodimer, after mixing the tagged and the non-tagged reduced monomers in different molar ratios. 1) Strepα^{WT} stock control, 2) Strepα^{WT} cross-linked homodimer control, 3 and 8) Strepα^{WT} and α$^{D\ 175N}$ homodimers loading control. Mixed Strepα^{WT}: α$^{D\ 175N}$ in 4) 2:1 ratio, 5) 1:1 ratio, 6) 1:2 ratio, 7) 1:4 ratio. 9) α$^{D\ 175N}$cross-linked homodimer control, 10) α^{D175N} stock control. 7.5 % SDS gel was used with samples ran under non-reducing conditions and stained using Coomassie blue.

Depending on the tag used in each case an appropriate affinity chromatography method was followed. Thus for Strep tags, purification occurred on gravity flow Strep-Tactin column using desthiobiotin to elute the protein. For the His tag cases purification occurred on gravity flow NiNTA column and proteins were eluted by imidazole. Elution of the bound dimers was initiated by applying very low concentration of disthiobiotin or imidazole that would only be sufficient for elution of the weaker affinity single–tagged heterodimers. Then a final elution stage occurred, using high concentration of desthiobiotin or imidazole, that would elute the remaining bound material (desthiobiotin was used at 0.1 and 2.5 mM, imidazole used at 20, 50 and 250 mM). Samples were collected after each step (flow-through, washes, initial elution, final elution) and visualised on non-reducing SDS gels (since the samples were previously cross-linked after the dimer recombination step it was possible to see the dimers on the gels). In order to improve the purification yield, samples which contained a mixture of non-tagged homodimers with single tagged heterodimers were collected and subjected to further purification cycles. Figure 3.16 shows the three affinity chromatography cycles used for the purification of the Strep$\alpha^{WT}\alpha^{D175N}$ heterodimer. Samples highlighted in red in fig 3.16 contained mostly the heterodimer and were pooled together.

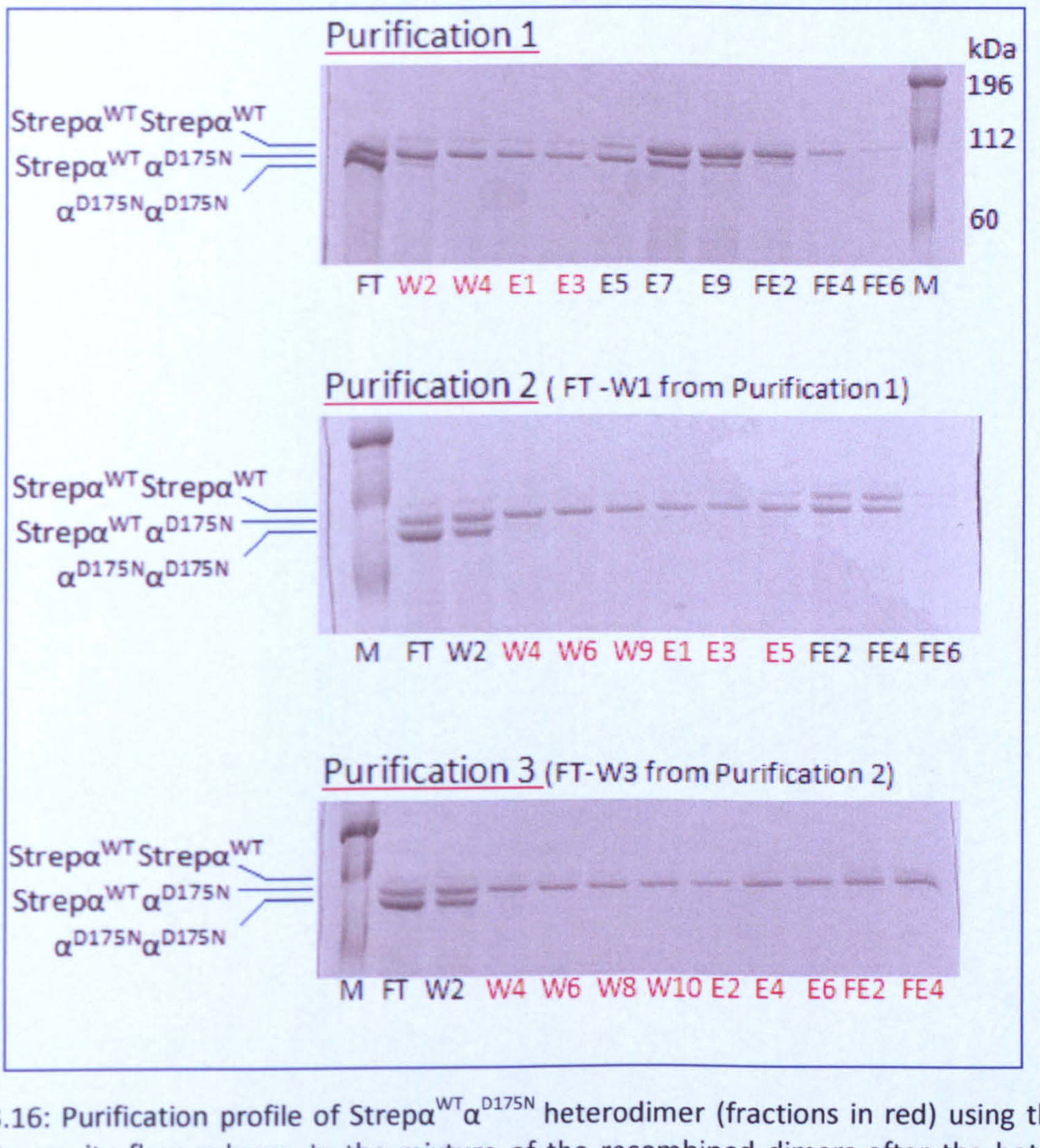

Fig 3.16: Purification profile of Strepα^{WT}α^{D175N} heterodimer (fractions in red) using the Strep-Tactin gravity flow column. In the mixture of the recombined dimers after the heterodimer formation experiment, the heterodimer is the middle band, the Strepα^{WT} homodimer is the upper band and the α^{D175N} homodimer is the lower band as shown previously in figure 3.10. In purification 1 (top gel) the untagged homodimer was eluted first in the flow through (FT) and the first wash (W1). Then the Strepα^{WT}α^{D175N} heterodimer was eluted with wash buffer (W2-W5) and with elution buffer (0.1 mM desthiobiotin) (E1-E3). The heterodimer together with the double-tagged Strepα^{WT} homodimer were co-eluted with the elution buffer (E4-E10) and final elution buffer (2.5 mM desthiobiotin) (FE1-FE6). The fractions containing the heterodimer of interest co-eluted with the mutant untagged homodimer were collected and subjected to further purification cycles 2 and 3. In detail the purification 1 included: Wash 5 x 4ml, Elution 10 x 1.5ml, Final Elution 6 x 1.5 ml. Purification 2: Wash 10 x 1.5 ml, Elution 5 x 1.5 ml, Final Elution 6 x 1.5 ml. Purification 3: Wash 10x 1.5 ml, Elution 6 x 1.5 ml, Final Elution 4 x 1.5 ml. 7.5 % SDS gels were used and samples ran under non-reducing conditions and stained using Coomassie blue.

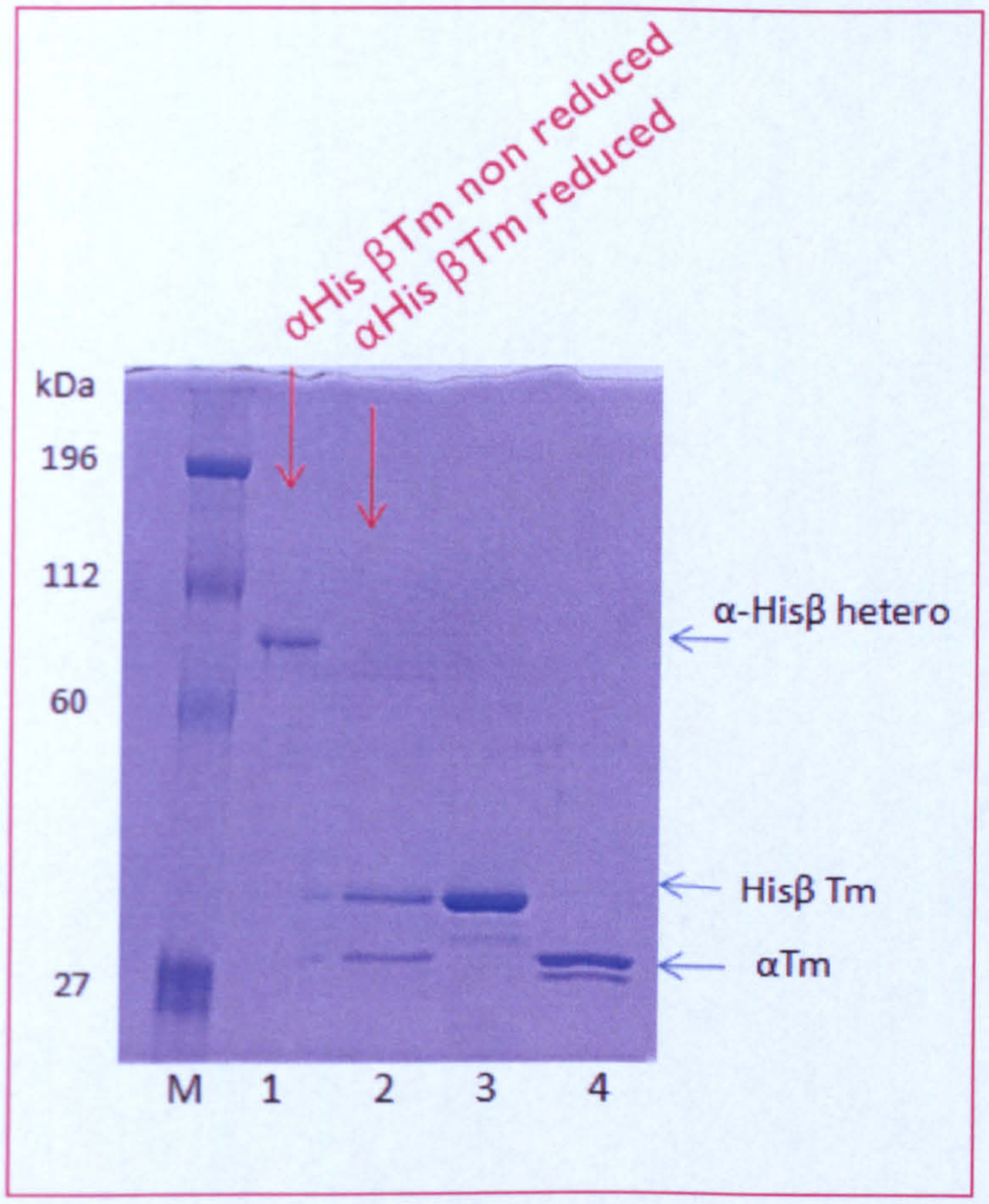

Fig 3.17: Purified α-Hisβ heterodimer run on SDS gel under non-reducing (lane 1) and reducing conditions (lane 2). When the heterodimer was loaded under reducing conditions it was broken down into the component subunits. Comparison with stock α and Hisβ controls that were loaded also under reducing conditions verifies that the purified sample was indeed the expected heterodimer, which was composed by the α and the Hisβ monomers. 7.5 % SDS gel was used and stained using Coomassie blue.

The purified bands that were expected to be the heterodimers were then checked on SDS gels under both non-reducing (no βME in sample buffer, no heating) and reducing conditions. Under reducing conditions each heterodimer was split into its component subunits. For each heterodimer tested, these component subunits ran on the gel exactly as the stock controls of the expected monomers. Therefore the purified bands were indeed the correct heterodimers. In figure 3.17 an example of α-Hisβ heterodimer is shown that was split into its component α and Hisβ monomers under reducing SDS-PAGE, which were identical to the stock controls of α and Hisβ.

3.5 Removal of affinity tags from purified heterodimers

After each heterodimer was purified the affinity tags were removed by FXa digestion. Independently of the type of the affinity tag present, all heterodimers were digested under the same conditions, since all of them contained the identical FXa protease restriction site sequence. Each heterodimer solution was incubated with FXa protease (10 unit/mg of protein) at 37 °C for 2 h and then placed at room temperature and continue the incubation overnight. The heterodimers were previously cross-linked therefore should remain associated during this digestion process. Complete digestion of the affinity tag was checked when the samples were loaded onto SDS gels together with non-digested controls (fig 3.18). After FXa digestion was completed, the samples passed through the Strep-Tactin or NiNTA columns. The cleaved tags were bound onto the column matrix while the digested/untagged heterodimers together with FXa protease were collected in the flow through. To further remove the FXa protease from the heterodimer, the mixture was incubated for 5 min with FXa removal resin (4 units of FXa protease can be bound onto 100 µl of slurry). After spinning for 5 min at 0.8 rpm the FXa protease was pelleted down together with the beads of the resin, while heterodimer was collected in the supernatant. As an example a non-reducing SDS gel is shown with the Strep$\alpha^{WT}\alpha^{D175N}$ and Strep$\alpha^{WT}\alpha^{E180G}$ heterodimers before and after the removal of the strep tag (fig 3.18). Unfortunately there was a significant amount of heterodimer still found in the pellet of the resin after centrifugation and this decreased the final purification yield of the heterodimer.

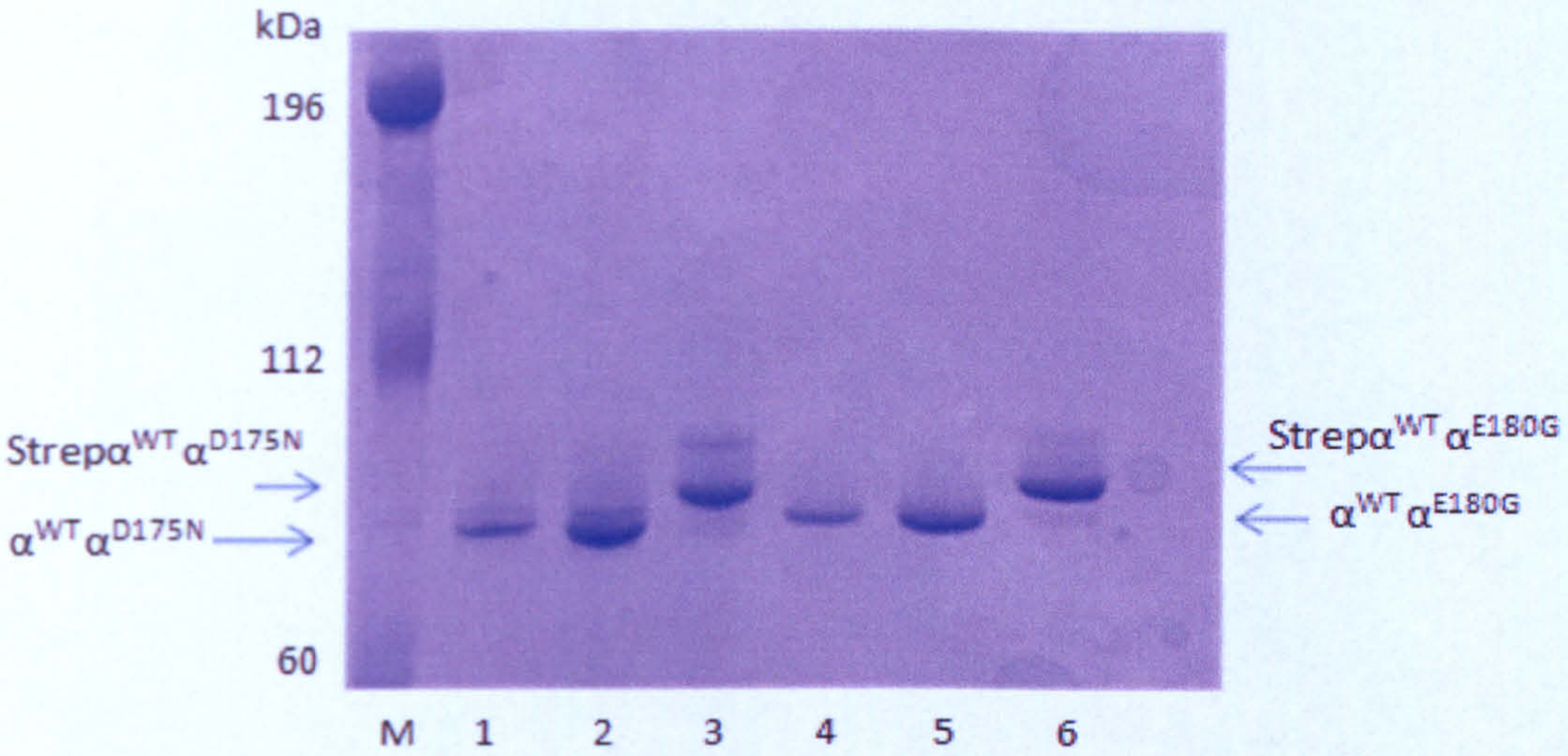

Fig 3.18: FXa digestions for removal of the Strep tag from Strepα^{WT}α^{D175N} and Strepα^{WT}α^{E180G} heterodimers. Samples ran under non-reducing conditions. Lanes 1 & 2 contain the digested α^{WT}α^{D175N} heterodimer and lane 3 is the undigested Strepα^{WT}α^{D175N} control. Lane 1 is the pellet of the FXa resin after centrifugation (during FXa protease removal step) and contained some heterodimer which could not be separated completely from the beads of the slurry. Lane 2 is the purified heterodimer collected from the supernatant after slurry centrifugation. Similar, lane 4 contain the α^{WT}α^{E180G} digested heterodimer that could not be further purified from FXa resin, lane 5 is the purified digested α^{WT}α^{E180G} heterodimer and lane 6 in the non-digested Strepα^{WT}α^{E180G} control. 7.5 % SDS gel was used and stained using Coomassie blue.

For each large scale heterodimer formation experiment 24 reaction tubes i.e. a total of 24 mg of homodimer mixture was used. Because the homodimers were mixed in a 3:1 ratio, the theoretical maximum amount of the heterodimer formed would be 50 % (i.e. 12 mg), assuming that all of the homodimer in shortage would be combined into heterodimer. About 5 mg of heterodimer was purified from the mixture of the recombined dimers. At the end of the FXa digestions about 3 mg of pure non-tagged heterodimer was obtained (i.e. 25 % yield).

3.6 Mass spectrometry

The homodimer stock solutions and the purified heterodimers that were subjected to FXa digestion were then analysed by electrospray mass spectrometry.

For the homodimer samples the mass spectrometry results were in agreement with the predicted molecular mass values:

Homodimer	Monomer mass		Dimer mass	
	Predicted	Mass Spec	Predicted	Mass Spec
α	32838.7	32839.18	65677.4	65677.4
β	32994.8	32995.3	65989.6	65990.32
α^{D175N}	32837.7	32837.8	65675.4	65675.62
α^{E180G}	32766.6	32762.18	65533.2	65417.37 **(-116)**

Table 3.1: Mass spectrometry analysis of the Tm homodimer samples. Both monomer and dimer molecular mass could be detected. The mass spectrometry results were largely in agreement with the predicted values.

Strangely the α^{E180G} sample had the correct molecular mass when found as monomer, but when formed dimers, the dimer molecular mass was 116 Da less than expected (i.e. this makes each chain of the dimer -58 Da).

The molecular mass of each heterodimer was estimated by adding up the molecular masses of the two component subunits (as was found from the homodimer mass spectrometry results shown in table 3.1 above). These predicted values were compared to the actual values obtained after mass spectrometry analysis. Because the heterodimer samples were cross-linked the mass spectrometry only showed the mass of the whole dimer and not of the individual subunits. The results are compared in the table 3.2 below.

Heterodimer	Predicted mass	Actual mass after mass spec
$\alpha^{WT}\alpha^{D175N}$	65676.98	65690.58 **(+14)**
$\alpha^{WT}\alpha^{E180G}$	65601.36	65561.41 **(-44)**
αβ	65834.48	66040.64 **(+207)**
$\alpha^{D175N}\beta$	65833.1	66023.59 **(+191)**
$\alpha^{E180G}\beta$	65757.48	65899.6 **(+138)**

Table 3.2: Mass spectrometry analysis of the cross-linked Tm heterodimer samples that were digested with FXa to remove the N-terminal tag. Both estimated mass and the mass spectrometry results are shown and the numbers in brackets show the difference between the two values.

The mass spectrometry results from table 3.2 indicate that:

$\alpha^{WT}\alpha^{D175N}$: the mass is +14 Da larger than the expected ; that could be due to methylation of the α chain.

$\alpha^{WT}\alpha^{E180G}$: the mass is -44 Da less than the expected; this could be due to the -58 Da that the α^{E180G} shows when found as dimer (as shown in the homodimer case, table 3.1) plus the +14 Da from the methylation of the α chain as noticed for the $\alpha\alpha^{D175N}$ heterodimer above.

αβ : the mass is +207 Da more than the expected; this could be explained by extra mass at the β chain due to wrong site of FXa digestion (fig 3.19). If the protease cuts after the residue E in the recognition site sequence IEGR instead of the expected residue R, then the dipeptide GR will remain attached on the β chain and its molecular mass will be 33208. Thus the αβ heterodimer expected molecular mass will then be 66047 i.e. very close to the obtained mass spectrometry result.

$\alpha^{D175N}\beta$: the mass is +191 Da more than the expected; this could be due to the extra GR dipeptide on the β chain as shown in the αβ heterodimer case above. The estimated molecular mass for the $\alpha^{D175N}\beta$ would then be 66046 i.e. -22 Da compared to the obtained mass spectrometry result.

$\alpha^{E180G}\beta$: the mass is +138 Da more than the expected; this could be due to the extra GR dipeptide on the β chain combined with the -58 Da mass loss due to the α^{E180G} dimer formation effect. The estimated molecular mass for the $\alpha^{E180G}\beta$ would then be 65912 i.e. -12 Da compared to the obtained mass spectometry result.

N-terminal sequencing of the constructs is required to verify the predictions above, but unfortunately there was no time to permit these controls to be carried out.

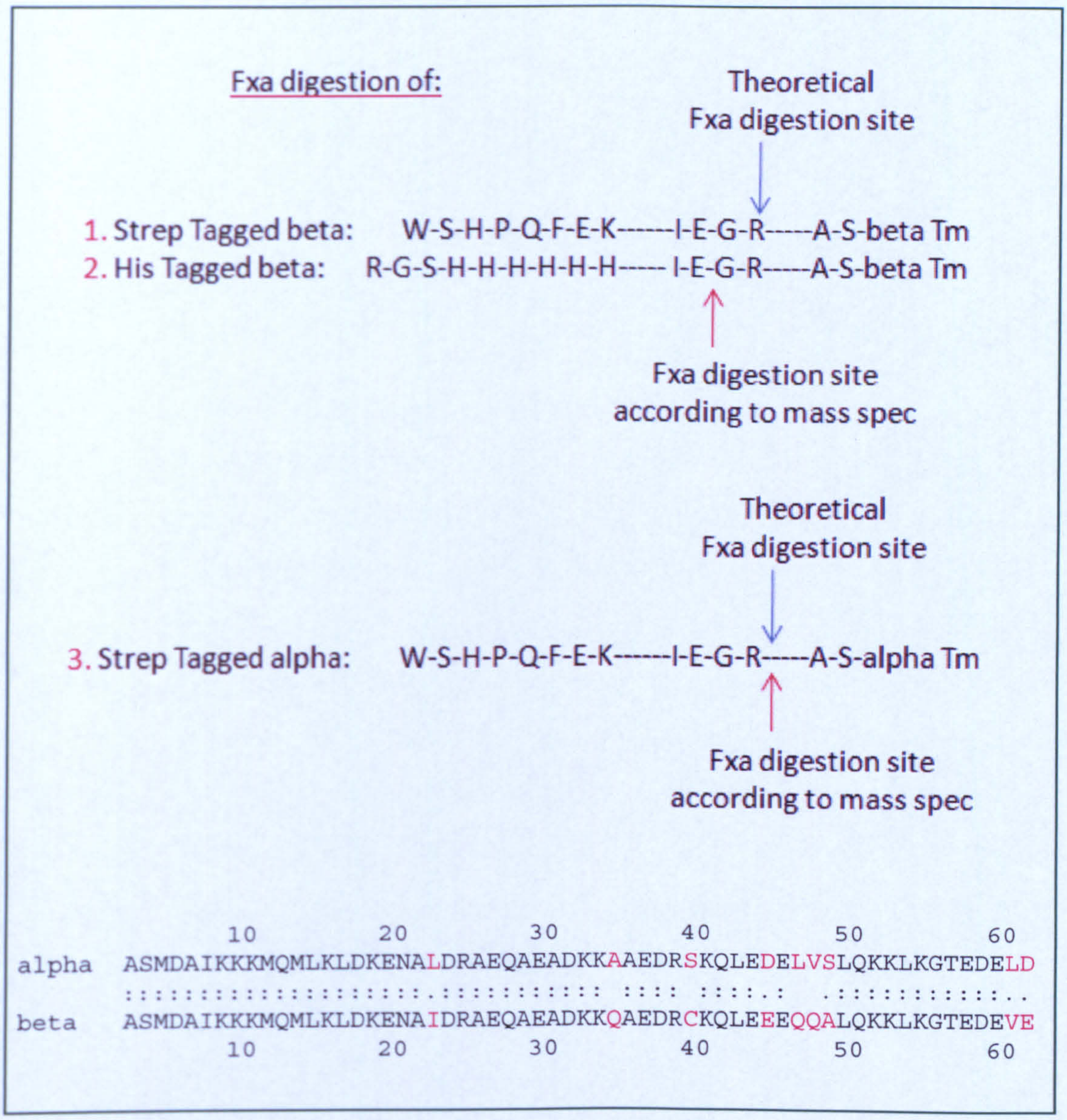

Fig 3.19: Predicted site of FXa digestions. According to the mass spectrometry results the FXa enzyme does not always cut after the last Arg in the recognition site IEGR. It can also cut after E, leaving the GR dipeptide at the N-terminal of the protein. This FXa digestion pattern does not depend on the type of the affinity tag prior to FXa site, since both His and Strep tag β Tms are digested after E residue. Instead it is dependent on the protein sequence itself since it can cut after R in the Strep tag α Tm, despite the fact that the α and the β Tms have very similar N-terminal sequences.

3.7 Conclusion

The novel method described in this chapter for the *in vitro* skeletal Tm heterodimer formation was successful in the formation of five different types of heterodimers i.e. the αβ, $\alpha^{WT}\alpha^{D175N}$, $\alpha^{WT}\alpha^{E180G}$, $\alpha^{D175N}\beta$ and $\alpha^{E180G}\beta$ heterodimers. Therefore, we are now capable of proceeding further into the characterisation of the pure skeletal αβ heterodimer and subsequently to compare its properties to the αα and the ββ homodimers. Also, heterodimers-carriers of a HCM mutation were made for the first time and can now be characterised. Subsequently the effect of the α^{E180G} or α^{D175N} mutations can be studied more extensively, since it is possible that these HCM mutants can be found both as homodimers or heterodimers in the diseased heart.

The most important element of this method was the ability to use and then remove the small affinity tags. Therefore the purification of the various heterodimers could be achieved by affinity chromatography. Without the affinity tags an adequate amount of heterodimer would be very difficult to obtain from the homodimers mixture using ion exchange or hydroxyapatite chromatography, since all of the dimers would be similar in ionic behaviour (the separation of native αα and αβ Tm dimers or of the untagged $\alpha^{WT}\alpha^{mutant}$ heterodimer from the homodimers mixture was tried as mentioned earlier, but proved to be very difficult). Also by tag removal after FXa treatment, the heterodimers obtained were very similar to the corresponding native acetylated heterodimers. Ideally for best purification it would be useful to have a heterodimer with two different tags on each chain. This way the heterodimer would be very easy to separate from the homodimers using a two-step affinity chromatography procedure. In the first step one type of the homodimer would be excluded and in the second step the other homodimer would be excluded. A combination of Strepα and Hisβ homodimers was used as starting materials for the Strepα-Hisβ double-tagged heterodimer formation but unfortunately they did not combine into the heterodimer.

When untagged α and β subunits were used as starting materials, heterodimer formation was not possible. In that case, when the α and β subunits were mixed they preferentially formed αα and ββ homodimers. The same unsuccessful result obtained

after mixing tagged αα homodimers with untagged ββ homodimers. However, the heterodimer did form when the tagged ββ homodimers were used (all experiments were performed under exactly the same conditions). Perhaps the untagged β subunits were preferentially recombined into the ββ homodimer, while in contrast the tagged β subunits were not preferentially recombined into the HisβHisβ homodimer. This way there would be Hisβ subunits available to interact with the α subunits and form heterodimers. This hypothesis was later confirmed by circular dichroism studies and the observations are discussed in chapter 6. *In vivo*, the α and the β monomers give rise only to the αα and the αβ dimers, while the ββ homodimer is unstable at physiological temperatures and not found. So if the ββ homodimer is indeed the preferential/less energy demanding dimer to form, *in vivo* this does not happen because ββ eventually falls apart. Therefore, the β chains have no other option *in vivo* than to combine with the α chains and form the αβ heterodimer which is more stable at physiological conditions.

Chapter 4

Characterisation of Tropomyosin Heterodimers

4.1 Introduction

Currently most of our knowledge on Tm comes from studies of Tm homodimers (of skeletal or smooth isoforms) and smooth Tm heterodimers.

It is known that in smooth muscles the predominant Tm dimer is the αβ heterodimer that can reach up to 95 % in chicken gizzard for example (Sanders *et al.* 1986). Thermal unfolding and refolding studies revealed that heterodimer of smooth Tm isoform was preferentially assembled over homodimers (Lehrer and Qian 1990; Lehrer and Stafford 1991). The smooth Tm heterodimer differs from either the αα or the ββ smooth Tm homodimers in having stronger end-to-end interactions as observed by thermal unfolding and viscosity measurements (Graceffa 1989; Jancso and Graceffa 1991). More recent studies revealed that smooth Tm heterodimers formed *in vitro* using bacterially expressed homodimers with an Ala-Ser N-terminal extension could bind actin as well as the native smooth Tm heterodimer. Furthermore, by creating a series of heterodimers with the N-terminal Ala-Ser extension on only one of the chains, it was concluded that the α chain of the smooth heterodimer contributed the most in actin binding (Coulton *et al.* 2006). Having succeeded in the *in vitro* formation of the skeletal αβ Tm heterodimer as shown in chapter 3, we are now in position to start its

characterisation and draw comparisons between the smooth and the skeletal heterodimers.

In the case of skeletal Tm isoforms there are many studies on the wild-type α Tm homodimers and their comparison to mutant α homodimers that cause familial cardiomyopathies. The α^{D175N} and the α^{E180G} mutations that cause hypertrophic cardiomyopathy are of great interest; they are both located in period 5, which is the most conserved amongst the seven periods of Tm (Hitchcock-DeGregori *et al.* 2002). Moreover the mutations α^{D175N} and α^{E180G} are found at positions g and e of the heptad repeat respectively, suggesting that they could have a direct effect on the ionic interactions between the two chains of the coiled-coil that stabilise the molecule and perhaps they may affect the binding of Tm to neighbouring actin or TnT. Skeletal muscle fibres from biopsy samples from patients carrying the α^{D175N} mutation were compared to wild-type muscle fibres from an unaffected individual. The comparison showed that the α^{D175N} had increased Ca^{2+} sensitivity over the wild type but no difference in maximum force or maximum shortening velocity (Bottinelli *et al.* 1998). In transgenic mice overexpressing the α^{D175N} mutant the Ca^{2+} sensitivity of the myofilaments was increased and the left ventricular relaxation rate was decreased in comparison to the wild-type (Evans *et al.* 2000). *In vitro* motility assays of actin filaments decorated with bacterially expressed α^{D175N} or α^{E180G} Tm over myosin showed that after addition of Ca^{2+} and skeletal Tn , the sliding velocity was 18 % increased for the α^{D175N} Tm and 21 % increased for the α^{E180G} Tm. In contrast, the increase in velocity of actin/α^{WT} Tm filaments was only 5 % upon addition of Ca^{2+} and Tn (Bing *et al.* 1997). However both mutations had less impact when cardiac Tn was used in the experiment (Bing *et al.* 2000). Characterisation of bacterially expressed α^{E180G} and α^{D175N} Tm homodimers was also performed in our laboratory. Measurement of S1 binding onto actin filaments decorated with the Tm of interest in the presence of either skeletal or cardiac Tn over a range of Ca^{2+} concentrations from pCa 8.9 to pCa 4.5 was performed using the stopped flow technique. The rate constants obtained were plotted against the pCa values and from the pCa curves it was shown that both mutants had slightly increased Ca^{2+} sensitivity compared to the wild-type, with the α^{E180G} having the strongest effect of 0.1 pCa unit shift (Boussouf *et al.* 2007). Both mutants also showed decreased affinity for actin as measured by actin cosedimentation assays. Moreover

from Differential Scanning Calorimetry (DSC) the α^{D175N} and the wild type Tm appear to have the same melting temperatures (i.e. ~50 ˚C for the N terminal peak and ~43˚C for the C-terminal peak). In contrast thermal unfolding of the α^{E180G} mutant occurred at lower temperatures 48.8˚C and 39.7˚C for the N and C termini respectively (Kremneva *et al.* 2004). Having succeeded in the *in vitro* formation of the skeletal Tm heterodimers that are carriers of the α^{E180G} and α^{D175N} mutants as shown in chapter 3, we are now in position to start their characterisation and investigate if they differ from the wild type and mutant homodimers.

In contrast to the smooth heterodimers and the skeletal Tm homodimers, there is little information on the skeletal Tm heterodimers. One thing is certain that the skeletal Tm isoforms do not follow the paradigm of the smooth isoforms in preferential assembling heterodimers over homodimers *in vitro*. However, skeletal Tm heterodimers do exist in cells and it is our hypothesis that they are different from the homodimers. As mentioned in section 1.3, because the coiled-coil of the Tm heterodimer is composed by two different chains, it could be different from the homodimers both in its interior and in the external surface. Therefore in the core of the coiled-coil the two chains could be different in how they interact and how tightly they hold the coiled-coil together. Subsequently, the heterodimer may have different thermal stability in comparison to the homodimers. Also the heterodimer presents different residues at its surface compared to the homodimers, therefore the heterodimer could be different in its interactions with partner proteins like actin and TnT. Tm heterodimers could also be different from the homodimers in the strength of their end-to-end interactions as it was reported in the smooth heterodimer case.

In this chapter the skeletal Tm heterodimers that were made in chapter 3, were characterised by three sets of experiments. With circular dichroism the thermal stability of each Tm heterodimer was investigated and compared to the thermal stability of the homodimers. Then the affinity of each Tm heterodimer for actin was measured. Tm affinity for actin was also measured in presence of the N-terminal part of TnT. Finally the regulation of S1 binding to actin filaments decorated with the Tm dimer of interest or Tm dimer together with skeletal Tn complex was observed by

stopped flow experiments. The results obtained here support our original hypothesis and show that Tm heterodimers are different from the homodimers. The heterodimers have different thermal stabilities and different binding affinities to actin in comparison to the homodimers of their component subunits. This leads us in a new hypothesis that the presence of different types of skeletal Tm dimers in skeletal muscle and heart is a mechanism of fine tuning muscle contraction.

4.2 Thermal unfolding of Tropomyosin monitored by Circular Dichroism spectroscopy

Circular dichroism (CD) measurements were carried out to investigate the thermal stability of each of the five Tm heterodimers that were formed *in vitro* and purified as was shown in chapter 3 plus the Tm homodimer samples for comparative studies. The CD spectrum of a Tm molecule (covering a range from 260 to 190 nm) shows three peaks which are typical in every coiled-coil structure; two negative peaks at 208 and 222 nm and one positive peak at 190 nm (fig 4.1). When the temperature was increased from 25 °C to 45 °C and finally to 80 °C, the percentage of coiled-coil structure in the sample was decreased (i.e. denaturation of Tm) as shown by the three indicator peaks that became progressively weaker.

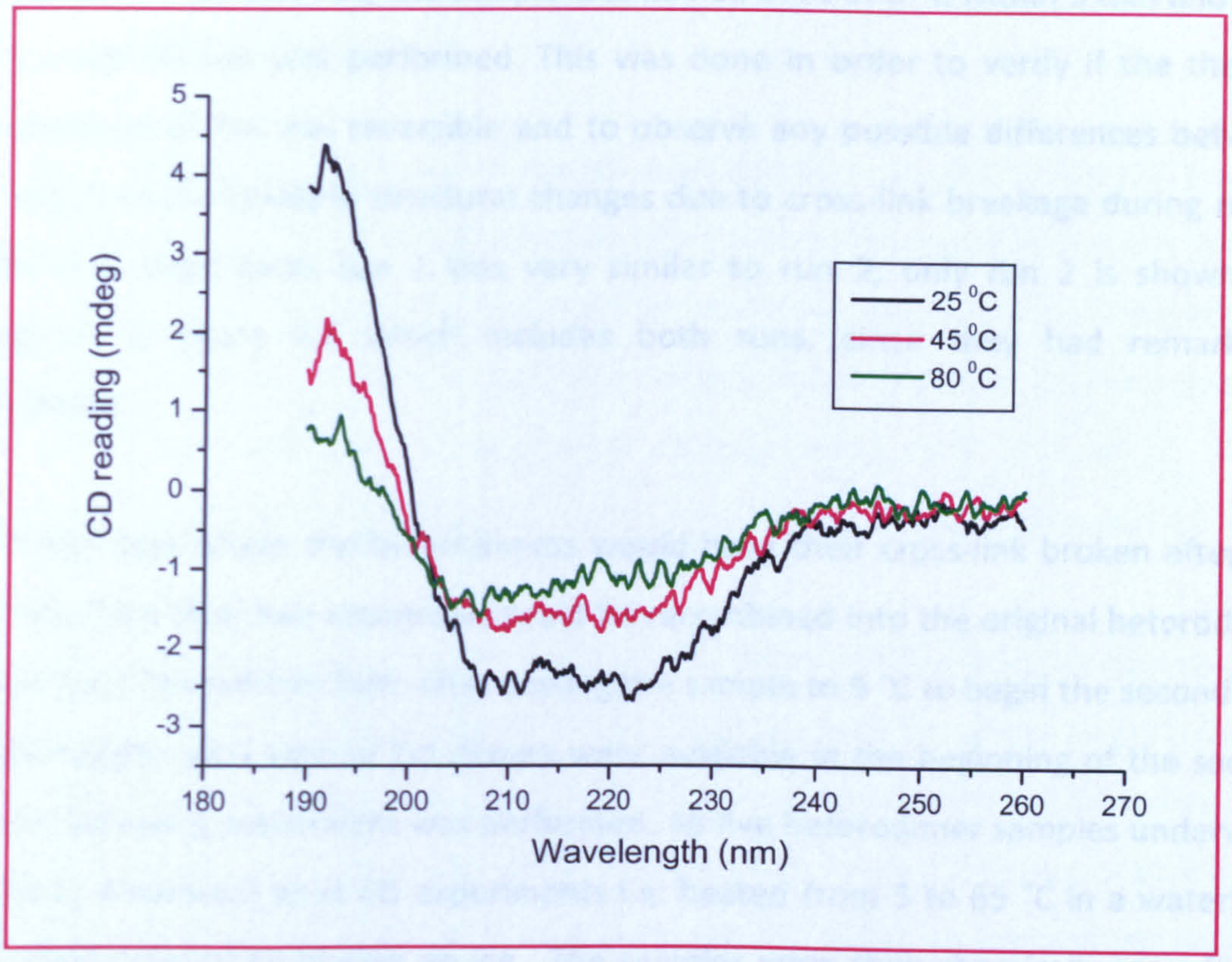

Fig 4.1: Circular Dichroism spectrum of α^{WT} Tm homodimer. Since Tm is a classic coiled-coil it showed three peaks in its CD spectrum at 190, 208 and 222 nm wavelength. These peaks can be seen better in the spectrum at 25 ˚C (in black) where Tm was folded. Upon thermal unfolding of Tm the peaks became weaker since coiled-coil structure was decreased. The traces were quite noisy because a small cuvette was used containing only 10 µl of 8 µM Tm sample.

In order to examine the thermal unfolding of each of the Tm dimers, CD readings were recorded as temperature was increasing at a constant rate of 1.5 ˚C /min from 5 to 65 ˚C. In this case the wavelength was set to 222 nm, which alone is sufficient to report any changes in the coiled-coil structure (method described in section 2.3.1).

For each of the Tm sample under examination two CD runs were taken. During the first run the signal was gradually increased until reached a constant - plateau phase at higher temperatures where no further change in the CD readings was observed. After reaching 65 ˚C in the first run, the Tm samples could have their cross-link broken. The experimental buffer contained DTT, to help maintain the samples in the reduced state after the first run and prevent disulphide cross-linking of the reduced Tm dimers. After

completion of the first run, the sample was cooled back at 5 °C within 3 min and then the second CD run was performed. This was done in order to verify if the thermal denaturation of Tm was reversible and to observe any possible differences between the two runs for example structural changes due to cross-link breakage during run 1. Because in most cases run 1 was very similar to run 2, only run 2 is shown. An exception is figure 4.4 which includes both runs, since they had remarkable differences.

In the case where the heterodimers would have their cross-link broken after the first run, then their two monomers could be recombined into the original heterodimer or into their homodimer form after cooling the sample to 5 °C to begin the second run. To investigate what kind of Tm dimers were available in the beginning of the second run the following experiment was performed. All five heterodimer samples underwent the same treatment as in CD experiments i.e. heated from 5 to 65 °C in a waterbath and rapidly cooled by placing on ice. The samples were then chemically cross-linked and loaded onto SDS gels under non-reducing conditions to view the newly formed dimers. Control stock heterodimers were also loaded for comparisons. There was no obvious difference between the stock samples and the samples that were treated as in a CD experiment. Only in $\alpha^{D175N}\beta$, $\alpha^{E180G}\beta$, and $\alpha^{WT}\beta$ heterodimers traces of extra bands appeared, and presumably these were newly recombined homodimers. The newly formed bands were much smaller in comparison to the original heterodimer band, so they shouldn't interfere much to the unfolding curves of the heterodimer taken for run 2.

4.2.1 Comparison of the thermal stability of the αβ heterodimer vs. the αα and ββ homodimers

The thermal unfolding curve of the αβ heterodimer is shown in figure 4.2 and is compared to the thermal unfolding curves of its subunit homodimers i.e. the αα and the ββ. To allow comparison between the three dimers, all curves were normalised from 0 to 1 to obtain curves with common starting and end points. This was done by subtracting the starting CD measurement corresponding to 5 °C from all of the recorded CD readings and dividing afterwards by the final CD measurement at 65 °C.

The thermal unfolding curve of any of the Tm dimers tested is highly complex and does not represent a single phase unfolding event. In each Tm dimer case (in fig 4.2 and in the following figures), at least three phases of unfolding were observed. The two blue lines that are drawn on the melting curves in figure 4.2 separate each curve in these three phases. The three phases were clearer in the αα homodimer case: 1) The first phase had a slow unfolding rate and in the case of the αα homodimer this extended up to 30 °C. 2) The unfolding rate then accelerated, since the slope of the curve became steeper, until about 45 °C. 3) After this point the slope of the curve changed again, indicating that another unfolding event occurred, and extended up to 54 °C. From this point on the unfolding was complete and no other change in CD readings was observed.

From fig 4.2 it is clear that the most stable dimer is the αα homodimer while the least stable dimer is the ββ homodimer. The melting temperature of each dimer can be estimated by the midpoint of the melting curve (the temperature at which the normalised CD signal = 0.5). If the melting curve was a single phase event then the midpoint would accurately describe the melting temperature of each dimer. However, since at least three phases are included, the midpoint is just an approximation of the melting temperature of each dimer. Differentiation of the sigmoidal thermal unfolding curve does not improve the estimation of the number of the transitions involved or of the midpoint of the transition, because the resulting derivative appears quite noisy and with a broad peak. Thus the probability of error in estimating the melting temperature is higher upon smoothing of the derivative and defining the centre of the

peak. On the other hand, the midpoint of each unfolding curve is taken at exactly 0.5 CD reading, thus it is a more reproducible approach to compare the various Tm dimers. Thus the melting temperature using the midpoint for the αα homodimer is about 44.7 ˚C. The melting temperature of the ββ homodimer is very low indeed about 38.4 ˚C. The αβ heterodimer has an intermediate melting profile in comparison to the homodimers and its melting temperature is about 39.5 ˚C. The αβ heterodimer thermal unfolding curve is more similar to that of the least stable ββ homodimer. The differences in the melting profile between the αβ and the ββ dimers are more noticeable at the third phase of the unfolding process.

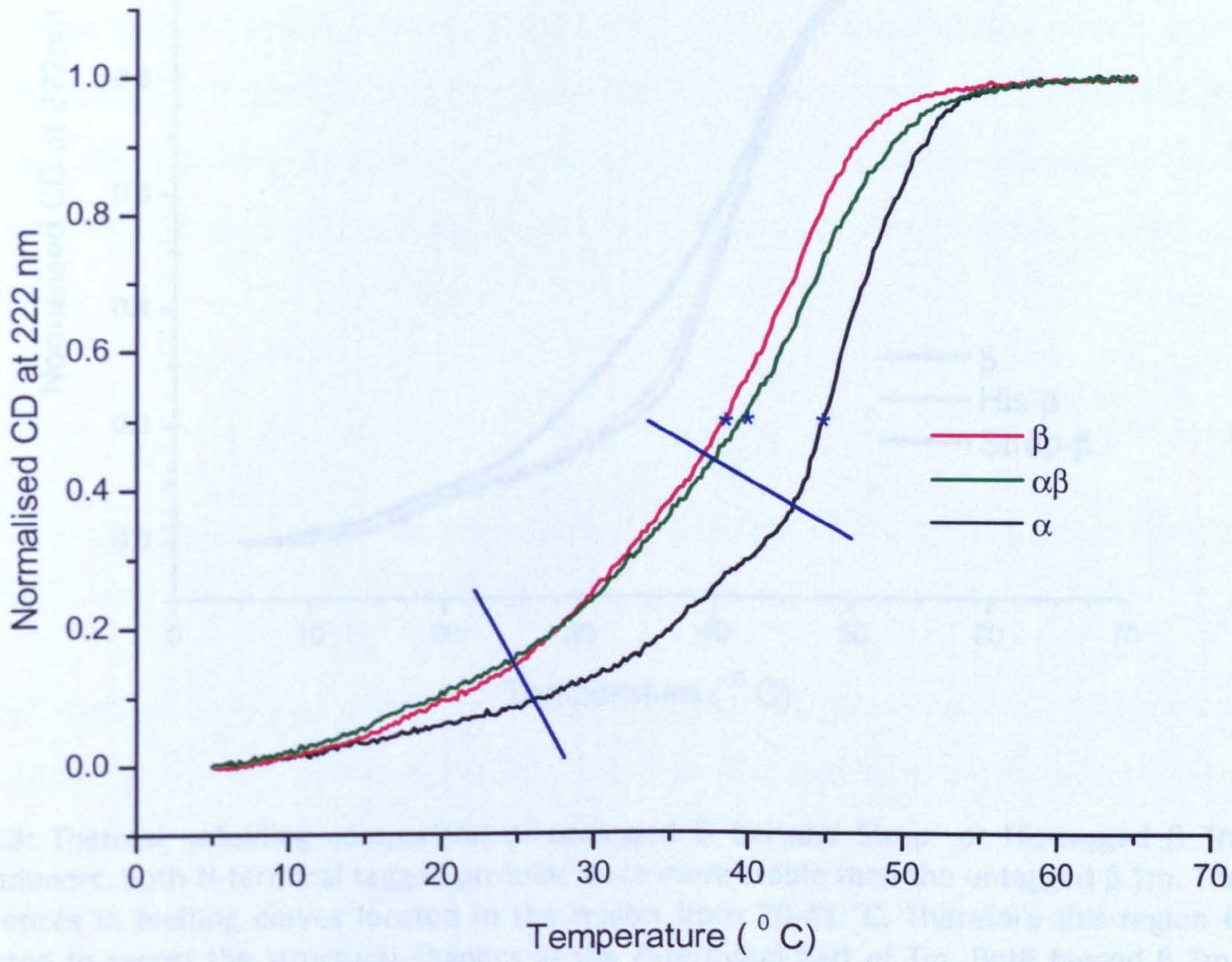

Fig 4.2: Thermal unfolding comparisons of αβ heterodimer vs. the αα and ββ homodimers. It is clear that the most stable dimer is the αα homodimer. The melting temperature of each dimer is estimated by the midpoint of each curve that is indicated by an asterisk (*). The least stable is the ββ homodimer with a melting temperature of ≈38.4 ˚C i.e. close to physiological temperature. The heterodimer has an intermediate thermal stability (melting temperature of ≈39.5 ˚C) compared to the homodimers and is more similar to the least stable ββ homodimer.

4.2.2 Comparison of the thermal stability of the ββ homodimer vs. the thermal stability of N-terminal affinity tagged ββ homodimers

In chapter 3 it was explained that for the formation of heterodimers containing one β subunit, Strep- or His-tagged β homodimers were used. Interestingly, the thermal unfolding of the untagged vs. the tagged β homodimers was very different as it can be observed in figure 4.3.

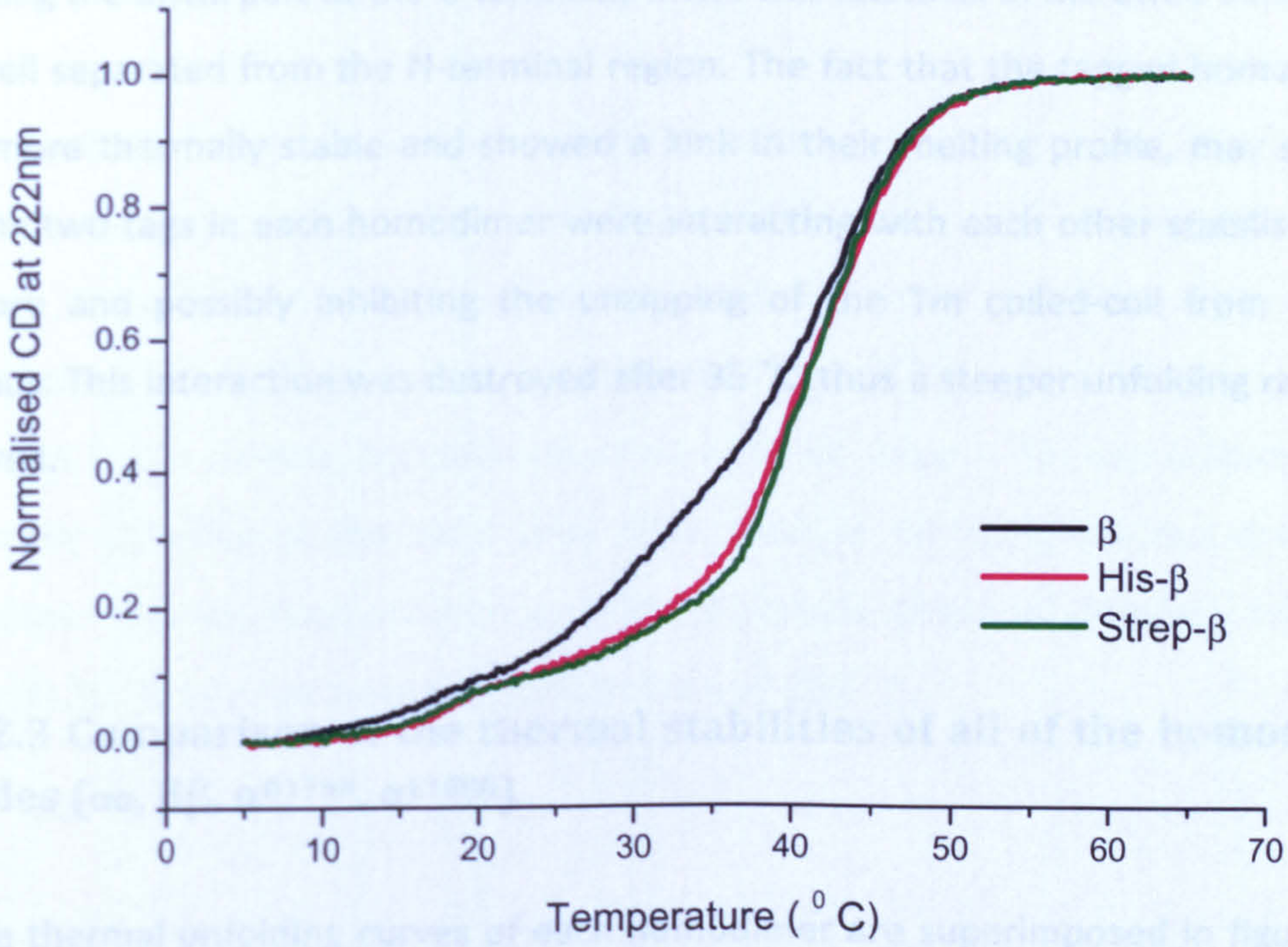

Fig 4.3: Thermal unfolding comparison of untagged β Tm and Strep- or His-tagged β Tm homodimers. Both N-terminal tagged proteins were more stable than the untagged β Tm. The differences in melting curves located in the region from 20-43 ˚C. Therefore this region is expected to report the structural changes at the N-terminal part of Tm. Both tagged β Tms showed the same melting profile and after 35 ˚C the rate of unfolding was increased. From 43 ˚C on all three dimers were identical in their thermal unfolding.

The tagged homodimers did not simply show a small kink within their melting curves that would correspond to a small local change in structure. Instead a large area from 20 to 43 ˚C was affected suggesting that within this area changes involving the N-terminal part can be found. Also it is shown clearly in figure 4.3 that both Strep- or His-tagged β Tm were more stable than the non-tagged β Tm.

The three homodimers had also distinct shape of melting curves. The wild type β Tm showed a rather smooth unfolding curve, in which the three phases were not distinct. Both tagged β Tms showed a more marked triphasic curve. In the tagged homodimers there was also a characteristic kink in the unfolding curve at 35 ˚C. Below this point there was a small change in CD reading but after passing 35 ˚C, a steeper unfolding rate was observed. However after 43 ˚C all three dimers showed a more synchronized behaviour in unfolding and reached the plateau phase at the same time. It can be assumed that this latter part of the curve (i.e. 43 -65 ˚C) gives information regarding the distal part of the C-terminal, which was identical in the three dimers and was well separated from the N-terminal region. The fact that the tagged homodimers were more thermally stable and showed a kink in their melting profile, may suggest that the two tags in each homodimer were interacting with each other stabilising the structure and possibly inhibiting the unzipping of the Tm coiled-coil from the N-terminus. This interaction was destroyed after 35 ˚C, thus a steeper unfolding rate was observed.

4.2.3 Comparison of the thermal stabilities of all of the homodimer samples (αα, ββ, α^{D175N}, α^{E180G})

The thermal unfolding curves of each homodimer are superimposed in figure 4.4. Two panels are shown in the figure and these correspond to the thermal unfolding curves obtained after the first run and after the second run of the CD experiment (as explained in pg 129). Both runs are presented because in the case of mutant α^{D175N} and α^{E180G} Tm homodimers, differences were observed in their melting profiles between the two runs. During the first run both mutants showed a shoulder in their CD curves prior to the main unfolding transition. Such shoulder was not observed for the α^{WT} Tm homodimer. This structural change in the mutant homodimers happened at an early stage during unfolding with the temperature being 32.2 ˚C for α^{D175N} and 23.8 ˚C for α^{E180G} Tm. This unfolding event was also observed in previous published DSC work (reported at 28 ˚C and 25 ˚C for α^{D175N} and α^{E180G} respectively, (Kremneva *et al.* 2004)). However this was an irreversible event that did not appear in the second run. This observation can be explained by both mutant homodimers being cross-linked during

the first run, which then had their cross-link broken after reaching 65 °C and so being reduced in the second run. In run 1 the location of both mutations close to the cross-link at position C190 caused a local structural instability, while in run 2 the mutations did not show any effect because they were not combined with a cross-link. Presumably when the cross-link was broken, the two mutant chains were not held tightly together within the coiled-coil and therefore could be more flexible at least locally in order to adopt a more favourable structural conformation. To verify the above observation, two CD experiments should be performed, one using fully chemically cross-linked dimers and the other using fully reduced dimers.

In run 2 all dimers showed at least three phases of unfolding and their melting temperatures were estimated by the mid-point of their thermal unfolding curves. The α^{WT} and the α^{D175N} homodimers had very similar thermal stabilities with melting temperatures of 44.7 °C and 45 °C respectively. The α^{E180G} homodimer appeared less stable and had a melting temperature of 41.4 °C. All three α Tm homodimers were completely unfolded at the same time after reaching 54 °C. In contrast the β Tm homodimer was the least stable one, reached plateau phase of complete unfolding earlier (at 50 °C) and had a melting temperature of 38.4 °C.

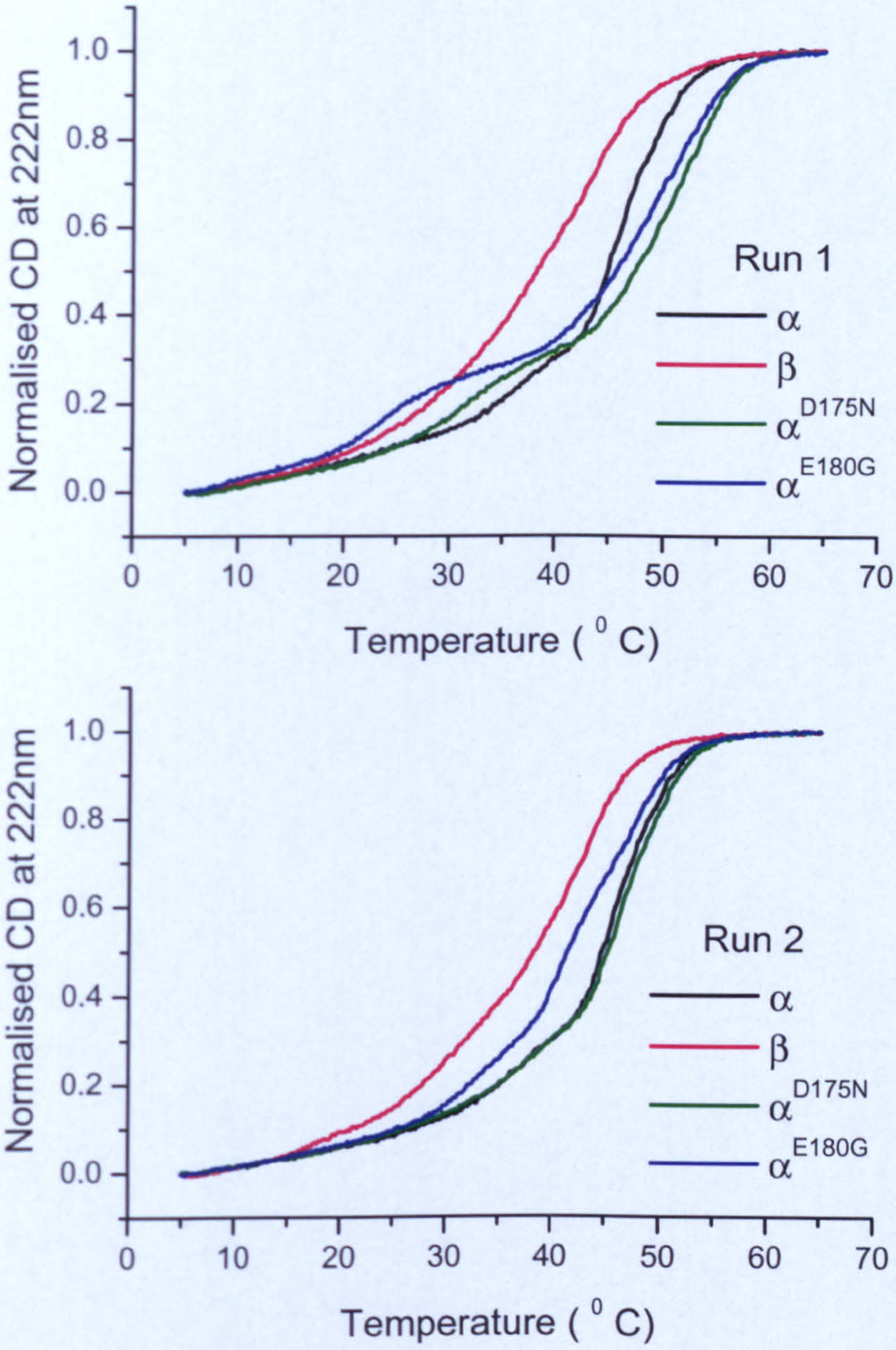

Fig 4.4: CD comparisons between the control homodimer samples. Panel A shows the Tm dimers during the first run and panel B shows the same dimers as in A that were run for a second time. Both mutant α^{D175N} and α^{E180G} Tm homodimers showed an early denaturation effect in panel A, at 32.2 ˚C and 23.8 ˚C respectively, which was irreversible and did not appear again in panel B. From the second run the α^{WT} Tm and the α^{D175N} Tm appear more stable than the α^{E180G} Tm (44.7, 45 and 41.4 ˚C respectively). The ββ homodimer was the least thermally stable from all.

Moreover figure 4.4 shows that the mutant homodimers in their cross-linked conformation (run 1) reached the plateau phase of complete unfolding at 59 °C, while when they were reduced (run 2) they reached plateau much earlier at 54 °C. In contrast the α^{WT} Tm homodimer was indistinguishable between the two runs. Mass spectrometry analysis of the α^{WT} Tm sample revealed the presence of monomers only, therefore the dimers in this particular batch of Tm were not cross-linked (*this was due to a variation in the α^{WT} protein's purification protocol where the heating step at 80 °C for 10 min of the bacterial lysate was skipped; if the protocol is followed as described in section 2.2.3a then most of the protein purified is cross-linked*). Therefore a non cross-linked dimer showed no difference particularly in the area from 54 °C to 65 °C. It can be concluded that within this last part of the melting curve changes in thermal stability due to breakage of cross-link can be reported. This is expected if we think that breaking a covalent bond should be the most energy demanding step during unfolding of Tm dimer.

These results are comparable to previous published observations using DSC experiments; Kremneva et al., reported that all of the α Tm homodimers under examination were less thermally stable when the cross-link was reduced and they observed a difference in the melting temperatures at the C-terminal region of the molecule. They reported that the melting temperatures for the N-terminal parts were 50 °C for α^{WT} and α^{D175N} and 49°C for α^{E180G} homodimer. For the C-terminal part of the reduced dimers the melting temperatures were 43 °C for α^{WT} and α^{D175N} and 40°C for α^{E180G}, while for the oxidised dimers were 54.3, 53.1 and 53.3 °C for α^{WT}, α^{D175N} and α^{E180G} respectively (Kremneva *et al.* 2004).

4.2.4 Comparison of the thermal stabilities of the heterodimers- carriers of hypertrophic cardiomyopathies vs. their constituent subunits' homodimers

Each set of the thermal unfolding curves of a heterodimer together with the corresponding homodimers are shown in figure 4.5 below in panels A-D.

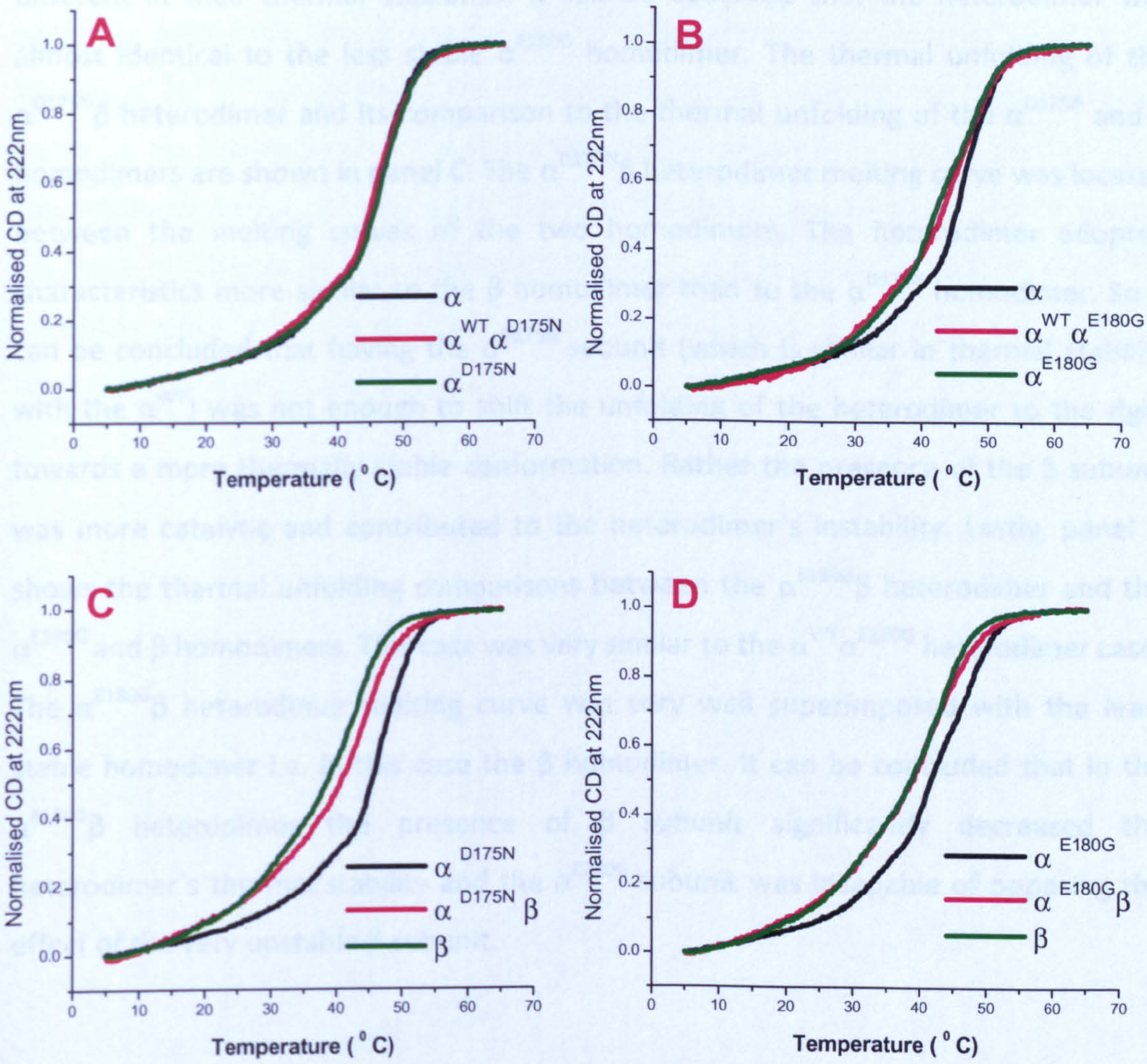

Fig 4.5: Thermal unfolding comparisons of heterodimers that carry a hypertrophic cardiomyopathy mutant copy vs. homodimers of their component subunits. In panel **A** the thermal unfolding curves of the $\alpha^{WT}\alpha^{D175N}$ heterodimer together with the α^{D175N} and α^{WT} homodimers are compared. Similarly in **B**: $\alpha^{WT}\alpha^{E180G}$ set, **C**: $\alpha^{D175N}\beta$ set and in **D**: $\alpha^{E180G}\beta$ set.

In figure 4.5, panel A shows the thermal unfolding of the $\alpha^{WT}\alpha^{D175N}$ heterodimer and compares it to the thermal unfolding of the α^{WT} and α^{D175N} homodimers. It can be observed that all three types of dimers had very well superimposed thermal unfolding curves. Since the two α^{WT} and α^{D175N} homodimers were no different in their thermal stability the heterodimer was indistinguishable as well. Panel B shows the thermal unfolding of the $\alpha^{WT}\alpha^{E180G}$ heterodimer compared to those of the α^{WT} and α^{E180G} homodimers. In the $\alpha^{WT}\alpha^{E180G}$ heterodimer case, the two homodimers were significant different in their thermal stabilities. It can be observed that the heterodimer was almost identical to the less stable α^{E180G} homodimer. The thermal unfolding of the $\alpha^{D175N}\beta$ heterodimer and its comparison to the thermal unfolding of the α^{D175N} and β homodimers are shown in panel C. The $\alpha^{D175N}\beta$ heterodimer melting curve was located between the melting curves of the two homodimers. The heterodimer adopted characteristics more similar to the β homodimer than to the α^{D175N} homodimer. So it can be concluded that having the α^{D175N} subunit (which is similar in thermal stability with the α^{WT}) was not enough to shift the unfolding of the heterodimer to the right towards a more thermally stable conformation. Rather the presence of the β subunit was more catalytic and contributed to the heterodimer's instability. Lastly, panel D shows the thermal unfolding comparisons between the $\alpha^{E180G}\beta$ heterodimer and the α^{E180G} and β homodimers. This case was very similar to the $\alpha^{WT}\alpha^{E180G}$ heterodimer case. The $\alpha^{E180G}\beta$ heterodimer melting curve was very well superimposed with the least stable homodimer i.e. in this case the β homodimer. It can be concluded that in the $\alpha^{E180G}\beta$ heterodimer the presence of β subunit significantly decreased the heterodimer's thermal stability and the α^{E180G} subunit was incapable of opposing the effect of the very unstable β subunit.

4.2.5 Comparison of the thermal stabilities of all of the heterodimers

Finally in figure 4.6 the thermal unfolding curves of all five heterodimers are superimposed. It can be observed from the figure that the least stable heterodimer was the $\alpha^{E180G}\beta$. Then $\alpha^{D175N}\beta$ together with $\alpha\beta$ followed. The thermal unfolding curves of the $\alpha^{D175N}\beta$ and the $\alpha\beta$ heterodimers were very similar as expected, since these heterodimers only differed in their α^{D175N} or α copy that have a very similar thermal unfolding behaviour. Fourth was the $\alpha^{WT}\alpha^{E180G}$ heterodimer and last and most stable was the $\alpha^{WT}\alpha^{D175N}$ heterodimer. Therefore it can be concluded that the most important factor in Tm heterodimer thermal stability is the presence or not of a β Tm copy. Heterodimers with a β copy were the least stable. A second factor would be the presence of a mutation. The least stable heterodimers were those carrying the α^{E180G} mutation rather than the α^{D175N} mutation, independently on whether the mutation was combined with an α or a β subunit.

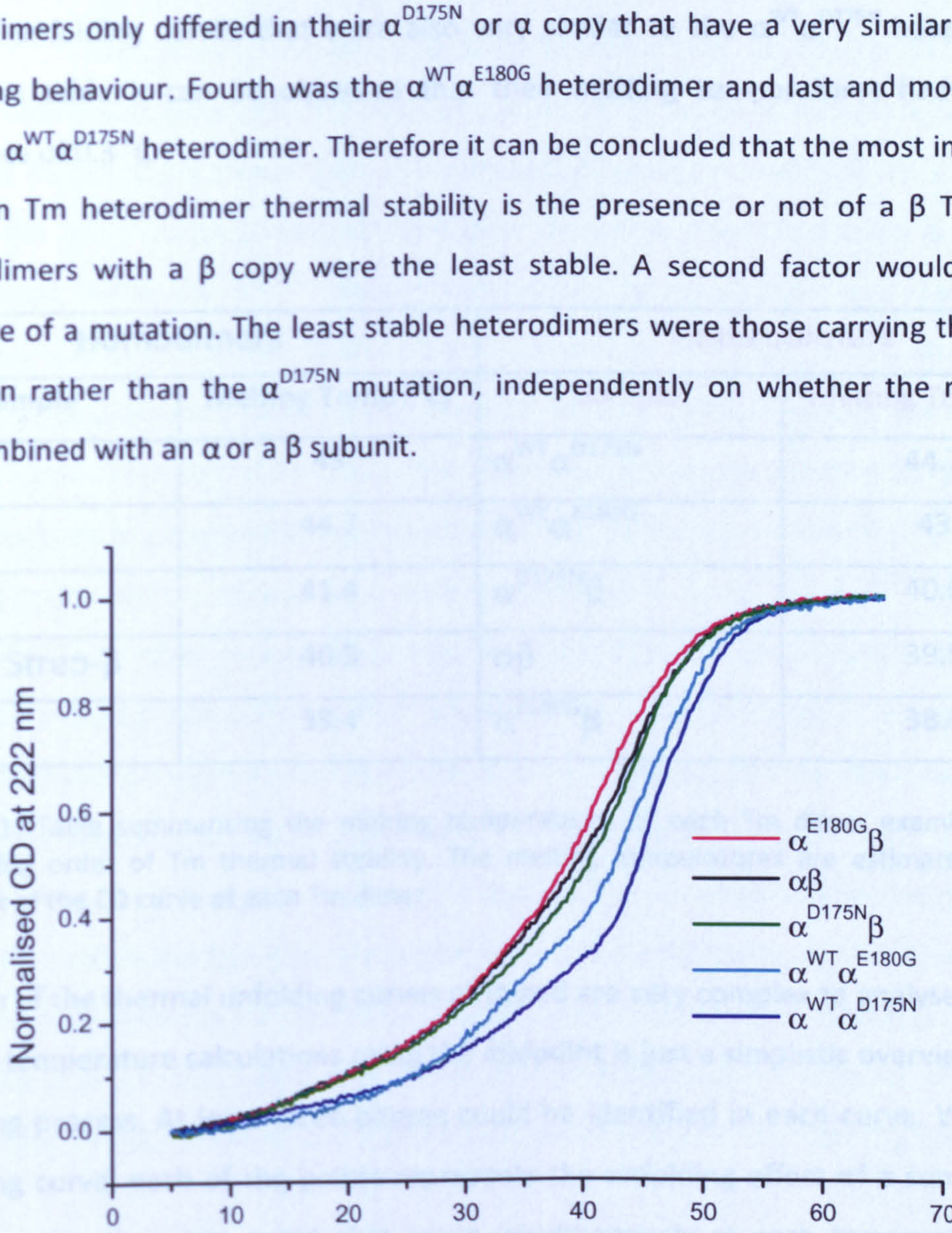

Fig 4.6: Comparison of the CD thermal unfolding curves of all heterodimer samples. From the graph it can be concluded that heterodimers carrying a β copy were the least stable. Also heterodimers carrying the α^{E180G} mutation were less stable that the corresponding heterodimers carrying the α^{D175N} mutation.

4.2.6 CD results summary

The melting temperatures as explained in section 4.2.1 are calculated from the midpoint of the thermal unfolding curves and they are only an estimate of the overall unfolding process (since each curve represents a more than one unfolding phases). The melting temperatures of each of the Tm heterodimers and homodimers examined are summarised in table 1. The homodimers α^{WT} and α^{D175N} had very well superimposed thermal unfolding curves that were also very similar to the $\alpha^{WT}\alpha^{D175N}$ heterodimer. From the table it can be observed that their melting temperatures had a small difference of 0.3 ˚C.

Homodimers		Heterodimers	
Sample	Melting Temp (˚C)	Sample	Melting Temp (˚C)
α^{D175N}	45	$\alpha^{WT}\alpha^{D175N}$	44.7
α	44.7	$\alpha^{WT}\alpha^{E180G}$	43
α^{E180G}	41.4	$\alpha^{D175N}\beta$	40.6
His- or Strep-β	40.5	αβ	39.5
β	38.4	$\alpha^{E180G}\beta$	38.6

Table 4.1: Table summarising the melting temperatures of each Tm dimer examined with descending order of Tm thermal stability. The melting temperatures are estimated as the midpoint of the CD curve of each Tm dimer.

Each of the thermal unfolding curves obtained are very complex to analyse and the melting temperature calculations using the midpoint is just a simplistic overview of the unfolding process. At least three phases could be identified in each curve. Within an unfolding curve, each of the points represents the unfolding effect of a summary of perhaps more than one event that occur simultaneously at each temperature. For example from the figure 4.3 showing the N-terminal tagged vs. the untagged β homodimers, it could be concluded that unfolding events of the N-terminal could be represented in the area from 20-43 ˚C. On the other hand, from figure 4.4 it was shown that events correlating with cross linking at C190 for the mutant homodimers could be represented in the area from 20-45 ˚C and also at the end of the unfolding

curve (area 54-65 °C). This proves that in the area 20-45 °C at least two unfolding events are included. It may be possible to analyse the N- and C-termini unfolding events separately by repeating the CD experiments with higher concentration of Tm in order to improve the data quality, or by performing DSC experiments.

The data on the thermal stabilities of skeletal Tm homodimers analysed in this section are in agreement with the published literature. CD experiments on α^{WT}, α^{D175N} and α^{E180G} homodimers reported melting temperatures of 43, 44 and 40.5 °C respectively (Golitsina *et al.* 1997; Golitsina *et al.* 1999) which is very close to what is reported in this study (from table 4.1 corresponding values are 44.7, 45 and 41.4). Overall the α^{D175N} mutant homodimer appear of similar thermal stability as the α^{WT} homodimer, while the α^{E180G} mutant homodimer is significantly less stable. This behaviour was also observed in DSC data (Kremneva *et al.* 2004). In DSC studies two major unfolding domains could be identified for Tm that corresponded to the N- and C-termini. Upon reduction of the cross-link of Tm, the C-terminal melting temperatures were significantly lower and the N-terminal melting temperature remained unaffected (melting temperatures of reduced C-terminal were 43 °C for α^{WT} and α^{D175N} and 40 °C for α^{E180G}). The rather strange local structural instability in both mutant α^{D175N} and α^{E180G} cross-linked homodimers that appeared as a shoulder prior to the major unfolding transition (fig 4.4) was also seen in the DSC studies. On the other hand the β Tm homodimer in this study is found to be extremely unstable with a melting temperature of 38.4 °C, which is close to a mammal's physiological body temperature. This could explain the fact that the β homodimer is rarely found *in vivo*. The result is comparable to previous CD studies on skeletal β homodimer that reported a melting temperature of 35 °C (Coulton *et al.* 2008). The presence of an N-terminal affinity tag (either Strep or His) enhances the thermal stability of the β homodimer (fig 4.3).

The findings on Tm heterodimers reported in the present study are novel and there is no other data published in literature to compare them with. The most stable heterodimers were the $\alpha^{WT}\alpha^{D175N}$ and $\alpha^{WT}\alpha^{E180G}$, while the least stable heterodimers were those carrying a β chain i.e. the αβ, $\alpha^{D175N}\beta$ and $\alpha^{E180G}\beta$ heterodimers. In any heterodimer that contained a α^{D175N} or α^{E180G} mutant chain there was no shoulder prior to the main unfolding transient indicating local structural instability as in the

α^{D175N} and α^{E180G} mutant homodimers case. Also in a mutant heterodimer it is important to which other subunit the mutation is combined. Thus the thermal unfolding of $\alpha^{D175N}\beta$ is distinct from that of $\alpha^{WT}\alpha^{D175N}$. The same is true for the α^{E180G} case. In general, each of the heterodimer appeared to be of intermediate stability when compared to homodimers of its component subunits and had a tendency to appear similar to the least stable homodimers of the two. Overall the presence of the β subunit is the most crucial factor in the instability of Tm dimers. The presence of α^{D175N} and α^{E180G} mutations also influences the stability of Tm dimers. The dimers containing the α^{E180G} subunit are less stable than those carrying the α^{D175N} subunit, independently if found as homodimers or as heterodimers combined with α or β subunit.

4.3 Affinity of Tropomyosin for Actin in the absence or presence of Troponin T1

In the present section each of the different Tm heterodimers and homodimers were characterised in relation to their interaction with partner proteins i.e. actin and Troponin T1 (TnT1, the N-terminal part of TnT, residues 1-160). The affinity of each Tm heterodimer and homodimer for actin in the presence or absence of TnT1 was measured by the actin cosedimentation assays as explained in section 2.3.2. According to the literature, the TnT1 domain binds Tm at the Tm overlap region, stabilising the end-to-end interactions between Tms and increasing their affinity for actin (as mentioned in section 1.4.1.c, pg 25) (Schaertl *et al.* 1995; Palm *et al.* 2001). Thus the experiments in the presence of TnT1 were performed to check if TnT1 had indeed an impact on the affinity of Tm for actin and also to check if TnT1 had a varying effect on the different Tm dimers.

4.3.1 Cosedimentation assays in the absence of TnT1

Figure 4.7 shows an example of a cosedimentation assay in which the Strep-tag $\alpha^{WT}\alpha^{D175N}$ Tm heterodimer was used. Because in this example a Tm heterodimer was used, it was broken down to Strep-α^{WT} and α^{D175N} chains under reducing SDS-PAGE, therefore two bands could be observed for any Tm sample.

It can be observed that in samples 1-8 most of the actin was found in the pellets with traces appearing in the supernatants. In a control sample containing Tm only (lane 9), most of Tm was in the supernatant with only traces appearing in the pellet. This verifies that in samples 1-8 the presence of Tm in pellets was due to Tm bound to actin. The fraction of the Tm bound to actin increased until the point where the actin filaments became saturated (lanes 5-6). From that point on the amount of Tm in pellets remained constant while the amount of free Tm in supernatants increased.

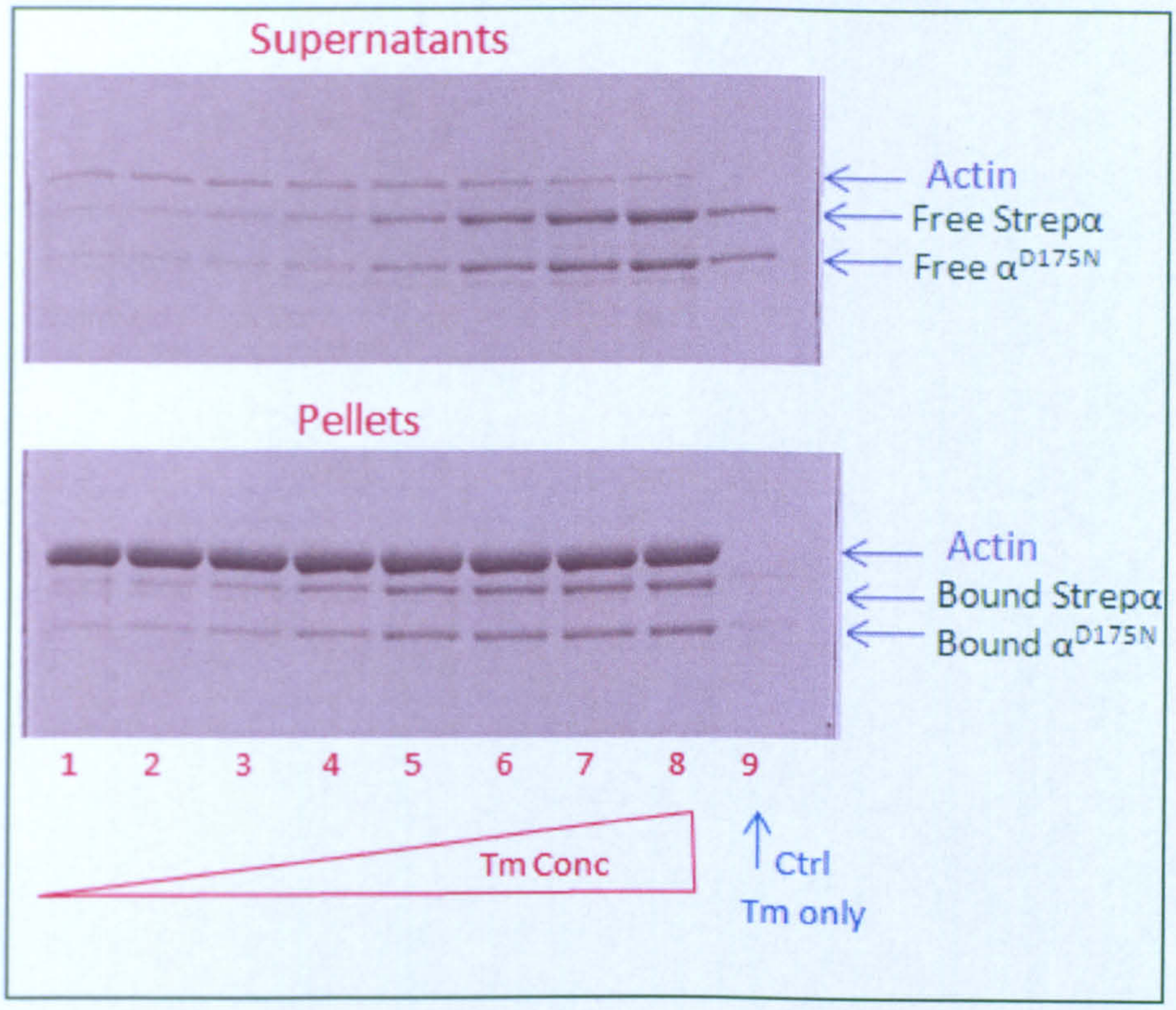

Fig 4.7: Actin and heterodimer Tm cosedimentation assay. The two proteins were mixed in a tube and ultracentrifuged. Pellets were separated from supernatants and loaded onto SDS gels. Actin was constant (9 μM) and Tm was increased (0.2, 0.4, 0.6, 1, 2, 3, 4, 5 μM in tubes 1-8 respectively). Tube 9 contained 2 μM of Tm alone as control and when ultracentrifuged most of Tm remained in supernatants. After lane 5 (i.e. 2 μM Tm) actin became saturated thus the amount of Tm in pellets did not change but the amount of Tm in supernatants was increased. Buffer used 100 mM KCl, 20 mM MOPS, 5 mM $MgCl_2$ at pH 7. 7.5 % SDS gels were used and the samples were run under reducing conditions and stained using Coomassie blue. The Tm used in this experiment was the Strepα^{WT}α^{D175N} Tm heterodimer, thus it was split into the Strepα^{WT} and α^{D175N} subunits under the reducing PAGE.

In the upper panel of figure 4.8 the total Tm density for each sample as measured by densitometry analysis was plotted against the known Tm concentration as used in the beginning of the experiment. In the lower panel of fig 4.8 the free Tm concentration was plotted against the fractional actin saturation (following the methodology described in section 2.3.2). The graph, in agreement with the published literature, was sigmoidal suggesting that Tm binding to actin was cooperative. The graph was fitted using Origin software with the Hill equation shown below. From the fit the apparent binding affinity of Tm for actin (K_d) and the Hill coefficient (n) of binding were estimated.

$$y = a\,[x]^n / K_d{}^n + [x]^n$$

Fitting parameters: a= amplitude, n = Hill coefficient, K_d = binding affinity of Tm to actin. Dependent variable y (Tm bound to actin and divided by actin pellet), Independent variable x (free Tm concentration).

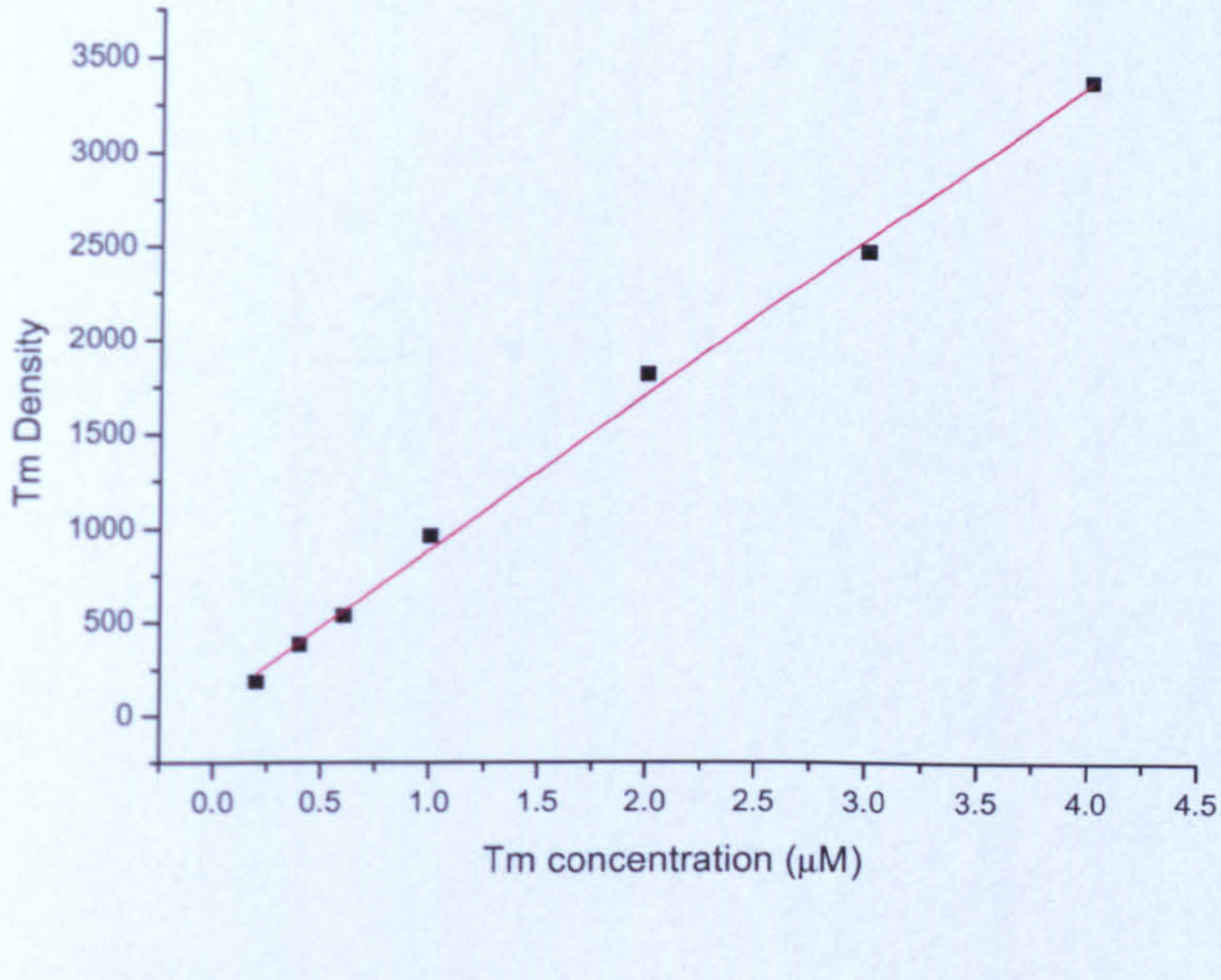

Fig 4.8: Estimation of Tm binding affinity for actin. The density of Strepα^{WT}α^{D175N} Tm heterodimer in each lane of gels in fig 4.7 was measured by densitometry and was plotted against the corresponding known Tm concentration. The graph in top panel is a straight line since Tm densities were directly proportional to Tm concentrations and the slope of the line gave the concentration of Tm per unit density. In the lower panel the free Tm densities from the supernatant gels were converted into free Tm concentrations and plotted against the fractional actin saturation (i.e. Tm pellets/actin pellets); a sigmoidal curve obtained, which is representative of the cooperative binding of Tm to actin. The apparent binding affinity was estimated by fitting to Hill equation (in this example $K_d = 0.37 \pm 0.03$ μM).

4.3.2 Cosedimentation assays in the presence of TnT1

The different Tm dimers were co-sedimented with actin as described previously but with 2 μM of TnT1 added in each tube. This amount of TnT1 would be in excess over the amount of Tm required to saturate actin, assuming that TnT1 binds Tm in a 1:1 stoichiometry. (K_d binding affinity of Tm to actin reported to be 0.18, 0.23, 0.51 and 0.68 μM for α^{WT}, β, α^{D175N} and α^{E180G} respectively, (Boussouf *et al.* 2007)).

In figure 4.9 the gels of a cosedimentation assay are shown for the α^{E180G} homodimer in the presence of TnT1. The analysis of these gels is shown in the top panel of figure 4.10. This panel also include the cosedimentation assay analysis of the α^{E180G} homodimer without TnT1 present. In the absence of TnT1 the affinity of α^{E180G} Tm for actin had a K_d of 0.55 μM. However, in presence of TnT1 the same α^{E180G} homodimer had an actin binding affinity K_d of 0.21 μM. Therefore it is clear that addition of TnT1 enhances the affinity of α^{E180G} Tm for actin. In figure 4.9 it can be observed that at lower concentrations of Tm where actin was not yet fully saturated (lanes 1-4) all of Tm was found in the pellets and only traces appeared in supernatants. In contrast, in cosedimentation assays without TnT1 it was observed that, within the same range of Tm concentrations, Tm was found in significant amounts in the supernatants although actin was not saturated (gels not shown here).

Another observation from fig 4.9 is that the TnT1 was found to exist in a constant ratio with the actin-bound Tm as shown in the gel of the pellets in the top panel. So it can be seen that the amount of TnT1 in pellets was gradually increased in each lane, following Tm's increase; when Tm concentration remained constant due to actin saturation, so was the amount of TnT1. The excess amount of TnT1 that was not used to bind the actin-bound Tm, was found in supernatants. So it can be concluded that TnT1 preferentially binds to actin-Tm complex than to Tm alone.

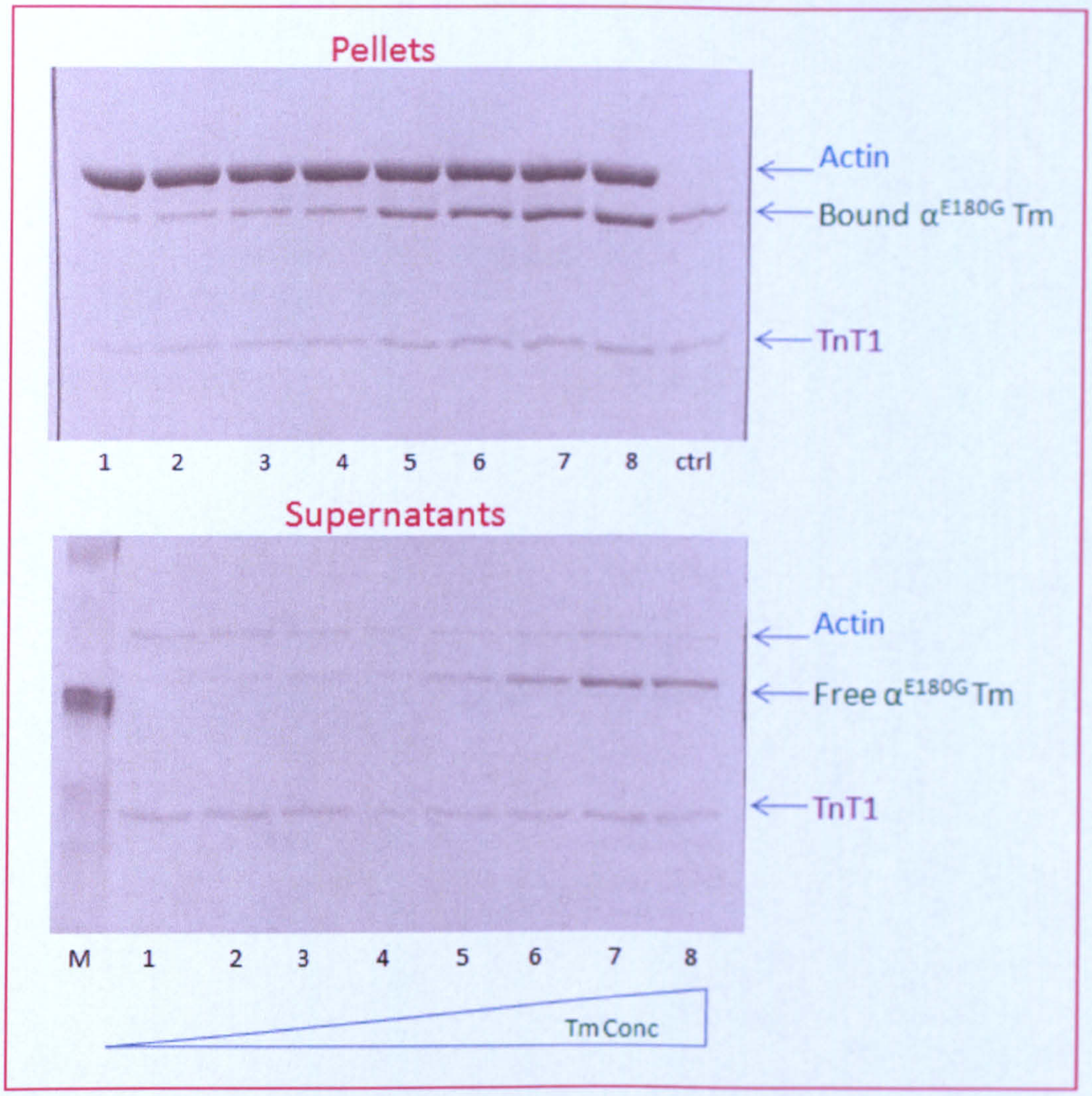

Fig 4.9: Actin and α^{E180G} Tm cosedimentation assay in presence of TnT1. Actin and TnT1 were kept constant (9 and 2 μM respectively) and Tm was gradually increased from 0.2-5 μM (similarly to fig 4.7). From top panel, it can be observed that the amount of TnT1 in pellets was kept in a standard proportion to the amount of Tm in the pellets. It seems that only when actin-bound Tm is saturated with TnT1, the excess TnT1 is found in supernatants to interact with the free Tm. 10 % SDS gels were used and the samples were run under reducing conditions and stained using Coomassie blue.

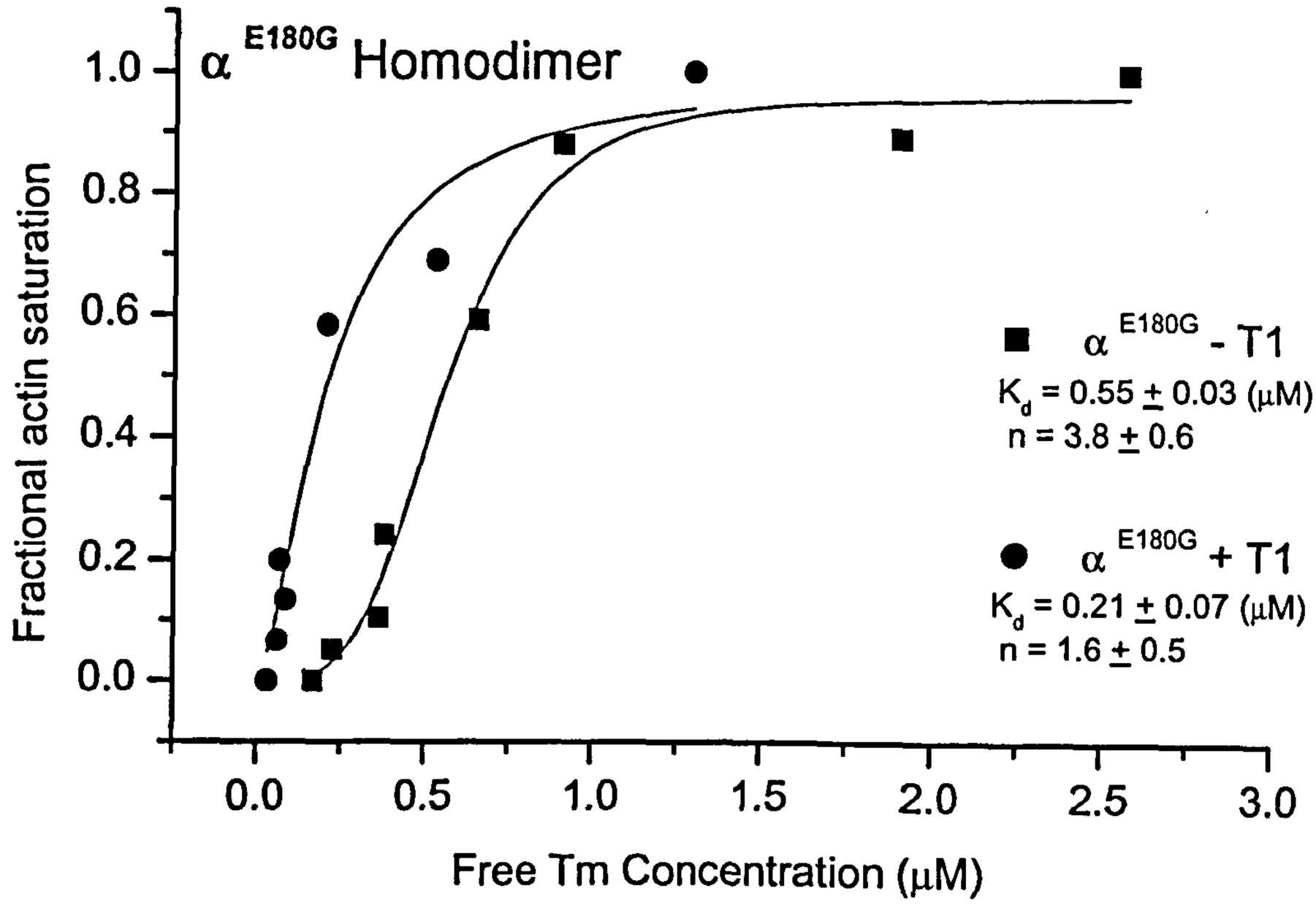

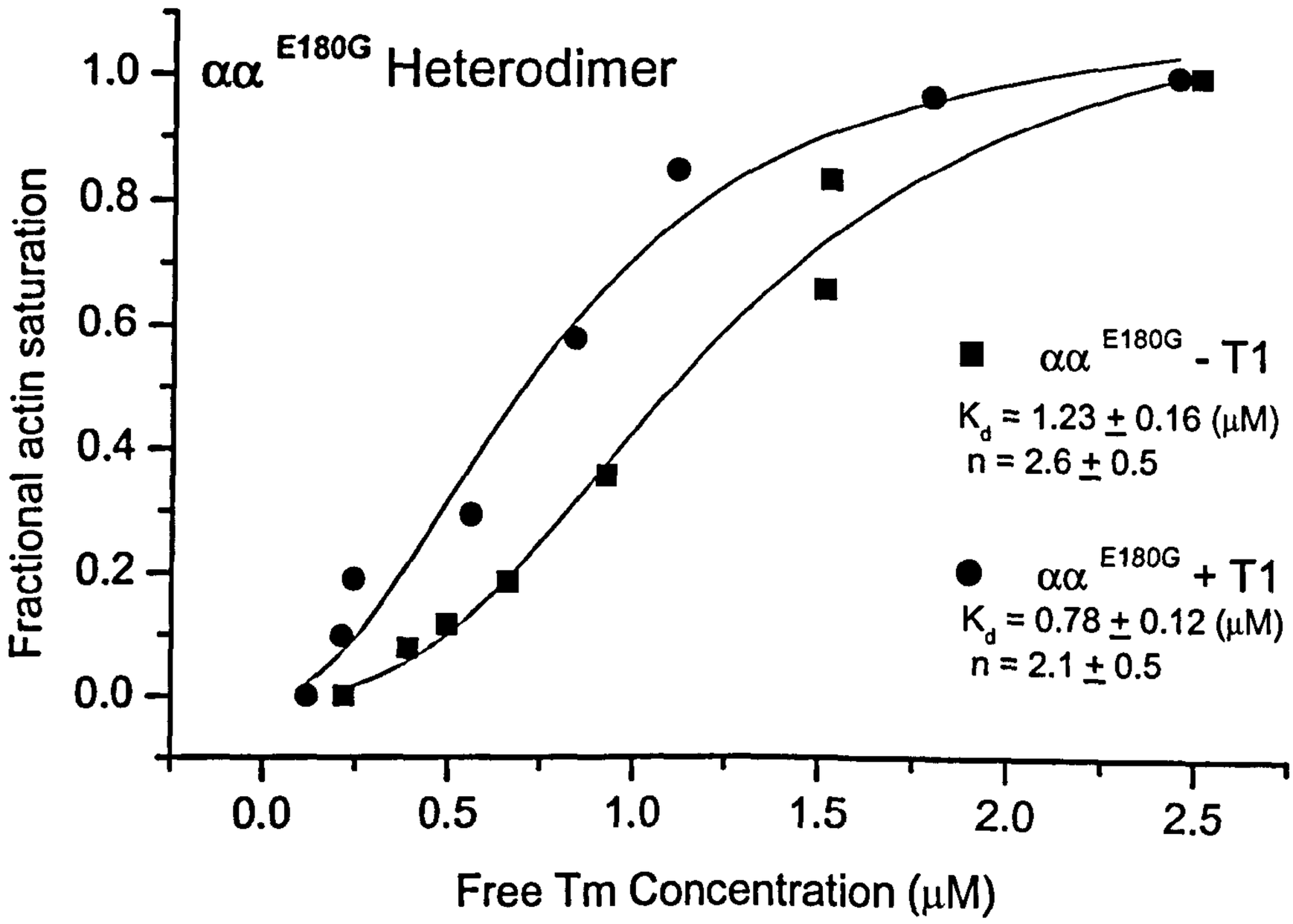

Fig 4.10: Comparison of actin binding affinities of homodimers and heterodimers of Tm upon addition of TnT1. Top panel shows the α^{E180G} homodimer, bottom panel shows the $\alpha^{WT}\alpha^{E180G}$ heterodimer. For each sample the actin binding affinity (K_d) and the Hill coefficient (n) values are indicated, as calculated from the individual experiments that are plotted here. Average values of the actin binding affinities and Hill coefficient are shown in table 4.2. The heterodimer had significantly lower actin binding affinities than the homodimer, either in the absence or the presence of TnT1. In the homodimer case the binding affinity to actin was increased x 2.6 fold after TnT1 addition. In the heterodimer experiment, addition of TnT1 increased the binding affinity to actin x 1.6 fold.

Figure 4.10 also shows the analysis of the cosedimentation experiment of the $\alpha^{WT}\alpha^{E180G}$ Tm heterodimer in the presence or the absence of TnT1 (bottom panel). As in the α^{E180G} homodimer case, the addition of TnT1 increases the binding affinity of the $\alpha^{WT}\alpha^{E180G}$ Tm heterodimer to actin (K_d = 1.23 or 0.78 in the absence and presence of TnT1 respectively, as obtained after fitting the individual curves shown in figure 4.10 to the Hill equation). In the α^{E180G} homodimer case, the affinity is increased more than x2 fold. In the $\alpha^{WT}\alpha^{E180G}$ Tm heterodimer case the affinity is increased x1.6 fold.

More importantly comparison of the α^{E180G} homodimer to the $\alpha^{WT}\alpha^{E180G}$ heterodimer from the two panels in figure 4.10, reveals that the heterodimer binds with significantly lower affinity to actin than the homodimer. In the absence of TnT1 the heterodimer binds actin x2.2 fold weaker and in the presence of TnT1 it binds x3.7 fold weaker compared to the homodimer.

4.3.3 Actin cosedimentations results summary

The actin cosedimentation assays were performed for each Tm dimer both in the absence and in the presence of TnT1. As will be explained in section 5.3, the TnT1 had a 6 residues C-terminal extension, which resulted by fault in molecular biology methods. For this reason only the actin cosedimentation experiments with the α and β Tm homodimers were repeated more than once in the presence of this faulty TnT1 peptide. The rest of the Tm samples were only tested once in the presence of TnT1, in order to roughly check if any obvious difference in the presence and absence of TnT1 could be observed. However the cosedimentation assays in the presence of TnT1 should be repeated for all Tm samples using the correct TnT1 peptide.

The results of the binding affinity (K_d) of each dimer to actin and cooperativity (n) of binding together with the number of observations (N) are summarised in table 4.2. In the case where the number of observation was more than one, the values of K_d and n are averages of the individual experiments thus for each average value the standard deviation error is indicated. In the case where the experiment was not repeated, the K_d and n values shown in table 4.2 are obtained after fitting each individual curve to the the Hill equation; in that case the error indicates the error of the fit. In the cooperativity values the error was quite large, thus n was not very well defined.

Tm Dimer	–TnT1		+ TnT1		Ratio of K_d(-T1)/ K_d(+T1)
	K_d ± SD (μM)	n ± SD	K_d ± SD (μM)	n ± SD	
αα	0.31 ± 0.09 (N=3)	1.9 ± 0.39	0.19 ± 0.005 (N=2)	1.6 ± 0.47	1.6
α^{D175N} α^{D175N}	0.46 ± 0.07 (N=3)	2.1 ± 0.6	0.37 ± 0.03 (N=1)	1.1 ± 0.05	1.2
α^{E180G} α^{E180G}	0.53 ± 0.003 (N=2)	2.5 ± 1.1	0.21 ± 0.07 (N=1)	1.6 ± 0.5	2.5
ββ	0.13 ± 0.06 (N=3)	1.6 ± 0.1	0.21 ± 0.11 (N=4)	2 ± 0.44	0.6
α^{WT} α^{D175N}	1.32 ± 0.41 (N=3)	1.6 ± 0.08	0.5 ± 0.06 (N=1)	3.3 ± 1.05	2.6
α^{WT} α^{E180G}	1.36 ± 0.16 (N=2)	2.1 ± 0.54	0.78 ± 0.12 (N=1)	2.1 ± 0.5	1.7
αβ	0.96 ± 0.12 (N=3)	1.9 ± 0.73	0.78 ± 0.14 (N=1)	3.6 ± 2.2	1.2
α^{D175N} β	1.7 ± 1.13 (N=2)	2.4 ± 1.68	1.32 ± 0.06 (N=1)	1.8 ± 0.09	1.3
α^{E180G} β	1.15 ± 0.23 (N=2)	2.4 ± 1.34	1.09 ± 0.27 (N=1)	1.9 ± 0.49	1.1

Table 4.2: Actin binding affinities (K_d) in blue and cooperativity of binding (n) in purple of Tm homodimers and heterodimers in absence or presence of TnT1. The affinities of heterodimers to actin are significantly weaker than the affinities of the homodimers. TnT1 increases the affinity for actin in both homo and hetero dimers (exception the β Tm homodimer which is not very different in the presence of TnT1). For each experiment the number of repeats (N) is indicated. In cases where N is more than 1, the K_d and n are average values of several individual experiments and the standard deviation error is indicated. In cases where N=1, K_d and n are the values obtained after fitting each binding curve to the Hill equation and the error indicated shows just the error of the fit. The K_d was better defined in the case of the homodimers than the heterodimers as indicated by the standard deviation values. In any case the error in the estimation of the n value was quite large.

As can be observed from table 4.2, the homodimers of Tm appeared to bind actin with a higher affinity than the heterodimers. In the absence of TnT1, the α^{WT}, β, α^{D175N} and α^{E180G} homodimers had an affinity of 0.3, 0.13, 0.46, and 0.53 respectively which is in agreement with previously published values (0.2, 0.2, 0.5, 0.7 (Boussouf *et al.* 2007)). Also the cooperativity of binding n was found to be 1.9, 1.6, 2.1 and 2.5 for α^{WT}, β, α^{D175N} and α^{E180G} homodimers respectively and was comparable with previously published values (1.9, 2.7, 2.9, 3.9 respectively, (Boussouf *et al.* 2007)). The increased value of n in the mutant homodimers suggests that these dimers had sigmoidal curves with steeper slopes. The steeper slopes mean that the initiation of Tm polymerisation on actin was more difficult. Therefore, a higher concentration of Tm was populated on actin surface to initiate polymerisation; thus when polymerisation finally was initiated then fewer dimers needed to fully saturate the actin filament and subsequently saturation occurred faster and the slope of the curve was steeper.

The heterodimers appeared to bind actin with significantly weaker affinities in comparison to the homodimers. For example the αβ heterodimer had a x3 and x7 fold weaker affinity to actin when compared to the α and the β homodimers respectively. However the affinities of the different Tm heterodimers were very similar (0.96-1.36 μM), taking into account that the SD error in the heterodimers case was quite large. The binding of the $\alpha^{D175N}\beta$ heterodimer to actin was not well defined and it will be useful to repeat this measurement few more times.

The cooperativity number n was comparable between the homodimers and the heterodimers. In heterodimers the cooperativity numbers were: 1.6, 1.9, 2.1, 2.4 and 2.4 (for the $\alpha^{WT}\alpha^{D175N}$, αβ, $\alpha^{WT}\alpha^{E180G}$, $\alpha^{D175N}\beta$ and $\alpha^{E180G}\beta$ respectively) thus the cooperativity of binding was very similar to the homodimers. Unfortunately in any case the n values were not well defined. The error in the homodimers case was within 1.1 and in the heterodimers within 1.7. Since the error was quite large, the n values should not be strictly accounted thus safe comparisons between the cooperativity amongst the different Tm homodimers and heterodimers cannot be drawn.

In the presence of TnT1 the actin binding affinities in all of the Tm dimers were increased. In homodimers there was a 1.2 – 2.5 fold increase and in the heterodimers a 1.1 – 2.6 fold increase. Therefore the effect of TnT1 was similar in each case. However, the increase on actin binding affinity in the presence of TnT1 would physiologically be of more importance to the heterodimers that could not bind very well actin rather than to the homodimers that had a tight affinity for actin even in the absence of TnT1. An exception was the β Tm homodimer, which was found to bind actin with very tight affinity even in the absence of TnT1, thus did not appear with significantly enhanced actin binding affinity upon TnT1 addition.

Also in the presence of TnT1 the cooperativity of binding, n, was increased in most cases. The actin binding curves in the presence of TnT1 were steeper than in the absence of TnT1, suggesting that the Tm polymerised on actin surface more readily. This was perhaps due to the TnT1 association on the Tm-Tm overlap region, promoting stability between adjacent Tm dimers and thus assisting Tm polymerisation. However, in the case of mutant α^{D175N} and α^{E180G} homodimers the value of n was decreased upon TnT1 addition. This could probably mean that TnT1 addition stabilised the overlap region between adjacent mutant Tm homodimers promoting polymerisation, as in the rest of the dimers. But this effect minimised the requirement for a large initial Tm concentration on the actin surface to initiate the polymerisation.

Interestingly some of the Tm heterodimers that were not digested with FXa protease and still carried the N-terminal Strep tag were subjected to actin cosedimentation assays and found to bind actin very well. These were the Strep-$\alpha^{WT}\alpha^{E180G}$ and the Strep-$\alpha^{WT}\alpha^{D175N}$ heterodimers (cosedimentation gels and analysis shown in fig 4.7 and 4.8) that both had a K_d of 0.4 μM (mean value of 4 independent experiments with SD 0.1 and 0.06 respectively). Thus the presence of a 12 or 13 residues N-terminal extension in one of the chains does not interfere with the binding of Tm to actin. However, cosedimentation experiments in the presence of TnT1 with these tagged heterodimers were not performed. It is expected that the N-terminal peptide extension would probably interfere with the binding of TnT1 on the Tm overlap region.

4.4 Tm and Tn regulation of S1 binding onto actin thin filaments monitored by Stopped-flow experiments

Myosin binding to actin filaments that are labelled by a fluorescent probe causes a quenching in the fluorescence signal. Actin and myosin can be rapidly mixed together using a stopped flow spectrofluorimeter and the traces showing the decrease in actin fluorescence upon binding of myosin can be monitored. Analysis of the results gives information on the actomyosin association kinetics.

In the experiments described in this section, actin filaments were labelled by pyrene fluorophore at Cys374 and were rapidly mixed with S1 using the stopped flow machine (method described in section 2.3.3). The actin filaments were decorated with a Tm dimer of interest to investigate how the presence of Tm would affect the S1 binding to actin.

For each of the Tm dimer tested, four experiments were performed. The first one served as control and only contained pyrene-actin pushed against S1. The second set was the binding of S1 onto pyrene-actin reconstituted with the Tm dimer of interest. The third set monitored binding of S1 onto actin reconstituted with both Tm and the Tn complex (purified from rabbit skeletal muscle) in the absence of Ca^{2+} (i.e. 2 mM EGTA in the buffer). The last set monitored binding of S1 onto pyrene-actin decorated with Tm and the Tn complex in the presence of Ca^{2+} (i.e. 1 mM $CaCl_2$ in the buffer).

In particular, 5 μM S1 were pushed against 0.5 μM actin, 0.2 μM Tm and 0.2 μM Tn (syringe concentrations before mixing). The amount of Tm and Tn used would be enough to fully decorate the actin filaments (taking in account the K_d values measured in the previous section for each Tm with TnT). To assemble the thin filaments, actin was incubated with Tm or Tm and Tn at higher concentrations for 20 min and then the experimental buffer was added to dilute the filaments into the working concentration. S1 was chosen to be in excess over the thin filaments in order to be economical with the quantity of the Tm heterodimer used.

Because S1 was in excess over the thin filaments, the reaction was pseudo-first order and could be analysed by single exponential fitting. Only the main body of the transient was used for the fitting, excluding its initial part. This is because the initial part showed a lag phase. When S1 is in excess over the thin filaments, as in the experiments described in the current section, an initial lag phase is expected to be observed because a portion of the few actin sites will not be available for binding. In contrast, in experiments where the thin filaments are in excess over S1, then the lag phase is not expected to be observed. In that case the same portion of the actin sites will be again not available for binding but since there will be more actins than S1 molecules, the remaining available actin sites will be enough for the few S1 molecules present.

Furthermore, in any of the Tm dimers tested, the lag phase was more marked in the case were Tn was present and Ca^{2+} was absent. This was expected, because under these conditions the thin filaments were in the blocked and closed positions and the probability of S1 binding on actin was decreased.

In every set of experiments binding of S1 on actin filaments caused a quenching of the pyrene fluorescence signal as expected. For example, figure 4.11 shows the transients obtained after S1 binding on thin filaments decorated with the αβ heterodimer (middle panel). For comparison, the transients of S1 binding on thin filaments decorated with αα (top panel) and ββ (bottom panel) Tm homodimers are also shown. In figure 4.11, the transients in red describe binding of S1 on actin/Tm filaments and transition from the closed to the open state since Tm under these conditions does not occupy the blocked position. The green transients represent the S1 binding on thin filaments decorated with Tm and Tn in the absence of Ca^{2+}. In this case the TnI subunit was at the inhibitory site on actin and Tm was at the blocked position, so the thin filament transition from the blocked to closed to open states is represented. The blue transients describe the S1 binding on thin filaments decorated with Tm and Tn in the presence of Ca^{2+}. When both Tn and Ca^{2+} are present the Tm does not occupy the blocked state and binding of S1 describes the transition of the filaments from the closed to the open states. In agreement with previous observations (Boussouf and Geeves 2007), the time needed to reach 50 % of pyrene fluorescence is

longer in the absence of Ca^{2+} than in the presence of Ca^{2+} and is relevant to the actin sites available for S1 binding. Lastly the transients in black serve as controls and describe S1 binding on undecorated actin filaments. From figure 4.11 it is clear that the αα, the αβ and the ββ Tm dimers had very similar transients in all of the conditions examined and all could regulate the S1 binding to actin together with the skeletal Tn complex.

The heterodimers of Tm containing a cardiomyopathy mutation were also examined. All heterodimers showed similar transients as the αβ heterodimer described above. The experiments with the $\alpha^{WT}\alpha^{D175N}$ and the $\alpha^{WT}\alpha^{E180G}$ heterodimers are shown in figure 4.12. The experiments with the $\alpha^{D175N}\beta$ and the $\alpha^{E180G}\beta$ heterodimers are shown in figure 4.13. It can be concluded that all heterodimers (and the control homodimers tested) were functional and all could regulate, with the skeletal Tn, the S1 binding on the thin filaments.

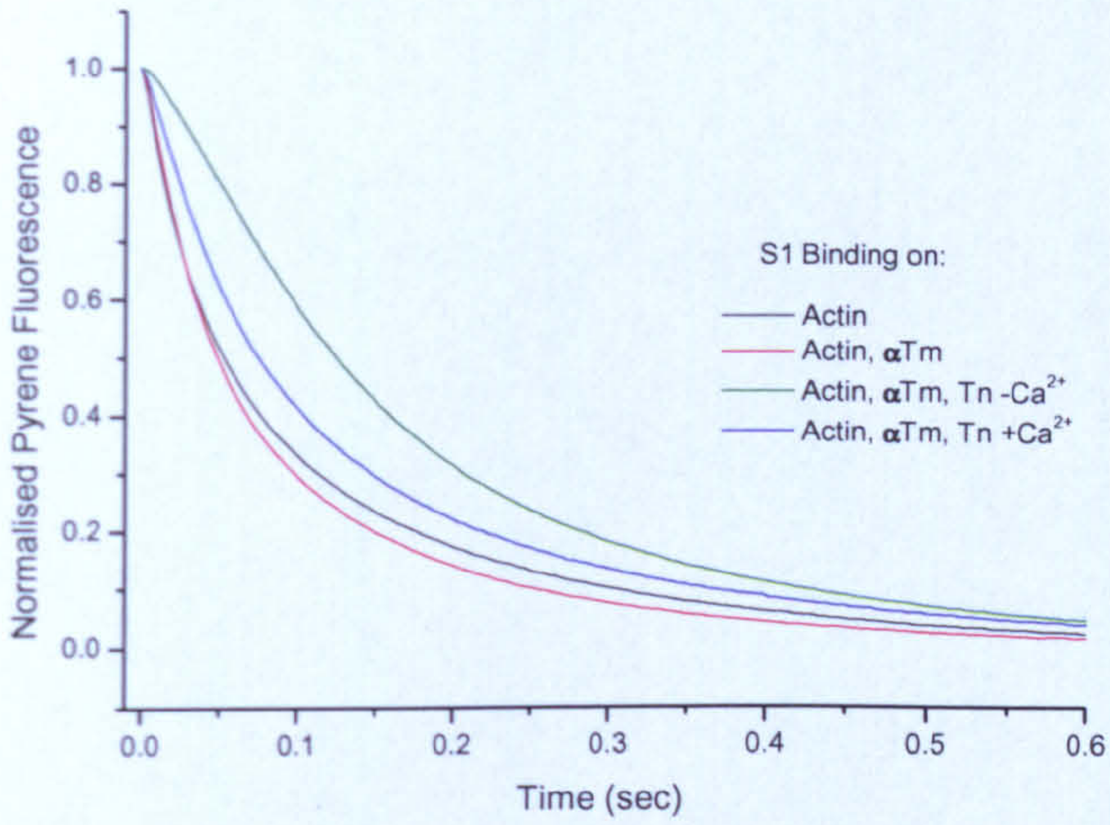

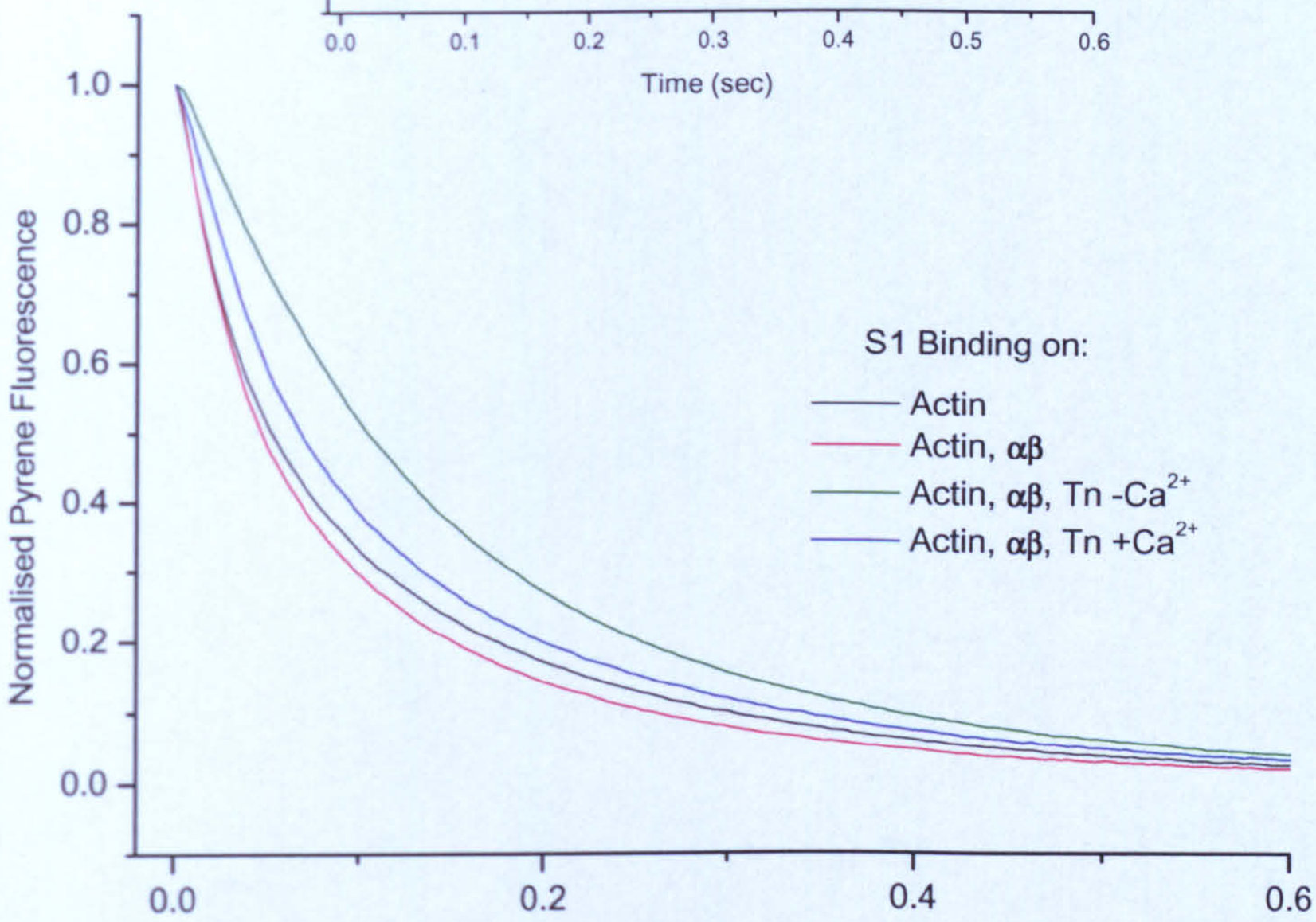

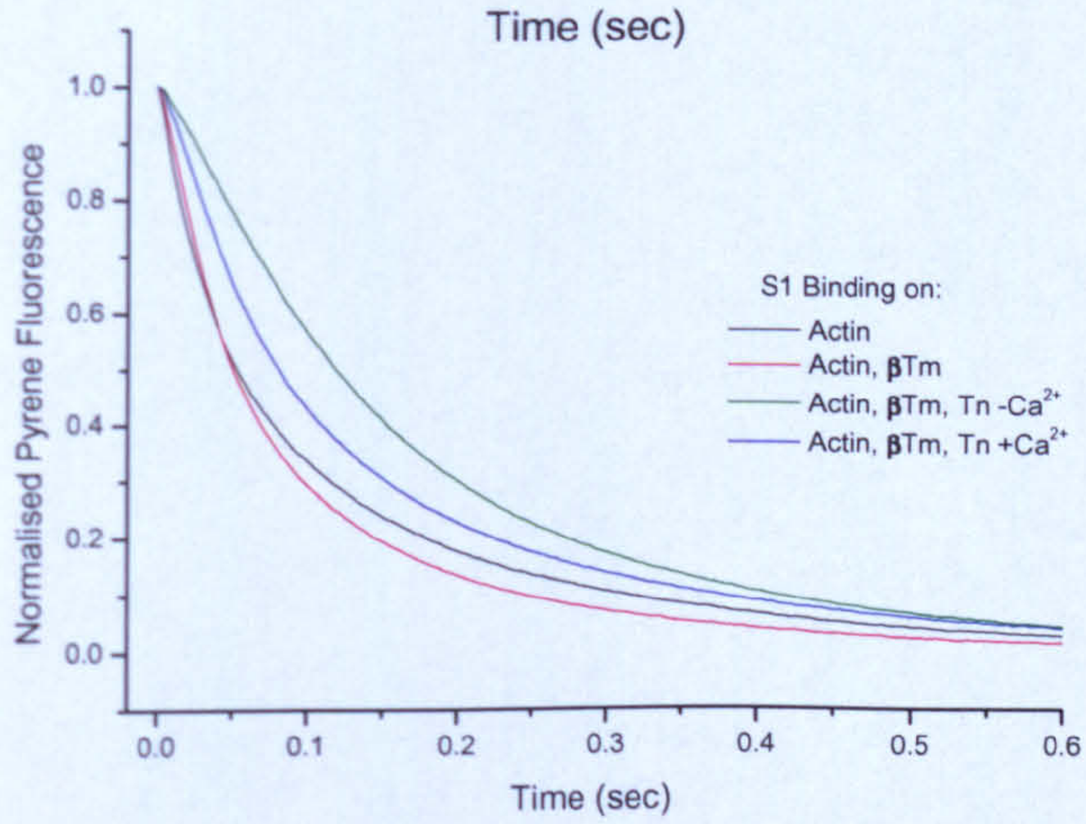

Fig 4.11: Binding of excess S1 on pyrene actin thin filaments monitored by stopped-flow experiments. The black transient shows binding of S1 on thin filaments containing actin only. In red S1 binding to Actin/Tm. In green S1 binding to Actin/Tm/Tn in the absence of Ca^{2+}. In blue S1 binding on Actin/Tm/Tn in the presence of Ca^{2+}. In absence of Ca^{2+}more time is needed to reach 50 % of pyrene fluorescence than in the presence of Ca^{2+}, because in the absence of Ca^{2+} the majority of Tm is at the blocked position and therefore the probability for S1 to bind on an actin site is decreased. The thin filaments shown in this example are decorated with the αβ heterodimer (middle). The transients are compared to the αα (top), or ββ (bottom) homodimers. In any case, the transients were very similar.

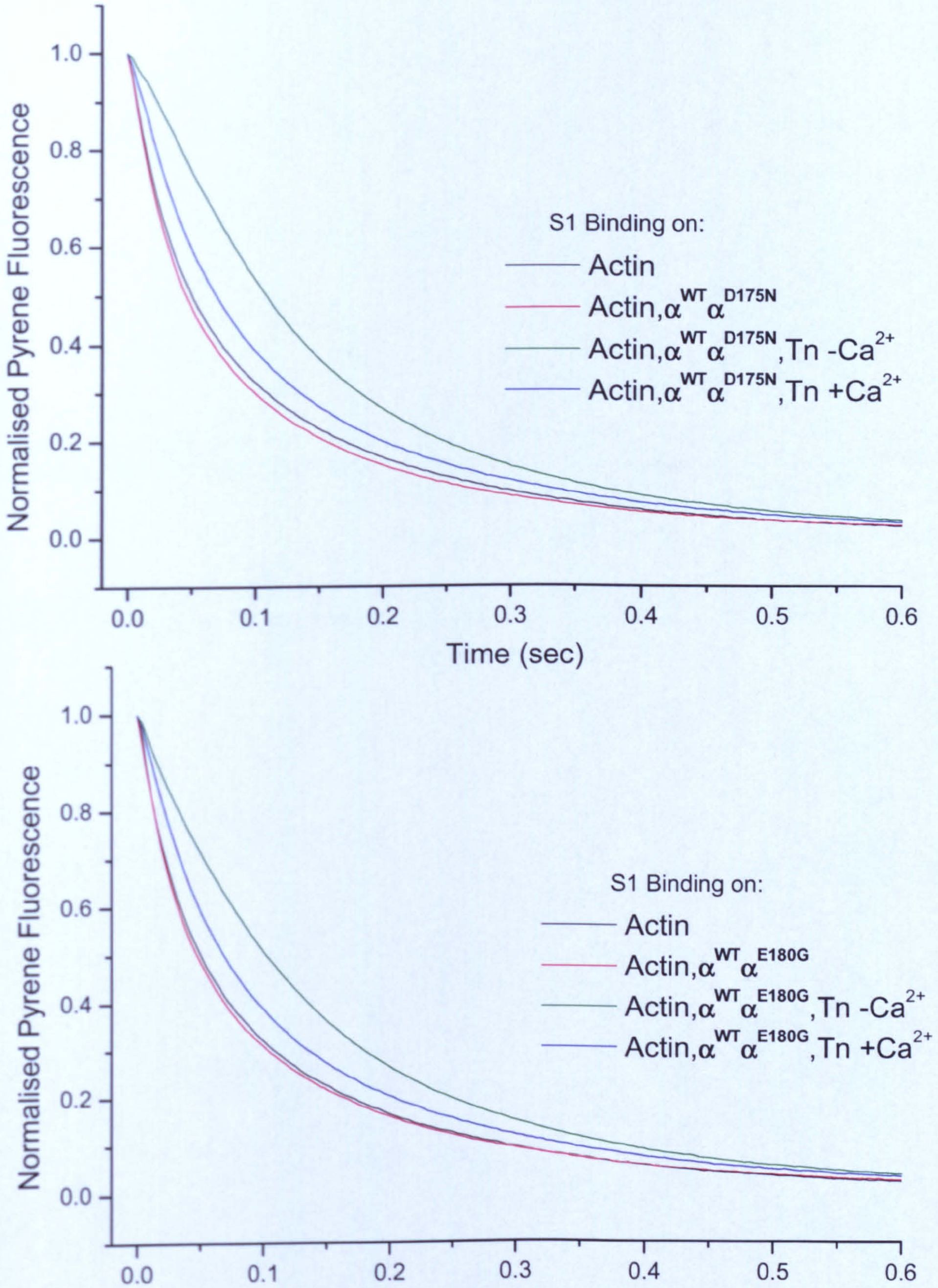

Fig 4.12: Binding of S1 to actin filaments decorated with the $\alpha^{WT}\alpha^{D175N}$ or the $\alpha^{WT}\alpha^{E180G}$ heterodimer (top and bottom panels respectively). The colour code of the transients is the same as described in figure 4.12. Both heterodimers could successfully regulate with the Tn complex the S1 binding to the thin filaments.

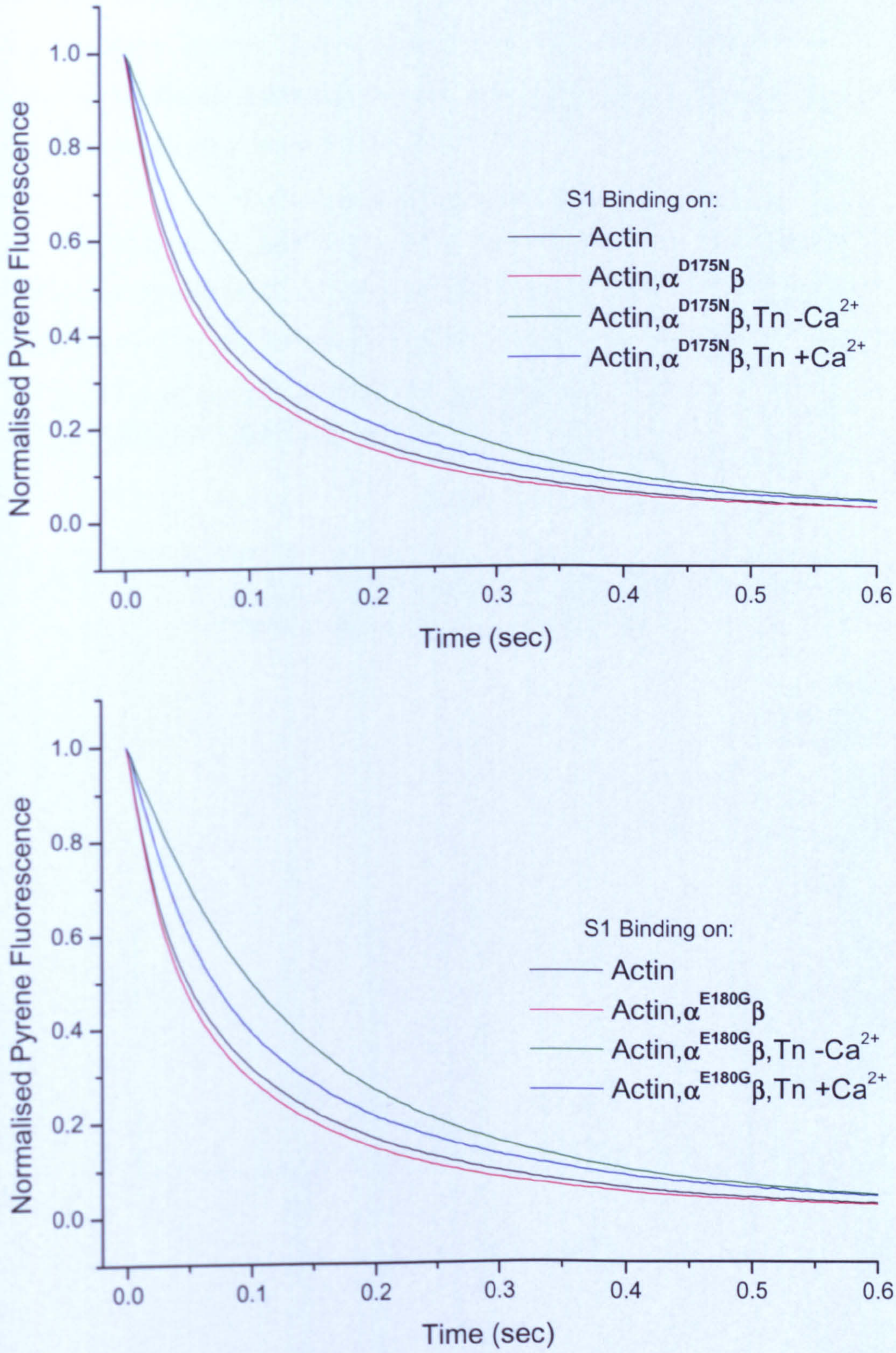

Fig 4.13: Binding of S1 to actin filaments decorated with the $\alpha^{D175N}\beta$ or the $\alpha^{E180G}\beta$ heterodimer (top and bottom panels respectively). The colour code of the transients is the same as described in figure 4.12. Both heterodimers could successfully regulate with the Tn complex the S1 binding to the thin filaments.

Figure 4.14 shows all the transients obtained from the binding of S1 on actin filaments containing the different Tm dimers (no Tn). In figure 4.15, panel A shows all the transients obtained from the binding of S1 on actin filaments containing the different Tm dimers plus the Tn complex in the absence of Ca^{2+}, while panel B shows the same transients in the presence of Ca^{2+}.

In each case, no significant differences were observed between the filaments containing the different Tm dimers and all transients were well superimposed. Fitting the main body of the transients to single exponentials estimated the observed rate constants k_{obs} of the S1 binding to the thin filaments, which were similar in any case. The k_{obs} values are summarised in table 4.3.

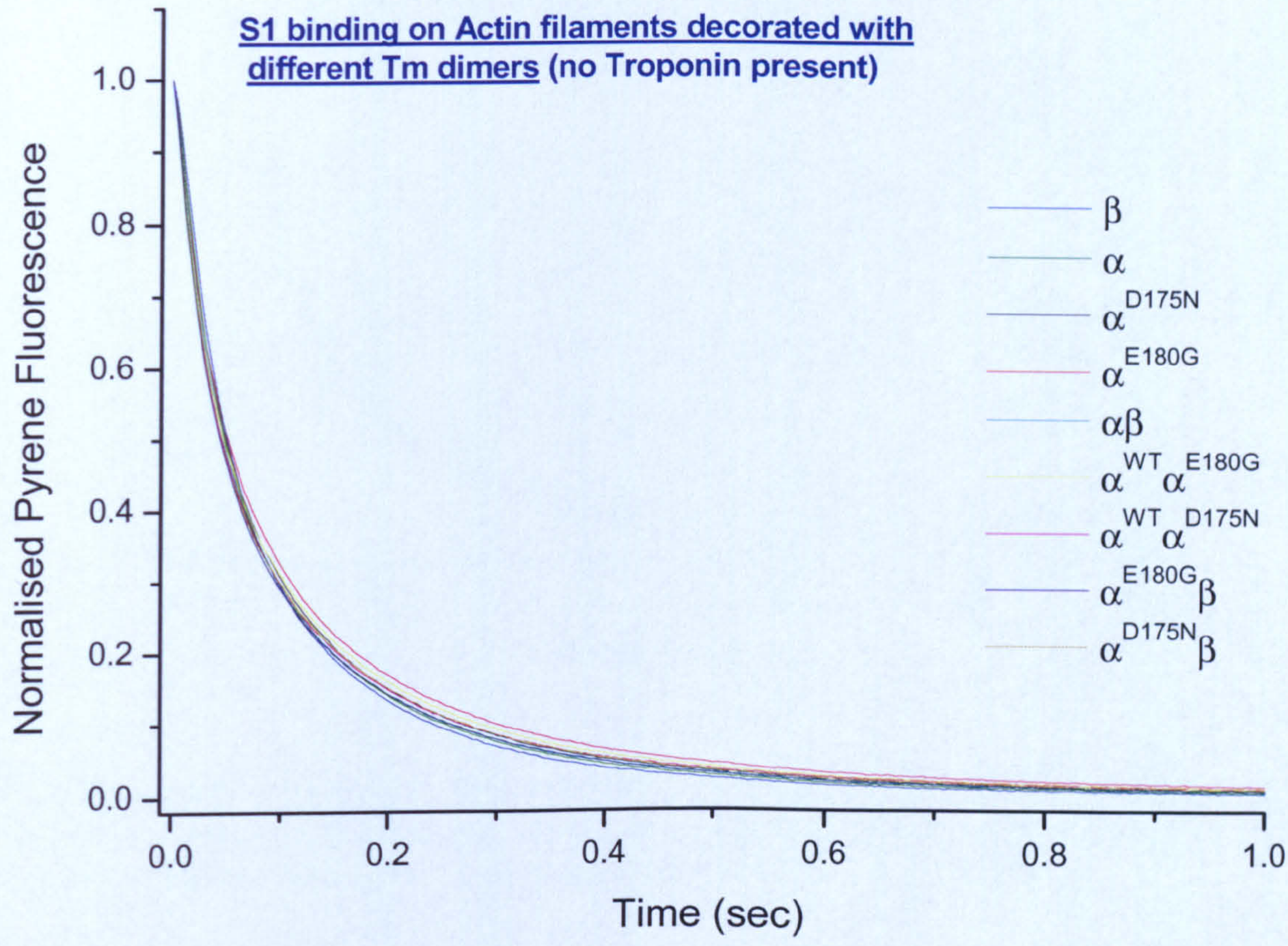

Fig 4.14: Binding of S1 onto actin filaments decorated with the different Tm dimers (no Tn present). No apparent difference can be observed between the different types of filaments.

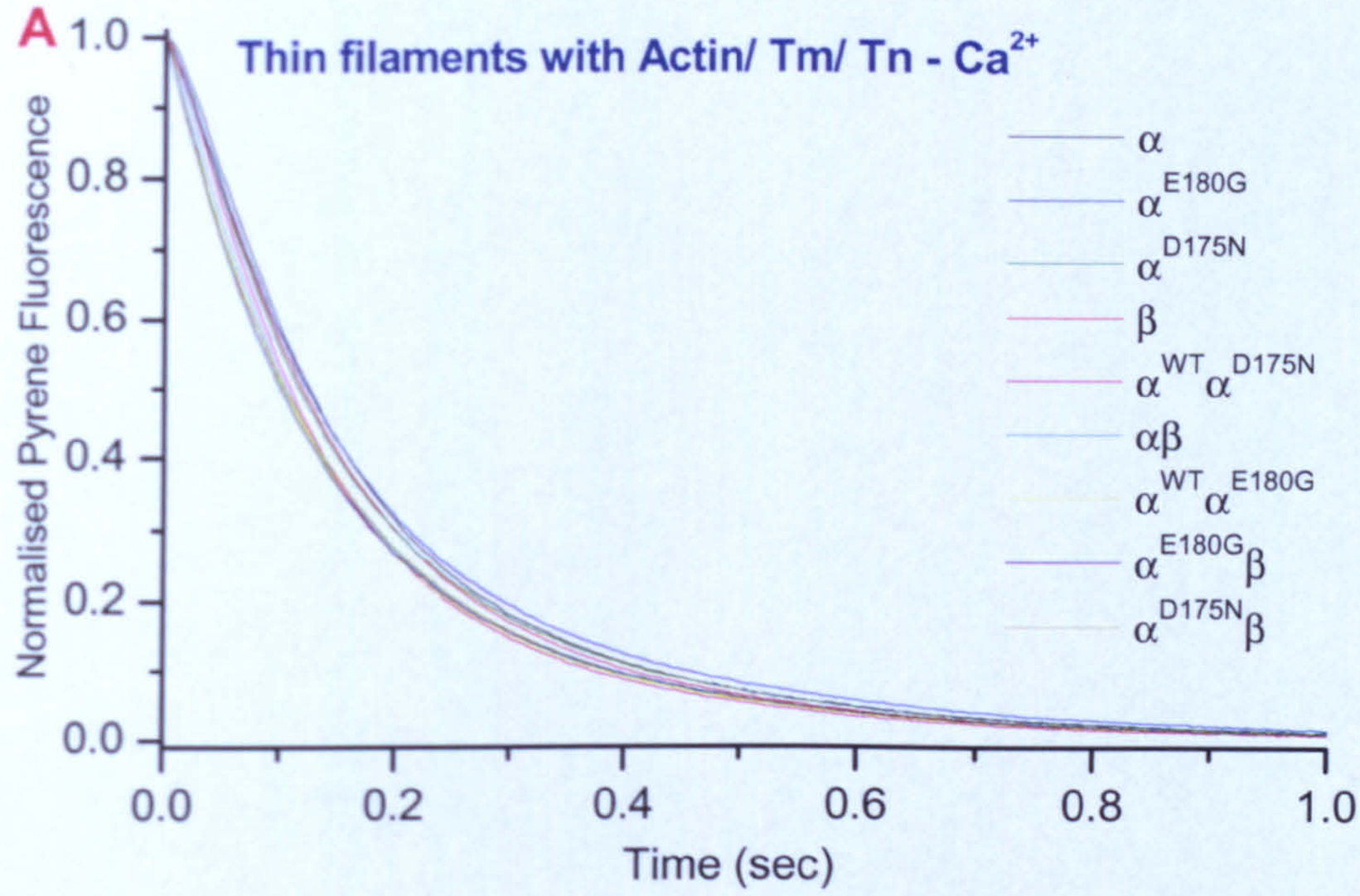

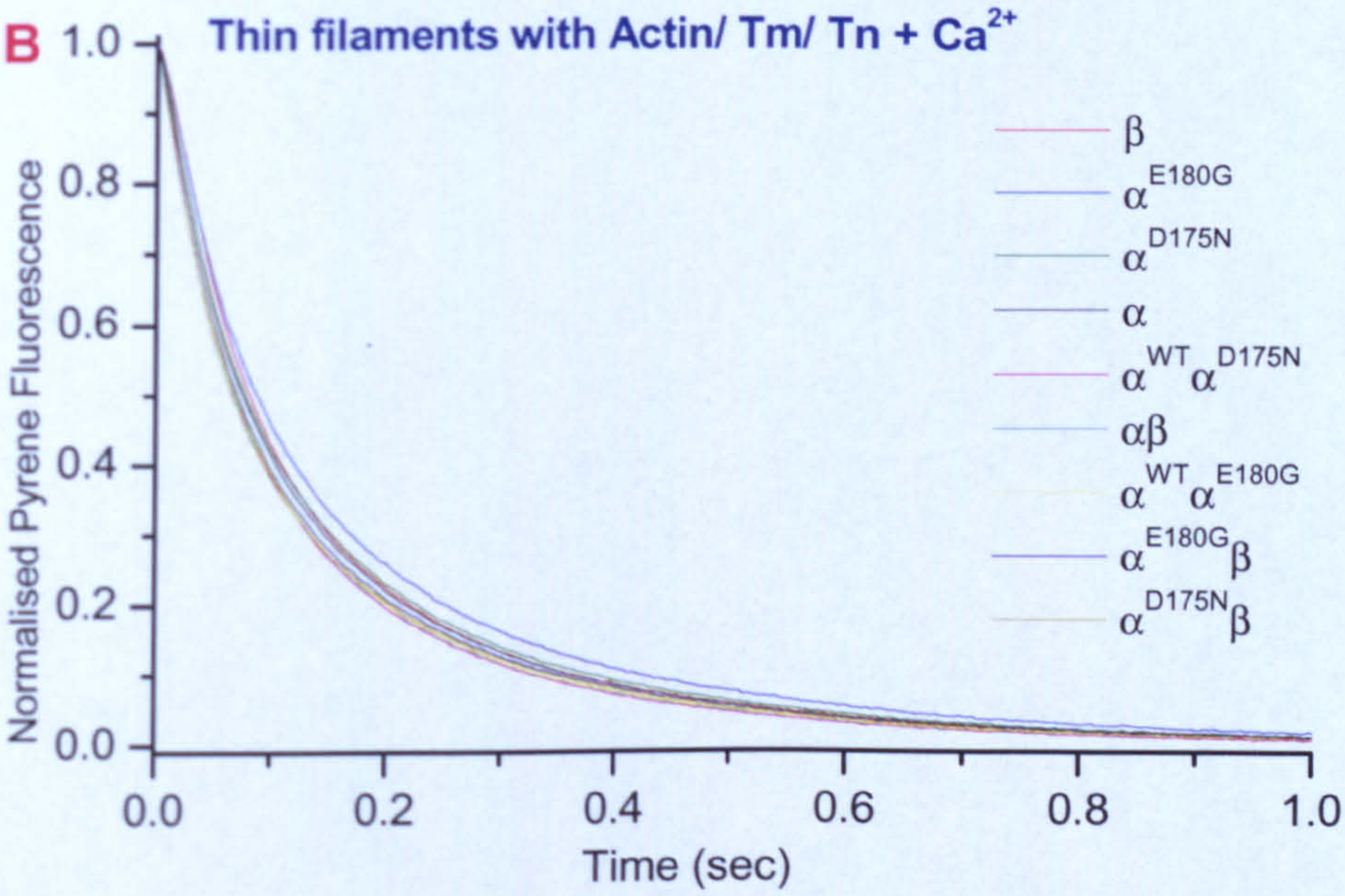

Fig 4.15: Binding of S1 to actin filaments decorated with the different Tm dimers plus the skeletal Tn complex in the absence (panel A) or presence (panel B) of Ca^{2+}. In any case, no apparent difference can be observed between the different types of filaments.

Tm dimer	k_{obs}			
	Actin only	Actin/Tm	Actin/Tm/Tn + Ca^{2+}	Actin/Tm/Tn - Ca^{2+}
αα	8.23	9.74	7.05	6.59
ββ	7.99	9.84	7.27	6.69
$\alpha^{D175N}\alpha^{D175N}$	8.29	8.97	7.24	6.66
$\alpha^{E180G}\alpha^{E180G}$	7.65	8.11	6.91	6.24
αβ	8.02	9.52	7.72	6.73
$\alpha^{WT}\alpha^{D175N}$	8.37	9.2	7.91	7.3
$\alpha^{WT}\alpha^{E180G}$	8.09	8.36	7.93	6.85
$\alpha^{D175N}\beta$	7.95	8.17	7.09	6.53
$\alpha^{E180G}\beta$	7.77	8.83	7.3	6.79
Mean	8.04	8.97	7.38	6.71
SD	0.22	0.62	0.36	0.27

Tm dimer	Normalised k_{obs}		
	Actin/Tm	Actin/Tm/Tn + Ca^{2+}	Actin/Tm/Tn - Ca^{2+}
αα	1.18	0.857	0.8
ββ	1.23	0.91	0.84
$\alpha^{D175N}\alpha^{D175N}$	1.08	0.87	0.8
$\alpha^{E180G}\alpha^{E180G}$	1.06	0.9	0.82
αβ	1.18	0.96	0.84
$\alpha^{WT}\alpha^{D175N}$	1.1	0.95	0.87
$\alpha^{WT}\alpha^{E180G}$	1.03	0.98	0.85
$\alpha^{D175N}\beta$	1.03	0.89	0.82
$\alpha^{E180G}\beta$	1.14	0.94	0.87
Mean	1.11	0.92	0.83
SD	0.07	0.04	0.03

Table 4.3: The top table shows the observed rate constants k_{obs} obtained after binding of S1 to actin filaments decorated with the various Tm dimers. The k_{obs} values for the filaments containing actin or actin/Tm, or actin/Tm/Tn/+Ca^{2+} or actin/Tm/Tn/-Ca^{2+} are shown. The actin control was varied from 7.65-8.23, but it should be the same in any case. From the mean 8.04 and the SD 0.22 of the actin control it can be estimated that the precision of the measurement is ± 2.7 %. The k_{obs} values in each set of experiments were normalised by dividing with the k_{obs} value of their corresponding actin control. The normalised values are shown in the lower table. These values were very similar indeed in every set of experiments and the SD value was very small.

Apart from the k_{obs}, the half time $t_{1/2}$ was also measured. This is the time required for S1 to bind actin and reduce the pyrene fluorescence signal to 50 %. Theoretically, from the equation showing the exponential decrease of the actin fluorescence:

$$[A]_t = [A]_o e^{-k_{obs} t}$$

the $t_{1/2}$ can be calculated, by solving the equation for $[A]_t = [A]_o / 2$

This gives $t_{1/2} = 0.69/k_{obs}$.

However the calculation of $t_{1/2}$ by dividing 0.69 by the k_{obs} values that were previously calculated, is not entirely accurate. This is because the above equation that shows the exponential decrease of the actin's signal does not include any possible lag phases. For the calculation of the k_{obs} the initial lag phase of the transient was not included and the k_{obs} was measured by fitting an exponential to the main body of the transient. By measuring the $t_{1/2}$ manually, any lag phase that might exist in the transient is also included in the period needed to reduce the signal to 50 %.

The $t_{1/2}$ values are summarised in table 4.4 for the thin filaments containing Actin/Tm/Tn in the presence and absence of Ca^{2+}. In either case, it can be observed that $t_{1/2}$ was very similar between the different filaments. It is obvious from the table that more time was required to reduce the pyrene signal in the absence of Ca^{2+}. This is because in that case the filaments occupied the blocked state as well, thus there were fewer actin sites available for binding than in the presence of Ca^{2+}.

Tm dimer	$t_{1/2}$ (msec)	
	+ Ca^{2+}	- Ca^{2+}
αα	76	125
ββ	80	118
$\alpha^{D175N}\alpha^{D175N}$	77	115
$\alpha^{E180G}\alpha^{E180G}$	88	124
αβ	68	104
$\alpha^{WT}\alpha^{D175N}$	69	107
$\alpha^{WT}\alpha^{E180G}$	69	103
$\alpha^{D175N}\beta$	66	103
$\alpha^{E180G}\beta$	70	101
Mean	74	111
SD	7	9

Table 4.4: The time required for S1 to bind to the actin filaments and reduce the pyrene signal down to 50 % ($t_{1/2}$) is shown for the actin filaments decorated with Tm and Tn in the presence and absence of Ca^{2+}. The $t_{1/2}$ was larger in the absence of Ca^{2+}. In any case, no significant differences were observed in the thin filaments decorated with the various Tm dimers.

4.5 Conclusion points from the Characterisation of different Tm Homodimers and Heterodimers

The different skeletal Tm homodimers and heterodimers were characterised by three set of experiments. From the characterisation experiments correlations between cardiomyopathies and the αβ heterodimer or the α^{D175N} or α^{E180G} mutants can be drawn and these are discussed in the final chapter 6.

From the thermal unfolding of the different Tm dimers using CD experiments it was concluded that the heterodimers adopted melting profiles similar to those of the homodimers of their least stable subunit. Also a pattern of thermal stability was revealed, according to which amongst the heterodimers, those carrying a β subunit were the least stable. Also amongst the dimers that carried the α^{D175N} or α^{E180G} mutations the least stable were the dimers that carried the α^{E180G} copy. The β

homodimer appeared to be extremely unstable and perhaps this explains its absence from normal muscle tissues.

From the actin binding experiments, comparison of homodimers vs. heterodimers revealed that the homodimers had significantly higher affinities for actin. However, the heterodimers had comparable cooperativity values to the homodimers. The presence of TnT1 caused an increase in the actin binding affinity in all homodimers and heterodimers.

Finally, monitoring of S1 binding on thin filaments by stopped flow indicates that all of the heterodimer produced were functional and could regulate together with Tn the binding of S1 to the actin filaments. The Tm heterodimers showed transients almost identical to those of the homodimers. The k_{obs} obtained after fitting the transients to single exponentials and the $t_{1/2}$ values were very similar.

As a future study, it will be useful to perform equilibrium experiments in order to calculate the equilibrium constants of K_T or K_1 or K_2 (as indicated in fig 1.25). In our laboratory the above equilibriums can be precisely estimated using the titration experiments where S1 is continuously titrated on thin filaments and binding can be followed as pyrene-actin fluorescence is decreased. The resulting curves can be fitted to the three state model of regulation and the value of each equilibrium constant can be estimated. Currently an on-going project aims to improve these S1 titration experiments in order to be able to use less thin filaments (and therefore be economic on the amount of heterodimers used) while obtaining precisely the equilibrium values at the same time. When the new method will be fully developed it will be of extreme interest to run all experiments with the different Tm dimers and define the equilibrium constants for each one.

Chapter 5

Cloning, Expression and Characterisation of TnT1 mutants

5.1 Introduction

In parallel with the major aim of this thesis of forming and purifying the skeletal Tm heterodimer, a secondary project was initiated. This project is described in the current chapter and aimed in exploring the effects of mutations in the Troponin T gene that cause hypertrophic cardiomyopathies (HCM).

As explained in section 1.4.1.c, TnT can be cleaved by proteolysis into the N-terminal and C-terminal domains known as TnT1 and TnT2 respectively (Morris and Lehrer 1984). The TnT2 binds to TnI, TnC and Tm and contributes to the Ca^{2+} sensitivity of the thin filament. The TnT1 binds to Tm only and in its presence the cooperative unit size of actin/Tm filaments is increased from 6 to 9 units. In contrast the TnT2 (in complex with TnI and TnC) does not have an effect in the cooperativity of the actin/Tm filament (Schaertl *et al.* 1995).

In the project presented here, the characterisation of the HCM TnT mutants was focused in experiments that would investigate the interactions of these mutants with Tm. For the characterisation experiments the TnT1 fragment was used instead of the whole TnT protein. This is because TnT1 alone interacts with Tm and binds at the

overlap region between adjacent Tms (Jackson *et al.* 1975; Pearlstone and Smillie 1977). Furthermore it stabilises the Tm overlap region and promotes the binding of Tm to actin (Palm *et al.* 2001). Also it is more soluble and easier to handle than the whole TnT.

The primarily aim of the project was to introduce point mutations in the wild-type TnT1 peptide. As mentioned in section 1.6, amongst the thin filament proteins, cardiomyopathy mutations are the most frequent in TnT and counts for the 15 % of the total HCM cases (Thierfelder *et al.* 1994; Redwood *et al.* 1999). The majority of those mutations are located within the TnT1 region as can be seen from figures 1.31 and 5.1. Therefore there were plenty of HCM TnT1 candidates to choose for this study. In figure 5.1 some of the cardiomyopathy mutations in the cardiac TnT gene are shown together with the gene's exon organisation.

From figure 5.1 it can be observed that the TnT1 peptide, which includes the first 160 residues, extends from exon 1 to the beginning of exon 12. The part of TnT1 that interacts with the Tm overlap region includes exon 10, exon 11 and the start of exon 12. Thus the mutations were chosen to be from this area. The mutations R92Q, A104V and F110I were chosen (highlighted in red in figure 5.1). All of these mutations cause hypertrophic cardiomyopathies. Furthermore all of them are located within the same exon, the exon 10. The R92Q is at the beginning of the exon and at the edge with the Tm overlap region. The A104V is at the middle and the F110I is at the end of exon 10.

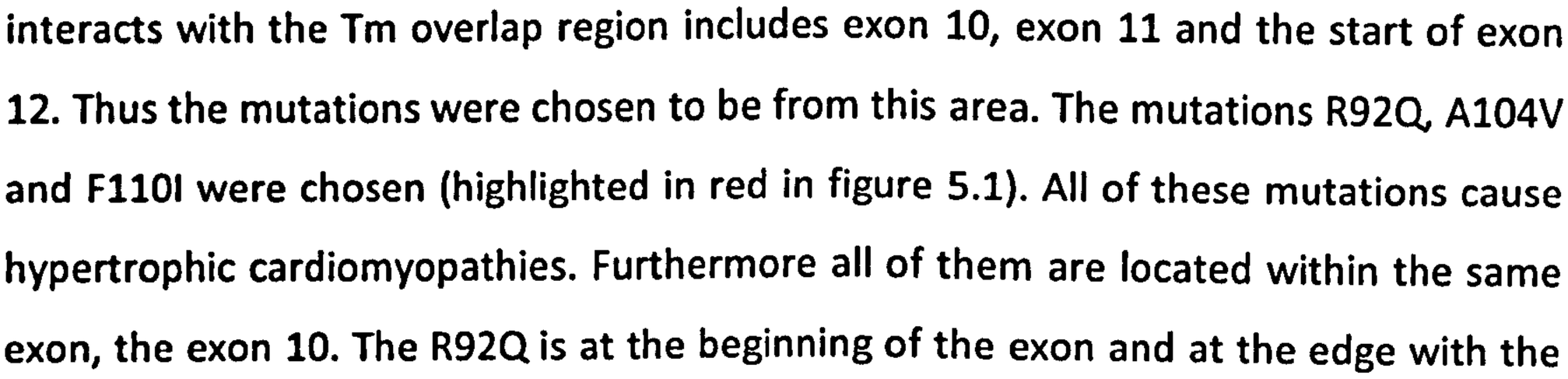

Fig 5.1: Organisation of exons and location of cardiomyopathy mutations in the human cardiac TnT gene. The HCM mutations R92Q, A104V and F110I are located within exon 10, which interacts with the Tm overlap region (Gomes *et al.* 2004).

The three TnT1 point mutations were introduced into the wild-type TnT1 DNA template (that was amplified from the human cardiac TnT, isoform 3) using PCR site-directed mutagenesis. The three mutants were successfully cloned and expressed in bacteria cells and purified by ion exchange chromatography. Then the interactions of each mutant with the bacterially expressed α Tm homodimer were investigated and compared to the wild-type TnT1 peptide. From actin cosedimentation assays, the affinity of each TnT1 for Tm was measured. Also, the affinity of Tm for actin was measured in the presence of the various TnT1s.

5.2 TnT1 mutants cloning and expression

The three TnT1 mutants R92Q, A104V and F110I were made by site directed mutagenesis using wt TnT1 as template DNA. The primers used are described in materials and methods (section 2.1.1). DNA sequencing of several plasmids revealed those successfully mutagenised. The positive TnT1 inserts were then cloned into the expression vector pJC20. BL21 cells were transformed with the expression plasmid and streaked onto LB/Amp agar plates. Five colonies of each of the transformed BL21 cells were then used to inoculate 5 ml of LB/Amp media. The mini liquid cultures were then induced with IPTG to check for protein expression levels. All colonies showed good expression levels of the mutant TnT1 when analysed by SDS-PAGE (fig5.2). Together with the IPTG-induced liquid cultures, purified wt TnT1 protein was also loaded to indicate the position of the TnT1 mutants on the gels.

Fig 5.2: Protein expression in BL21 cells transformed with plasmids containing the different TnT1 mutants. 5 mini-cultures were tested for each mutant. In each lane, the whole bacterial lysate was loaded and the most dense bands corresponded to the TnT1 mutants. The different TnT1 mutants ran at about the same level as the wt TnT1 purified protein control.

5.3 TnT1 purification

For the purification of the whole Troponin T usually a two step protocol is followed; first the lysate mixture is applied onto a cation exchanger (like CM sepharose), the fractions containing TnT are pooled together and then applied onto an anion exchanger (like DEAE sepharose) (Krüger *et al.* 2003). This coupled cation and anion exchange chromatography is used because the charge is unevenly distributed within the TnT protein, with the N-terminal part having a pI of 4.4 and the C-terminal part having a pI of 10.24. However in the case of the TnT1 peptide, the fragment is mostly negative with pI of 4.4. Therefore a new TnT1 purification protocol was developed that included only the anion exchange chromatography step using the weak anion exchanger DEAE sepharose column (method described in section 2.2.3d). The lysate mixture was applied onto the DEAE sepharose column and the bound proteins were eluted using a salt gradient from 0 to 0.6 M KCl within 24 column volumes (120 ml). At the end of this first purification cycle, the eluted fractions were loaded on SDS gels. From the gels the TnT1 fragments looked already free from most of the lysate protein contaminants (fig 5.3) but they were high in nucleotide contaminants (as shown in chromatograms by the red peak showing absorbance at 260 nm). Thus the TnT1 fractions were further polished by repeating the purification procedure. The fractions containing TnT1 were pooled together, dialysed in equilibration buffer A overnight at 4 °C and the second purification cycle was performed under exactly the same conditions as the first cycle. The second chromatogram showed some improvement in the nucleotide contamination, since the 260 nm peak was decreased (the ratio of 260/280 peaks was 2.3 in first run and 1.9 in second run) (fig 5.4). There were still nucleotide contaminants present but these should not interfere with the future actin binding experiments. The fractions within the peaks of the chromatogram were loaded onto SDS gels, and those containing TnT1 were pooled together. From the gels, the TnT1 containing fractions appeared free from most protein contaminants (fig 5.4). The concentration of each TnT1 protein was measured using the Bradford method (Bradford 1976) instead of the routinely used UV spectroscopy to avoid inaccuracies caused by the presence of the nucleotide contaminants. The yield was about 25 mg of protein per litre of bacterial culture.

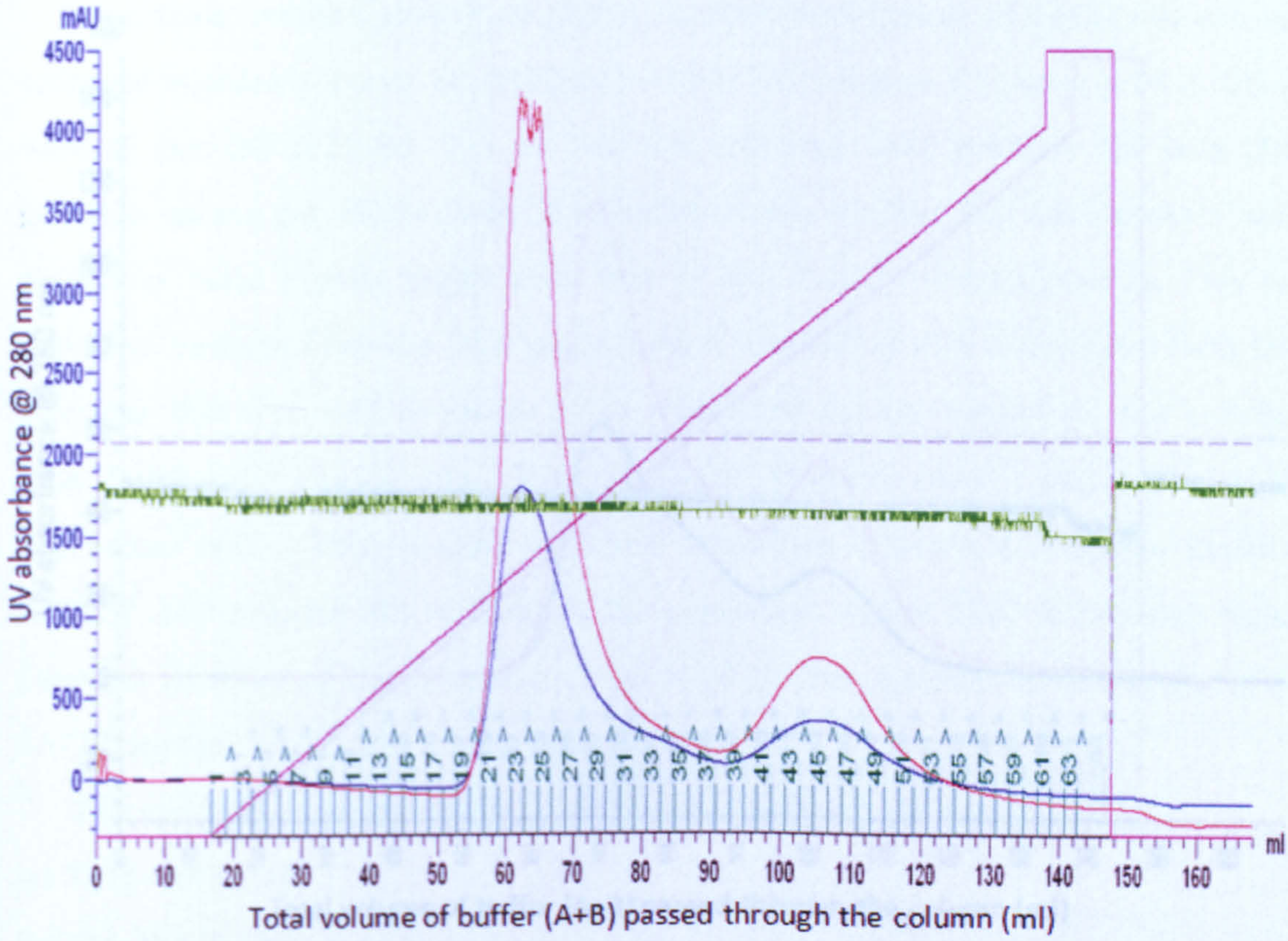

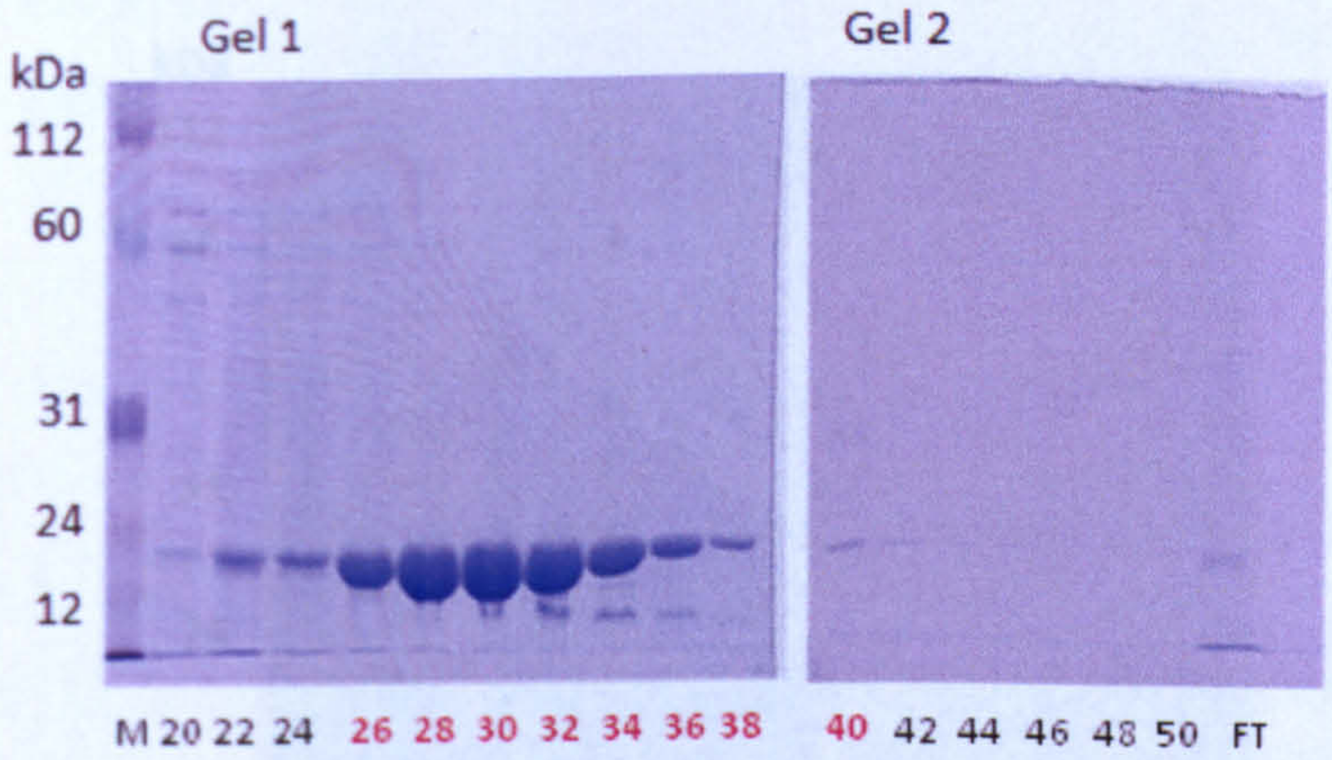

Fig 5.3: First cycle of anion exchange chromatography on DEAE column for the purification of F110I TnT1 mutant. The peak in blue shows the absorbance at 280 nm and the peak in red the absorbance at 260 nm. Elution achieved with a salt gradient 0-0.6 M KCl (pink line) over 120 ml. Fractions 20-50 that lied within the peaks of the chromatogram were loaded onto 12 % SDS gels. The fractions 26-40 had the least contaminated TnT1 and were pooled together to undergo a second purification cycle. Although in the chromatogram the fractions 20-24 were included in the peak, in the SDS gels these fractions did not show any large amount of protein present.

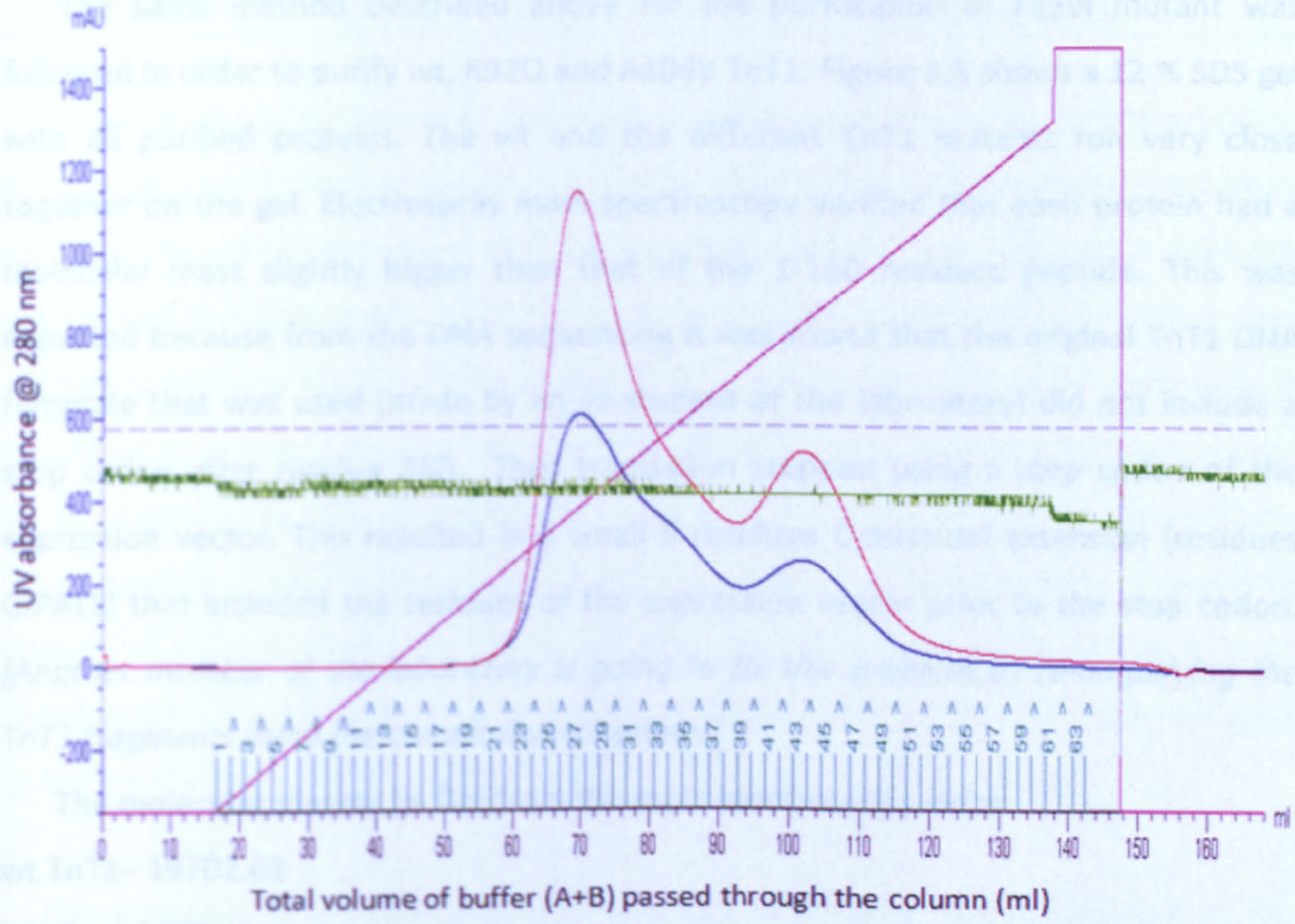

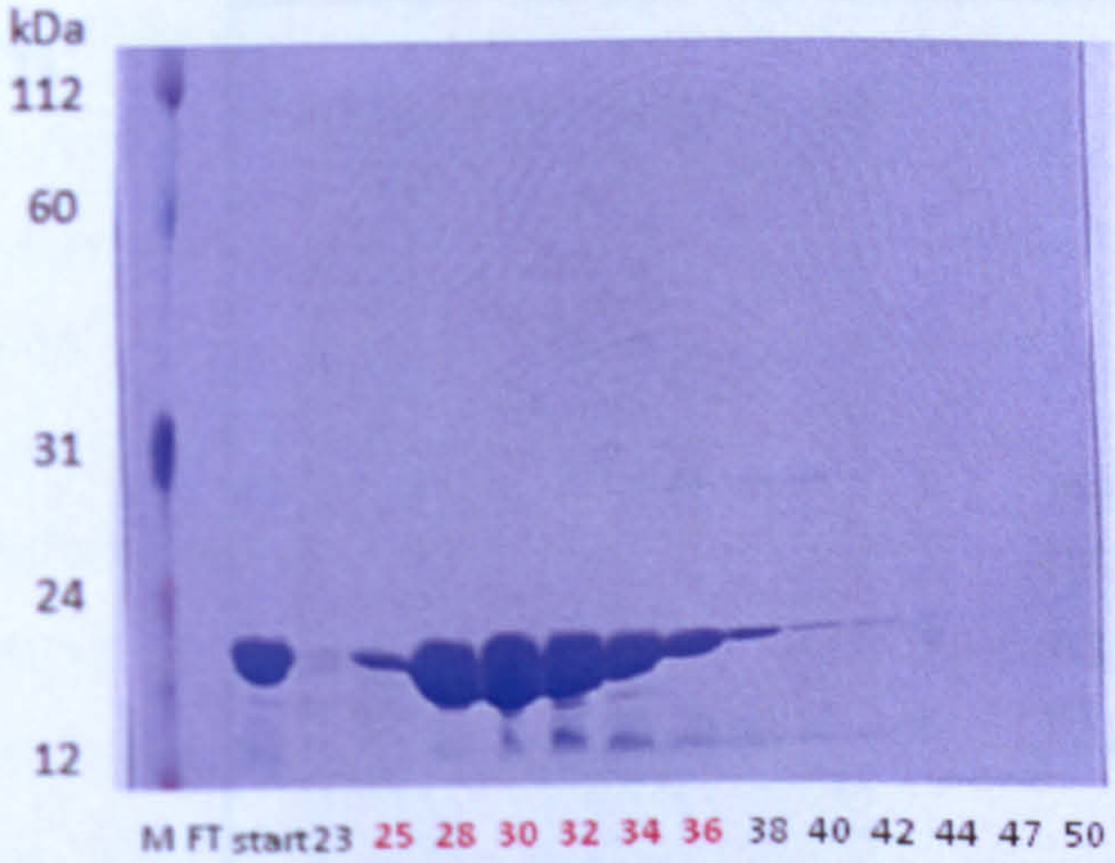

Fig 5.4: Second cycle of anion exchange chromatography on DEAE column for the purification of F110I TnT1 mutant. Same conditions were followed as in fig 5.3. The fractions that appeared within the peaks of the chromatogram were loaded onto an SDS gel. Fractions 25-36 were pooled together. F110I TnT1 appeared clean from most protein contaminants. Also there was less nucleotide contamination in comparison to the first purification cycle, as indicated by the absorbance at 260 nm (red peak). In the chromatogram the colour code is the same as in fig 5.3.

The same method described above for the purification of F110I mutant was followed in order to purify wt, R92Q and A104V TnT1. Figure 5.5 shows a 12 % SDS gel with all purified proteins. The wt and the different TnT1 mutants run very close together on the gel. Electrospray mass spectroscopy verified that each protein had a molecular mass slightly bigger than that of the 1-160 residues peptide. This was expected because from the DNA sequencing it was found that the original TnT1 DNA template that was used (made by an ex-student of the laboratory) did not include a stop codon after residue 160. Thus translation stopped using a stop codon of the expression vector. This resulted in a small 6 residues C-terminal extension (residues GIPALS) that included the residues of the expression vector prior to the stop codon. *[Another member of the laboratory is going to fix this problem by re-amplifying the TnT1 fragments using the correct reverse primer]*

The molecular masses (in Da) from the mass spectroscopy were:

wt TnT1– 19702.68

R92Q – 19675.19

A104V – 19730.87

F110I – 19668.73

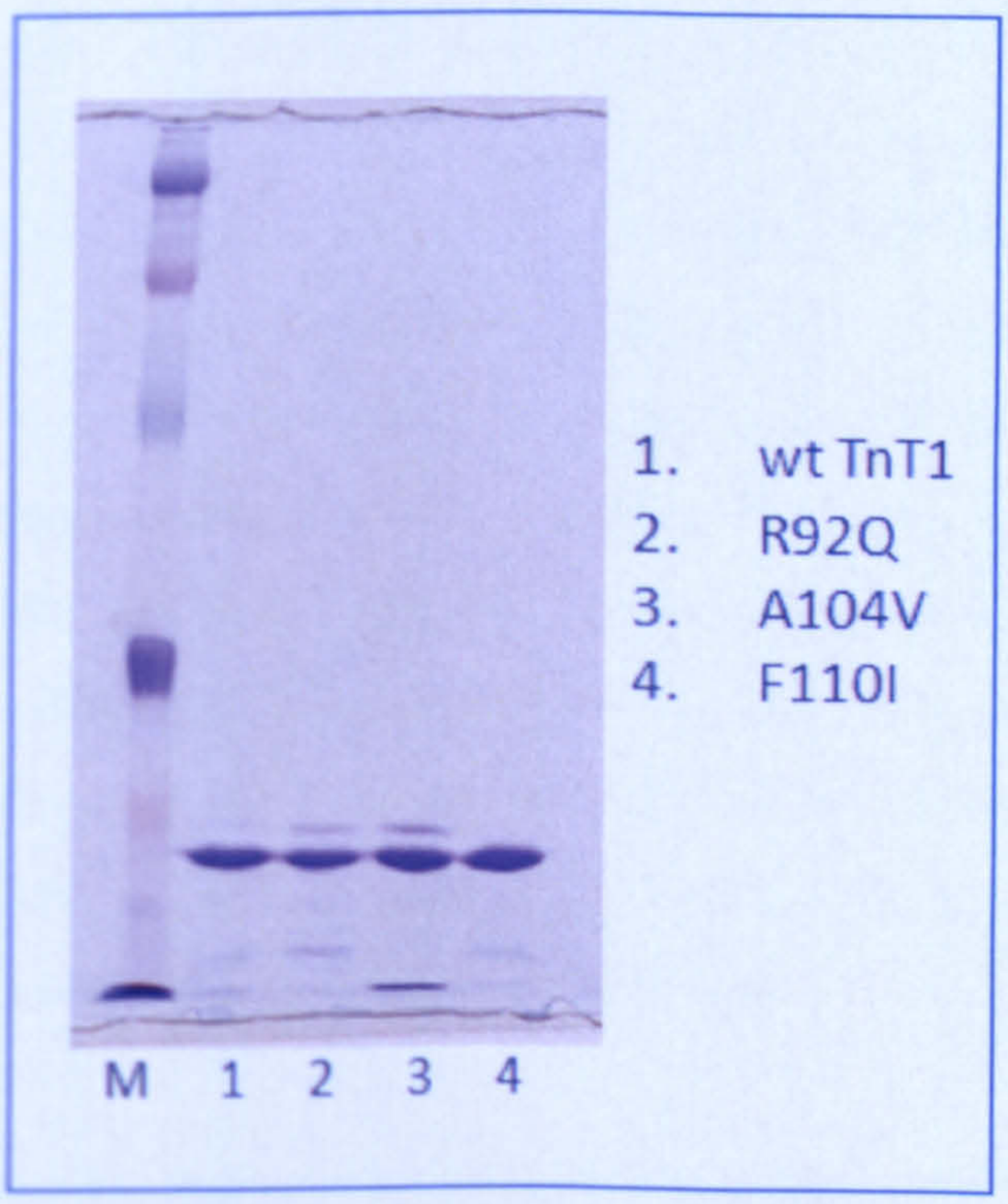

Fig 5.5: Summary of the wt and mutant TnT1 proteins purified. All proteins were purified by anion exchange chromatography under the same conditions. 3 µg of each were loaded for the SDS-PAGE. The bands were of equal density, indicating that for each protein the concentration was measured correctly using the Bradford method. The R92Q and A104V mutants appeared with minor contaminants. All TnT1 proteins run at the same level on the 12 % SDS gel.

5.4 Affinity of α Tm for actin in the presence of mutant TnT1

For the characterisation of the various TnT1 peptides, actin cosedimentation experiments were performed where the actin and the TnT1 concentrations remained constant throughout the assay, while the concentration of Tm was increased. With this experiment the binding affinity of Tm for actin and the cooperativity of binding were estimated in the presence of the various TnT1s, using exactly the same procedure as described in section 4.3.2. The same batches of actin and α Tm homodimer were used in all experiments. The concentration of actin was 9 μM, of TnT1 2 μM and the concentration of Tm was increased from 0.2 to 5 μM. The amount of TnT1 would be enough to saturate the actin bound Tm, assuming that TnT1 binds to Tm in a 1:1 stoichiometry and taking into account that the affinity of α Tm for actin in the absence of TnT1 is 0.3 μM.

An example of a Tm/Actin cosedimentation assay that was performed in the presence of the mutant R92Q TnT1 is shown in figure 5.6. It can be observed from the gel showing the pellets that Tm bound actin until the actin filaments became saturated (lane 5). When saturation of actin was reached the amount of Tm remained constant in pellets and accumulated in the supernatants. From the gel showing the pellets it can also be observed that in each lane the ratio of Tm density vs. TnT1 density was constant. This indicates that TnT1 was preferentially binding to the filamentous Tm in the pellets, until they became saturated with the TnT1. The excess amount of TnT1 that did not bind to the Tm/Actin (after Tm became saturated) was found in supernatants. In lane 1, where the Tm concentration was very low, it can be observed that only a trace of TnT1 was found in the pellets following the small amount of Tm. The rest of TnT1 was found in the supernatants. This means that TnT1 alone did not bind actin directly, otherwise it would be found in the pellets.

Also from the gels, it can be seen that some minor protein contaminants of the R92Q sample could be found in the supernatants and not in the pellets. Thus these contaminants should not interfere with the binding event. Moreover the α Tm appeared as a doublet on the gel. This is due to a portion of α Tm being cleaved at the N-terminal as found from mass spectrometry results. The lower band of the α Tm is

the cleaved band and is found in the supernatants only, thus it is not interfering with the binding. From densitometry analysis it was calculated that this band accounts for the 9.5 % of the total α Tm density, thus the initial α Tm concentration was corrected for this number.

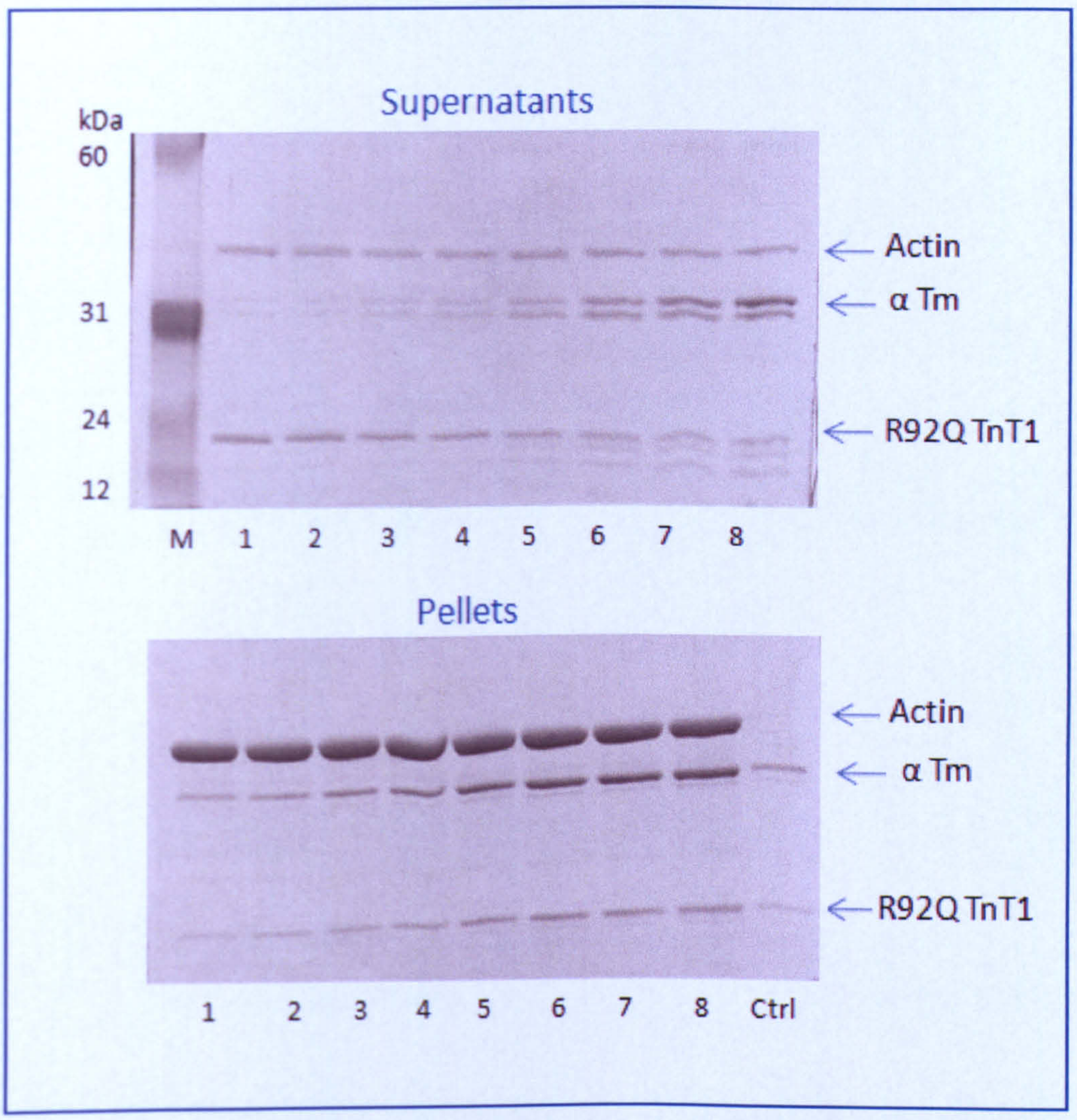

Fig 5.6: Cosedimentation assay of actin with Tm in the presence of the mutant R92Q TnT1. Actin and TnT1 concentrations were kept constant in tubes 1-8, while Tm concentration was increased from 0.2-5 μM. Tm was binding to the actin filaments until they became saturated (after lane 5). After actin's saturation the Tm accumulated in the supernatants. The R92Q TnT1 bound to the Tm filaments in the pellets and it can be seen that in any sample 1-8 of the pellets the ratio of TnT1 : Tm was constant. The excess of TnT1 was found in the supernatants. The control in the gel of the pellets contained Tm and TnT1 (at concentrations same as in lane 5) and it can be seen that the two proteins without the presence of actin are not pelleted down (only traces appear in the control sample).

The graphs obtained after the cosedimentation gels analysis are shown in figure 5.7, for each one of the TnT1 proteins tested. The graphs of the free Tm concentration vs. the fractional saturation of actin had a sigmoidal shape, showing that the binding of Tm to actin was cooperative. By fitting the graphs to the Hill equation, the K_d and n values were obtained.

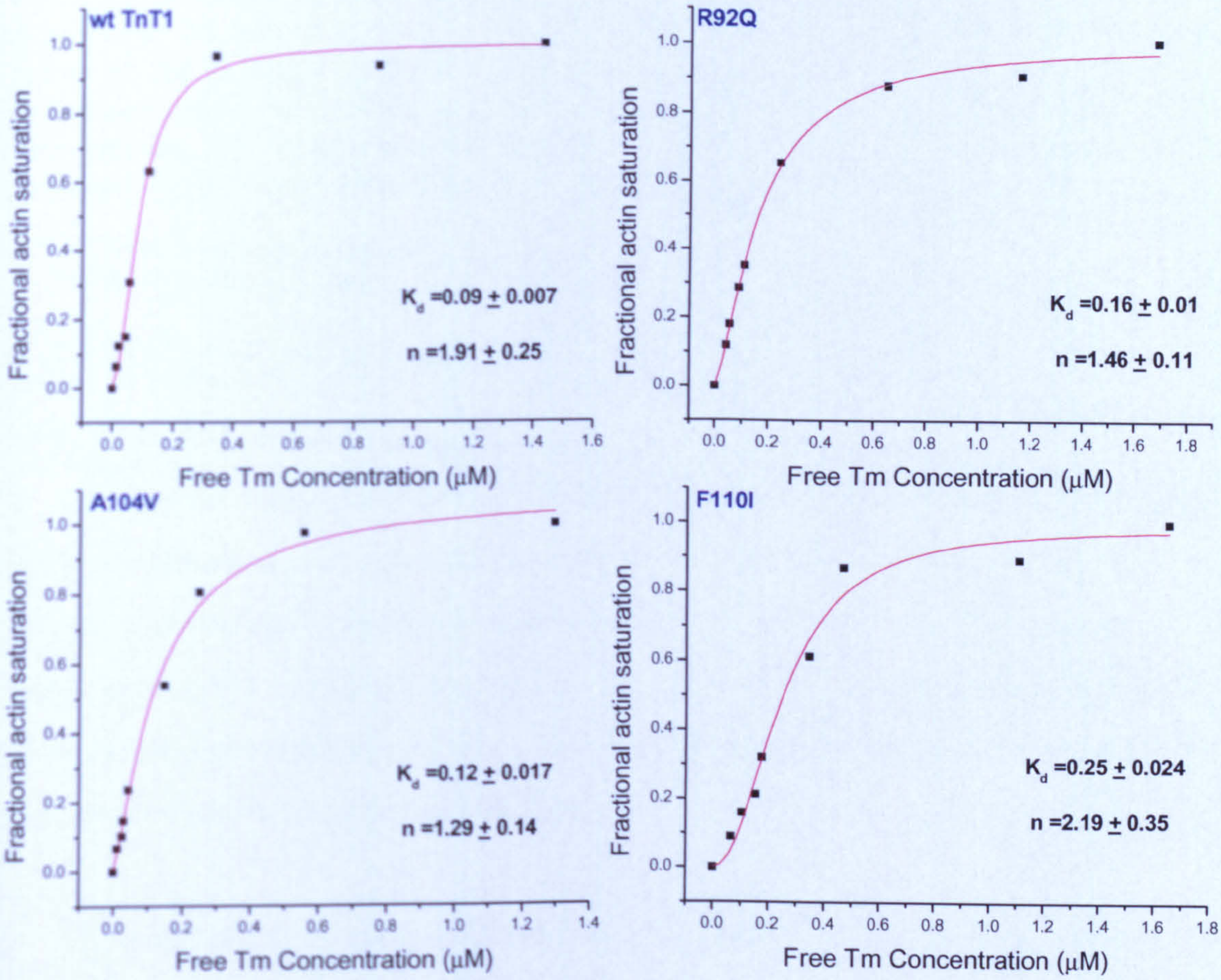

Fig 5.7: Calculation of the binding affinity of the α Tm homodimer to actin and of the cooperativity of binding in the presence of the wild-type and mutant TnT1s. In each panel the type of TnT1 that was present in the cosedimentation experiment is indicated. The free Tm concentration was plotted against the fractional actin saturation. The K_d (affinity of Tm for actin) and n (cooperativity of binding) values were calculated by fitting to the Hill equation.

Unfortunately, apart from the experiment with the wt TnT1 that is exactly the same as in section 4.3.2, the rest of the cosedimentation experiments were only performed once because of time limitations. The preliminary results are summarised in table 5.1. Therefore it is not possible to tell if they are reproducible and what is the accuracy of the measurement.

TnT1	K_d (μM)	n
no TnT1	0.34 ± 0.05	1.58 ± 0.23
wt	0.09 ± 0.007	1.91 ± 0.25
R92Q	0.16 ± 0.01	1.46 ± 0.11
A104V	0.12 ± 0.017	1.29 ± 0.14
F110I	0.25 ± 0.024	2.19 ± 0.35

Table 5.1: Summary of the affinity of α Tm for actin and cooperativity of binding in the presence of the different TnT1s. Values are shown together with the degree of error after fitting to Hill equation. Since the cosedimentations with the mutant TnT1s were only performed once it is not known if they are reproducible and what is the accuracy of the measurement. For comparison the K_d and n values calculated from a cosedimentation experiment of α Tm with actin in the absence of TnT1 (from section 4.3.1) are also shown.

5.5 Affinity of the various TnT1 mutants for α Tm

The second experiment performed for the characterisation of the various TnT1s, again in relation to their interactions with Tm, was to measure their binding affinities for Tm. For this experiment the same principles of the actin cosedimentation assay were applied (as explained in section 2.3.2). In order to obtain more accurate comparisons on the affinities of each TnT1 for Tm, the same batches of actin and α Tm homodimer were used in all experiments.

The actin and α Tm concentrations were constant in samples 1-8 of the assay (9 μM and 2 μM respectively). Therefore, after ultracentrifugation, in every sample the distribution of actin-Tm between the pellets and the supernatants would be constant. From the densitometry analysis it was estimated that 80 % of the Tm was needed to saturate actin and was constantly found in the pellets, while the rest 20 % was found in the supernatants. The TnT1 was assayed by using increasing concentrations from 0.4 - 6 μM in the samples 1-8. At any point in the assay a portion of TnT1 was bound onto the actin/Tm filaments in the pellet; the rest of TnT1 was found free in supernatants. It can be observed that at very low TnT1 concentrations (lanes 1 and 2 for example) where saturation of actin/Tm was far from being reached almost all of TnT1 was found in pellets and none was found in supernatants. This shows that TnT1 preferentially binds to the 80 % of the Tm found as actin/Tm filaments, than to the rest 20 % of the

free Tm in the supernatants. The TnT1 was binding to the actin/Tm filaments in the pellets until Tm became saturated. In the gels shown in figure 5.8 saturation was reached after lane 5. From this point it can be seen that the amount of TnT1 was constant in pellets and increased in supernatants.

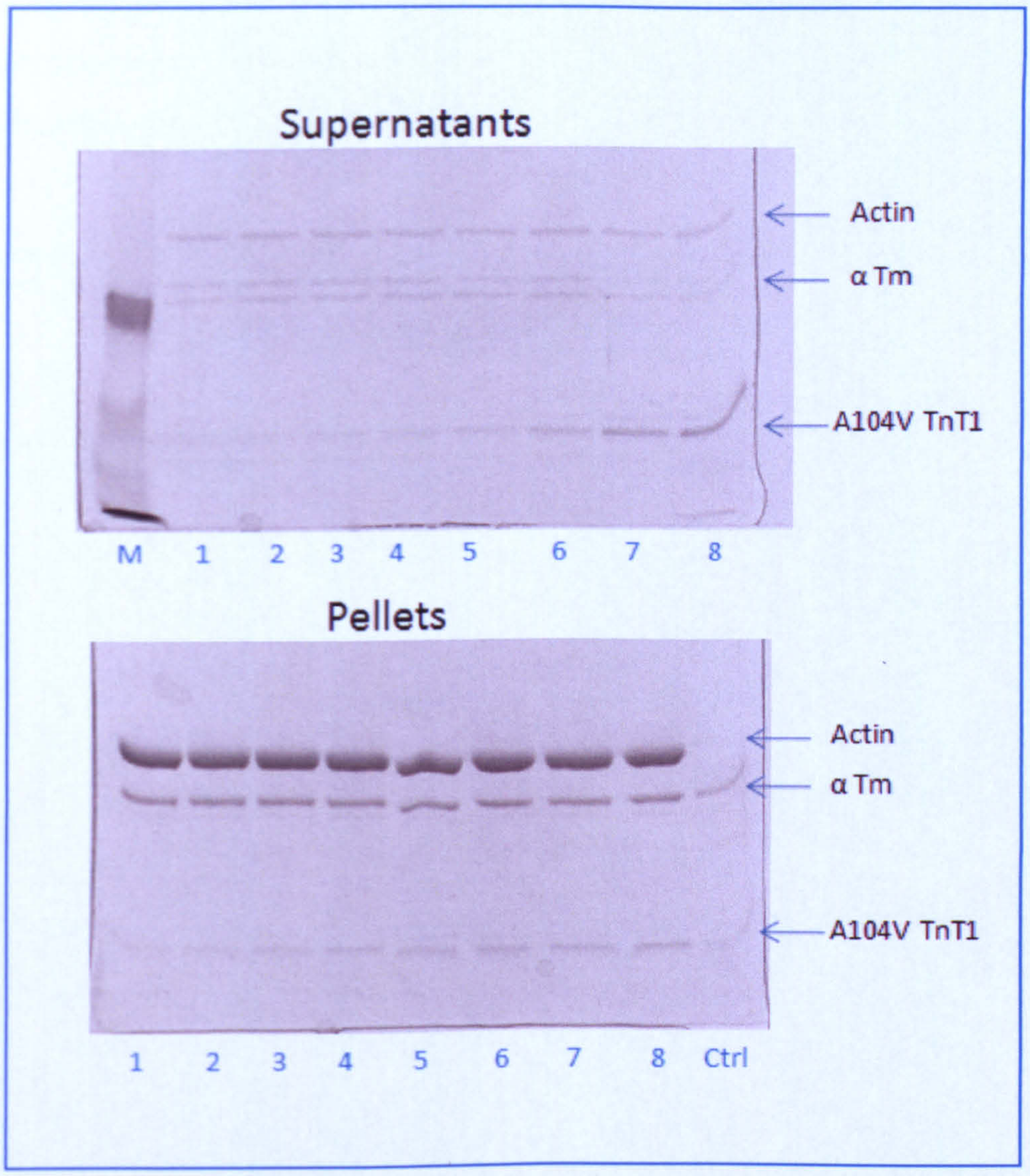

Fig 5.8: SDS gels containing the supernatant and pellet samples of A104V TnT1 and α Tm/actin cosedimentation assay. The amount of actin/Tm was constant in all samples. TnT1 preferentially bound to Tm in pellets, until Tm became saturated (lane 5). When saturation of filamentous Tm in pellets was reached, TnT1 amount in pellets remained constant and TnT1 in supernatants was increased. In the ctrl lane 2 μM Tm and 2 μM TnT1 were ultracentrifuged without actin and their pellet showed only traces of the two proteins.

By densitometry analysis of the gels as explained in section 2.3.2, the amount of free TnT1 concentration can be estimated and plotted against the Tm fractional saturation (pellet TnT1/ pellet Tm). By fitting the resulting graph to a hyperbola:

$$y = a\,[x] / K_d + [x]$$

(because binding of TnT1 to Tm is not cooperative), the affinity K_d of each TnT1 for Tm can be calculated. The graphs after the cosedimentation gels analysis for each TnT1 protein are shown in figure 5.9 and the calculated affinities are summarised in table 5.2.

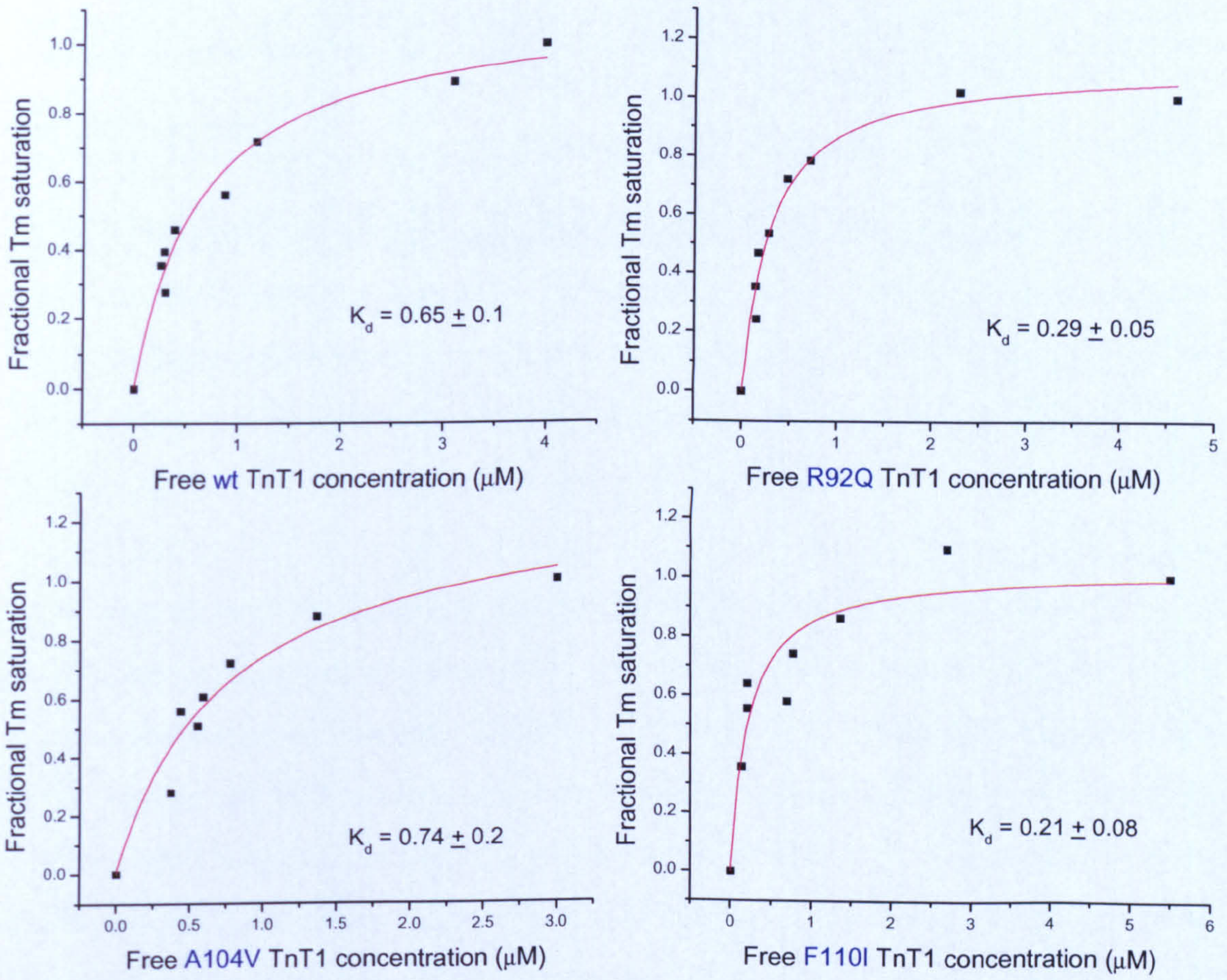

Fig 5.9: Calculation of the binding affinity of the wild-type and mutant TnT1s for the α Tm homodimer. In each panel the type of TnT1 that was examined is indicated. The free TnT1 concentration was plotted against the fractional Tm saturation (pellet of TnT1/pellet of Tm). The K_d affinity of TnT1 for Tm was estimated by fitting the curve to the hyperbola equation $y = a\,[x] / K_d + [x]$.

As in section 5.4, these are preliminary results, obtained from single experiments. All of the experiments should be repeated to check if they are reproducible.

TnT1	K_d (μM)
wt	0.65 ± 0.1
R92Q	0.29 ± 0.05
A104V	0.74 ± 0.2
F110I	0.21 ± 0.08

Table 5.2: Summary of the affinities of the wild-type and the mutant TnT1s for Tm. From these preliminary results, it can be observed that the A104V mutant has similar affinities to Tm as the wild-type TnT1. However the R92Q and the F110I bind to Tm with higher affinities in comparison to the wt TnT1. All experiments should be repeated to check for reproducibility.

5.6 Discussion

In this chapter the interactions of the N-terminal peptide of Troponin T, which is known as TnT1, with the bacterially expressed α Tm homodimer were investigated. The TnT1 is known to bind to the head-to-tail overlap region between adjacent Tms and stabilise this site (Pato *et al.* 1981; Pearlstone and Smillie 1981; Brisson *et al.* 1986).

A large 15 % of the hypertrophic cardiomyopathy mutations exist in the TnT gene (Thierfelder *et al.* 1994) and from these more than ≈2/3 lie within the TnT1 region. Three mutations in the cardiac TnT gene namely the R92Q, the A104V and the F110I were created by PCR using DpnI-mediated site directed mutagenesis. The three mutants were successfully cloned and expressed in BL21 cells. The mutants and the wild-type TnT1 proteins were also successfully purified by anion exchange chromatography using a variation of a protocol that is used for the purification of the whole TnT protein.

The interaction of TnT1 with Tm was investigated at two levels. From chapter 4 it was observed that the wild-type TnT1 could increase the binding affinity of Tm for actin. The three TnT1 mutants were also examined using exactly the same methodology to check if they would differ from the wild-type TnT1. It was found that

the presence of the wild-type TnT1 could increase the Tm's binding affinity to actin x 3.5 fold; in the absence of TnT1 the α Tm had an affinity of 0.3 μM and in the presence of TnT1 the affinity was increased to 0.09 μM. The results of the TnT1 mutants are preliminary and needs to be repeated. From these early observations, the A104V was very similar to the wild-type and increased the Tm's binding affinity to actin x3 fold. However the mutants R92Q and F110I only caused a x2 and a x1.3 fold increase in the binding affinity respectively. The F110I mutant caused the lowest binding affinity of Tm for actin, and was similar to the binding affinity of Tm in the absence of any TnT1. The n values were very similar amongst all of the TnT1s.

A second experiment was performed in order to measure the binding affinity of the various TnT1 proteins for α Tm. From the preliminary results it was found that the affinity of the wild-type protein to actin/Tm was 0.65 μM. Once again the mutant A104V was very similar to the wild-type TnT1 with an affinity of 0.74 μM. However the R92Q and the F110I mutants bound actin/Tm x2-3 fold tighter.

From the results of the two experiments it is indicated that those TnT1 proteins that could bind to Tm with very strong affinities, caused the least increase of the Tm's binding affinity to actin. The F110I mutation had the tightest affinity for Tm which was 3 times stronger compared to the wild-type TnT1. At the same time the presence of F110I had a minor effect on the Tm's affinity for actin; there was only a 1.3 fold increase in the K_d value of Tm for actin compared to the K_d value obtained in the absence of TnT1.

A possible explanation for the above observation is that the TnT1 proteins like the F110I mutant, that can bind to Tm very tightly, may result in a super-stable Tm overlap region. In this case the end-to-end interactions between the Tm molecules may become stiffer. This further suggests that some degree of flexibility at least locally at the Tm overlap regions may increase the affinity of Tm for actin. This does not mean however that flexible end-to-end interactions are a requirement for Tm binding to actin, since the F110I results suggest that even in the case of a potential loss of flexibility the Tm still binds actin efficiently.

However, if the R92Q and the F110I mutants in the TnT do cause an increased stiffness of the Tm filament, then there will be further consequences in the regulation of muscle contraction. Tm needs to be constantly relocating between the blocked the closed and the open states of the thin filament in order to accurately regulate the binding of myosin. To complement this function, flexible end-to-end interactions between Tms are of great advantage because they can sustain the stress that is building up in the Tm overlap regions (Singh and Hitchcock-DeGregori 2006; Minakata *et al.* 2008). If a Tm filament would have to break due to increased stress, the only potential breaking points would be the end-to-end interactions. Thus by having some degree of flexibility in this vulnerable area, it will be less probable to break the continuous Tm filament during its dynamic movement.

Moreover, if the binding of TnT1 mutants causes an increased stiffness of Tm filaments at the end-to-end interactions, this will result in an increase in the cooperative unit size as explained in section 1.4.3 (Geeves and Lehrer 2002; Sumida *et al.* 2008). Having a larger cooperative unit size, would cause the binding of a single S1 on the filament to turn on more actin sites. The thin filaments would then move towards the open state more readily. This means that perhaps less Ca^{2+} would be required from the system to turn the filaments on i.e. an increase in the Ca^{2+} sensitivity would be observed. Indeed most of the HCM mutations are associated with an increase in the Ca^{2+} sensitivity (Robinson *et al.* 2007). Chandra et al have reported exactly this observation for the R92Q mutant i.e. they observed an increased Ca^{2+} sensitivity of the R92Q myofilaments and linked that to altered Tm-Tn interactions (Chandra *et al.* 2001). Hernandez et al have also reported that muscle fibres of transgenic mice expressing the F110I mutant had an increased in the Ca^{2+} sensitivity of force development and ATPase activity (Hernandez *et al.* 2005). In contrast, another group has reported that the F110I mutant had no effect in the cooperativity or in the Ca^{2+} sensitivity of myofibrils (Nakaura *et al.* 1999).

From the experiments performed in this chapter there cannot be a correlation of the mutant A104V TnT1 with cardiomyopathies. From another comparative study between various TnT mutants, the A104V was found to have the least effect in the Ca^{2+} sensitivity and behaved very similarly to the wild-type (Harada and Potter 2004).

Although the A104V mutation is associated with a malignant form of HCM and has a high incidence of sudden cardiac death (Nakajima-Taniguchi *et al.* 1997), the molecular mechanism of the disease remains unknown.

The preliminary results of the binding affinities of the various TnT1 for Tm presented in this chapter are not in complete agreement with previous published observations. Palm et al have reported that the A104V mutant binds to Tm with similar affinity as the wt TnT, in agreement to our results. However, they have reported that the mutant R92Q had slightly lower affinity for Tm and the mutant F110I had almost 2 fold reduced affinity for Tm when compared to the wild-type protein (Palm *et al.* 2001). However, the TnT1 peptide used in the present study extends from residue 1 to residue 160 (plus the small 6 residue extension). In contrast, in the Palm et al study a TnT1 peptide was used that included residues 70-170. Also in the Palm study the affinity of each TnT1 peptide for Tm was measured using a different approach. They have used Tm-sepharose columns, applied the TnT peptides on the column and then measured the concentration of salt required to elute the TnT1 peptide from the column. Thus in their experiment the affinity of the various TnT1s for Tm was measured. In contrast, the experiment performed here measured the affinity of TnT1 for the Tm-actin complex.

As a future experiment, the binding assays of the TnT1 that were presented in sections 5.4 and 5.5 must be repeated to check the reproducibility of the results. Also the experiments can be performed using the αβ Tm heterodimer. In the heart of bigger size organisms both αα and αβ Tm dimers can be found (as mentioned in section 1.2). Although physiologically the αβ heterodimers are found in lower levels than the αα homodimers, they do exist in the heart and they are potential binding partners to TnT1.

More importantly it will be useful to check the Ca^{2+} sensitivity and the cooperative unit size of each mutant. This can be achieved by stopped flow and S1 titration experiments (according to Boussouf *et al.* 2007). For these experiments the whole TnT protein will be used to reconstruct the Tn complex together with the wild-type TnI and TnC. A similar experiment as the one described in section 4.4 can be performed where

the binding of S1 to the thin filaments decorated with the Tn complex of interest can be monitored at different Ca^{2+} concentrations. Then the k_{obs} values can be plotted against the Ca^{2+} concentration to obtain the $pCa_{50\%}$ values. Also from the stopped flow experiment the K_B equilibrium between the blocked and closed states can be estimated. From the fluorescence titrations of S1 into the thin filaments decorated with the various Tn complex of interest, the binding of S1 can be monitored as a decrease in the actin's fluorescence signal. The resulting titration curves can be fitted to the equation describing the three-state model of regulation as proposed by McKillop and Geeves. From the fit, the cooperative unit size and the K_T equilibrium from the closed to the open states can be calculated.

From these future experiments, hopefully more information on the regulatory properties of the various TnT mutants can be obtained and perhaps then it will be possible to tell why these mutants cause cardiomyopathies.

Chapter 6

Closing Discussion

The regulation of heart muscle contraction is very similar to the regulation of the skeletal muscle contraction. In both systems, the thin filament mediated regulation of muscle contraction is achieved by Ca^{2+}, the troponin complex and tropomyosin (reviewed in Gordon *et al.* 2000). The components of the troponin complex between the heart and the skeletal muscle tissues differ because different tissue-specific isoforms are expressed in each case (Parmacek and Solaro 2004). However the same tropomyosin isoforms, namely the skeletal α and β isoforms, are expressed in both skeletal and heart tissue (Lewis and Smillie 1980). These isoforms are found *in vivo* as αα homodimer or αβ heterodimer coiled-coils (Leger *et al.* 1976). A major difference between the heart and the skeletal muscle tissues is in their αβ heterodimer content. In skeletal muscle the αβ heterodimer can be up to 50 % of the total Tm, depending on the type of muscle fibre. In contrast, in heart muscle the αβ heterodimer can reach up to 20 % only in larger size organisms that have slower beating hearts (like humans) and it is absent in the hearts of smaller animals which have faster beating hearts (like rat and rabbit) (Bronson and Schachat 1982; Pieples and Wieczorek 2000). Overexpression of the β isoform in heart increases the amount of the αβ heterodimer and is associated with cardiomyopathies (Muthuchamy *et al.* 1995; Muthuchamy *et al.* 1998).

To understand how the αβ heterodimer regulates the heart muscle contraction and why it can be associated with cardiomyopathies, it is necessary to obtain a large amount of pure skeletal αβ heterodimer and run a number of characterisation

experiments. An efficient amount of the αβ heterodimer could possibly be obtained by chain dissociation of the αα and ββ homodimers and subsequent chain exchange. This method was demonstrated in 1990 and was successful in the production of the smooth αβ heterodimer using smooth isoform αα and ββ homodimers as starting materials (Lehrer *et al.* 1989; Lehrer and Qian 1990; Jancso and Graceffa 1991; Lehrer and Stafford 1991). When the smooth α and the β subunits were mixed together in a 1 : 1 ratio, more than 95 % of heterodimer was formed. From CD studies it was reported that the smooth heterodimer is formed at temperatures below its thermal unfolding transition. From viscosity measurements it was reported that the end-to-end interactions were stronger in the smooth αβ heterodimers than in the smooth αα and ββ homodimers (Lehrer and Qian 1990; Jancso and Graceffa 1991; Lehrer and Stafford 1991). Since 1990 though, the *in vitro* formation and the subsequent characterisation of the skeletal αβ heterodimer remained unsuccessful. In contrast to the smooth heterodimer, the skeletal heterodimer is not preferentially formed *in vitro*. From previous published observations and from the current study, it was found that when reduced skeletal α and β monomers were mixed to allow dimer assembly, they preferentially formed the αα and the ββ homodimers . Therefore to date there is only information on the regulation of skeletal and heart muscle contraction by the αα homodimer while the exact functional properties of the αβ heterodimer remain unknown. The major aim of the current research proposal was to develop a method for the *in vitro* formation of the skeletal αβ heterodimer that would allow the isolation of an efficient amount of pure protein and would further make possible the subsequent characterisation of its intriguing properties.

After many unsuccessful trials, which lasted for the majority of the project's duration, eventually a reproducible method for the formation of the αβ heterodimer was developed. The heterodimer was made by chain dissociation and chain exchange of the αα and the HisβHisβ homodimers. It was absolutely necessary to use the N-terminal affinity tag ββ homodimers as starting material. When combinations of untagged ββ and αα homodimers or tagged αα homodimers with untagged ββ were used, the αβ heterodimer could not be formed. This led to the conclusion that in any of the experiments where the ββ homodimer was used as a starting material, when the two homodimers were reduced into monomers and then mixed to be recombined,

the β subunit was preferentially combined into the ββ homodimer, leaving the other type of subunit no choice but to reform its original homodimer as well. This conclusion is supported by the fact that the ββ homodimer is the least thermally stable molecule amongst the various Tms, as it is reported from the CD results here (≈38.4 °C) and from other studies (Coulton *et al.* 2008). If the ββ homodimer requires the least amount of energy to break into the β monomers then the β monomers would require the least amount of energy to compose the ββ homodimer. From the CD data reported here the tagged ββ homodimers, either with a Strep or with a His tag, appear more thermally stable (≈40.5 °C) than the untagged ββ homodimer. The thermal stability of the tagged ββ homodimer was similar to that of the αβ heterodimer (≈39.5 °C, i.e. as measured for the untagged αβ heterodimer that had its His-tag removed). Thus theoretically the tagged β monomers should not have a strong thermodynamic preference to be recombined into the tagged homodimer or into the requested heterodimer and indeed in practice both of these dimers were obtained during the heterodimer formation experiments.

The method developed for the *in vitro* formation of the skeletal αβ heterodimer was also successful for the formation of more types of heterodimers that were carriers of the α^{D175N} and α^{E180G} HCM mutations. Each of these mutants was combined with either the wild-type α or β subunits. For the same reasons as explained previously, the heterodimers that contained the β subunit, were made using the tagged β homodimer (Strep-tag) as a starting material. For the heterodimers that contained α subunits only, the use of affinity tags was not necessary for the formation of the heterodimers but it was absolutely required for their subsequent purification.

There was no preference in using the His-tag or the Strep-tag homodimers as starting materials for the heterodimer formation experiment. Both had the same success in formation or purification of the heterodimers. The only difference was that the His-tagged homodimers should be kept diluted in a large volume of buffer after their purification to avoid precipitation after imidazole removal. The Strep-tagged homodimers did not have any problem with precipitation even when they were more concentrated.

About 3 mg of heterodimer was obtained from a total of 24 mg of starting Tm homodimers. The homodimers were used in a 3:1 ratio to improve the purification yield of the heterodimer, therefore the theoretical maximum yield of heterodimer would be 50 % i.e. 12 mg. Thus the actual heterodimer yield was about 25 %. In the current experiments the FXa protease was used to digest the affinity tag from the heterodimers and then it was removed using the recommended by the supplier FXa resin. When the mixture of heterodimer/FXa protease (obtained after the FXa was applied for the tag digestion) was added into the FXa resin solution, the FXa protease was precipitated with the resin after centrifugation. However the resin did not form a compact pellet and beads were still visible in a layer between the supernatant containing the heterodimer and the pellets containing the FXa protease. Thus some amount of heterodimer could not be removed from these beads completely and this decreased the final purification yield. The heterodimer yield can be improved up to 40 % if a better method for separating the heterodimer from the FXa protease were developed. This is because from the 5 mg of pure heterodimer that were purified from the recombined dimers mixture (using 24 mg of homodimers as starting materials) and were used at the start of the FXa removal step, only 3 mg could be purified at the end of the procedure. Thus it will be worth trying ion exchange or gel filtration chromatography to separate the heterodimer from the FXa protease.

Also further improvements can be made regarding the FXa digestions. In all cases where a Strep- or a His-tag was to be removed from the β subunit, the FXa digestion was not very reliable. This is because instead of cutting after the last Arg in the recognition sequence IEGR, the enzyme found to cut after the Glu. This resulted in an extra 2 residues at the N-terminal of all heterodimers containing one β subunit, as indicated by the mass spectroscopy analysis. N-terminal sequencing of the protein is required to verify the above conclusion. Thus the conditions of the FXa digestions can be altered to check if the enzyme will cut at the expected site. For example, FXa digestions can be performed using a higher concentration of the enzyme, or a longer incubation at 37 °C or even try an FXa enzyme from a different company. The tests are not necessary to be performed on the valuable heterodimer but they can be done on the tagged ββ homodimers that can be expressed and purified in large amounts.

The heterodimers carrying HCM mutation were made because in a diseased heart the mutant subunits that are expressed is possible not only to form homodimers. The mutant subunits have also the probability to be recombined with the wild-type α and β subunits that may be present in the heart making the corresponding heterodimers. However information on the HCM or DCM Tm mutations to date come only from the studies of their homodimers, because when these mutants are bacterially expressed they do naturally form and subsequently are purified as homodimers. The carrier-mutant heterodimers though could be different from the mutant homodimers. This was indeed the case in the current study. Therefore the novel method developed for the *in vitro* formation of the skeletal Tm heterodimers may well be applied for the formation and the subsequent characterisation of more Tm heterodimers. Heterodimers that carry other α Tm HCM mutations or DCM mutations may be formed and investigated.

More importantly, the new method can be applied for the formation of αβ heterodimers which carry a mutant β copy. Recently, many disease-causing mutations on the TPM2 gene encoding the skeletal β Tm have been reported. All of these mutations may cause a variety of skeletal muscle disorders and have not been found to be associated with cardiomyopathies. For example the R91G and R133W mutations on β Tm cause distal arthrogryposis (Sung *et al.* 2003; Robinson *et al.* 2007; Tajsharghi *et al.* 2007). The β E117K and β Q147P mutations cause nemaline myopathy (Donner *et al.* 2002). The β E41K mutant can cause nemaline myopathy and cap disease (Tajsharghi *et al.* 2007). Deletion of the glutamate at position 139 on the β Tm causes cap disease (Laing 2007; Lehtokari *et al.* 2007). Characterisation of these β Tm mutants has started in order to investigate how each mutant can lead to the disease. Currently the characterisation experiments are performed using the β Tm mutant homodimers. However this is physiologically of low importance, since it is known that the β Tm homodimer is unstable and does not exist in muscle cells. The β Tm that is expressed in the muscle is expected to be found as the more stable αβ heterodimer (Leger *et al.* 1976). Therefore, the method developed during this project, for the *in vitro* formation and purification of the skeletal αβ heterodimer, may well be applied for the formation of αβ heterodimers carriers of the β mutants and thus provide a significant step forward.

Having formed and purified pure Tm heterodimers makes now possible their subsequent characterisation.

From the CD studies important information was extracted. The skeletal αβ heterodimer was found to be much less thermally stable than the αα homodimer and only slightly more stable than the ββ homodimer. Therefore the skeletal and the smooth Tm heterodimers are very different in this manner. The smooth heterodimer is reported to be the most stable dimer in comparison to the αα and the ββ homodimers (Lehrer and Stafford 1991). The melting temperature of the skeletal αβ heterodimer was estimated to be ≈39.5 °C. It can be hypothesised that when the temperature is increased in a heart that has a higher amount than expected of the αβ heterodimers, these heterodimers may not remain associated. The αβ heterodimers will fall apart and the regulation should be achieved using the remaining αα homodimers. The higher the amount of the αβ heterodimer in the diseased heart, the lower will be the percentage of the remaining αα homodimers and the tougher it will be for them to anticipate in the regulation of the heart contraction. However, it must be taken into account that the αβ heterodimer, as any other Tm dimer, is expected to be more stable when bound to actin. From DSC studies of skeletal Tm homodimers it was found that binding of the various Tm dimers to actin increased their thermal stability from 1 to 4 °C, depending on the dimer tested (Kremneva *et al.* 2004).

The mutant α^{E180G} homodimer was also found to be thermally less stable than the wild-type αα homodimer. This was in agreement with previously published reports (Kremneva *et al.* 2004). The novel findings here included the characterisation of α^{E180G}-containing heterodimers. When the α^{E180G} subunit was combined with an α subunit, the heterodimer was only slightly more stable than the α^{E180G} homodimer. When however it was combined with the β subunit, the resulting $\alpha^{E180G}\beta$ heterodimer was very unstable. The melting temperature was estimated to be around 38.6 °C thus very similar to the ββ homodimer (38.4 °C). Physiologically this could mean that the $\alpha^{E180G}\beta$ heterodimer may not be observed at all *in vivo* as is the case of the ββ homodimer of similar stability. Therefore in the diseased heart expressing the α^{E180G} mutant, it is likely to find the mutant as α^{E180G} homodimer or as $\alpha^{WT}\alpha^{E180G}$ heterodimer with melting temperatures of 41.4 and 43 °C respectively. The percentage of the α^{E180G} homodimer

vs. the $\alpha^{WT}\alpha^{E180G}$ heterodimer in the heart is expected to be influenced by the expression levels of each of the α^{WT} and α^{E180G} subunits in the heart i.e. the disease gene penetrance.

The mutant α^{D175N} was as stable as the wild type α subunit. The $\alpha^{D175N}\beta$ heterodimer was similar to the αβ heterodimer with melting temperatures of 40.6 and 39.5 °C respectively. Thus the $\alpha^{D175N}\beta$ heterodimer was not very thermally stable but this was because of the presence of the β subunit and not due to the presence of the α^{D175N} mutant. Therefore the α^{D175N} - caused cardiomyopathies is unlikely to be correlated to thermal stability issues.

The melting temperatures calculated for each dimer in the present CD data are only estimates of the overall thermal unfolding process. It would be nice to repeat the thermal unfolding studies with DSC to double-check the results. With DSC experiments the melting temperatures for the N- and the C-terminal domains can be estimated separately for each Tm dimer, thus DSC interprets more accurately the unfolding process. Also with the DSC the thermal stability of the various Tm dimers bound to actin filaments can be investigated.

The affinity of each heterodimer for actin was also measured and compared to the affinities of the homodimers. In the homodimer cases, the actin binding affinity (K_d) and the cooperativity of binding (n) values that are reported here are in agreement with previously published data (Boussouf *et al.* 2007). The αα and the ββ homodimers had the highest K_d while the α^{D175N} and the α^{E180G} homodimers had decreased K_d. Thus a first comment is that the ββ homodimer has a problem with its thermal stability but appears normal in its interactions with actin at 20 °C.

The binding of Tm to actin follows a sigmoidal curve. The various parts of the curve represent the different stages of Tm polymerisation on actin's surface in agreement with the Gestalt-binding theory (described in pg 31). Figure 6.1 shows the correlation between the different parts of the actin binding curve with the Tm polymerisation stages proposed in the Gestalt binding theory (Holmes and Lehman 2008). In stage 1, individual Tm molecules bind on actin with very low affinity due to their shape

complementarity. This affinity is not measurable and is not represented on the graph. In stage 2 subsequent Tm molecules start polymerising on actin surface and this event is represented at the beginning of the graph. In stage 3 the binding of subsequent Tm molecules is essentially the Tm polymerisation process and a steeper binding rate is observed. Finally at stage 4 full actin filament decoration is achieved and the graph shows a plateau phase. Upon fitting to the Hill equation, the K_d and the n values are calculated. The actin binding affinity K_d corresponds to the Tm concentration required to reach 50 % saturation of the actin filaments. The Hill coefficient n defines the steepness of the actin binding curve. An increase in the steepness means that the promotion from stage 2 to stage 3 (and subsequently stage 4) becomes faster. This promotion depends on a) the initial concentration of Tm required to populate the thin filament and initiate Tm polymerisation at stage 2 and b) on the rate of Tm polymerisation itself i.e. efficiency of the Tm's head-to-tail interactions. Therefore K_d and n can give information on the Tm concentration required to reach 50 % actin saturation and to initiate Tm polymerisation respectively.

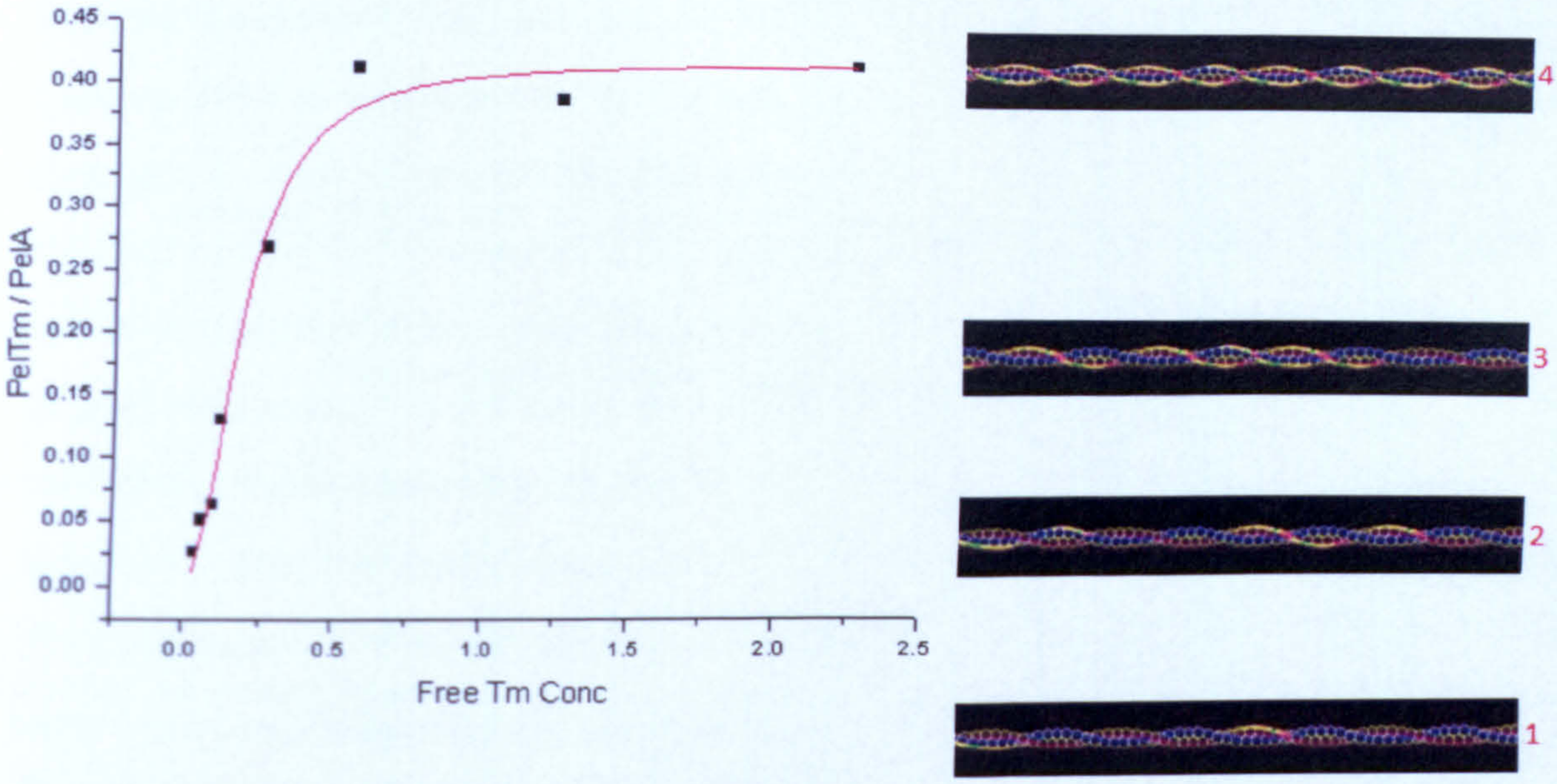

K_d – Tm's affinity for actin
correlates with concentration of Tm required for 50% actin filament saturation

n – steepness of curve,
correlates with starting concentration of Tm required to initiate Tm polymerisation on actin surface

Figure 6.1: Correlation of the Gestalt-binding theory stages with the different parts of the Tm's actin binding curve. The initial part of the curve depicts the start of the polymerisation of Tm on the actin surface. The binding of Tm occurs cooperatively thus a sigmoidal curve is obtained. The final part of the curve represents the full saturation of actin filaments by Tm. Fitting the curve to the Hill equation gives information on the K_d (the concentration of Tm required to saturate half of the actin filament) and on the steepness of slope n (depending on factors correlating with Tm polymerisation on the actin surface). (Panels 1-4 adopted by Holmes and Lehman 2008.)

Surprisingly, all of the heterodimers tested had decreased affinity for actin when compared to the homodimers. In some cases the decrease in K_d between a heterodimer and a corresponding homodimer was as high as x5 fold. It is not clear why such a big difference between the heterodimers and the homodimers is observed. The decreased heterodimer affinity for actin could be caused by two reasons:

1) Difficulties in the polymerisation of Tm heterodimers on the surface of actin.

If the Tm heterodimers have abnormal end-to-end interactions then it is likely that they will not polymerise into filaments as easy as the homodimers. That will reflect particularly on the beginning of the polymerisation process.

Some of the heterodimers had not the expected N-terminals that would mimic the native protein as was observed by the mass spectrometry results. The heterodimers carrying a β subunit had a GR dipeptide extension as mentioned before. However the heterodimers $\alpha^{WT}\alpha^{D175N}$ and $\alpha^{WT}\alpha^{E180G}$ that were digested by FXa precisely and only had an extra of +14 Da mass (probably due to N-terminal methylation) had also decreased K_d values. Thus it cannot be explained how the dipeptide extension or the methylation can cause such a big effect on the K_d values. On the other hand, it could be possible that these small extensions do not affect the molecule, and it is a real intrinsic property of the heterodimer not to form strong end-to-end interactions.

To answer these questions viscosity measurements should be taken for the various Tm heterodimers and homodimers and also from the tissue purified αβ heterodimer. If the viscosity measurements between the recombinant and the native αβ heterodimers differ markedly then indeed there must be a problem with the end-to-end interactions due to the N-terminal extensions. In that case it will be useful to optimise the FXa digestion conditions as mentioned earlier or even use a different protease for the removal of the affinity tag, like for example a TEV protease.

2) Decreased structural compatibility between the Tm heterodimer and the actin filament surface.

Another reason why the heterodimers have decreased K_d values when compared to the homodimers could be that they do not have the required structure to associate with the actin filaments and initiate the polymerisation event. According to the Gestalt binding theory the structural compatibility between actin and Tm dimers is the absolute requirement to initiate Tm polymerisation on the actin surface (Holmes and Lehman 2008). To answer this question it will be useful to perform electron microscopy experiments. From EM reconstructions of the actin filament decorated with the various Tm dimers, it can be observed if the various dimers have any distinguishable characteristic. If for example a dimer is found at a large distance from the actin filament axis, then this may well be due to decreased structural compatibility between the two. Therefore in that case the decreased K_d values obtained in this study

may be a real property of the heterodimers and not just a misinterpretation due to technical artefacts.

Another relevant issue that must be addressed is to examine the affinity of a heterodimer for actin in the presence of other Tm dimers. In any striated muscle, there is not just a single type of a Tm dimer present. It could be possible that in a mixture of dimers, those that have the best compatibility with the actin surface initiate the polymerisation of Tm. After this initiation is complete then Tm dimers that have less compatible structures can be added up next to the pre-existing Tm dimers. Thus in that case the apparent K_d of the heterodimer for actin will be higher. Cosedimentation assays were performed with the tissue extracted αβ heterodimers and αα homodimers. The preliminary results showed that the two dimers had comparable K_d values. However as mentioned in section 3.2 and figure 3.4 the native αβ heterodimer was contaminated with a small amount of the αα homodimer. Thus the presence of a small amount of αα homodimer would be enough to initiate the polymerisation event if it had a preferable structural compatibility with actin and to cause subsequently an increase in the obsevrved K_d value of the αβ heterodimer for actin. 100 % pure native αβ heterodimer could not be purified to test them in isolation. However the same experiment can be performed using recombinant heterodimer and homodimer mixtures. Thus the recombinant αβ heterodimers can be mixed with the αα homodimers and the affinity of the dimer mixture and of each dimer separately can be calculated by the actin cosedimentation assays. (This is because from the gel densitometry analysis, the α and the β subunit densities can be measured separately and from there the concentration of each of the αα and the αβ dimers can be calculated in any sample of the assay.) Therefore it can be tested whether the K_d value of the αβ heterodimer will be enhanced in the presence of the αα homodimers.

Although the various Tm heterodimers appeared to have decreased affinity for actin when compared to the homodimers, they could all regulate the binding of S1 onto the actin filaments when combined with the skeletal Tn as measured by the stopped-flow experiments.

For the characterisation of the heterodimers it would be also of great interest to perform Ca^{2+} sensitivity tests. These have been done with the stopped flow spectrofluorimeter for the mutant α^{D175N} and α^{E180G} homodimers (Boussouf *et al.* 2007) and it was reported that only the α^{E180G} homodimer showed an increase in the Ca^{2+} sensitivity of 0.1 pCa units compared to the α^{WT} homodimer. It would be interesting to observe if there is any alteration in the Ca^{2+} sensitivity of the filaments containing the α^{E180G} heterodimers or the αβ heterodimer. This is because alteration in the Ca^{2+} sensitivity of a system is strongly linked to the HCM or DCM disease phenotypes (Robinson *et al.* 2007).

Another experiment that can be performed is the equilibrium studies after S1 is titrated into thin filaments decorated with the various Tm dimers of interest. From these experiments the equilibrium constant between the closed and open states (K_T) as well as the cooperative unit size of the thin filament can be calculated. Also, as explained briefly in section 5.6, stopped flow experiments can be performed in which the thin filaments would be in excess over S1, for the measurement of the K_B equilibrium between the blocked and closed states. Thus information on the transition of each of the Tm dimers between the three states can be obtained.

Clearly there are still more questions regarding the Tm heterodimers than answers. However the method presented in this thesis for the *in vitro* formation and purification of the heterodimers is reproducible and the skeletal heterodimers are now available. Therefore we are now in a position to begin addressing these questions and expand our knowledge towards a better understanding of the cardiac muscle regulation.

Alahyan, M., M. R. Webb, S. B. Marston and M. El-Mezgueldi (2006). "The mechanism of smooth muscle caldesmon-tropomyosin inhibition of the elementary steps of the actomyosin ATPase." J Biol Chem **281**(28): 19433-48.

Ansari, S., M. Alahyan, S. B. Marston and M. El-Mezgueldi (2008). "Role of caldesmon in the Ca2+ regulation of smooth muscle thin filaments: evidence for a cooperative switching mechanism." J Biol Chem **283**(1): 47-56.

Anyanful, A., Y. Sakube, K. Takuwa and H. Kagawa (2001). "The third and fourth tropomyosin isoforms of Caenorhabditis elegans are expressed in the pharynx and intestines and are essential for development and morphology." Journal of Molecular Biology **313**(3): 525-537.

Arad, M., B. J. Maron, J. M. Gorham, W. H. Johnson, Jr., J. P. Saul, A. R. Perez-Atayde, P. Spirito, G. B. Wright, R. J. Kanter, C. E. Seidman and J. G. Seidman (2005). "Glycogen storage diseases presenting as hypertrophic cardiomyopathy." N Engl J Med **352**(4): 362-72.

Assouline, Z., R. Graham, R. C. Miller, Jr., A. J. Warren and D. G. Kilburn (1995). "Processing of fusion proteins with immobilized factor Xa." Biotechnol Prog **11**(1): 45-9.

Bailey, K. (1948). "Tropomyosin; a new asymmetric protein component of the muscle fibril." Biochem J **43**(2): 271-9.

Balasubramanian, M. K., D. M. Helfman and S. M. Hemmingsen (1992). "A new tropomyosin essential for cytokinesis in the fission yeast S. pombe." Nature **360**(6399): 84-87.

Basi, G. S., M. Boardman and R. V. Storti (1984). "Alternative splicing of a Drosophila tropomyosin gene generates muscle tropomyosin isoforms with different carboxy-terminal ends." Mol Cell Biol **4**(12): 2828-36.

Bauer, C. B., H. M. Holden, J. B. Thoden, R. Smith and I. Rayment (2000). "X-ray structures of the apo and MgATP-bound states of Dictyostelium discoideum myosin motor domain." J Biol Chem **275**(49): 38494-9.

Bernstein, B. W. and J. R. Bamburg (1982). "Tropomyosin binding to F-actin protects the F-actin from disassembly by brain actin-depolymerizing factor (ADF)." Cell Motil **2**(1): 1-8.

Bers, D. M. (2002). "Cardiac excitation-contraction coupling." Nature **415**(6868): 198-205.

Bing, W., A. Knott, C. Redwood, G. Esposito, I. Purcell, H. Watkins and S. Marston (2000). "Effect of hypertrophic cardiomyopathy mutations in human cardiac muscle alpha -tropomyosin (Asp175Asn and Glu180Gly) on the regulatory properties of human cardiac troponin determined by in vitro motility assay." J Mol Cell Cardiol **32**(8): 1489-98.

Bing, W., C. S. Redwood, I. F. Purcell, G. Esposito, H. Watkins and S. B. Marston (1997). "Effects of two hypertrophic cardiomyopathy mutations in alpha-tropomyosin, Asp175Asn and Glu180Gly, on Ca2+ regulation of thin filament motility." Biochem Biophys Res Commun **236**(3): 760-4.

Blanchoin, L., T. D. Pollard and S. E. Hitchcock-DeGregori (2001). "Inhibition of the Arp2/3 complex-nucleated actin polymerization and branch formation by tropomyosin." Curr Biol **11**(16): 1300-4.

Bonne, G., L. Carrier, P. Richard, B. Hainque and K. Schwartz (1998). "Familial hypertrophic cardiomyopathy: from mutations to functional defects." Circ Res **83**(6): 580-93.

Bottinelli, R., D. A. Coviello, C. S. Redwood, M. A. Pellegrino, B. J. Maron, P. Spirito, H. Watkins and C. Reggiani (1998). "A mutant tropomyosin that causes hypertrophic cardiomyopathy is expressed in vivo and associated with an increased calcium sensitivity." Circ Res **82**(1): 106-15.

Boussouf, S. E., B. Agianian, B. Bullard and M. A. Geeves (2007). "The regulation of myosin binding to actin filaments by Lethocerus troponin." J Mol Biol **373**(3): 587-98.

Boussouf, S. E. and M. A. Geeves (2007). "Tropomyosin and troponin cooperativity on the thin filament." Adv Exp Med Biol **592**: 99-109.

Boussouf, S. E., R. Maytum, K. Jaquet and M. A. Geeves (2007). "Role of tropomyosin isoforms in the calcium sensitivity of striated muscle thin filaments." J Muscle Res Cell Motil **28**(1): 49-58.

Bradford, M. M. (1976). "A rapid and sensitive method for the quantitation of microgram quantities of protein utilizing the principle of protein-dye binding." Anal Biochem **72**: 248-54.

Brisson, J. R., K. Golosinska, L. B. Smillie and B. D. Sykes (1986). "Interaction of tropomyosin and troponin T: a proton nuclear magnetic resonance study." Biochemistry **25**(16): 4548-55.

Bronson, D. D. and F. H. Schachat (1982). "Heterogeneity of contractile proteins. Differences in tropomyosin in fast, mixed, and slow skeletal muscles of the rabbit." J Biol Chem **257**(7): 3937-44.

Brown, J. H., K. H. Kim, G. Jun, N. J. Greenfield, R. Dominguez, N. Volkmann, S. E. Hitchcock-DeGregori and C. Cohen (2001). "Deciphering the design of the tropomyosin molecule." Proc Natl Acad Sci U S A **98**(15): 8496-501.

Brown, J. H., Z. Zhou, L. Reshetnikova, H. Robinson, R. D. Yammani, L. S. Tobacman and C. Cohen (2005). "Structure of the mid-region of tropomyosin: bending and binding sites for actin." Proc Natl Acad Sci U S A **102**(52): 18878-83.

Bryce, N. S., G. Schevzov, V. Ferguson, J. M. Percival, J. J. Lin, F. Matsumura, J. R. Bamburg, P. L. Jeffrey, E. C. Hardeman, P. Gunning and R. P. Weinberger (2003). "Specification of actin filament function and molecular composition by tropomyosin isoforms." Mol Biol Cell **14**(3): 1002-16.

Chandra, M., V. L. Rundell, J. C. Tardiff, L. A. Leinwand, P. P. De Tombe and R. J. Solaro (2001). "Ca(2+) activation of myofilaments from transgenic mouse hearts expressing R92Q mutant cardiac troponin T." Am J Physiol Heart Circ Physiol **280**(2): H705-13.

Chang, A. N. and J. D. Potter (2005). "Sarcomeric protein mutations in dilated cardiomyopathy." Heart Fail Rev **10**(3): 225-35.

Clark, K. A., A. S. McElhinny, M. C. Beckerle and C. C. Gregorio (2002). "Striated muscle cytoarchitecture: an intricate web of form and function." Annu Rev Cell Dev Biol **18**: 637-706.

Clos, J. and S. Brandau (1994). "pJC20 and pJC40--two high-copy-number vectors for T7 RNA polymerase-dependent expression of recombinant genes in Escherichia coli." Protein Expr Purif **5**(2): 133-7.

Cooper, J. A. (2002). "Actin Dynamics: Tropomyosin Provides Stability." Current Biology **12**(15): R523-R525.

Coulton, A., S. S. Lehrer and M. A. Geeves (2006). "Functional homodimers and heterodimers of recombinant smooth muscle tropomyosin." Biochemistry **45**(42): 12853-8.

Coulton, A. T., K. Koka, S. S. Lehrer and M. A. Geeves (2008). "Role of the head-to-tail overlap region in smooth and skeletal muscle beta-tropomyosin." Biochemistry **47**(1): 388-97.

Craig, R. and W. Lehman (2001). "Crossbridge and tropomyosin positions observed in native, interacting thick and thin filaments." J Mol Biol **311**(5): 1027-36.

Criddle, A. H., M. A. Geeves and T. Jeffries (1985). "The use of actin labelled with N-(1-pyrenyl)iodoacetamide to study the interaction of actin with myosin subfragments and troponin/tropomyosin." Biochem J **232**(2): 343-9.

Cummins, P. and S. V. Perry (1973). "The subunits and biological activity of polymorphic forms of tropomyosin." Biochem J **133**(4): 765-77.

Cummins, P. and S. V. Perry (1974). "Chemical and immunochemical characteristics of tropomyosins from striated and smooth muscle." Biochem J **141**(1): 43-9.

Donner, K., M. Ollikainen, M. Ridanpaa, H. J. Christen, H. H. Goebel, M. de Visser, K. Pelin and C. Wallgren-Pettersson (2002). "Mutations in the beta-tropomyosin (TPM2) gene--a rare cause of nemaline myopathy." Neuromuscul Disord **12**(2): 151-8.

Drees, B., C. Brown, B. G. Barrell and A. Bretscher (1995). "Tropomyosin is essential in yeast, yet the TPM1 and TPM2 products perform distinct functions." J Cell Biol **128**(3): 383-92.

Dye, B. T., M. Buvoli, S. A. Mayer, C. H. Lin and J. G. Patton (1998). "Enhancer elements activate the weak 3' splice site of alpha-tropomyosin exon 2." RNA **4**(12): 1523-36.

Ebashi, S. (1963). "THIRD COMPONENT PARTICIPATING IN THE SUPERPRECIPITATION OF 'NATURAL ACTOMYOSIN'." Nature **200**: 1010.

Ebashi, S. and A. Kodama (1965). "A new protein factor promoting aggregation of tropomyosin." J Biochem **58**(1): 107-8.

Ebashi, S., T. Wakabayashi and F. Ebashi (1971). "Troponin and its components." J Biochem **69**(2): 441-5.

Eisenberg, E. and W. W. Kielley (1974). "Troponin-tropomyosin complex. Column chromatographic separation and activity of the three, active troponin components with and without tropomyosin present." J Biol Chem **249**(15): 4742-8.

Evans, C. C., J. R. Pena, R. M. Phillips, M. Muthuchamy, D. F. Wieczorek, R. J. Solaro and B. M. Wolska (2000). "Altered hemodynamics in transgenic mice harboring mutant tropomyosin linked to hypertrophic cardiomyopathy." Am J Physiol Heart Circ Physiol **279**(5): H2414-23.

Eyre, H., P. A. Akkari, S. D. Wilton, D. C. Callen, E. Baker and N. G. Laing (1995). "Assignment of the human skeletal muscle alpha-tropomyosin gene (TPM1) to band 15q22 by fluorescence in situ hybridization." Cytogenet Cell Genet **69**(1-2): 15-7.

Fatkin, D. and R. M. Graham (2002). "Molecular mechanisms of inherited cardiomyopathies." Physiol Rev **82**(4): 945-80.

Fisher, C. L. and G. K. Pei (1997). "Modification of a PCR-based site-directed mutagenesis method." Biotechniques **23**(4): 570-1, 574.

Flashman, E., L. Korkie, H. Watkins, C. Redwood and J. C. Moolman-Smook (2008). "Support for a trimeric collar of myosin binding protein C in cardiac and fast skeletal muscle, but not in slow skeletal muscle." FEBS Letters **582**(3): 434-438.

Foth, B. J., M. C. Goedecke and D. Soldati (2006). "New insights into myosin evolution and classification." Proc Natl Acad Sci U S A **103**(10): 3681-6.

Fukuda, N., H. L. Granzier, S. Ishiwata and S. Kurihara (2008). "Physiological functions of the giant elastic protein titin in mammalian striated muscle." J Physiol Sci **58**(3): 151-9.

Galinska-Rakoczy, A., P. Engel, C. Xu, H. Jung, R. Craig, L. S. Tobacman and W. Lehman (2008). "Structural basis for the regulation of muscle contraction by troponin and tropomyosin." J Mol Biol **379**(5): 929-35.

Geeves, M. A. and K. C. Holmes (1999). "Structural mechanism of muscle contraction." Annu Rev Biochem **68**: 687-728.

Geeves, M. A. and K. C. Holmes (2005). "The molecular mechanism of muscle contraction." Adv Protein Chem **71**: 161-93.

Geeves, M. A. and S. S. Lehrer (1994). "Dynamics of the muscle thin filament regulatory switch: the size of the cooperative unit." Biophys J **67**(1): 273-82.

Geeves, M. A. and S. S. Lehrer (2002). "Modeling Thin Filament Cooperativity." Biophysical Journal **82**(3): 1677-1679.

Geisterfer-Lowrance, A. A. T., S. Kass, G. Tanigawa, H.-P. Vosberg, W. McKenna, C. E. Seidman and J. G. Seidman (1990). "A molecular basis for familial hypertrophic cardiomyopathy: A [beta] cardiac myosin heavy chain gene missense mutation." Cell **62**(5): 999-1006.

Golitsina, N., Y. An, N. J. Greenfield, L. Thierfelder, K. Iizuka, J. G. Seidman, C. E. Seidman, S. S. Lehrer and S. E. Hitchcock-DeGregori (1997). "Effects of two familial hypertrophic cardiomyopathy-causing mutations on alpha-tropomyosin structure and function." Biochemistry **36**(15): 4637-42.

Golitsina, N., Y. An, N. J. Greenfield, L. Thierfelder, K. Iizuka, J. G. Seidman, C. E. Seidman, S. S. Lehrer and S. E. Hitchcock-DeGregori (1999). "Effects of two familial hypertrophic cardiomyopathy-causing mutations on alpha-tropomyosin structure and function." Biochemistry **38**(12): 3850.

Gomes, A. V., J. A. Barnes, K. Harada and J. D. Potter (2004). "Role of troponin T in disease." Mol Cell Biochem **263**(1-2): 115-29.

Gordon, A. M., E. Homsher and M. Regnier (2000). "Regulation of contraction in striated muscle." Physiol Rev **80**(2): 853-924.

Graceffa, P. (1989). "In-register homodimers of smooth muscle tropomyosin." Biochemistry **28**(3): 1282-7.

Graceffa, P. and R. Dominguez (2003). "Crystal structure of monomeric actin in the ATP state. Structural basis of nucleotide-dependent actin dynamics." J Biol Chem **278**(36): 34172-80.

Greenfield, N. J., Y. J. Huang, G. V. Swapna, A. Bhattacharya, B. Rapp, A. Singh, G. T. Montelione and S. E. Hitchcock-DeGregori (2006). "Solution NMR structure of the junction between *tropomyosin* molecules: implications for actin binding and regulation." J Mol Biol **364**(1): 80-96.

Gregorio, C. C., A. Weber, M. Bondad, C. R. Pennise and V. M. Fowler (1995). "Requirement of pointed-end *capping by tropomodulin to maintain* actin filament length in embryonic chick cardiac myocytes." Nature **377**(6544): 83-6.

Gromak, N., A. Rideau, J. Southby, A. D. Scadden, C. Gooding, S. Huttelmaier, R. H. Singer and C. W. Smith (2003). "The PTB interacting protein raver1 regulates alpha-tropomyosin alternative splicing." EMBO J **22**(23): 6356-64.

Gulick, A. M., C. B. Bauer, J. B. Thoden, E. Pate, R. G. Yount and I. Rayment (2000). "X-ray structures of the Dictyostelium discoideum myosin motor domain with six non-nucleotide analogs." J Biol Chem **275**(1): 398-408.

Gunning, P., G. O'Neill and E. Hardeman (2008). "Tropomyosin-based regulation of the actin cytoskeleton in time and space." Physiol Rev **88**(1): 1-35.

Gusev, N. B. (2001). "Some properties of caldesmon and calponin and the participation of these proteins in regulation of smooth muscle contraction and cytoskeleton formation." Biochemistry (Mosc) **66**(10): 1112-21.

Hancock, C. R., J. J. Brault and R. L. Terjung (2006). "Protecting the cellular energy state *during contractions: role of AMP deaminase*." J Physiol Pharmacol **57 Suppl 10**: 17-29.

Hanke, P. D., H. M. Lepinske and R. V. Storti (1987). "Characterization of a Drosophila cDNA clone that encodes a 252-amino acid non-muscle tropomyosin isoform." J Biol Chem **262**(36): 17370-3.

Harada, K. and J. D. Potter (2004). "Familial hypertrophic cardiomyopathy mutations from different functional regions of troponin T result in different effects on the pH and Ca2+ sensitivity of cardiac muscle contraction." J Biol Chem **279**(15): 14488-95.

Herman, I. M. (1993). "Actin isoforms." Curr Opin Cell Biol **5**(1): 48-55.

Hernandez, O. M., D. Szczesna-Cordary, B. C. Knollmann, T. Miller, M. Bell, J. Zhao, S. G. Sirenko, Z. Diaz, G. Guzman, Y. Xu, Y. Wang, W. G. Kerrick and J. D. Potter (2005). "F110I and R278C troponin T mutations that cause familial hypertrophic cardiomyopathy affect muscle contraction in transgenic mice and reconstituted human cardiac fibers." J Biol Chem **280**(44): 37183-94.

Herzberg, O. and M. N. James (1985). "Structure of the calcium regulatory muscle protein troponin-C at 2.8 A resolution." Nature **313**(6004): 653-9.

Hill, T. L., E. Eisenberg and L. Greene (1980). "Theoretical model for the cooperative equilibrium binding of myosin subfragment 1 to the actin-troponin-tropomyosin complex." Proc Natl Acad Sci U S A **77**(6): 3186-90.

Hitchcock-DeGregori, S. E. (2008). "Tropomyosin: function follows structure." Adv Exp Med Biol **644**: 60-72.

Hitchcock-DeGregori, S. E. and R. W. Heald (1987). "Altered actin and troponin binding of amino-terminal variants of chicken striated muscle alpha-tropomyosin expressed in Escherichia coli." J Biol Chem **262**(20): 9730-5.

Hitchcock-DeGregori, S. E., P. Sampath and T. D. Pollard (1988). "Tropomyosin inhibits the rate of actin polymerization by stabilizing actin filaments." Biochemistry **27**(26): 9182-5.

Hitchcock-DeGregori, S. E., Y. Song and N. J. Greenfield (2002). "Functions of tropomyosin's periodic repeats." Biochemistry **41**(50): 15036-44.

Holmes, K. C. (1998). "A molecular model for muscle contraction." Acta Crystallogr A **54**(Pt 6 Pt 1): 789-97.

Holmes, K. C., I. Angert, F. J. Kull, W. Jahn and R. R. Schroder (2003). "Electron cryo-microscopy shows how strong binding of myosin to actin releases nucleotide." Nature **425**(6956): 423-7.

Holmes, K. C. and M. A. Geeves (2000). "The structural basis of muscle contraction." Philos Trans R Soc Lond B Biol Sci **355**(1396): 419-31.

Holmes, K. C. and W. Lehman (2008). "Gestalt-binding of tropomyosin to actin filaments." J Muscle Res Cell Motil **29**(6-8): 213-9.

Holmes, K. C., D. Popp, W. Gebhard and W. Kabsch (1990). "Atomic model of the actin filament." Nature **347**(6288): 44-9.

Holmes, K. C., R. R. Schroder, H. L. Sweeney and A. Houdusse (2004). "The structure of the rigor complex and its implications for the power stroke." Philos Trans R Soc Lond B Biol Sci **359**(1452): 1819-28.

Hunt, C. C., H. J. Eyre, P. A. Akkari, C. Meredith, S. M. Dorosz, S. D. Wilton, D. F. Callen, N. G. Laing and E. Baker (1995). "Assignment of the human beta tropomyosin gene (TPM2) to band 9p13 by fluorescence in situ hybridisation." Cytogenet Cell Genet **71**(1): 94-5.

Huxley, A. F. and R. Niedergerke (1954). "Structural changes in muscle during contraction; interference microscopy of living muscle fibres." Nature **173**(4412): 971-3.

Huxley, H. and J. Hanson (1954). "Changes in the cross-striations of muscle during contraction and stretch and their structural interpretation." Nature **173**(4412): 973-6.

Ishikawa, R., S. Yamashiro and F. Matsumura (1989). "Differential modulation of actin-severing activity of gelsolin by multiple isoforms of cultured rat cell tropomyosin. Potentiation of protective ability of tropomyosins by 83-kDa nonmuscle caldesmon." J Biol Chem **264**(13): 7490-7.

Jackson, P., G. W. Amphlett and S. V. Perry (1975). "The primary structure of troponin T and the interaction with tropomyosin." Biochem J **151**(1): 85-97.

Jancso, A. and P. Graceffa (1991). "Smooth muscle tropomyosin coiled-coil dimers. Subunit composition, assembly, and end-to-end interaction." J Biol Chem **266**(9): 5891-7.

Kabsch, W., H. G. Mannherz, D. Suck, E. F. Pai and K. C. Holmes (1990). "Atomic structure of the actin:DNase I complex." Nature **347**(6288): 37-44.

Kagawa, H., K. Sugimoto, H. Matsumoto, T. Inoue, H. Imadzu, K. Takuwa and Y. Sakube (1995). "Genome Structure, Mapping and Expression of the Tropomyosin Genetmy-1ofCaenorhabditis elegans." Journal of Molecular Biology **251**(5): 603-613.

Kee, A. J., G. Schevzov, V. Nair-Shalliker, C. S. Robinson, B. Vrhovski, M. Ghoddusi, M. R. Qiu, J. J. Lin, R. Weinberger, P. W. Gunning and E. C. Hardeman (2004). "Sorting of a nonmuscle tropomyosin to a novel cytoskeletal compartment in skeletal muscle results in muscular dystrophy." J Cell Biol **166**(5): 685-96.

Klenchin, V. A., S. Y. Khaitlina and I. Rayment (2006). "Crystal Structure of Polymerization-Competent Actin." Journal of Molecular Biology **362**(1): 140-150.

Koppe, R. I., P. L. Hallauer, G. Karpati and K. E. Hastings (1989). "cDNA clone and expression analysis of rodent fast and slow skeletal muscle troponin I mRNAs." J Biol Chem **264**(24): 14327-33.

Kostyukova, A. S. (2008). "Capping complex formation at the slow-growing end of the actin filament." Biochemistry (Mosc) **73**(13): 1467-72.

Kranias, E. G. and R. J. Solaro (1982). "Phosphorylation of troponin I and phospholamban during catecholamine stimulation of rabbit heart." Nature **298**(5870): 182-184.

Kremneva, E., S. Boussouf, O. Nikolaeva, R. Maytum, M. A. Geeves and D. I. Levitsky (2004). "Effects of two familial hypertrophic cardiomyopathy mutations in alpha-tropomyosin, Asp175Asn and Glu180Gly, on the thermal unfolding of actin-bound tropomyosin." Biophys J **87**(6): 3922-33.

Krüger, M., G. Pfitzer and R. Stehle (2003). "Expression and purification of human cardiac troponin subunits and their functional incorporation into isolated cardiac mouse myofibrils." Journal of Chromatography B **786**(1-2): 287-296.

Laemmli, U. K. (1970). "Cleavage of structural proteins during the assembly of the head of bacteriophage T4." Nature **227**(5259): 680-5.

Laing, N. G. (2007). "Congenital myopathies." Curr Opin Neurol **20**(5): 583-9.

Lamb, G. D. (2000). "Excitation-contraction coupling in skeletal muscle: comparisons with cardiac muscle." Clin Exp Pharmacol Physiol **27**(3): 216-24.

Landis, C., N. Back, E. Homsher and L. S. Tobacman (1999). "Effects of tropomyosin internal deletions on thin filament function." J Biol Chem **274**(44): 31279-85.

Leger, J., P. Bouveret, K. Schwartz and B. Swynghedauw (1976). "A comparative study of skeletal and cardiac tropomyosins: subunits, thiol group content and biological activities." Pflugers Arch **362**(3): 271-7.

Lehman, W. and R. Craig (2008). "Tropomyosin and the steric mechanism of muscle regulation." Adv Exp Med Biol **644**: 95-109.

Lehman, W., V. Hatch, V. Korman, M. Rosol, L. Thomas, R. Maytum, M. A. Geeves, J. E. Van Eyk, L. S. Tobacman and R. Craig (2000). "Tropomyosin and actin isoforms modulate the localization of tropomyosin strands on actin filaments." J Mol Biol **302**(3): 593-606.

Lehrer, S. S. and D. Joseph (1987). "Differences in local conformation around cysteine residues in alpha alpha, alpha beta, and beta beta rabbit skeletal tropomyosin." Arch Biochem Biophys **256**(1): 1-9.

Lehrer, S. S. and Y. Qian (1990). "Unfolding/refolding studies of smooth muscle tropomyosin. Evidence for a chain exchange mechanism in the preferential assembly of the native heterodimer." J Biol Chem **265**(2): 1134-8.

Lehrer, S. S., Y. D. Qian and S. Hvidt (1989). "Assembly of the native heterodimer of Rana esculenta tropomyosin by chain exchange." Science **246**(4932): 926-8.

Lehrer, S. S. and W. F. Stafford, 3rd (1991). "Preferential assembly of the tropomyosin heterodimer: equilibrium studies." Biochemistry **30**(23): 5682-8.

Lehtokari, V. L., C. Ceuterick-de Groote, P. de Jonghe, M. Marttila, N. G. Laing, K. Pelin and C. Wallgren-Pettersson (2007). "Cap disease caused by heterozygous deletion of the beta-tropomyosin gene TPM2." Neuromuscul Disord **17**(6): 433-42.

Lewis, W. G. and L. B. Smillie (1980). "The amino acid sequence of rabbit cardiac tropomyosin." J Biol Chem **255**(14): 6854-9.

Li, M. X., S. M. Gagne, S. Tsuda, C. M. Kay, L. B. Smillie and B. D. Sykes (1995). "Calcium binding to the regulatory N-domain of skeletal muscle troponin C occurs in a stepwise manner." Biochemistry **34**(26): 8330-40.

Li, Y., S. Mui, J. H. Brown, J. Strand, L. Reshetnikova, L. S. Tobacman and C. Cohen (2002). "The crystal structure of the C-terminal fragment of striated-muscle alpha-tropomyosin reveals a key troponin T recognition site." Proc Natl Acad Sci U S A **99**(11): 7378-83.

Lin, J. J. C., K. S. Warren, D. D. Wamboldt, T. Wang, J. L. C. Lin and W. J. Kwang (1997). Tropomyosin Isoforms in Nonmuscle Cells. International Review of Cytology, Academic Press. **Volume 170: 1-39.**

Liu, H. and A. Bretscher (1992). "Characterization of TPM1 disrupted yeast cells indicates an involvement of tropomyosin in directed vesicular transport." J Cell Biol **118**(2): 285-99.

Liu, H. P. and A. Bretscher (1989). "Disruption of the single tropomyosin gene in yeast results in the disappearance of actin cables from the cytoskeleton." Cell **57**(2): 233-42.

Lorenz, M., K. J. V. Poole, D. Popp, G. Rosenbaum and K. C. Holmes (1995). "An Atomic Model of the Unregulated Thin Filament Obtained by X-ray Fiber Diffraction on Oriented Actin-Tropomyosin Gels." Journal of Molecular Biology **246**(1): 108-119.

Lymn, R. W. and E. W. Taylor (1971). "Mechanism of adenosine triphosphate hydrolysis by actomyosin." Biochemistry **10**(25): 4617-24.

Maass, A. H. and L. A. Leinwand (2003). "Mechanisms of the pathogenesis of troponin T-based familial hypertrophic cardiomyopathy." Trends Cardiovasc Med **13**(6): 232-7.

Margossian, S. S. and S. Lowey (1982). "Preparation of myosin and its subfragments from rabbit skeletal muscle." Methods Enzymol **85 Pt B**: 55-71.

Maron, B. J., J. M. Gardin, J. M. Flack, S. S. Gidding, T. T. Kurosaki and D. E. Bild (1995). "Prevalence of hypertrophic cardiomyopathy in a general population of young adults. Echocardiographic analysis of 4111 subjects in the CARDIA Study. Coronary Artery Risk Development in (Young) Adults." Circulation **92**(4): 785-9.

Marston, S., D. Burton, O. Copeland, I. Fraser, Y. Gao, J. Hodgkinson, P. Huber, B. Levine, M. el-Mezgueldi and G. Notarianni (1998). "Structural interactions between actin, tropomyosin, caldesmon and calcium binding protein and the regulation of smooth muscle thin filaments." Acta Physiol Scand **164**(4): 401-14.

Marston, S. B. and C. S. Redwood (1993). "The essential role of tropomyosin in cooperative regulation of smooth muscle thin filament activity by caldesmon." J Biol Chem **268**(17): 12317-20.

Maytum, R., M. A. Geeves and S. S. Lehrer (2002). "A modulatory role for the troponin T tail domain in thin filament regulation." J Biol Chem **277**(33): 29774-80.

Maytum, R., M. Konrad, S. S. Lehrer and M. A. Geeves (2001). "Regulatory properties of tropomyosin effects of length, isoform, and N-terminal sequence." Biochemistry **40**(24): 7334-41.

Maytum, R., S. S. Lehrer and M. A. Geeves (1999). "Cooperativity and switching within the three-state model of muscle regulation." Biochemistry **38**(3): 1102-10.

McElhinny, A. S., S. T. Kazmierski, S. Labeit and C. C. Gregorio (2003). "Nebulin: The Nebulous, Multifunctional Giant of Striated Muscle." Trends in Cardiovascular Medicine **13**(5): 195-201.

McKillop, D. F. and M. A. Geeves (1993). "Regulation of the interaction between actin and myosin subfragment 1: evidence for three states of the thin filament." Biophys J **65**(2): 693-701.

McLachlan, A. D. and M. Stewart (1976). "The 14-fold periodicity in alpha-tropomyosin and the interaction with actin." J Mol Biol **103**(2): 271-98.

McLachlan, A. D., M. Stewart and L. B. Smillie (1975). "Sequence repeats in [alpha]-tropomyosin." Journal of Molecular Biology **98**(2): 281-291.

McLaughlin, P. J., J. T. Gooch, H. G. Mannherz and A. G. Weeds (1993). "Structure of gelsolin segment 1-actin complex and the mechanism of filament severing." Nature **364**(6439): 685-692.

Minakata, S., K. Maeda, N. Oda, K. Wakabayashi, Y. Nitanai and Y. Maeda (2008). "Two-crystal structures of tropomyosin C-terminal fragment 176-273: exposure of the hydrophobic core to the solvent destabilizes the tropomyosin molecule." Biophys J **95**(2): 710-9.

Molkentin, J. D., J. R. Lu, C. L. Antos, B. Markham, J. Richardson, J. Robbins, S. R. Grant and E. N. Olson (1998). "A calcineurin-dependent transcriptional pathway for cardiac hypertrophy." Cell **93**(2): 215-28.

Monteiro, P. B., R. C. Lataro, J. A. Ferro and C. Reinach Fde (1994). "Functional alpha-tropomyosin produced in Escherichia coli. A dipeptide extension can substitute the amino-terminal acetyl group." J Biol Chem **269**(14): 10461-6.

Morimoto, S. (2008). "Sarcomeric proteins and inherited cardiomyopathies." Cardiovasc Res **77**(4): 659-66.

Mornet, D., P. Pantel, E. Audemard and R. Kassab (1979). "The limited tryptic cleavage of chymotryptic S-1 : An approach to the characterization of the actin site in myosin heads." Biochemical and Biophysical Research Communications **89**(3): 925-932.

Morris, E. P. and S. S. Lehrer (1984). "Troponin-tropomyosin interactions. Fluorescence studies of the binding of troponin, troponin T, and chymotryptic troponin T fragments to specifically labeled tropomyosin." Biochemistry **23**(10): 2214-20.

Mudd, J. O. and D. A. Kass (2008). "Tackling heart failure in the twenty-first century." Nature **451**(7181): 919-28.

Mullen, M. P., C. W. Smith, J. G. Patton and B. Nadal-Ginard (1991). "Alpha-tropomyosin mutually exclusive exon selection: competition between branchpoint/polypyrimidine tracts determines default exon choice." Genes Dev **5**(4): 642-55.

Muthuchamy, M., G. P. Boivin, I. L. Grupp and D. F. Wieczorek (1998). "Beta-tropomyosin overexpression induces severe cardiac abnormalities." J Mol Cell Cardiol **30**(8): 1545-57.

Muthuchamy, M., I. L. Grupp, G. Grupp, B. A. O'Toole, A. B. Kier, G. P. Boivin, J. Neumann and D. F. Wieczorek (1995). "Molecular and physiological effects of overexpressing striated muscle beta-tropomyosin in the adult murine heart." J Biol Chem **270**(51): 30593-603.

Nakajima-Taniguchi, C., H. Matsui, Y. Fujio, S. Nagata, T. Kishimoto and K. Yamauchi-Takihara (1997). "Novel Missense Mutation in Cardiac Troponin T Gene Found in Japanese Patient with Hypertrophic Cardiomyopathy." Journal of Molecular and Cellular Cardiology **29**(2): 839-843.

Nakajima-Taniguchi, C., H. Matsui, S. Nagata, T. Kishimoto and K. Yamauchi-Takihara (1995). "Novel missense mutation in alpha-tropomyosin gene found in Japanese patients with hypertrophic cardiomyopathy." J Mol Cell Cardiol **27**(9): 2053-8.

Nakaura, H., F. Yanaga, I. Ohtsuki and S. Morimoto (1999). "Effects of missense mutations Phe110Ile and Glu244Asp in human cardiac troponin T on force generation in skinned cardiac muscle fibers." J Biochem **126**(3): 457-60.

Nowak, K. J., G. Ravenscroft, C. Jackaman, A. Filipovska, S. M. Davies, E. M. Lim, S. E. Squire, A. C. Potter, E. Baker, S. Clement, C. A. Sewry, V. Fabian, K. Crawford, J. L. Lessard, L. M. Griffiths, J. M. Papadimitriou, Y. Shen, G. Morahan, A. J. Bakker, K. E. Davies and N. G. Laing (2009). "Rescue of skeletal muscle alpha-actin-null mice by cardiac (fetal) alpha-actin." J Cell Biol **185**(5): 903-15.

Nyitrai, M., R. Rossi, N. Adamek, M. A. Pellegrino, R. Bottinelli and M. A. Geeves (2006). "What Limits the Velocity of Fast-skeletal Muscle Contraction in Mammals?" Journal of Molecular Biology **355**(3): 432-442.

Oda, T., M. Iwasa, T. Aihara, Y. Maeda and A. Narita (2009). "The nature of the globular- to fibrous-actin transition." Nature **457**(7228): 441-5.

Odronitz, F. and M. Kollmar (2007). "Drawing the tree of eukaryotic life based on the analysis of 2,269 manually annotated myosins from 328 species." Genome Biol **8**(9): R196.

Offer, G. (1990). "Skip residues correlate with bends in the myosin tail." J Mol Biol **216**(2): 213-8.

Ohtsuki, I. and S. Morimoto (2008). "Troponin: regulatory function and disorders." Biochem Biophys Res Commun **369**(1): 62-73.

Olson, E. N. and R. S. Williams (2000). "Calcineurin signaling and muscle remodeling." Cell **101**(7): 689-92.

Otterbein, L. R., P. Graceffa and R. Dominguez (2001). "The crystal structure of uncomplexed actin in the ADP state." Science **293**(5530): 708-11.

Palm, T., S. Graboski, S. E. Hitchcock-DeGregori and N. J. Greenfield (2001). "Disease-Causing Mutations in Cardiac Troponin T: Identification of a Critical Tropomyosin-Binding Region." Biophysical Journal **81**(5): 2827-2837.

Parmacek, M. S. and R. J. Solaro (2004). "Biology of the troponin complex in cardiac myocytes." Prog Cardiovasc Dis **47**(3): 159-76.

Passier, R., H. Zeng, N. Frey, F. J. Naya, R. L. Nicol, T. A. McKinsey, P. Overbeek, J. A. Richardson, S. R. Grant and E. N. Olson (2000). "CaM kinase signaling induces cardiac hypertrophy and activates the MEF2 transcription factor in vivo." J Clin Invest **105**(10): 1395-406.

Pato, M. D., A. S. Mak and L. B. Smillie (1981). "Fragments of rabbit striated muscle alpha-tropomyosin. II. Binding to troponin-T." J Biol Chem **256**(2): 602-7.

Pearlstone, J. R. and L. B. Smillie (1977). "The binding site of skeletal alpha-tropomyosin on troponin-T." Can J Biochem **55**(10): 1032-8.

Pearlstone, J. R. and L. B. Smillie (1981). "Identification of a second binding region on rabbit skeletal troponin-T for alpha-tropomyosin." FEBS Lett **128**(1): 119-22.

Pearson, D. S., D. R. Swartz and M. A. Geeves (2008). "Fast pressure jumps can perturb calcium and magnesium binding to troponin C F29W." Biochemistry **47**(46): 12146-58.

Pelham, R. J., Jr., J. J. Lin and Y. L. Wang (1996). "A high molecular mass non-muscle tropomyosin isoform stimulates retrograde organelle transport." J Cell Sci **109 (Pt 5)**: 981-9.

Perry, S. V. (1998). "Troponin T: genetics, properties and function." J Muscle Res Cell Motil **19**(6): 575-602.

Perry, S. V. (2001). "Vertebrate tropomyosin: distribution, properties and function." J Muscle Res Cell Motil **22**(1): 5-49.

Phillips, G. N., Jr. (1986). "Construction of an atomic model for tropomyosin and implications for interactions with actin." J Mol Biol **192**(1): 128-31.

Pieples, K. and D. F. Wieczorek (2000). "Tropomyosin 3 increases striated muscle isoform diversity." Biochemistry **39**(28): 8291-7.

Pirani, A., C. Xu, V. Hatch, R. Craig, L. S. Tobacman and W. Lehman (2005). "Single particle analysis of relaxed and activated muscle thin filaments." J Mol Biol **346**(3): 761-72.

Poole, K. J., M. Lorenz, G. Evans, G. Rosenbaum, A. Pirani, R. Craig, L. S. Tobacman, W. Lehman and K. C. Holmes (2006). "A comparison of muscle thin filament models obtained from electron microscopy reconstructions and low-angle X-ray fibre diagrams from non-overlap muscle." J Struct Biol **155**(2): 273-84.

Potter, J. D. and J. Gergely (1975). "The calcium and magnesium binding sites on troponin and their role in the regulation of myofibrillar adenosine triphosphatase." J Biol Chem **250**(12): 4628-33.

Rall, J. A. (1985). "Energetic aspects of skeletal muscle contraction: implications of fiber types." Exerc Sport Sci Rev **13**: 33-74.

Rayment, I., W. R. Rypniewski, K. Schmidt-Base, R. Smith, D. R. Tomchick, M. M. Benning, D. A. Winkelmann, G. Wesenberg and H. M. Holden (1993). "Three-dimensional structure of myosin subfragment-1: a molecular motor." Science **261**(5117): 50-8.

Redwood, C. S., J. C. Moolman-Smook and H. Watkins (1999). "Properties of mutant contractile proteins that cause hypertrophic cardiomyopathy." Cardiovasc Res **44**(1): 20-36.

Rios, E. and G. Pizarro (1991). "Voltage sensor of excitation-contraction coupling in skeletal muscle." Physiol Rev **71**(3): 849-908.

Robinson, P., P. J. Griffiths, H. Watkins and C. S. Redwood (2007). "Dilated and hypertrophic cardiomyopathy mutations in troponin and alpha-tropomyosin have opposing effects on the calcium affinity of cardiac thin filaments." Circ Res **101**(12): 1266-73.

Robinson, P., S. Lipscomb, L. C. Preston, E. Altin, H. Watkins, C. C. Ashley and C. S. Redwood (2007). "Mutations in fast skeletal troponin I, troponin T, and beta-tropomyosin that cause distal arthrogryposis all increase contractile function." FASEB J **21**(3): 896-905.

Rould, M. A., Q. Wan, P. B. Joel, S. Lowey and K. M. Trybus (2006). "Crystal structures of expressed non-polymerizable monomeric actin in the ADP and ATP states." J Biol Chem **281**(42): 31909-19.

Sahota, V. K., B. F. Grau, A. Mansilla and A. Ferrus (2009). "Troponin I and Tropomyosin regulate chromosomal stability and cell polarity." J Cell Sci.

Sanders, C., L. D. Burtnick and L. B. Smillie (1986). "Native chicken gizzard tropomyosin is predominantly a beta gamma-heterodimer." J Biol Chem **261**(27): 12774-8.

Schaertl, S., S. S. Lehrer and M. A. Geeves (1995). "Separation and characterization of the two functional regions of troponin involved in muscle thin filament regulation." Biochemistry **34**(49): 15890-4.

Shaffer, J. F., R. W. Kensler and S. P. Harris (2009). "The myosin-binding protein C motif binds to F-actin in a phosphorylation-sensitive manner." J Biol Chem **284**(18): 12318-27.

Singh, A. and S. E. Hitchcock-DeGregori (2003). "Local destabilization of the tropomyosin coiled coil gives the molecular flexibility required for actin binding." Biochemistry **42**(48): 14114-21.

Singh, A. and S. E. Hitchcock-DeGregori (2006). "Dual requirement for flexibility and specificity for binding of the coiled-coil tropomyosin to its target, actin." Structure **14**(1): 43-50.

Singh, A. and S. E. Hitchcock-DeGregori (2007). "Tropomyosin's periods are quasi-equivalent for actin binding but have specific regulatory functions." Biochemistry **46**(51): 14917-27.

Siththanandan, V. B., L. S. Tobacman, N. Van Gorder and E. Homsher (2009). "Mechanical and kinetic effects of shortened tropomyosin reconstituted into myofibrils." Pflugers Arch.

Skoumpla, K., A. T. Coulton, W. Lehman, M. A. Geeves and D. P. Mulvihill (2007). "Acetylation regulates tropomyosin function in the fission yeast Schizosaccharomyces pombe." J Cell Sci **120**(Pt 9): 1635-45.

Somlyo, A. P. and A. V. Somlyo (1994). "Signal transduction and regulation in smooth muscle." Nature **372**(6503): 231-6.

Spudich, J. A. and S. Watt (1971). "The regulation of rabbit skeletal muscle contraction. I. Biochemical studies of the interaction of the tropomyosin-troponin complex with actin and the proteolytic fragments of myosin." J Biol Chem **246**(15): 4866-71.

Squire, J. M. (1975). "Muscle filament structure and muscle contraction." Annu Rev Biophys Bioeng **4**(00): 137-63.

Straussman, R., J. M. Squire, A. Ben-Ya'acov and S. Ravid (2005). "Skip Residues and Charge Interactions in Myosin II Coiled-coils: Implications for Molecular Packing." Journal of Molecular Biology **353**(3): 613-628.

Sugden, P. H. (2001). "Signalling pathways in cardiac myocyte hypertrophy." Ann Med **33**(9): 611-22.

Sumida, J. P., E. Wu and S. S. Lehrer (2008). "Conserved Asp-137 imparts flexibility to tropomyosin and affects function." J Biol Chem **283**(11): 6728-34.

Sun, Y. B., F. Lou and M. Irving (2009). "Calcium- and myosin-dependent changes in troponin structure during activation of heart muscle." J Physiol **587**(Pt 1): 155-63.

Sung, S. S., A. M. Brassington, K. Grannatt, A. Rutherford, F. G. Whitby, P. A. Krakowiak, L. B. Jorde, J. C. Carey and M. Bamshad (2003). "Mutations in genes encoding fast-twitch contractile proteins cause distal arthrogryposis syndromes." Am J Hum Genet **72**(3): 681-90.

Szent-Gyorgyi, A. G. (1975). "Calcium regulation of muscle contraction." Biophys J **15**(7): 707-23.

Tajsharghi, H., E. Kimber, D. Holmgren, M. Tulinius and A. Oldfors (2007). "Distal arthrogryposis and muscle weakness associated with a beta-tropomyosin mutation." Neurology **68**(10): 772-5.

Tajsharghi, H., M. Ohlsson, C. Lindberg and A. Oldfors (2007). "Congenital myopathy with nemaline rods and cap structures caused by a mutation in the beta-tropomyosin gene (TPM2)." Arch Neurol **64**(9): 1334-8.

Takeda, S., A. Yamashita, K. Maeda and Y. Maeda (2003). "Structure of the core domain of human cardiac troponin in the Ca2+-saturated form." Nature **424**(6944): 35-41.

Taylor, M. R., E. Carniel and L. Mestroni (2004). "Familial hypertrophic cardiomyopathy: clinical features, molecular genetics and molecular genetic testing." Expert Rev Mol Diagn **4**(1): 99-113.

Thierfelder, L., H. Watkins, C. MacRae, R. Lamas, W. McKenna, H. P. Vosberg, J. G. Seidman and C. E. Seidman (1994). "Alpha-tropomyosin and cardiac troponin T mutations cause familial hypertrophic cardiomyopathy: a disease of the sarcomere." Cell **77**(5): 701-12.

Trinick, J. (1996). "Cytoskeleton: Titin as a scaffold and spring." Current Biology **6**(3): 258-260.

Tskhovrebova, L. and J. Trinick (2008). "Giant proteins: sensing tension with titin kinase." Curr Biol **18**(24): R1141-2.

Varnava, A. M., P. M. Elliott, C. Baboonian, F. Davison, M. J. Davies and W. J. McKenna (2001). "Hypertrophic cardiomyopathy: histopathological features of sudden death in cardiac troponin T disease." Circulation **104**(12): 1380-4.

Varnava, A. M., P. M. Elliott, N. Mahon, M. J. Davies and W. J. McKenna (2001). "Relation between myocyte disarray and outcome in hypertrophic cardiomyopathy." Am J Cardiol **88**(3): 275-9.

Vinogradova, M. V., D. B. Stone, G. G. Malanina, C. Karatzaferi, R. Cooke, R. A. Mendelson and R. J. Fletterick (2005). "Ca(2+)-regulated structural changes in troponin." Proc Natl Acad Sci U S A **102**(14): 5038-43.

Vlahovich, N., A. J. Kee, C. *Van der Poel,* E. Kettle, D. Hernandez-Deviez, C. Lucas, G. S. Lynch, R. G. Parton, P. W. Gunning and E. C. Hardeman (2009). "Cytoskeletal tropomyosin Tm5NM1 is required for normal excitation-contraction coupling in skeletal muscle." Mol Biol Cell **20**(1): 400-9.

Vlahovich, N., G. Schevzov, V. Nair-Shaliker, B. Ilkovski, S. T. Artap, J. E. Joya, A. J. Kee, K. N. North, P. W. Gunning and E. C. Hardeman (2008). "Tropomyosin 4 defines novel filaments in skeletal muscle associated with muscle remodelling/regeneration in normal and diseased muscle." Cell Motil Cytoskeleton **65**(1): 73-85.

Watkins, H., D. Conner, L. Thierfelder, J. A. Jarcho, C. MacRae, W. J. McKenna, B. J. Maron, J. G. Seidman and C. E. Seidman (1995). "Mutations in the cardiac myosin binding protein-C gene on chromosome 11 cause familial hypertrophic cardiomyopathy." Nat Genet **11**(4): 434-7.

Webb, R. C. (2003). "Smooth muscle contraction and relaxation." Adv Physiol Educ **27**(1-4): 201-6.

Weber, A., C. R. Pennise, G. G. Babcock and V. M. Fowler (1994). "Tropomodulin caps the pointed ends of actin filaments." J Cell Biol **127**(6 Pt 1): 1627-35.

Wegner, A. (1982). "Kinetic analysis of actin assembly suggests that tropomyosin inhibits spontaneous fragmentation of actin filaments." Journal of Molecular Biology **161**(2): 217-227.

Weinberger, R., G. Schevzov, P. Jeffrey, K. Gordon, M. Hill and P. Gunning (1996). "The molecular composition of neuronal microfilaments is spatially and temporally regulated." J Neurosci **16**(1): 238-52.

Weisberg, A. and S. Winegrad (1996). "Alteration of myosin cross bridges by phosphorylation of myosin-binding protein C in cardiac muscle." Proc Natl Acad Sci U S A **93**(17): 8999-9003.

Whitby, F. G. and G. N. Phillips, Jr. (2000). "Crystal structure of tropomyosin at 7 Angstroms resolution." Proteins **38**(1): 49-59.

Wilkinson, J. M. and R. J. Grand (1978). "Comparison of amino acid sequence of troponin I from different striated muscles." Nature **271**(5640): 31-5.

Wilton, S. D., H. Eyre, P. A. Akkari, H. C. Watkins, C. MacRae, N. G. Laing and D. C. Callen (1995). "Assignment of the human a-tropomyosin gene TPM3 to 1q22-->q23 by fluorescence in situ hybridisation." Cytogenet Cell Genet **68**(1-2): 122-4.

Wilton, S. D., L. Lim, S. D. Dorosz, H. C. Gunn, H. J. Eyre, D. F. Callen and N. G. Laing (1996). "Assignment of the human alpha-tropomyosin gene TPM4 to band 19p13.1 by fluorescence in situ hybridization." Cytogenet Cell Genet **72**(4): 294-6.

Wolska, B. M. and D. M. Wieczorek (2003). "The role of tropomyosin in the regulation of myocardial contraction and relaxation." Pflugers Arch **446**(1): 1-8.

Yamauchi-Takihara, K., C. Nakajima-Taniguchi, H. Matsui, Y. Fujio, K. Kunisada, S. Nagata and T. Kishimoto (1996). "Clinical implications of hypertrophic cardiomyopathy associated with mutations in the alpha-tropomyosin gene." Heart **76**(1): 63-5.

Zot, H. G. and J. D. Potter (1982). "A structural role for the Ca2+-Mg2+ sites on troponin C in the regulation of muscle contraction. Preparation and properties of troponin C depleted myofibrils." J Biol Chem **257**(13): 7678-83.

Books

Carlo Reggiani and Roberto Botinelli. Chapter 5 pg 125-169 "Myosin II: Sarcomeric myosins, the motors of contraction in skeletal and cardiac muscles" from *Myosins: A Superfamily of Molecular Motors©2008 Springer, L.M .Collucio (ed.)*

Websites

http://faculty.etsu.edu/forsman/Histologyofmuscleforweb.htm

http://www.merck.com/mmhe/print/sec03/ch026/ch026a.html

http://kc.njnu.edu.cn/swxbx/shuangyu/6.files/image016.gif

http://www.ch.embnet.org/software/LALIGN_form.html

http://www.iba-biotagnology.com/downloads/pdf/cycle.pdf

http://www.kpl.com/images/His-tagged2.jpg

http://www.iba-go.com/prottools/prot_fr01_01.html

http://www.iba-go.com/downloads/pdf/2-1437-000pASK-IBA37plus.pdf